DOCTOR OF PHILOSOPHY

The effects of intensive sports training on the growth plate and subsequent biomechanical development of long bones
a pilot study

Stephen, Ashley Elizabeth

Award date:
2013

DOCTOR OF PHILOSOPHY

The effects of intensive sports training on the growth plate and subsequent biomechanical development of long bones

a pilot study

Ashley Elizabeth Stephen

2013

University of Dundee

The Effects of Intensive Sports Training on the Growth Plate and Subsequent Biomechanical Development of Long Bones: A Pilot Study

By

Ashley Elizabeth Stephen

BSc (Hons) Forensic Anthropology

PhD

University of Dundee

November 2013

Table of Contents

List of Figures

List of Tables

Abbreviations

3D – Three Dimensional

Ag – Silver

AIIS – Anterior Inferior Iliac Spine

AMTI® – Advanced Mechanical Technology Incorporated

ASCII – American Standard Code for Information Interchange

ASIS – Anterior Superior Iliac Spine

BMI – Body Mass Index

BMP – Bone Morphogenic Proteins

C3D – Coordinate 3-Dimensional file

CAHId – Centre for Anatomy and Human Identification

CD – Compact Disc

Cl – Chlorine

CLUT – Colour look-up table

CMAS – Clinical Movement Analysis Society

CRC – Clinical Research Centre

DESS – Dual Echo Steady State

DICOM – Digital Imaging and Communications in Medicine

ECM – Extra Cellular Matrix

FA – Football Association

FL – Forefoot Loading

FS – Foot Strike

Fx – Force vector in the sagittal plane (x)

Fy – Force vector in the frontal plane (y)

Fz – Force vector in the vertical plane (z)

GRF – Ground Reaction Force

HS – Heel Strike

HO – Heel Off

Hz – Hertz

Ihh – Indian Hedgehog (signalling factor)

IMAR – Institute of Motion Analysis and Research

IS – Initial Swing

ISE – Institute of Sport and Exercise

kg – Kilograms

kPa – Kilo Pascals

LR – Loading Response

MA – Motion Analysis

MATLAB®– Matrix Laboratory

MRI – Magnetic Resonance Imaging

MS – Mid-stance or Mid-swing depending on phase of gait cycle

MSP – Mid-swing Phase

N – Newtons

NHS – National Health Service

N/m – Newtons per metre

Nm/kg – Newtons per kilogram

PACS – Picture Archiving and Communications System

PAR – Parity archive

PS – Pre-swing

PTHrP – Parathyroid Hormone-Related Protein

ROI – Region of Interest

SPA – Swing Phase Absorption or Stance Phase Absorption depending on phase of gait cycle

SPG – Swing Phase Generation or Stance Phase Generation depending on phase of gait cycle

SPR – Swing Phase Reversal

T_1 – Spin-Lattice Relaxation Time: *type of magnetic resonance imaging scan defined as the time to reduce the difference between the longitudinal magnitisation and the equilibrium magnetisation by a factor of e.*

T_2 – Spin-Spin Relaxation Time: *type of magnetic resonance imaging scan defined as the time to reduce the transverse magnetisation by a factor of e.*

TMSi™ – Twente Medical Systems International

TO – Toe Off

TORT – Tayside Orthopaedic and Rehabilitation Technology

TS – Terminal Stance or Terminal Swing depending on phase of gait cycle

VPI – Virtual Path Identifier

W/kg – Watts per kilogram

Acknowledgements

Firstly, I wish to sincerely thank my supervisors, Professor Sue Black and Professor Rami Abboud, for their inspirational guidance, support, strength and patience throughout the last few years. I am forever grateful for this privileged opportunity and words cannot fully convey the heartfelt appreciation I have for the enthusiasm, knowledge and inspiring influences that Sue and Rami inadvertently exude, both professionally and personally.

I would like to extend my deepest gratitude to all of the staff at Rangers Football Club, in particular Phillip Yeates and Dr Paul Jackson, in addition to all of the boys and families who kindly volunteered to support this research – I am truly thankful.

Special thanks go to the following departments, whose invaluable expertise and technological help played a key role in the development and progression of this research:

CAHID – All of the staff and fellow students for creating a warm, amiable atmosphere for creative ideas to flourish. Special mention of thanks go to Prof Soames, Dr Paul Felts, Viv, Marj, Gill, Lucina, Roos, Chris, Andrew and Nurul.

CRC – Dr Barry Oliver for acting as the clinical radiologist assigned to this research and the exceptional work, time and friendship of the lovely Pat Martin and her team of radiographers (Elena, Karen, Kay, Susan and Ruth).

IMAR – Inordinate gratitude of thanks go to Dr Graham Arnold, Sadiq Nasir, Dr Ahmad Dahrouj and Mr & Mrs Gibbs for their precious time collectively teaching me the necessary skills, patience and appreciation for working with the advanced biomechanical technology and software in the gait lab. I treasure all of the staff who create another wonderful working environment, however, special mention of thanks also go to Dr Weijie Wang (for his statistical support), Mr Ian Christie (for his illustrative eye), Sheila and June.

ISE – Brian Ewing and Dr Audrey Duncan for their continued support.

Medical Physics – Dr Stephen Gandy for his investment of precious time assisting with the inter-observer measurements and dedication working together with Dr Ian Cavin and Mr Marko Erdtel to design, develop and define the final MRI acquisition settings required to conduct this scientific research.

I would personally like to thank Dianna Bruce and John Payne for their support, understanding and flexibility while I have worked part-time as a member of their team. I truly value the friendship and opportunities which helped me to appreciate the important little things in life which kept me grounded in the 'real' world.

I also would to extend my heartfelt appreciation and thanks to all of my fabulous family and friends who are the stars of my life – although we do not always get to see each other, I know that they are always sparkling close by. Finally, I wish to thank my parents and Kev as I would not be the person I am today without their endless love, support, pride, inspiration, belief and friendship – for this I owe them everything.

Declaration

I hereby declare that this thesis has been compiled by me, that this is a record of work completed by myself under the direct supervision of Professor Sue Black and Professor Rami Abboud, and that it has not previously been accepted for a higher degree at this University or any other institution of learning.

……

Ashley E Stephen

Abstract

Introduction and Aim

Football is renowned for being the most popular international team sport and the attraction of a prosperous professional career is enticing for young enthusiasts. This has led to a greater number of increasingly younger individuals participating in organised training regimes that use repetitious exercises in order to develop specialist skills. While obesity and inactivity is a mounting problem for the general population, the increased intensity of complex skills practised by competitive young athletes is just as perturbing with respect to the unknown health risks associated with prolonged intensive exercise.

The lack of scientific guidelines to prevent overtraining is partly due to the limited number of longitudinal studies which assess growing athletes over many years. The gap in the literature leads to a weakness in scientific understanding; thus the potential to uniquely combine Motion Analysis (MA) and Magnetic Resonance Imaging (MRI) to assess the development of young athletes. This research may affect the design of future health support mechanisms to protect the vulnerable area of bone growth (the epiphyseal plate). The aim of this research is to broaden scientific understanding with respect to the epiphyseal plate and subsequent development of long bones; in addition to exploring the influence exercise has on the biomechanics of gait and the future health and welfare of amateur and professional athletes.

Materials and Method

This study assessed 15 young male footballers aged between 12-14 years who attend Rangers Youth Academy. This active group were compared to an age-matched cohort of 15 non-trained school boys who lead a more sedentary lifestyle. Motion of the musculoskeletal system of individuals walking and running was captured using Vicon® in combination with concealed AMTI® force plates prior to being analysed using Polygon®. The in-shoe pressure was simultaneously measured using Pedar® while electromyography was recorded for 4 muscles on the dominant leg using the TMS International Mobi®. The MRI scans non-invasively generate images of the internal anatomical structures; thus enabling epiphyseal plate dimensions and volumes to be calculated and visualised in 3-D. Three different software programs were used

(OsiriX™, Endpoint and MatLab™) to quantify the volume of each epiphyseal plate around the knee and foot.

Results

Significant differences were encountered in the kinetic and kinematic data when comparing the MA of the active and control groups. The influence that intensive sport training has on the biomechanical development of the young athletes is particularly evident in relation to the difference in running styles adopted by the active and control groups; the active individuals tend to adopt an efficient toe-running technique which dramatically differs from the heel-running style selected by individuals in the control group.

The growth plate volumes of the two groups did not statistically reach a level of significant difference. However, the MRI findings highlighted there is a complex trend that is present between the active and control groups indicating that intensive training has a distinct influence on the development of long bones.

Discussion and Conclusions

Ultimately this research provided greater insight as to the appropriate prescription of training for young athletes. If an individual's biomechanics are found to place detrimental stress and strain across the lower limb joints, or if MRI reveals otherwise hidden micro-damage to the epiphyseal plate, clinical analysis of the motion can enable beneficial intervention to assist with their running and exercise techniques. If this research could extend longitudinally, it could potentially provide information on the levels of exercise required to induce positive changes in growth while eliminating any negative changes, therefore enabling us to prevent possible long-term health risks and give a better understanding of how bones adapt to our changing lifestyles.

Chapter 1

Introduction and Aim of Thesis

1.1 Introduction

Football is renowned for being the most popular international team sport (Dunning, 2000; Dvorak *et al.*, 2012) and the attraction of a prosperous professional career is enticing for young enthusiasts. This has led to a greater number of increasingly younger individuals participating in organised training regimes (Rowland, 1996; Loh, 2012) that use repetitive exercises to develop specialist skills (Gerrard, 1993). While obesity and inactivity are mounting problems for the general population (Brewis, 2012), the increased intensity of complex skills practised by competitive young football players is perturbing with respect to the unknown health risks associated with intensive exercise and the lack of scientific guidelines to prevent overtraining (Brenner *et al.*, 2007; Hartwig *et al.*, 2009).

The significant weakness in current scientific understanding stems from the possibility that children may incur irreversible damage to the growing region of long bones (Colvin and Lynn, 2010) which are particularly vulnerable to trauma when compared with the fully fused structure of adult bone. Unfortunately there is a lack of defined upper limits as to when the volume, intensity or level of exercise is attained before the beneficial health effects associated with fitness are negated (Babraj *et al.*, 2009; Lynch *et al.*, 2007) and may instead induce detrimental micro-trauma to the cellular and structural elements of bone. The major shortfall in current literature is the paucity of longitudinal studies (Malina *et al.*, 2000) as most datasets are cross-sectional in nature, or research is founded on single case studies which are incomparable as a consequence of different sample sizes, age ranges, number of individuals, sport played and the skill level of individuals.

The development of a stable training programme is both necessary and desirable to promote competitive skills. Ericsson *et al.* (1993) demonstrated that approximately ten years of intensive training are required prior to achieving the level of expert performance as depicted in Figure 1.1. In Scotland, one example of a specialised youth development programme is Glasgow Rangers Youth Academy, located at Murray Park

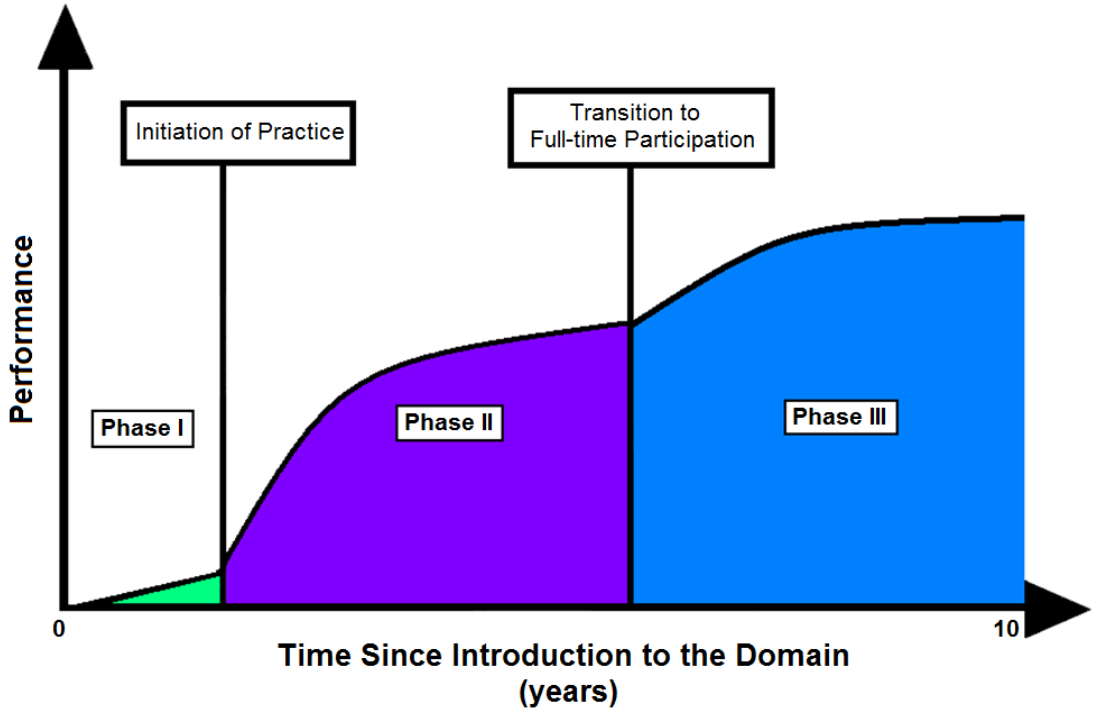

<u>Figure 1.1</u> – Three phases of development toward expert performance (Adapted from Ericsson *et al.*, 1993).

training grounds, where world-class facilities provide the optimal setting to recruit, shape and train young athletes from nine years of age through to the beginning of a professional career at the age of seventeen. The augmented intensive levels of elite and competitive skills having to be practiced continuously through the ages of peak skeletal growth raise particular concerns to the subsequent development of long bones (Caine *et al.*, 2006; Tobias *et al.*, 2007; Emery, 2009) as well as the influence this may have on

an individual's health which continues to manifest benefits and detriments long into adult life (Johannsen *et al.*, 2003; Kontulainen *et al.*, 2003). The mounting psychological pressure imposed on young athletes to perform and achieve success in the sporting field (Yarrow *et al.*, 2009) may inadvertently motivate an athlete to ignore and endure progressively painful, repetitive physical stresses that are regularly encountered during training (Liebling *et al.*, 1995). Successful training regimes recognise individual needs and potential, and can implement various modalities of teaching and practicing skills without necessarily focusing on repetition of the same tasks; consequentially the benefits that moderate exercise can have on the development of a healthy individual may be reaped long into adult life with rewards of a reduced risk of cardiovascular disease and osteoporosis (Haskell *et al.*, 2007; Lynch *et al.*, 2007; Brown *et al.*, 2012). Intensive sports training is more likely to induce injury if underlying biomechanical anomalies are present (Neely, 1998) and the risk of harm is significantly increased during periods of increased growth (Brenner *et al.*, 2007); thus supporting the unique design that this research attains with regard to providing a holistic understanding of the biomechanics and the resultant changes that may occur particularly at the "growing ends" of the long bones.

1.2 Aim and objectives

The scientific literature does not address adequately the effect that biomechanical influences have on the lower limb growth plates in relation to intensive training regimes. Ultimately this research is designed to fulfil the aim of broadening the scientific understanding of the influence that exercise may have on the development of long bones by analysing both the volume of growth plates and musculoskeletal biomechanics of young, elite footballers and comparing them to age matched controls.

The primary objective of this pilot project is to determine potential health risks/benefits that may be experienced as a consequence of intensive sports training and how this may influence changes to exercise regimes to ensure the future welfare of individuals in society up to the professional athlete level. To accomplish the desired aim and objectives, it is necessary to outline a clear hypothesis that can be tested and therefore accepted or rejected; therefore validating the final argument of whether intensive sports training has an effect (whether positive, negative or neutral) on the growth and development of long bones.

Hypothesis (H_1) – Intensive sports training **has an effect** on the normal growth of the epiphyseal plate and development of long bones in the lower limb.

The hypothesis can be divided into specific components:

- $H_{1\text{-}1}$ – The growth plate volumes in the active group are significantly different from those of the control group.
- $H_{1\text{-}2}$ – There is a significant difference in plantar pressures exhibited by the active group compared with the control group.
- $H_{1\text{-}3}$ – The lower limb kinetics of the active group differ significantly compared with those of the control group.
- $H_{1\text{-}4}$ – The lower limb kinematics of the active group differ significantly compared with those of the control group.

Null Hypothesis (H_{01}) – Intensive sports training **has no** influence on the normal growth of the epiphyseal plate and the development of long bones in the lower limb.

The null hypothesis can also be divided into specific components:

H_{01-1} – There is no significant difference in the volume of the growth plate between the active and control groups.

H_{01-2} – There is no significant difference in plantar pressures between the active and control groups.

H_{01-3} – The lower limb kinetics of the active group do not differ significantly from those of the control group.

H_{01-4} – The lower limb kinematics of the active group do not differ significantly from those of the control group.

Chapter one has introduced the motivation for undertaking this research and outlines the aim and objectives before Chapter two considers the relevant anatomical structures and functional processes that are encountered during normal growth; taking into consideration the principles of biomechanics and the gait cycle. Chapter two also reviews the current literature on this subject and will address the current limitations preventing a full understanding of the effects of intense training regimes on the growing skeleton of athletes. The design of this research is explained in Chapter three by providing a detailed account of the sample groups and equipment utilised in addition to the method in which the participant's data was prepared, captured and analysed. Chapter four presents the results obtained and statistical methods applied in the two stages of data collection:

1. Magnetic Resonance Imaging - to calculate the growth plate volume and discern any incidental findings with regard to pathology, and

2. Biomechanics - to calculate the kinematic, kinetic and in-shoe pressure differences.

Chapter five deliberates the research aims and objectives in light of the results and findings of the study and discusses the relevance of applying the knowledge and understanding achieved within this research to improving the field of sports performance. The limitations of the study and recommendations for future research are also explored with the conclusions of the research detailed in Chapter six.

Chapter 2

Review of the Literature

2.1 Growth Plate

To fully comprehend the effects of intensive sporting activities on the development of long bones, it is imperative to appreciate the key processes and biomechanical factors that may influence the progression of normal growth in the epiphyseal plate. Scientific research remains at a rudimentary stage with respect to understanding the regulation and cellular control of the growth plate (Bush *et al.,* 2008) and particular focus of future research might be advised to target the influence of intrinsic and extrinsic factors, which collectively shape the overall skeletal structure (Moreland, 1980).

The epiphyseal plate (also known as the growth plate or the physis) in long bones is a specialised, discoid junction between the diaphysis and epiphysis separating the two adjacent areas of growing bone. The principal function of the epiphyseal plate is to ensure that longitudinal growth and circumferential extension of bone diameter occur in a regulated manner as the bone grows (Rang, 1969) while at the same time directing forces and transmitting loads (body weight) in an efficient and effective manner (Bright *et al.,* 1974).

2.1.1 Form and Function

Skeletal development of the long bones results from a highly complex and regulated series of events that lead to co-ordinated increases in size through a process of conversion of cartilage into bone (endochondral ossification). The diaphyseal bone is separated from the epiphysis by the growth plate which is confined at the periphery by the annulus of chondrocytes that establish the perichondrium (Hochberg, 2002). Vascularisation of the growth plate via both diaphyseal and epiphyseal vessels is fundamental to deliver essential nutrients, including calcium, phosphates and vitamin

D, to the dispersed chondrocytes and in particular to the progenitor cells located in the germinal zone (Brookes, 1971; Laor *et al.*, 2006). The increased cellular organisation of each successive zone of the epiphyseal plate demonstrates the greater demand for a healthy blood supply to provide a sufficient level of essential core requirements to support the normal developmental processes of calcification and osteogenesis. Figure 2.1 depicts the histological appearance of the four discrete, cellular zones that form the growth plate.

The germinal zone is named after the quiescent nature of the chondroprogenitor cells which differentiate into, and are protected structurally by, radially orientated collagen fibres (Nilsson *et al.,* 2005). The chondroprogenitor cells establish a cartilaginous template for the subsequent development of the long bone and are derived from dense,

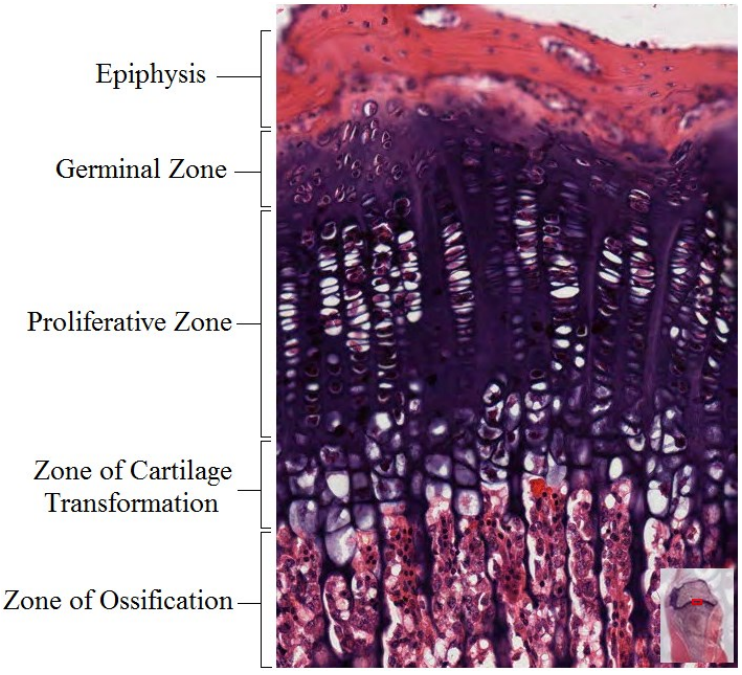

<u>Figure 2.1</u> – Histological overview of the zones of a diaphyseal growth plate of a long bone depicting the transition of cellular layers . Photograph acquired from histology slide 22 – foetal rabbit tibia stained with Haemotoxylin and Eosin.

irregularly arranged mesenchymal cells that are encased within an abundant cartilaginous extracellular matrix (Mackie *et al.*, 2011). Proteoglycans are dispersed throughout the extracellular matrix (ECM) and influence the interaction of cell membranes with secreted proteins, thus creating a concentration gradient to regulate chondrocyte interactions (de Andrea and Hogendoom, 2012). The structurally slender germinal zone is where the resting precursor chondrocytes are positioned and remain relatively dormant until triggered into activation. In the proliferating zone of the epiphyseal plate the activated chondrocytes mature and undergo cell division which is induced by the synchronised expression of bone morphogenic proteins (BMP) and Indian hedgehog (Ihh) signalling factor (Minina *et al.*, 2001). A number of morphological changes occur to each chondrocyte as the flattened shape begins to become fuller and more rectangular to acquire the necessary palisaded structural alignment and adhesion within the ECM. The proliferative zone contributes to approximately half of the growth plate where the mitotic palisades of highly organised, longitudinal columns of chondrocytes mature, prior to transitioning into the zone of cartilage transformation (Ogden, 2000). The chondrocytes in the zone of cartilage transformation undergo hypertrophy and degenerate progressively through the increased secretion of parathyroid hormone-related protein (PTHrP). A negative feedback loop, involving the interaction of Ihh and PTHrP, is the key regulation to maintain equilibrium between the proliferation and hypertrophy of chondrocytes progressing to this zone of the epiphyseal plate (Byres *et al.*, 2000). Hydroxyapatite crystals form calcified, structural partitions (Ulijaszek *et al*., 1998) and the chondrocytes prepare for this mineralisation of the cartilaginous ECM by altering the cell's ability to synthesise type-X collagen (de Andrea and Hogendoom, 2012). The natural degeneration of cells in this layer, by the action of calcium, phosphates and

vitamin D supplied through the vascular system (Laor *et al.*, 2006), is an important component in the ossification process; however, the loss of collagen in this layer of calcified structural partitions leaves a weak region that is susceptible to damage and could impact on normal bone growth. The final zone of ossification is highly vascular to enable mineralisation of the trabecular tissue and ECM, as well as promote the osteoclastic activity of remodelling and restructuring newly formed bone at the metaphysis (Siegling, 1941).

Inevitably, the viscoelastic nature of the growth plate results in a vulnerable discontinuity within the fibrous tissue which renders this area 2-5 times less resistant to external shear and tensile forces (Larson and McMahan, 1966) leading to a biomechanical area of concern and potential weakness, particularly for active youths who are more likely to experience injury. The architecture and growth of bone alters and remodels as a consequence of biomechanical stresses and strains, stimulating and stretching the intermolecular bonds (Frost, 1994). However, there are many additional factors that influence ossification including vascularity, nutritional status, genetics, disease and endocrine processes (Rose and Gamble, 1994; Bush *et al.*, 2008).

2.1.2 Growth

The metabolism of bone has a broadly circadian and seasonal component with respect to growth (Gelander *et al.*, 1994) and varies as a consequence of hormonal changes occurring during the three different phases of growth; infancy, childhood and adolescence (Stokes, 2002). Figure 2.2 depicts the three different phases of growth. Initially, the first infantile growth curve is regulated through nutrition as well as insulin-like growth factors 1 and 2 (Bush *et al.,* 2008) and follows a non-linear, dramatically decelerating pattern until around the age of three years. During childhood

around the age of five, the velocity of skeletal growth slows and the curve levels at a steady rate due to alterations in growth hormone. During pronounced growth spurts, the height of an individual increases in advance of increases in muscle and body mass which may not occur in a symmetrically synchronised nature for each side of the body (Malina *et al.*, 2000; Boisseau *et al.*, 2007). This results in the epiphyseal plate becoming increasingly susceptible to injury (Caine *et al.*, 2006; Neeley, 1998), which may be linked to the reduced flexibility and diminished strength caused by a delay in the musculoskeletal response to catch up with the rate of bone growth (Rowland, 1996). Rapid increments of growth are also associated with imbalance, reduced co-ordination of movements and can affect the physical endurance of individuals (Hodson, 1999).

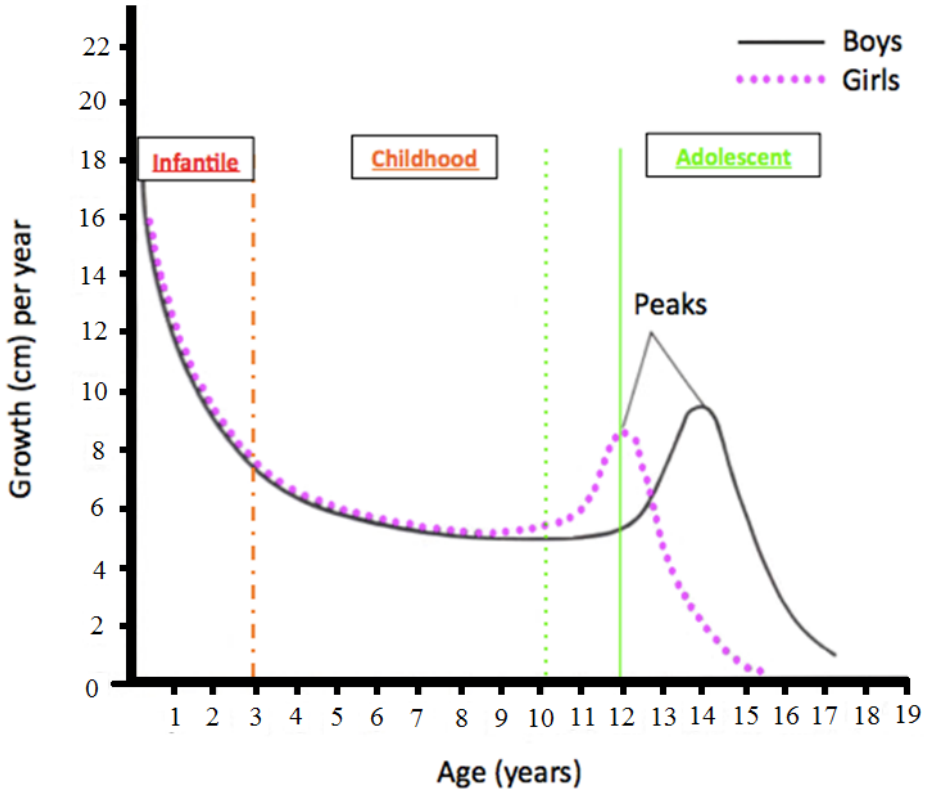

Figure 2.2 – Graph demonstrating the three phases of growth. The rapid rate of growth at the onset of birth decreases in velocity throughout infancy and slows during early childhood until a large surge of hormones induces a sharp peak of growth during puberty (Image adapted from Tanner *et al.*, (1966)).

Essentially, the longitudinal growth of long bones must maintain a synchronous response to the elongation of muscles and attaching tendons; therefore minimising the potential predisposition a growing athlete has of encountering an injury when repetitive muscular stresses may create biomechanical imbalances (Caine *et al*., 2006). If any alterations or skeletal deformities arise as a consequence of a delayed muscular response or damage, the continued growth process is an imperative way to correct and remodel any changes back to an efficient biomechanical and functional form (LeVeau and Bernhardt, 1984).

2.1.3 Cessation of Growth

Throughout life, bone undergoes continuous remodelling processes through the carefully balanced dynamic action of osteoclast and osteoblast cells to ensure that any microdamage to bone is fully restored and repaired (Tervo *et al.*, 2009). Various factors influence skeletal growth and the final height of an individual can be affected by socio-economic factors, genetics, health, ancestry and sex (Bush *et al.*, 2008). Typically, skeletal development in children follows a distinct and defined pattern; however the process of osseous differentiation and calcification does not necessarily occur at the same chronological age or progress at the same rate in all individuals. During childhood, for example, ill health has been found to inhibit skeletal growth by up to five months (Bush *et al.*, 2008) although following such restrictions the phenomenon of 'catch-up' growth may negate any visible delays due to the chondrocytes exhibiting a greater proliferative capacity and restoring any height that may have temporarily been lost (Rogol *et al.*, 2002; Nilsson and Baron, 2004). *The Radiographic Standard of Reference for the Growing Knee* (Pyle and Hoerr, 1969) and the *Radiographic Atlas of Skeletal Development of the Foot and Ankle* (Hoerr *et al.*,

1962) are two specially complied atlases that detail the chronological ages at which bone growth is expected to attain a respective stage of maturation or skeletal age providing the child is healthy and well nourished (Pyle and Hoerr, 1969; Hoerr *et al.*, 1962; Tanner *et al*., 1966; Scheuer and Black, 2000). Dr Thomas Wingate Todd initially collated the reference population dataset in 1927 by selecting healthy children in the Cleveland area of the United States of America who represented the 'ideal' growth environment thereby developing a gold standard for the time. The children were anthropometrically measured and radiography of the left hand/wrist, elbow, shoulder, hip, knee, and foot/ankle was undertaken initially on a six monthly basis and subsequently each year. This eventually became the founding roots for the longitudinal Brush Foundation Study and provided growth and maturation relevant records for over 4483 children (Pyle and Hoerr, 1969). The radiographic data represent an accurate temporal snapshot of the pace at which skeletal maturation and fusion is attained within a known population in a defined temporal window.

Differences in skeletal development can be attributed to many factors including disparities in health, nutrition, environmental and economic conditions; therefore the ability to gauge the natural unhindered or optimal progression of the growth of an individual is extremely helpful when considering the potential maturational discrepancy from chronological age. Unlike the growth and height curves that were also developed over 50 years ago (in 1966) and are now largely obsolete due to the secular trend of increased height (Wright *et al*., 2002); publications from a recent study by Hackman (2012) have established that the radiographic standards are still applicable as a reference to gauge the maturation of individuals in a clinical and forensic setting for a modern population (Hackman and Black, 2013). The radiographic standards rely on visualising the subsequent development of the epiphyseal plate and subsequent

cessation of growth which is governed by the intricate control of genetic, vascular, biomechanical and hormonal factors to regulate the rate of advancing development (ElBaradie *et al.*, 2011; Stokes, 2002). The dominant sex-steroid hormone, oestrogen, is a direct stimulant that aids in the initiation of the overall decline in rate of linear growth and subsequent narrowing of growth plate height (Emons *et al*., 2005); which also reflects a significant influence that oestrogen has over bone mineral density in later life (Riggs *et al*., 2004). The histological height of the growth plate has been found to correlate with the equivalent rate of growth (Villemure and Stokes, 2009), which is supported by the fact that increased levels of growth hormone trigger an amplification of the cellular component with respect to the physeal columns in the zone of proliferation (Bush *et al.*, 2008). Higher levels of oestrogen elucidate a reason why cessation of growth in females is precocious to males (Carter, 2009; Villemure and Stokes, 2009).

2.2 Biomechanical forces acting on bone

The dynamic, viscoelastic nature of the growth plate renders bone sensitive to external biomechanical forces which can influence skeletal remodelling (Villemure and Stokes, 2009). As previously stated, the architecture of bone enables it to be altered as a consequence of distributing the stresses, strains, forces and loads which stimulate and stretch the intermolecular bonds between the osseous units (Arkin and Katz, 1956; Bright *et al*., 1974; Frost, 1994) as illustrated in Figure 2.3.

Since Julius Wolff published *Das Gesetz der Transformation der Knocken* in 1892 (Kushner, 1940; Prendergast and Huiskes, 1995), the concept that functional remodelling of the external and internal structural form of bone is directly correlated

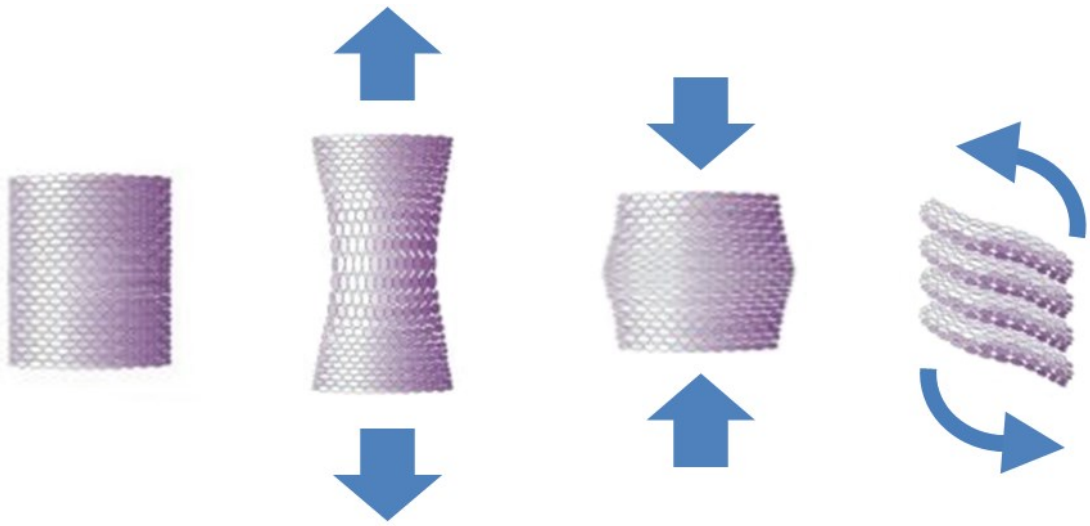

Figure 2.3 – Reaction of the intermolecular bonds between the osseous units of bone under the following biomechanical conditions:

(a) No force,

(b) Tensile forces,

(c) Compressive forces,

(d) Torsional forces.

(Adapted from Lujan and White, 2011)

with the biomechanical stresses applied to the bone has been defined as the 'law of bone transformation'. An additionally well-documented observation of the adaptations of skeletal architecture was made through the combined theories of Richard Von Volkman and Carl Heuter in 1862 (Willy *et al.*, 2008), which recognise that pressure and mechanical loading stimulate the appositional growth of bone and influence the rate of longitudinal ossification (Arkin and Katz, 1956). Unfortunately the 'laws' of Wolff and Heuter-Volkman are not truly scientific, as a scientific law by definition is required to predict a definitive effect that can be calculated by a mathematical formula (Frost, 1994); in reality however, only the mechanical influence of pressure is

mentioned without a mathematical expression to calculate a precise reaction of bone to the complex interaction of stimuli which currently cannot be simplified into one law (Pearson and Lieberman, 2004; Bush *et al.*, 2008). The external cortical morphology, and internal trabecular architecture of bone, adjusts as a response to the applied stresses and strains by increasing the cortical diameter and narrowing the medullary cavity respectively (Woo *et al.*, 1981).

Stress is defined as the force acting within an area of bone which can generate differing intensities of force and these stresses produce resultant magnitudes of strain within the bone that cause displacement in terms of length (Pearson and Lieberman, 2004). If the stress exerted on the bone is less than the tensile limit, positive accrual of bone will facilitate in the development of densely mineralised skeletal structures that are better equipped to resist the applied stresses (Vicente-Rodriguez *et al.*, 2003; Forwood *et al.*, 2006; Tobias *et al.*, 2007; Ducher *et al.*, 2009). The rate of newly formed bone will gradually become inhibited as the load and compressional stresses increase. Alternatively, if immature bone is subjected to decreased forces then the growth rate will accelerate (Arkin and Katz, 1956; Villemure and Stokes, 2009). If an unparallel load is exerted across the growth plate and is not directly perpendicular to the columnar palisades of chondrocytes, the subsequent longitudinal extension of bone will deflect along the line of deformational force (LeVeau and Bernhardt, 1984). The mechano-transductional responses of the cellular components of bone are least resilient to these unparallel, torsional forces (Moreland, 1980) and many clinical conditions concerning the skeletal frame typically occur prior to skeletal maturation as a consequence of abnormal biomechanical loading (Villemure and Stokes, 2009).

The growth plate is less resilient to stress, shear and tensile forces when compared to the surrounding skeletal bone, articular cartilage and muscular tissues (Caine *et al.*,

2006). Differences in the biomechanics across adjacent articulating surfaces can ultimately lead to the emergence of asymmetric, undulating morphological variances in growth plate shape (Stokes, 2002; Amini *et al.*, 2010). At present it is hypothesised that repetitive compressive loading and shearing forces applied at the growth plate can result in microfractures within the zone of cartilage transformation (Liebling *et al.*, 1995). The strains encountered across the respective zones of the growth plate have been found to be significantly lower in the germinal zone (which was 0.043mm) compared to both the proliferative zone (recorded at 0.081mm) and zone of cartilage transformation (measured at an increased strain of 0.096mm) (Fujii *et al.*, 2000). Histological analysis of rabbit growth plates by Fujii *et al.* (2000) revealed that the differential effects may be due to biochemical compositional differences in relation to the increased extracellular matrix volume and collagen content found within the protected germinal zone. In 1975, Lanyon *et al.* discerned that the principal strain encountered along the long axis of the human tibia during walking arose at the final stages of the stance phase just prior to toe off, which is further amplified during the act of running. Highly repetitive impact loads encountered during intensive sports training sessions can cause microfractural disturbance to the zone of cartilage transformation (Ogden, 2000); thus leading to a widened growth plate as the germinal and proliferative zones are thought to continue advancing while the zone of transformation is temporarily unable to complete the functional processes to advance the chondrocytes to attain ossification.

2.3 Anatomy of the lower limb

The main function of the lower limb is to provide stability and support for the axial skeleton without exerting excessive muscular energy during locomotion (Drake *et al.*,

2005). Bipedal locomotion has evolved to conserve the metabolic energy in the cascade of balanced temporal events which define human gait, while remaining in the erect, upright stance (Vaughan, 2003). Efficient locomotion focuses on the complimentary form and functional design of the lower limb to fulfil the following four distinct functions:

1. Generating a propulsive force,
2. Maintaining upright stability while continually recovering from the unbalanced swaying motion generated by the shifting weight of the upper body,
3. Limiting and absorbing the impact of the ground reaction force when the foot strikes the floor,
4. Minimising the overall muscular energy necessary to complete the gait cycle (Perry, 1992). This is detailed in Section 2.4.

The biologically versatile nature of locomotion is extremely difficult to simulate mechanically (Afshar and Ren, 2012); thus demonstrating the complex interaction and synergistic feedback system implemented in order to maintain effortlessly the balanced posture of the standing skeletal frame. The dynamic interaction and superimposition of the lower limb muscles are depicted in Figure 2.4 and represent the well-established, interconnected nature of the complex muscular layers.

2.3.1 Hip Joint

The hip joint consists of a robust ball and socket synovial joint between the acetabular cup of the pelvis and the femoral head (Palastanga *et al.*, 2008). The pelvis provides integral support while completing the junction of the upper axial skeleton with the pelvic girdle and lower limbs via articulation at the sacroiliac joint; thus dispersing

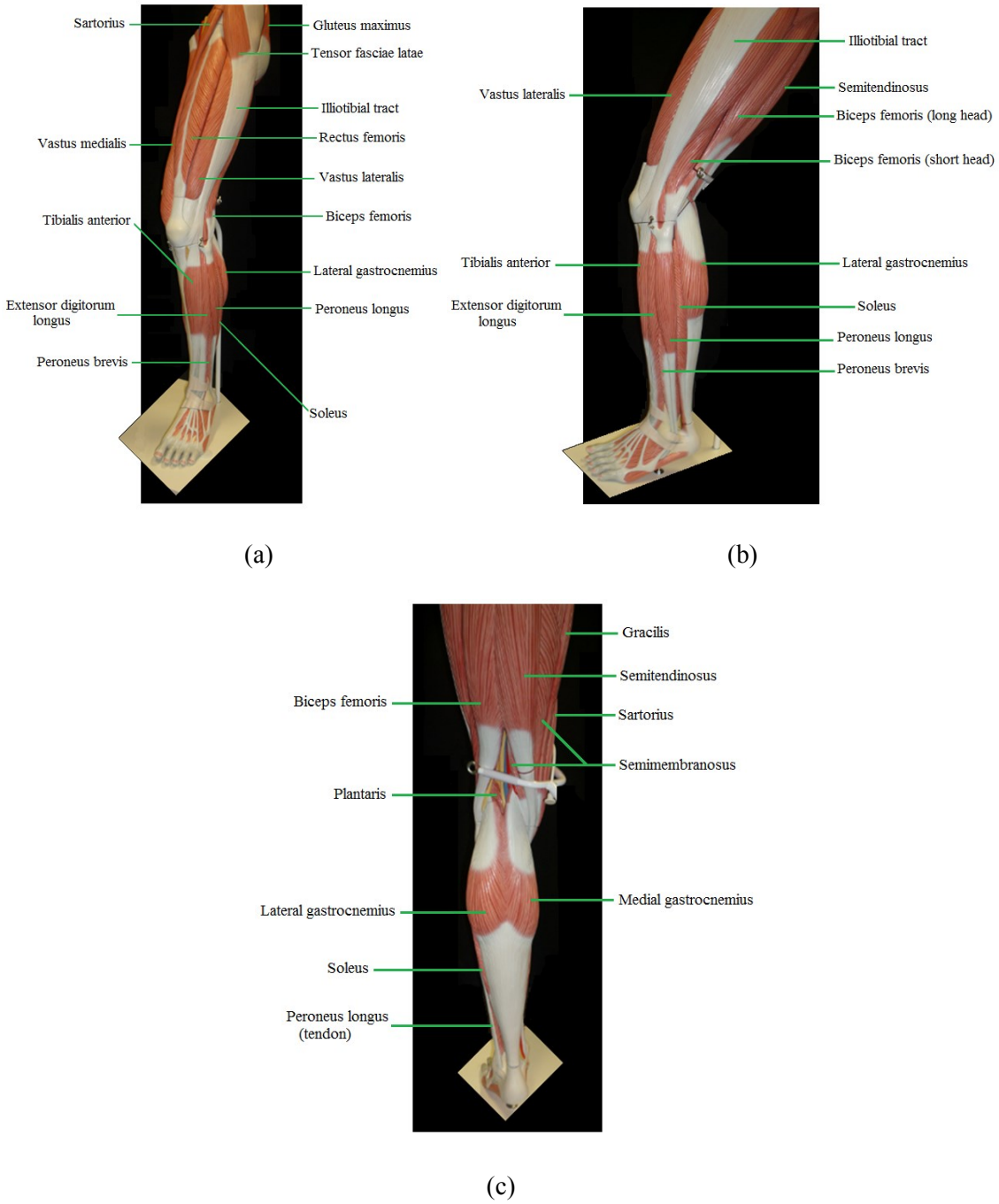

<u>Figure 2.4</u> – Musculature of the lower limb.

(a) Depiction of the anterior view of the left lower limb.

(b) Associated musculature from a lateral view of the left lower limb.

(c) Posterior view of the left lower limb.

body weight in a biomechanically efficient manner. Consequently, body weight transfers distally across the hip joint, into the femoral head where the trabecular and cortical structure of the bone reveals the internal paths of weight distribution (Hall, 1961; Ryan and Krovitz, 2006). The pelvis follows two arcs of motion during locomotion; extension at the hip joint primarily acts to stabilise the body during stance whereas flexion at the hip joint controls the limb during the swing phase (Perry, 1992).

2.3.2 Knee Joint

The hip joint is synchronously complimented by the design of the knee which is a modified bicondylar hinge and synovial joint formed by the articulation of the distal femur, proximal tibia and patella (Agur and Dalley, 2005). The knee is complex; as the joint must provide great stability yet maintain the necessary flexion, extension and rotational movements required for smooth locomotion (Goldblatt and Richmond, 2003). The three main functional roles of the knee are fulfilled due to the unique articular design and 'locking mechanism' that naturally occurs to conserve energy expenditure. The locking mechanism is accomplished through the curved and rounded posterior surface of the femoral condyles creating a smooth, effortlessly rolling articulating surface with the tibia, to facilitate flexion at the knee (Drake *et al.*, 2005). During extension, however, the articular surface favours the position of the broad, inferior aspect of the femoral condyles. The resultant flat surface forms a stable platform with the level tibial plateau and is secured by the various ligaments and membranes detailed in Figure 2.5.

The knee traces four arcs of motion during a typical walking cycle which are described in greater detail in Section 2.4.1. The flexion and extension motions of the knee joint affect the sagittal kinematics; ultimately facilitating the supporting limb to progress

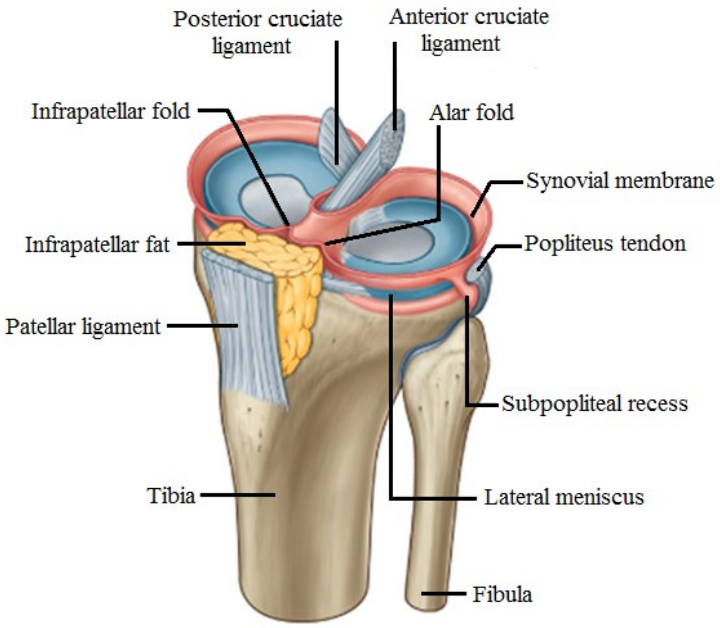

(a)

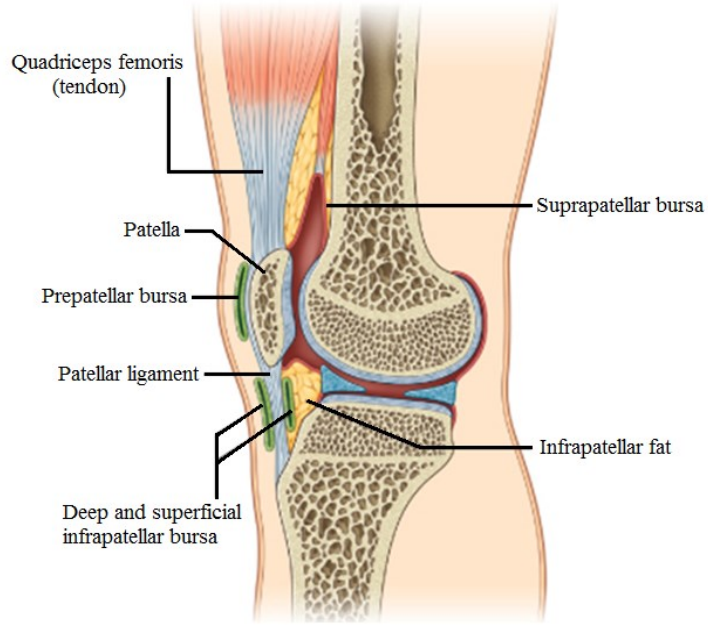

(b)

<u>Figure 2.5</u> – Anatomy of the knee.

(a) Illustration of the cruciate ligaments and cushioning design of the synovial membrane.

(b) Medial view of the sagittal plane of the knee.

(Adapted from Drake *et al.*, 2005)

during stance while advancing the limb through the swing phase. The resultant arc of motion at the knee joint during swing is evidently the largest and most prevalent of all the joints, while in the coronal and transverse planes the arcs remain small as a consequence of the smaller rotational action of the knee to accommodate and stabilise the alignment of the limb (Perry, 1992).

2.3.3 Ankle Joint

The junction connecting the leg and foot is the ankle joint, which is formed by the articulation of the distal tibia and distal fibula with the proximal (or dorsal) surface of the talus in the foot via a complex synovial joint (Palastanga *et al.*, 2008). In relation to the biomechanics of locomotion, there are three principal joints within the foot which articulate in a unique fashion to transfer the encountered forces efficiently when the foot reacts to contact with the ground (Muniz and Nadal, 2009). The subtalar, midtarsal and metatarsophalangeal joints act collectively to support and angle the foot in relation to the ankle joint, where the total compressive, rotatory, tensile and shearing forces encountered during the gait cycle have to be directed (Abboud, 2002). The anatomical form of the articular surface of the talus reflects the vital weight bearing function, with Figure 2.6(a) demonstrating that the anterior surface is significantly wider when compared to the narrow posterior surface. Figure 2.6(b) depicts the natural outline of the lateral longitudinal arch of the foot. Ultimately, the articulation of the hinge-like pivot ankle joint is most stable when the foot is dorsiflexed and the broad, anterior talar surface slots directly into the deep socket formed by the tibia and fibula (Drake *et al.*, 2005). The ankle additionally follows four arcs of motion (Perry, 1992) however not to as great an extent of motion as the knee during normal walking.

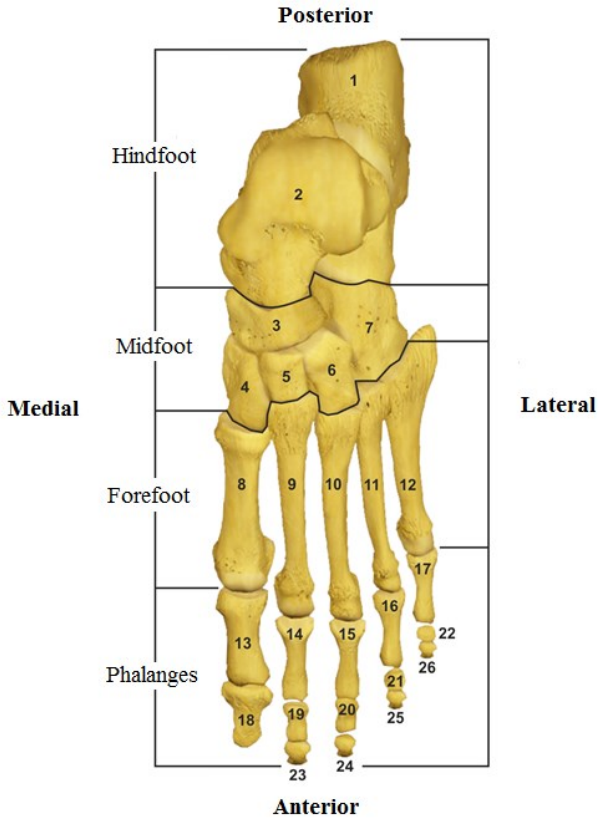

(a)

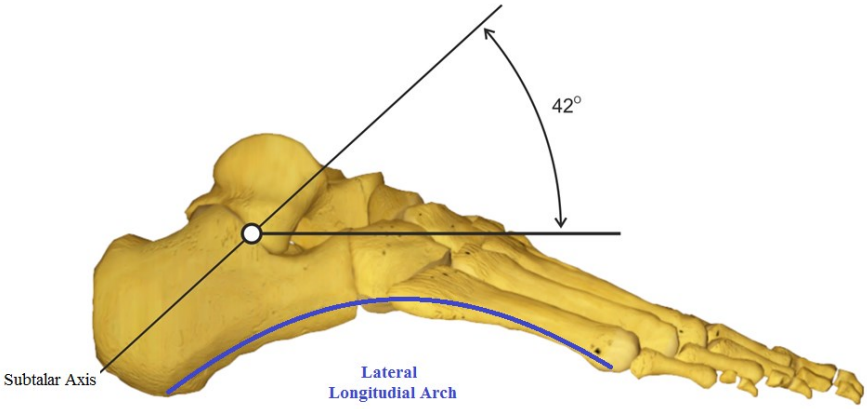

(b)

Figure 2.6 – Skeletal anatomy of the foot.

(a) Dorsal view identifying the bones and relevant regions of the left foot.

(b) Lateral view of the subtalar axis and outline of the longitudinal arch of the right foot.

2.3.4 Movement and muscles of interest

Movement and arcs of motion occur as a result of the activation and relaxation of phasically timed muscle interactions across specific joints. The types of lower limb movements are detailed in Figure 2.7 where the arrows demonstrate the respective actions of extension, flexion, adduction, abduction, dorsiflexion, plantarflexion, inversion and eversion.

An intricate interaction of specific lower limb muscles is required to perform the necessary arcs of motion resulting in walking and running, with Figure 2.8 illustrating the relationship of different muscles activating at certain points in the gait cycle. To discern where muscular attachments are more likely to influence the development of bone due to the effects of intense or repetitive actions, it is necessary to understand which muscular action will govern key biomechanical exertions at specific anatomical landmarks. The following descriptions detail the key actions, attachment sites and unique features which identify the form and functional role of each important muscle within the respective regions of the lower limb.

Of the seven muscles which contribute to forming the **gluteal region**, the three most superficial muscles are *Gluteus maximus*, *Gluteus medius*, and *Gluteus minimus*. *Gluteus maximus* is the largest of the three muscles and acts to extend the thigh whilst also providing assistance to stabilise the trunk against flexion of the hip during running (Lieberman *et al.*, 2006). The site of origin spans from the posterior aspect of the ilium, down along the dorsal surface of the sacrum, continuing onto the lateral coccygeal surface and the sacrotuberous ligament (Agur and Dalley, 2005). The majority of *Gluteus maximus* fibres insert distally into the iliotibial tract, whereas the

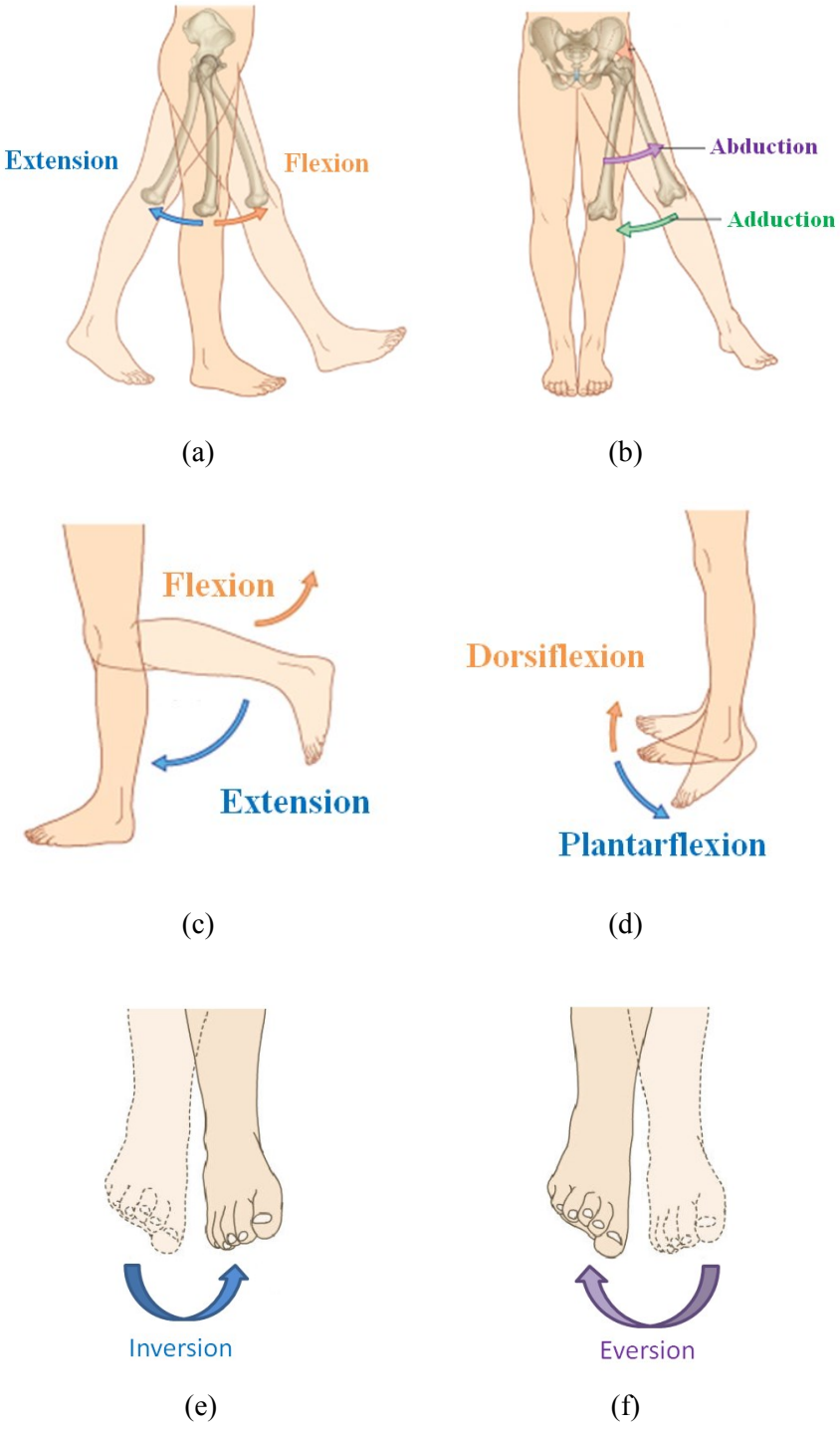

<u>Figure 2.7</u> – Movements of the lower limb.

(a) Extension and flexion at the hip joint.

(b) Abduction and adduction at the hip joint.

(c) Extension and flexion at the knee joint

(d) Dorsiflexion and plantarflexion at the ankle joint.

(e) and (f) illustrate inversion and eversion respectively.

(Adapted from Drake *et al.*, 2005)

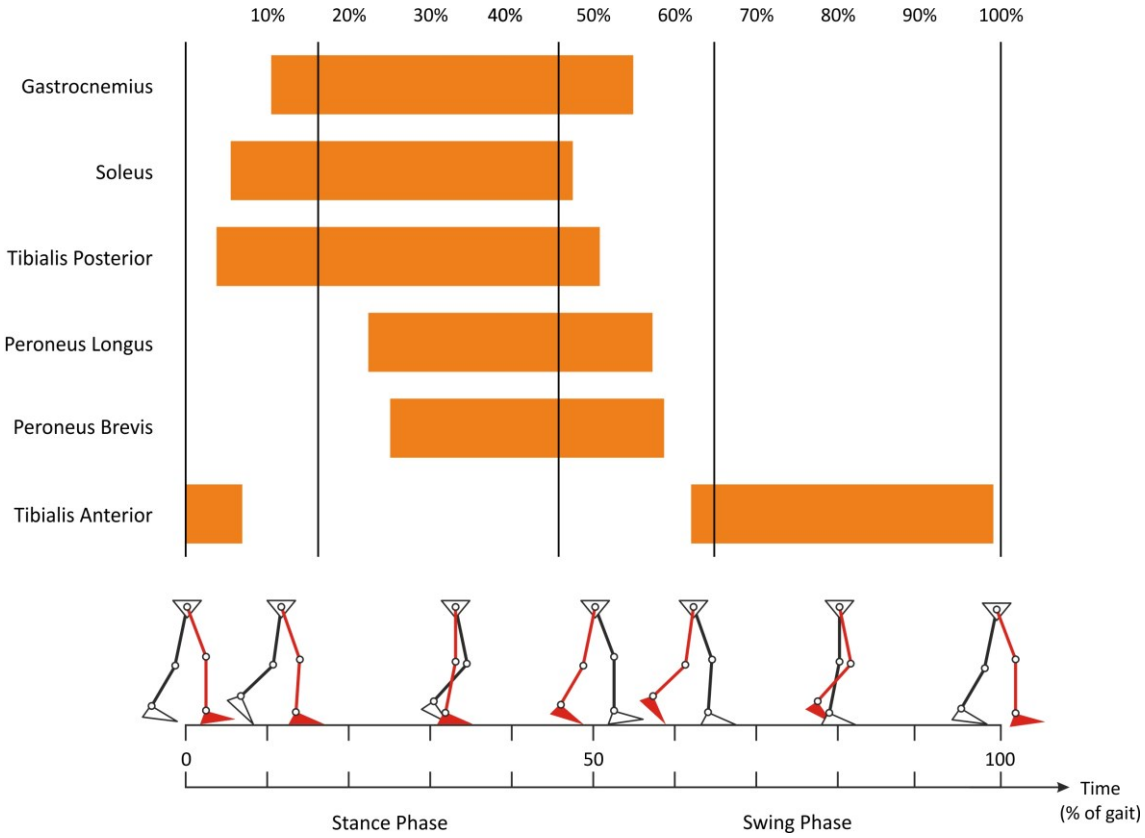

Figure 2.8 – Phasic activation of key muscles during the swing and stance phase of the walking gait cycle.

deeper fibres attach to the gluteal tuberosity of the proximal femur (Drake *et al.*, 2005). *Gluteus medius* and *Gluteus minimus* are innervated by the superior gluteal nerve, differing from *Gluteus maximus* whose innervation instead stems from the inferior gluteal nerve, and their combined actions abduct and medially rotate the thigh (Agur and Dalley, 2005). The proximal attachment site for *Gluteus medius* and *Gluteus minimus* arise from the external surface of the ilium between the anterior and inferior gluteal lines. The muscle fibres of *Gluteus minimus* converge distally to form a tendon that inserts onto the anterior surface of the greater trochanter of the femur, thus differing from *Gluteus medius* which attaches onto the lateral surface of the greater trochanter (Drake *et al.*, 2005). An important function of *Gluteus medius* and *Gluteus*

minimus during the gait cycle is to contract on the supporting limb in stance phase and therefore act to secure the position of the pelvis and avoid excessive pelvic tilt while the opposite limb is in the swing phase (Lovejoy, 1988).

The **anterior compartment of the thigh** encloses *Quadriceps femoris* (the combination of four muscles: *Rectus femoris*, *Vastus lateralis*, *Vastus medialis* and *Vastus intermedius*), *Iliopsoas* (the convergence of *Psoas major* and *Iliacus*) in addition to *Sartorius*. The most superficial muscle of this compartment is *Sartorius* which arises from the anterior superior iliac spine (ASIS) and travels diagonally to attach onto the medial surface of the proximal tibia (Ng and Vesely, 2012). This location on the tibia also demarcates the recognisable insertion site of *Gracilis* and *Semitendinosus*, that together create a unique 'goosefoot' pattern often referred to as pes anserinus, which can clinically present as an area of injury in the form of tendinitis or bursitis (Rennie and Saifuddin, 2005).

Quadriceps femoris is the dominant muscle mass of the anterior thigh and is innervated by the femoral nerve with additional contributions from lumbar spinal segments (Drake *et al.*, 2005). *Rectus femoris* is the most superficial of the four muscles and originates from the anterior inferior iliac spine (AIIS) and superior surface of the acetabular area of the ilium. *Rectus femoris* crosses both the hip and knee joints before inserting onto the base of the patella with *Vastus lateralis*, *Vastus medialis* and *Vastus intermedius* whose tendinous fibres consequently continue distally to form the patellar ligament and insert onto the tibial tuberosity (Agur and Dalley, 2005). The anatomical arrangement acts to stabilise the hip joint and assist *Iliopsoas* to flex the thigh, whilst also providing the primary function of extending the leg at the knee joint (Andersson *et al.*, 1997).

Activity of *Vastus lateralis* also causes extension of the leg at the knee joint and the muscle is similarly innervated by the femoral nerve (Palastanga *et al.*, 2008). The resultant extensional motion is due to the proximal site of attachment originating from the greater trochanter of the femur and lateral lip of the linea aspera and its insertion onto the base of the patella and tibial tuberosity as part of the *Quadriceps femoris* tendon (Agur and Dalley, 2005). This insertion site is also true of *Vastus medialis* and *Vastus intermedius,* however, the proximal origins are the intertrochanteric line plus the medial lip of the linea aspera and the anterolateral surface of the femur respectively. During the gait cycle the muscle action does not begin until the final stages of swing, which leads to a rapid peak of intensive activity when the forefoot responds to loading body weight (Perry, 1992; Liikavainio *et al.*, 2007).

The **posterior compartment of the thigh** comprises the musculature arrangement of *Biceps femoris, Semitendinosus* and *Semimembranosus* that are colloquially defined as the hamstrings. *Biceps femoris* is the most laterally positioned muscle in this compartment and arises from two separate origins; thus differentiating the long head of *Biceps femoris* from the short head. The long head of *Biceps femoris* is innervated by the tibial division of the sciatic nerve and proximally attaches to the ischial tuberosity while distally attaching to the lateral aspect of the fibular head (Drake *et al.*, 2005). The tendinous fibres from the short head of *Biceps femoris* blend with the long head fibres to distally insert onto the head of the fibula, however, as a consequence of arising from the lateral ridge of the linea aspera, the innervation is supplied via the common peroneal division of the sciatic nerve (Agur and Dalley, 2005). The primary action of *Biceps femoris* is to flex the leg at the knee joint, extend the thigh at the hip joint and permit lateral rotation at both the hip and knee joints (Woods *et al.*, 2004).

Semitendinosus lies superficial to *Semimembranosus* and both muscles are situated medial to *Biceps femoris*. Although both *Semitendinosus* and *Semimembranosus* originate from the ischial tuberosity, *Semimembranosus* distally attaches to the groove on the posterior aspect of the medial tibial condyle and *Semitendinosus* inserts onto the medial surface of the proximal tibia (Beltran *et al.*, 2012). The tibial division of the sciatic nerve also innervates these muscles, therefore the main functions closely follow *Biceps femoris* with the exception of *Semitendinosus* and *Semimembranosus* collectively acting to medially rotate the thigh and leg instead (Drake *et al.*, 2005).

Tibialis anterior, *Extensor hallucis longus*, *Extensor digitorum longus* and *Peroneus tertius* are the four muscles which form the **anterior compartment of the leg**. *Tibialis anterior* is located in the anterior compartment of the leg and acts mainly to dorsiflex at the ankle and invert the foot by raising the midfoot medially. Consequently this acts to provide dynamic support of the medial arch (Whittle, 2007). The proximal attachment site of *Tibialis anterior* is the lateral condyle of the proximal tibia, superior lateral surface of the tibia and the interosseous membrane and it inserts distally onto the medial and inferior surface of the medial cuneiform and base of the first metatarsal (Agur and Dalley, 2005). Innervation of *Tibialis anterior*, as with all muscles in the anterior compartment, is derived from the deep peroneal nerve which activates prior to limb swing and works intensively during locomotion to control dorsiflexion of the ankle and control antagonistic plantarflexion (Cappellini *et al.*, 2006).

Extensor hallucis longus originates from the medial surface of the fibula and associated anterolateral surface of the interosseous membrane. The principle function of this muscle is to extend the great toe, which is made possible through the functional design of the long tendon running antero-medially across the foot and inserting on the dorsal surface of the hallux at the base of the distal phalanx (Drake *et al.*, 2005).

The deepest, most posteriorly positioned muscle within the anterior compartment of the thigh is *Extensor digitorum longus.* This muscle originates from the lateral tibial condyle, deep interosseous membrane and medial surface of the proximal fibula and ultimately forms a tendon that continues into the foot (Agur and Dalley, 2005). The tendon of *Extensor digitorum longus* divides into dorsal digital expansions which distally attach onto the individual bases of the middle and distal phalanges of the lateral four digits. The main action of this muscle is to extend the lateral four toes while assisting dorsiflexion at the ankle joint (Reynard *et al.*, 2009). *Peroneus tertius* is closely connected and associated with *Extensor digitorum longus,* however, the tendon eventually deflects laterally on the dorsal aspect of the foot to insert on the medial base of the fifth metatarsal (Witvrouw *et al.*, 2006). This lateral position can aid eversion of the foot while also providing the main function of dorsiflexion at the ankle.

The **lateral compartment of the leg** contains *Peroneus longus* and *Peroneus brevis*. *Peroneus longus* facilitates eversion of the foot and weakly plantarflexes at the ankle (Palastanga *et al.*, 2008). The proximal attachment of *Peroneus longus* is the fibular head and superior two thirds of the lateral surface of the fibula and it inserts distally onto the base of the first metatarsal and medial cuneiform (Agur and Dalley, 2005). This inferior attachment results in the tendon following a path posterior to the lateral malleolus, curving under the fibular trochlea of the calcaneus into the cuboid groove under the base of the foot; thus secondarily supporting the lateral and transverse arches of the foot (Drake *et al.*, 2005). The superficial peroneal nerve innervates *Peroneus longus* which ultimately begins to relax during the middle of pre-swing (Perry, 1992).

Peroneus brevis lies deep to *Peroneus longus* and is also innervated by the superficial peroneal nerve. This smaller muscle arises from the inferior two thirds of the lateral fibular shaft and subsequently forms a tendon that also travels posterior to the lateral

malleolus before laterally inserting onto the dorsal surface of the fifth metatarsal base (Palastanga *et al.*, 2008). The main muscular function is eversion of the foot and also to assist with plantarflexion at the ankle joint.

The **posterior compartment of the leg** can be subdivided into the **superficial** muscular group (*Gastrocnemius, Soleus* and *Plantaris*) and the group of **deep** muscles (*Popliteus*, *Flexor hallucis longus*, *Flexor digitorum longus* and *Tibialis posterior*). *Gastrocnemius* is the most superficial muscle in the posterior compartment of the lower leg and, although regarded as one muscle, the two heads have distinct sites of origin and can be referred separately as *Lateral gastrocnemius* and *Medial gastrocnemius*. *Gastrocnemius* acts to plantarflex at the ankle, flex at the knee and elevate the heel from the ground (Whittle, 2007). *Lateral gastrocnemius* originates from the lateral aspect of the lateral femoral condyle whereas *Medial gastrocnemius* attaches proximally to the popliteal surface of the distal femur, superior to the medial condyle (Drake *et al.*, 2005). *Lateral gastrocnemius* inserts distally onto the posterior surface of the calcaneus after uniting with *Soleus* and the medial head of *gastrocnemius* to form the tendocalcaneus or Achilles tendon (Agur and Dalley, 2005). Innervation of *Lateral gastrocnemius* originates from the tibial nerve and aids in contributing to 93% of the theoretical plantarflexor torque during gait (Perry, 1992; Monaghan *et al.*, 2010).

The tibial nerve supplies all of the muscles in the posterior compartment of the leg (including the deep muscles) and activates *Soleus* and *Plantaris* to plantarflex the foot at the ankle joint (Drake *et al.*, 2005). *Soleus* originates from the soleal line on the tibia, in addition to attaching proximally on the posterior surface of the fibular head, neck and shaft.

Plantaris is unique in the fact that the muscle belly is short in relation to the thin, elongated tendon that descends distally to form the medial portion of the calcaneal tendon (Spina, 2007). *Plantaris* arises from the distal aspect of the lateral supracondylar line of the femur and the oblique popliteal ligament of the knee. This aids *Gastrocnemius* in plantarflexing the foot at the ankle joint and flexing the leg at the knee joint (Drake *et al.*, 2005).

Of the four deep muscles of the posterior compartment of the leg, *Popliteus* is the most proximal and smallest in size. The origin of this muscle is on the posterior surface of the tibia, inferior to the distal attachment site of *Semimembranosus* yet superior to the soleal line, where *Popliteus* ascends obliquely to pass in a groove on the inferior aspect of the lateral femoral condyle prior to attaching to the anterior depression (Agur and Dalley, 2005). The primary functional role of *Popliteus* is to 'unlock' the knee joint by laterally rotating the femur whilst the tibia remains static and aiding flexion at the knee joint (Drake *et al.*, 2005).

Flexor hallucis longus attaches proximally on the posterior surface of the distal fibula and adjacent interosseous membrane (Agur and Dalley, 2005). This muscle descends inferiorly and forms a long tendon, shaping the groove on the inferior surface of the talus as well as the sustentaculum tali groove on the calcaneus, which inserts distally on the plantar aspect of the hallux at the base of the distal phalanx (Kirane *et al.*, 2008). The key action of *Flexor hallucis longus* is to flex the hallux and plantarflex the foot at the ankle joint. Activation is predominant during the toe-off phase of the gait cycle, however, the tendon is continually in a position to support the medial longitudinal arch of the foot (Whittle, 2007).

The most medial of the four muscles in the deep posterior compartment of the leg is *Flexor digitorum longus* which acts to flex the lateral four digits and assist with plantarflexion at the ankle joint, particularly during events at the end of the gait cycle (Perry, 1992). These actions arise due to the proximal attachment of *Flexor digitorum longus* originating from the posterior surface of the medial tibia distal to the soleal line and the tendon that subsequently develops, inserts distally onto the individual bases of the lateral four distal phalanges (Kumar and Sharma, 2011). The tendon also supports the longitudinal arches of the foot by crossing, inferior to the tendon of *Flexor hallucis longus*, the medial surface of the foot to distribute and divide at the position of the plantar surface of the cuboid bone (Drake *et al.*, 2005).

Tibialis posterior is the final muscle to support the medial arch of the foot due to the tendon curving inferiorly along the groove under the medial malleolus of the tibia and attaching to the tuberosity of the navicular and medial cuneiform (Edwards *et al*., 2008). The proximal attachment of *Tibialis posterior* lies deep on the interosseous membrane and neighbouring posterior surfaces of the lateral tibia and medial fibula (Agur and Dalley, 2005). The main function of this muscle is to invert the foot and plantarflex the foot at the ankle joint (Murley *et al*., 2009).

2.4 Gait Analysis

Motion resulting from muscular contractions which act on anatomical structures can be analysed and assessed biomechanically in terms of forces, moments and pressures (Abboud, 2002). Innovative technological systems (including Vicon®, Codamotion®, Templo®, and Novel®) have been devised to calculate the kinematic movements and kinetic forces that are utilised effectively in many clinical settings to manage, as well as assess, conditions including cerebral palsy, clubfoot and diabetes (Abboud *et al*., 2000; Desloovere *et al.*, 2006; Long *et al.*, 2007; Hidler *et al.*, 2008; Kapoor *et al.*, 2009; Karol and Jeans, 2011; Ramanathan and Abboud, 2010). There is a profuse number of conditions and diseases that can impair and negatively influence the gait cycle of an individual and, although the primary pathologies may differ greatly, the subsequent biomechanical abnormalities can be categorised into the following four major functional groups (Perry, 2002);

1. Musculoskeletal pain,

2. Muscle weakness,

3. Impaired control,

4. Deformity.

Biomechanical abnormalities can only be distinguished through the implementation of internationally recognised standards and protocols to calculate and define the normal limits and variables of human movement. Kinematics is a measure of movement described in terms of "displacements, velocities and accelerations" (Whittle, 2007). An example of a kinematic variable is the joint angular velocity, as there is no reference to the forces associated with the rate of movement of a joint (Thomas and Supan, 1990;

Granata *et al.*, 2000). The joint angular velocity can be measured in three planes (flexion/extension, abduction/adduction and internal/external rotation) and can assist by highlighting timing changes of a joint. Muscular activation timings of a joint can alter, potentially in response to compensating for agonistic and antagonistic muscular actions, which could be confirmed through the use of electromyography. Temporal-distance variables can be obtained from kinematic data as in the case of stride length, which is the horizontal distance travelled by the same point on the foot from initial contact with the ground to the successive ipsilateral contact with the ground.

Kinetics, on the other hand, is defined as the study of forces, moments, powers, energy and masses without reference to geometric position or orientation (Bartlett, 1999). A force vector constitutes both directionality and magnitude; therefore the moment of force can be calculated by the multiplication of the perpendicular distance along the lever starting from the fulcrum with the magnitude of the force (Whittle, 2007). Biomechanical moments can also be referred to as the 'turning force' or 'torque' and are measured in Newtons/metre (N/m). A moment provides an indication of the resultant muscle activity acting on a joint at a specific point in time (Kakihana *et al*., 2007; Almosnio *et al*., 2009). Power measures the rate of work and is calculated by the multiplication of the joint angular velocity (otherwise defined as the angle of rotational displacement from the 'fulcrum' or joint per second) with the biomechanical moment (Knudson, 2003).

2.4.1 Gait Cycle - Walking

Independent walking is typically instigated around the age of 10 to 17 months (Bertsch *et al.*, 2004) and the pattern of gait continues to change throughout childhood. Adult

gait differs slightly from the immature and less efficient pattern observed in children. The equilibrium of muscle coordination and overall balance during the dynamic gait cycle in children is destabilised, when compared with adults, partially as a consequence of changing limb length (Bosch and Rosenbaum, 2010). The duration of a gait cycle is termed the stride time and is commonly measured from the initial strike of the heel with the ground to the consecutive heel strike of the ipsilateral foot. Normal adult values for the stride length and cadence are usually achieved by the age of fifteen years once growth decelerates following the pubertal growth spurt. Figure 2.9 illustrates the specific events that occur in the normal gait cycle and also demonstrates how the stride time is separated into two major divisions; the stance phase accounting for approximately 60% of the cycle when the limb is weight bearing and the swing phase which accounts for the subsequent 40% when the limb is non-weight bearing.

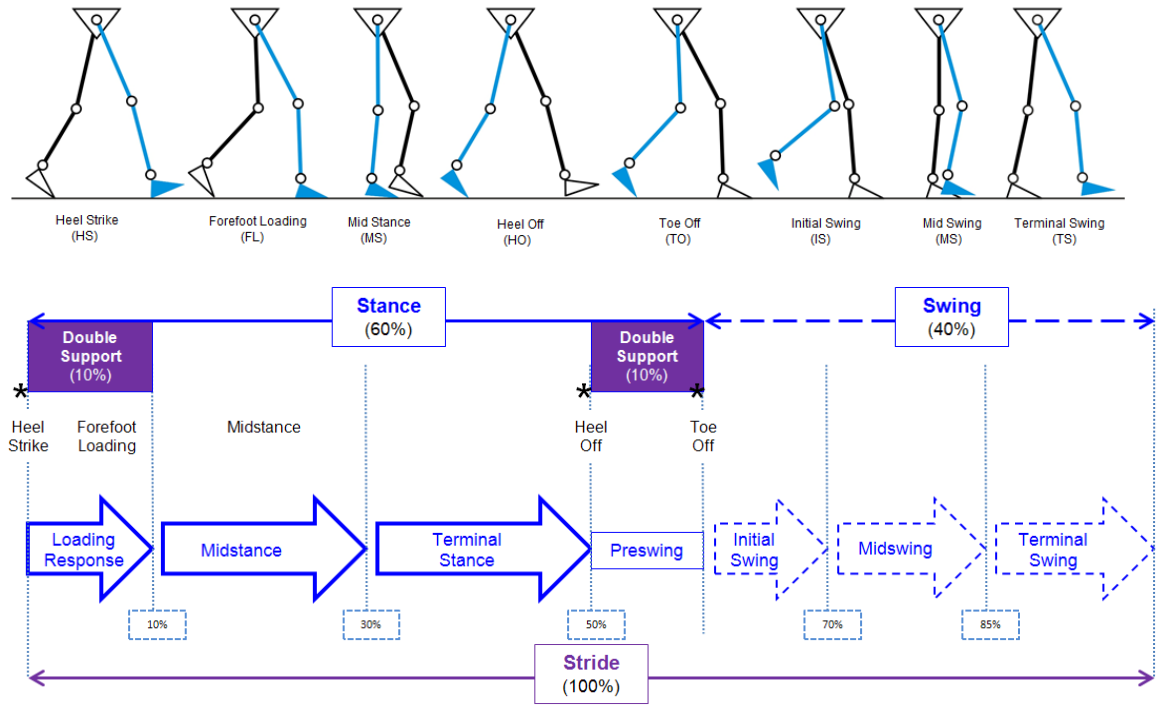

Figure 2.9 – Events of the gait cycle during walking (adapted from IMAR, 2013).

Initial contact of the foot with the ground is generally via the heel, which strikes the ground while the hip is approximately 25° flexed as the knee begins to flex out of a fully extended position and the ankle is in a plantigrade position. The key muscles that are acting during heel strike when the foot moves to a foot flat position are *Gluteus maximus*, *Semitendinosus*, *Semimembranosus*, *Biceps femoris*, *Tibialis anterior*, *Extensor digitorium longus* and *Extensor hallucis longus*. The subsequent force vector at this point is anterior to the hip yet posterior to the knee and ankle, which acts to convey stability to the lower limb (Thomas and Supan, 1990).

The **loading response (LR)** is facilitated by the pivotal action of the heel which acts as the first rocker to enable rotation of the forefoot into plantarflexion. The flexion moment generated at the hip decreases towards a neutral position and the knee begins to change from approximately 20° of flexion towards an extended position. Activation of the four quadriceps muscles *Rectus femoris*, *Vastus lateralis*, *Vastus intermedius* and *Vastus medialis* achieves the necessary shock absorption required to stabilise the knee by reducing flexion to approximately 15-18° (Ayyappa, 1997). The ankle undergoes approximately 10° of plantarflexion as a result of the ground reaction force and gravitational pull, consequently resulting in a valgus moment in the coronal plane. The relaxation of the antagonistic *Tibialis anterior* muscle is carefully coordinated to gradually decelerate and resist the ground reaction force (GRF) which acts to evert the forefoot; thus bringing the whole foot into controlled contact with the ground.

Midstance (MS) occurs at approximately 10% of the gait cycle and consists of a second pivotal rocker at the ankle generated by the anterior advancement of the tibia rolling over the supporting flat foot (Perry, 1992). The lower limb is elongated and extended at the knee through the activation of the previously mentioned quadriceps and the hip joint is further stabilised at the hip by the abductor muscles at a position of

180°. Jointly, *Gastrocnemius* and *Soleus* alleviate the instability of the limb in the sagittal plane when the force vector of the GRF progresses to become located anterior to the ankle and posterior to the knee and hip joints.

The **terminal stance (TS)** begins when the third forefoot rocker facilitates the 10° dorsiflexion of the ankle when the heel lifts off the ground while the knee extends (Vaughan *et al.*, 1999). The terminal stance is controlled chiefly by the action of *Gastrocnemius*, *Soleus*, *Flexor hallucis longus*, *Flexor digitorum longus* and *Tibialis posterior* with a contribution from *Peroneus longus*, *Peroneus brevis* and *Plantaris*. The plantarflexor muscles control the anteriorly displaced 'fall' of the upper body by stabilising the tibia at the ankle joint. At this point, the GRF is large and has progressed ahead of the foot and knee; consequently generating the second peak in normal 'm-shaped' ground reaction force graphs (Wearing *et al.*, 2000). The peak muscular response generated by an individual muscle is directly proportional to the antagonistic magnitude of force acting against this muscle to stabilise the limb.

The final division of the stance phase is **pre-swing (PS)** when the limb prepares to generate the propulsive force to clear the foot off the ground. The ground reaction force vector is still positioned anterior to the ankle joint, however, it has moved behind both the knee and hip joints. The contralateral foot at this stage helps to provide double support for the upper body, which in turn causes the extension moment at the hip joint to decelerate swiftly back to a neutral position. The knee joint undergoes flexion to approximately 40° via the contraction of *Adductor longus*. Prior to toe off, the ankle joint changes rapidly from dorsiflexion to 20° plantarflexion and this action completes the third rocker, which was initiated in the terminal stance (Perry, 2002). The prominently active muscle group during the stance phase of the gait cycle is the plantarflexors; therefore it is not surprising that during the transformation from stance

to swing phase the most prominent dorsiflexors prepare for accelerated activation during the swing phase (Hreljac, 2004).

Initial swing (IS) phase denotes the cessation of the double support and start of the swing phase. The hip joint undergoes 20° flexion which provides momentum to compliment the resultant propulsion generated by 60° flexion of the knee; ultimately ensuring that an energy effective stride length is obtained (Vaughan *et al.*, 1999). Dorsiflexion of the foot is implemented by the activation of *Tibialis anterior*, *Extensor digitorum longus* and *Extensor hallucis longus* to facilitate foot clearance by shortening the lower limb.

The three pretibial muscles (*Tibialis anterior*, *Extensor digitorum longus* and *Extensor hallucis longus*) are activated continuously throughout the swing phase; however by the **mid-swing phase (MSP)** there is reduced hip flexor activity as the hip angle remains constant and the knee undergoes passive extension (Perry, 2002).

Terminal Swing (TS) is the final stage of the gait cycle where the limb decelerates in preparation for the ipsilateral heel strike that completes the cycle. During this final part of swing phase it is the activation of *Biceps femoris*, *Semitendinosus* and *Semimembranosus* which contract to reduce the flexion of the hip and extension of the knee. The *Rectus femoris*, *Vastus lateralis*, *Vastus intermedius* and *Vastus medialis* muscles also activate to complete the extended position of the knee in advance of initial contact, which completes the cycle (Vaughan *et al.*, 1999). Table 2.1 illustrates the critical events during walking.

Table 2.1 – Summary of the critical events encountered by the lower limb during the walking gait cycle.

Interval of Gait	Diagram of Lower Limb Position	Critical Events	
		Actions	Muscles
Initial Contact		- Hip flexed - Knee extended - Ankle dorsiflexed	- Quadriceps (e.g Vastus lateralis) - Hamstrings - Pretibial muscles (e.g. Tibialis anterior)
Loading Response		- Hip flexed - Knee flexed - Foot flat	- Gluteus maximus - Quadriceps
Mid Stance		- Ankle dorsiflexed	- Quadriceps - Soleus - Gastrocnemius
Terminal Stance		- Hip extended - Knee extended - Ankle dorsiflexed	- Soleus - Gastrocnemius
Pre-Swing		- Hip is neutral - Knee flexed - Ankle plantarflexed	- Slight action from calf muscles - Adductor longus - Rectus femoris
Initial Swing		- Hip flexed - Knee flexed - Ankle plantarflexed (reduced)	- Iliacus - Pretibial muscles
Mid Swing		- Hip flexed (increased) - Knee flexed (reduced) - Ankle is neutral	- Hip flexors - Ankle dorsiflexors
Terminal Swing		- Hip flexed - Knee extended - Ankle is neutral	- Hamstrings - Quadriceps - Pretibial muscles

Adapted from source: Perry (1992)

2.4.2 Gait Cycle - Running

Running can be distinguished from walking by the presence of two float phases, when both limbs are non-weight bearing, with omission of the double support phases (Dugan and Bhat, 2005). The running cycle differs in that individuals do not necessarily adopt the same landing technique; therefore the term 'foot strike' (FS) is used to denote when the foot initially comes into contact with the ground. The velocity of running does not have a defined minimum or maximum, as long as the stance phase accounts for less than 50% of the gait cycle (Rodgers, 1988). The consequential impact and ground reaction forces encountered during running are extremely brief and the magnitude can range from as little as 2.5 times the body weight to approximately 5 times the body weight (Lilley *et al.*, 2011; Clinghan *et al*., 2008; Neeley, 1998). Most shod runners strike the ground with the heel first (Hrelijac, 2004); however the natural design of the unshod foot favours initial contact on the forefoot which dramatically reduces the excessive impact with the ground (Diebal *et al.,* 2011; Rolian *et al.*, 2009; Robbins and Hanna, 1987). The ground reaction force that is generated during forefoot running follows a single 'n' shaped curve (Damavandi *et al*., 2012) that is easily distinguished from the double peaked 'm' shaped graph recorded during heel strike running (Lieberman *et al*., 2010). The additional second peak of force generated by heel strike running is defined as the 'active peak' which occurs during the propulsive phase at approximately 60-75% of the stance phase (Hrelijac, 2004). The specific features and nomenclature of the running gait cycle are summarised in Figure 2.10 and due to the variable methods in which running can be achieved, the defining stages and events are slightly more accommodating by not being limited to standardised percentages.

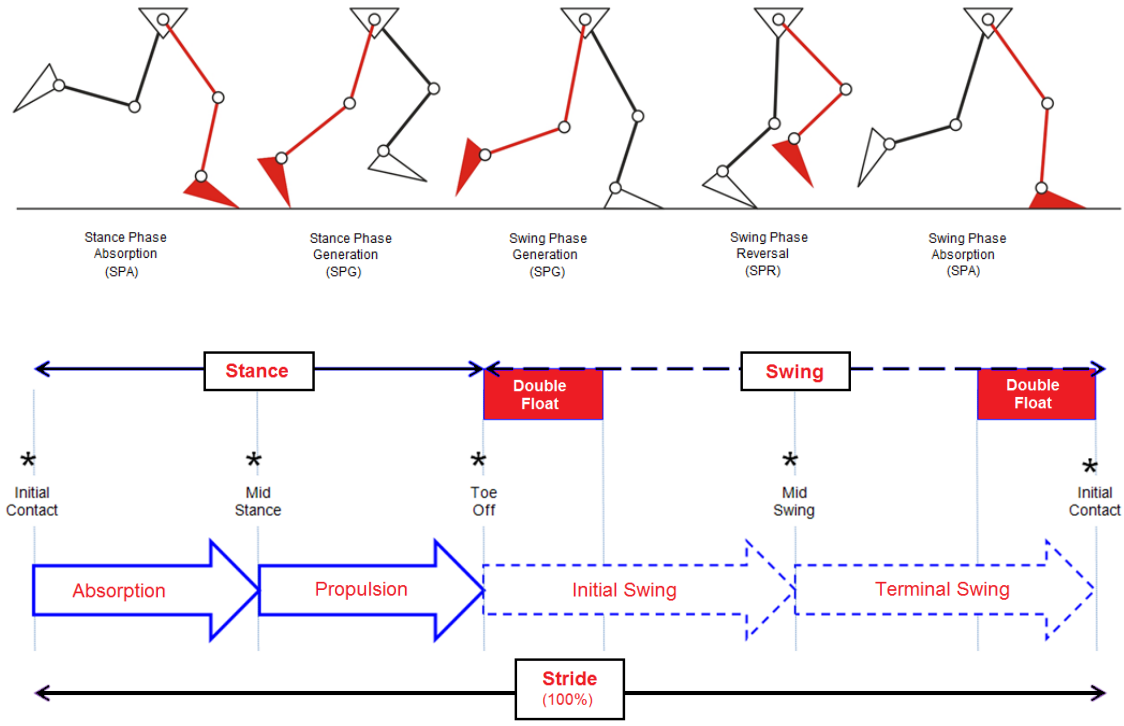

Figure 2.10 – Events of the gait cycle during running (adapted from IMAR, 2013).

The pattern of muscular activation during running is also influenced by running technique, with *Gastrocnemius* being the dominant muscle having to push the foot from the ground in contrast to forefoot running where the hamstring muscles facilitate extension of the thigh and flexion of the lower leg by pulling the foot from the ground. Interestingly, the presence of wearing shoes influences the behaviour of the forefoot dramatically by inhibiting sensory feedback, altering the distribution of pressure across the heads of the metatarsals and increasing the toe contact time (Soames, 1985); thus negating the intrinsic ability of the foot to absorb the peak impact forces naturally (Robbins and Hanna, 1987; Abboud, 2002).

Motion analysis involves synchronising multiple systems to improve the biomechanical understanding of an individual's gait cycle which may help to identify whether there

are underlying pathologies; subsequently facilitating rehabilitation of normal function. During the normal walking cycle, the majority of motion occurs in the sagittal plane; however, during running cycles there is an increased range of motion at the hip, knee and ankle in all three planes: sagittal, coronal and transverse planes (Õunpuu, 1994). Figures 2.11 and 2.12 demonstrate graphical representations of the normal kinematic pattern and overall range of motion expected to be observed during walking and running respectively. The kinetic patterns encountered during normal walking are typically less variable within an individual in comparison to the potential variability kinematic data can present within an individual (Õunpuu, 1994). The sagittal plane is where the hip, knee and ankle show the greatest arcs of motion with respect to kinematic data and Figure 2.13 represents an example of the associated normal kinetic data expected for walking while Figure 2.14 depicts running.

The kinematic graphs utilised by clinicians and researchers rely on an appropriate normalised dataset of healthy individuals from the same population being used as a template to define the minimum and maximum limits of healthy motion (as signified by the grey area in Figure 2.11(a) or dotted lines in Figures 2.11(b), 2.12, 2.13 and 2.14). Through the creation of an ideal database template, the knowledge that the kinematic results are comparable with respect to the averaged values (Bovi *et al*., 2011), which are measured with the same protocols, ensures that any divergence from the norm is not due to a difference in the population or the laboratory. Ultimately data for any research or clinical assessment should only be compared with data that has been ideally collected in the same location using the clearly defined protocols with regards to camera configuration/calibration, location of force plates, anthropometric measurements, marker/wand placement and the calculation of tibial torsion/shank rotation.

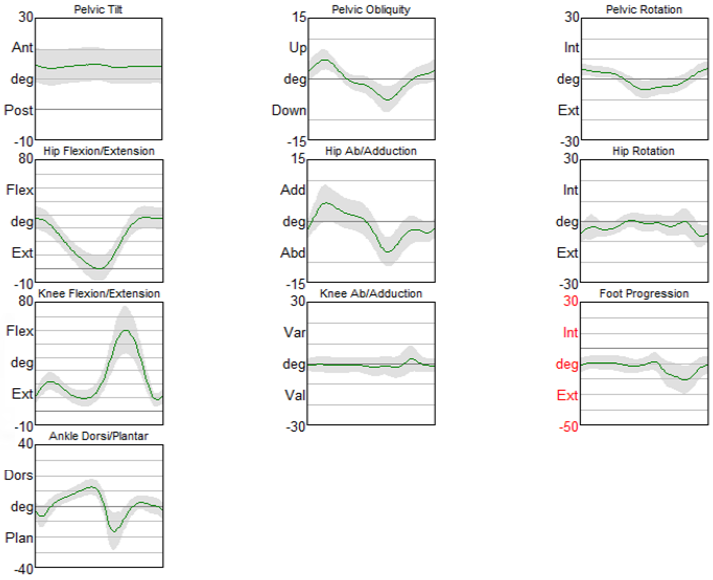

(a)

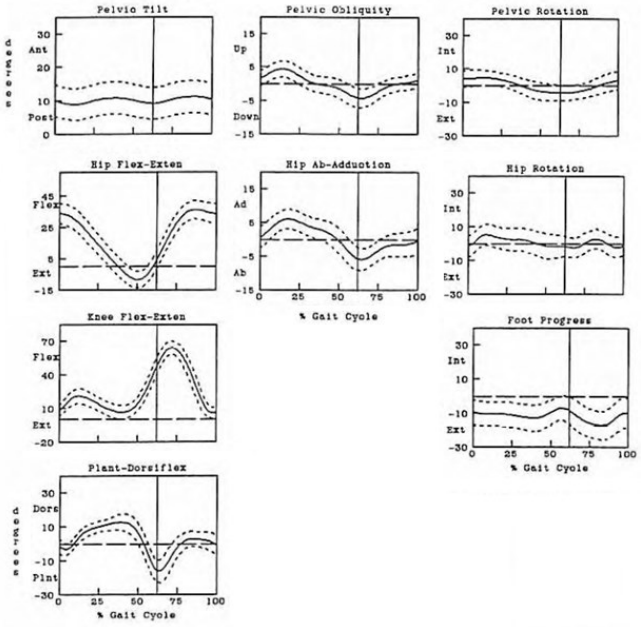

(b)

Figure 2.11 – Visualisation of the 'normalised' kinematic range of motion patterns that the pelvis, hip, knee and ankle should follow in healthy individuals while walking. (a) Averaged walking trials (denoted by green line with the gray shading marking the normal ranges) was created from 43 trials of healthy adults by the consultant clinical scientist in the Institute of Motion Analysis and Research. (b) Standard 'normalised' graphs found in the literature are in agreement with the template created using Polygon® software (image adapted from Õunpuu, 1994).

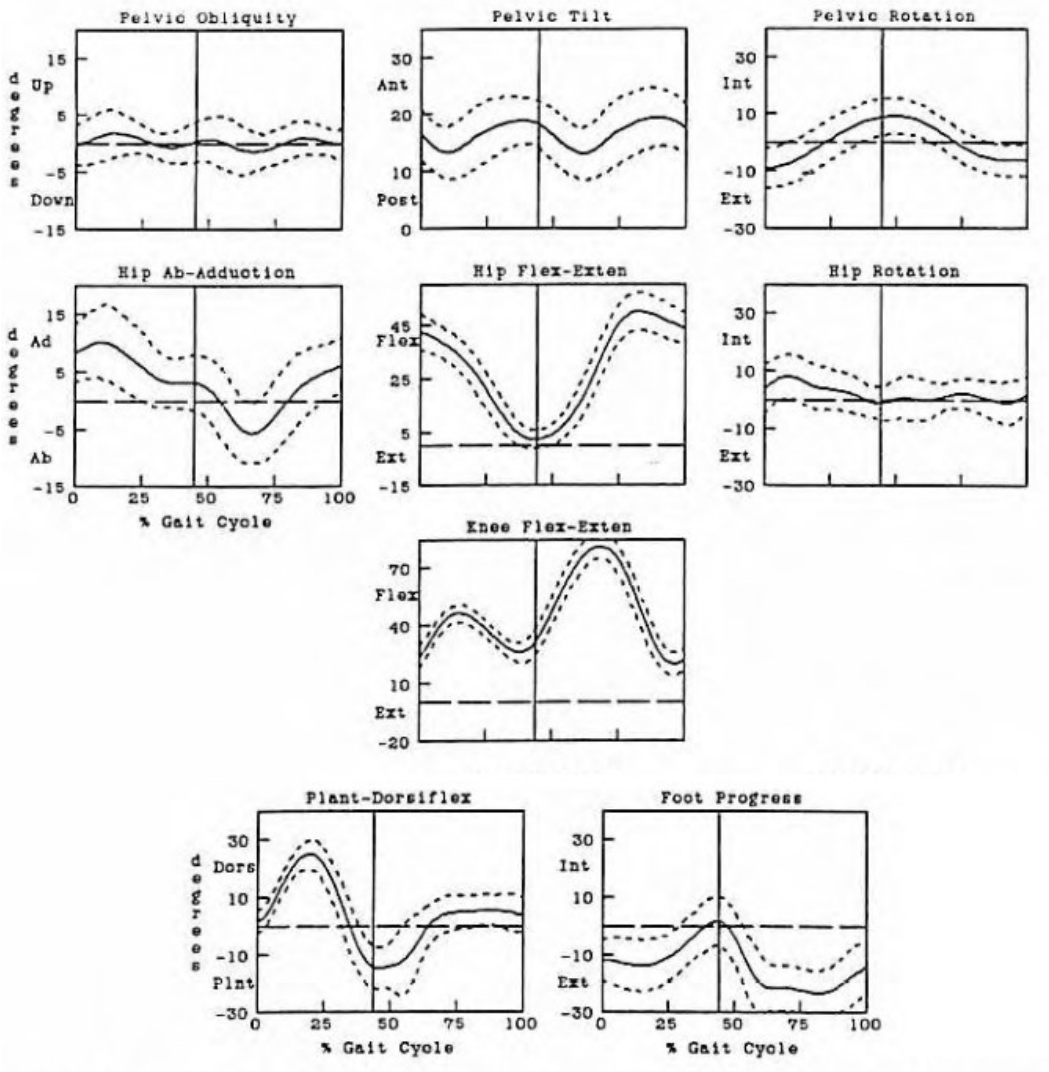

Figure 2.12 – A set of standard 'normalised' graphs enabling a visualisation of the normal kinematic patterns that the pelvis, hip, knee and ankle should follow in healthy individuals while heelstrike running (Adapted from Õunpuu, 1994). The single black lines represent the average while the dotted lines denote the minimum and maximum normal ranges.

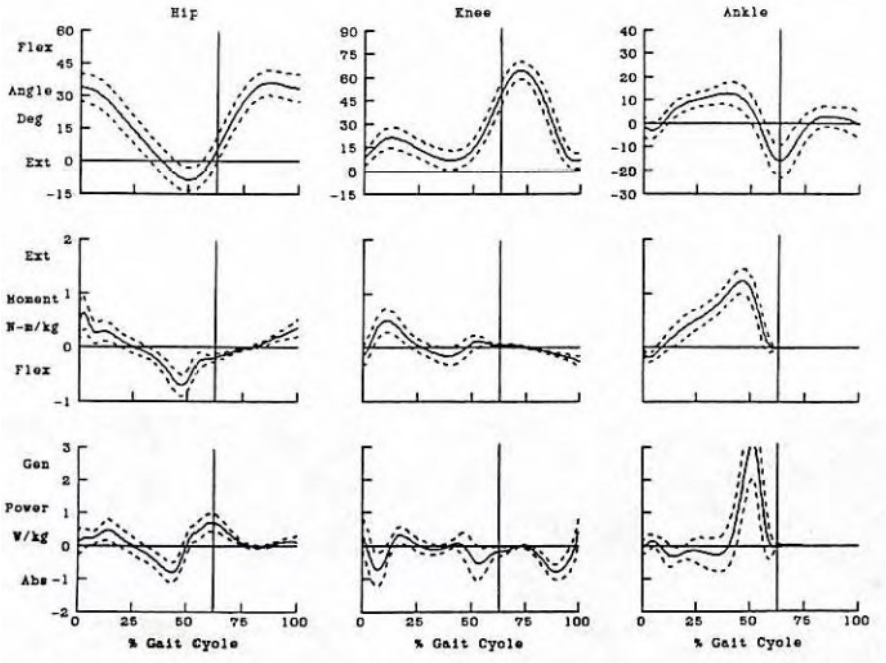

Figure 2.13 – Sagittal plane kinetics (moment and power) of walking are shown for the hip, knee and ankle. The first graph in each respective column is the relevant sagittal kinematic data to provide perspective (Adapted from Õunpuu, 1994).

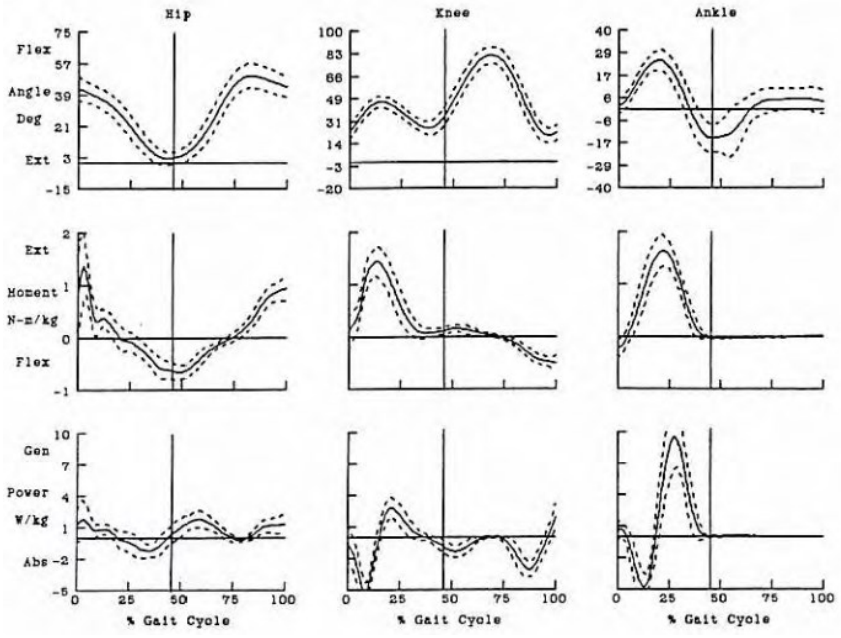

Figure 2.14 – Sagittal plane kinetics (moment and power) of running are shown for the hip, knee and ankle. The first graph in each respective column is the relevant sagittal kinematic data to provide perspective (Adapted from Õunpuu, 1994).

Velocity can influence the resultant range of motion of a joint and the slightest difference in the placement of anatomical markers can cause considerable experimental errors with regard to the expected pattern of gait (protocol is detailed in Section 3.2.2.3); thus the importance of interpreting and understanding the movements at each event in the cycle is fundamental to diagnosing any abnormality an individual may present.

2.4.3 Sport

The importance of sports biomechanics focuses on the drive athletes exhibit to push their functional boundaries to the limit (Perry, 1992) and the requirement to improve performance, while reducing injury, is key to sporting success (Bartlett, 1999). Football is a sport that requires an athlete to be exposed to excessive axial loading of the vertebral column as well as transfer, disperse and absorb disproportionate mechanical forces in the lower limbs (Kerssemakers *et al*., 2009). The addition of manipulating the ball while running adds to the necessity of players training and repeating movements to develop the skills of rapid acceleration and abrupt changes of direction while running (Christou *et al*., 2006).

A study by Rand and Ohtsuki (2000) measured the muscular responses generated when running direction is modified in response to open or cross manoeuvres regularly encountered during game play. Figure 2.15 shows a graphical representation of the electromyographic results generated from one individual straight running and the same individual performing an immediate stopping manoeuvre. The straight running trials act as a control to compare the timing differences in the activation of key lower limb muscles when the body attempts to stop forward acceleration suddenly by turning

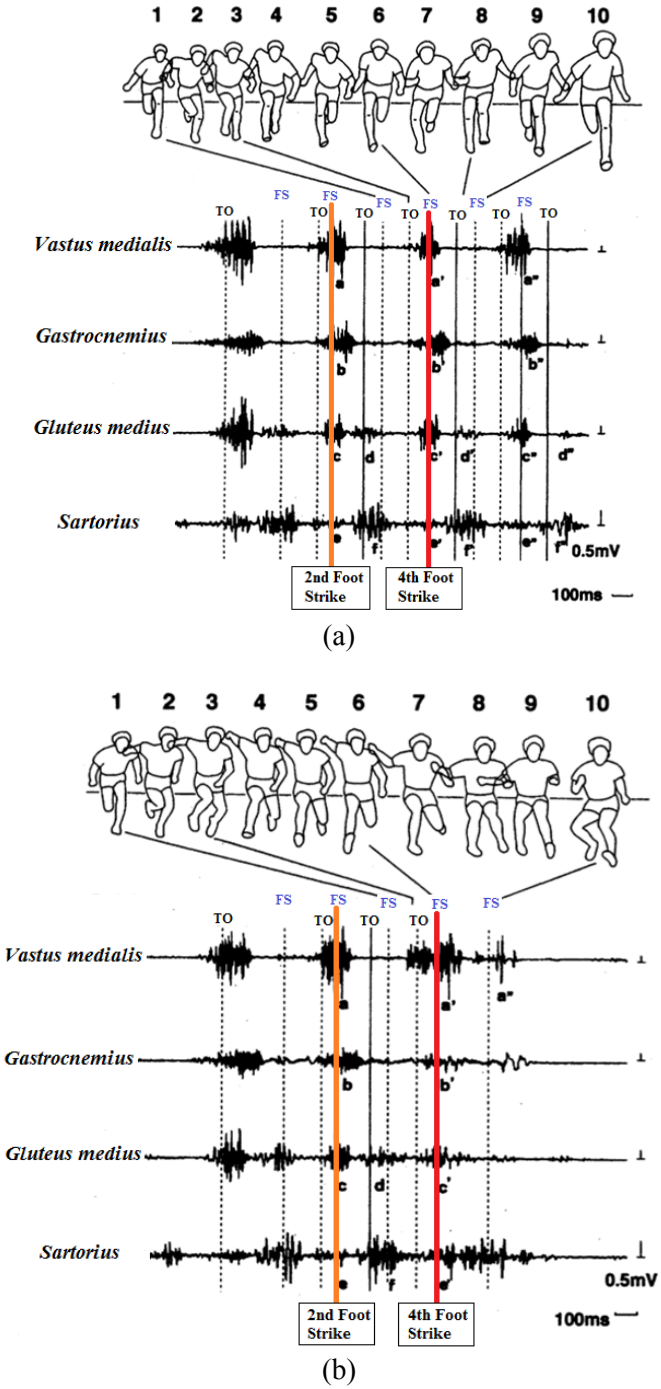

<u>Figure 2.15</u> – Electromyography graphs for four muscles (*Vastus medialis*, *Lateral gastrocnemius*, *Gluteus medius* and *Sartorius*) with toe off (TO) and foot strike (FS) signified by dotted lines. The second and forth foot strikes are accentuated by a continuous orange and red line respectively.

(a) Normal running data acting as a control.

(b) Changes that are experienced when opposing the excessive forces encountered during a self initiated cross maneuver to change running direction.

(adapted from Rand and Ohtsuki, 2000)

towards the direction of the supporting foot. The activation pattern is evidently altered in response to the dynamic differences of opposing the ground reaction forces, with particular attention drawn to the prolonged activity of *Vastus medialis* and the inhibited activity of *Gastrocnemius* after the fourth foot strike when running is forcefully stopped.

2.5 Injuries

The majority of research in the scientific literature which relates to growth plate injuries primarily focuses on acute injuries generally resulting from traumatic fractures; however there is little mention of altered biomechanical pressures that may have caused disturbance to specific sites of the growth plate.

2.5.1 Salter-Harris Fractures

Fractures are the most common cause of partial growth arrest (Sailhan *et al*., 2004) arising through traumatic disruption to the blood supply of the growth plate. The effect of intensive training on young athletes is thought to mimic this microvascular inhibition if the repetitive sporting actions induce trauma and exceeds the rate of bone repair (Laor *et al.*, 2006). Table 2.2 describes the classification of five fracture types that occur most frequently in immature long bones, which can be compared with the less traumatic and sometimes asymptomatic physeal extensions found in intensively trained athletes. These anomalies are similar to overuse injuries and are thought to differ from defined Salter-Harris type I fractures by the fact that broad physeal widenings extending into the metaphysis tend to be more focal in elite athletes. These physeal

extensions can be present without any indication of displacement or fracture through the cartilage which is unlike Satler-Harris fractures that are inflicted through acute trauma (Laor *et al.*, 2006).

Table 2.2 - Classification of Salter Harris fracture types (Adapted from Salter and Harris, 1963).

Salter-Harris Fracture Type	Diagram	Description
Type I		Physeal widening and complete separation of the epiphysis from the metaphysis without any bone fracture. Germinal cells of growth plate remain with the epiphysis, and the calcified layer remains with the metaphysis.
Type II		Line of separation extends along the growth plate, then out through a portion of the metaphysis, producing a triangular shaped metaphyseal fragment.
Type III		Intra-articular, extending from the joint surface to the weak zone of the growth plate and then extends along the growth plate to its periphery.
Type IV		Complete split as fracture extends from the joint surface through the epiphysis, across the full thickness of the growth plate and through a portion of the metaphysis.
Type V		Compression of the growth plate.

Overuse injuries can be defined as chronic injuries incurred through "high levels of physiological stress without sufficient recovery time" (Nanni *et al.*, 2005; Koh *et al.*, 2007). An overuse injury may progress into a stress fracture if the degree of repetition exceeds the ability of bone to recover by completing the natural reparative process to fully repair any damage incurred (Adirim and Barough, 2006; Brenner *et al.*, 2007). Overuse injuries tend to occur at areas of rapid muscular and skeletal growth (Gerrard, 1993) with the knee typically presenting as the joint that is most commonly affected (Lilley *et al.*, 2011).

In 2004, Hrelijac concluded that there was a lack of consensus in relation to the effects that individual anthropometric variables had on the incidence of developing an overuse injury due to the varied and multi-factorial nature of the aetiology. Figure 2.16 illustrates a generalised interaction that combines the level of stress and frequency with the point at which injury threshold occurs. This is thought to increase significantly with the presence of high longitudinal arches, leg length discrepancies and greater range of ankle motion in the sagittal plane which can be further influenced by the hardness of the playing surface and whether studded sports boots are worn (Bentley *et al.*, 2011).

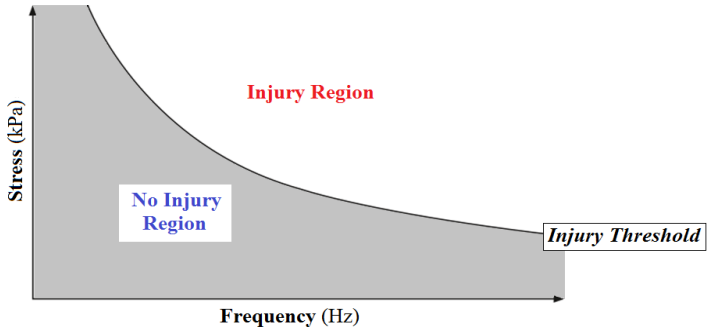

Figure 2.16 – Graphical depiction highlighting the threshold of inducing an injury with relation to the combined stress and frequency of excessive exercise (Adapted from Clinghan *et al.*, 2008).

2.5.2 Overuse injuries from sport

One of the initial studies that highlighted the potentially negative effects that football training may have on the developing skeleton was conducted by Hodson (1999). The Football Association (FA) carried out medical examinations on 34 young, elite players hoping to be accepted into the National School of Excellence in 1992 and the injuries discovered in this small cohort are summarised in Table 2.3.

Table 2.3 – 1992 FA medical examination findings from a sample of 34 boys (ages not stated).

Observation of Injury	Number of Incidences	Percentage of sample
Overuse	12	35%
Spondylolysthesis of lumbar vertebrae	5	15%
Tibial growth plate problems (Knee area)	2	6%
Stress fracture of fibula	1	3%
Osgood-Schlatter's disease (Knee)	2	6%
Sever's disease (Ankle)	1	3%
Bone Spur (Ankle)	1	3%
Total	24	

Source: Hodson (1999)

An overuse injury was defined as one which targets specific anatomical sites due to excessive repetitive activity over a period of time and the four predisposing factors involved load, technique, posture and equipment (Hodson, 1999). One factor the report accentuated related to the resultant skeletal damage that can be caused by an unequal transmission of weight across the vertebral column and pelvis as a result of leg length asymmetry. This inequality of force distribution is relatively common during the

pronounced adolescent growth spurt, as skeletal development is typically not symmetrical, which further increases the risk of young athletes developing chronic back pain as a consequence of spondylolysis of the vertebral column (Soler and Calderón, 2000). Unfortunately, the two cases of proximal tibial growth plate problems noted by Hodson (1999) were not discussed, further emphasising the need to investigate this neglected gap in the scientific literature.

Malina *et al.* (2004) tested the functional fitness capacity of 69 Portuguese football players aged between 13 and 15 years of age. Anthropometric measurements were taken to assess height and body mass which was standardised against the new United States growth charts to characterise the growth status of each individual. Although the new Centre for Disease Control and Prevention growth curves (Kuczmarski *et al.,* 2002) are approved by the World Health Organisation, the data is still sourced from as early as 1963 until 1994, and is therefore outdated by at least 16 years. In addition to this, an American reference sample may not be ideal for the Portuguese population, however, population specific growth data was not readily available. Sexual maturity of the young boys was estimated using Tanner stages to classify pubic hair development and overall it was found that biological maturity status was a key contributor to the discrepancies in functional capacity performance (Malina *et al.*, 2000). Interestingly, Malina *et al.* (2000) established that maturity-associated variation appears to reflect a trend in the position played by individuals as their tallest, heaviest players were forwards and the smallest, lightest footballers were either defenders or midfielders. This trend correlates with the associated variation in secondary sexual maturation, as the majority of players who were selected for forward positions demonstrated greater biological maturity status and improved functional performance.

Their research has been developed and extended more recently by Figueirdo *et al.* (2010) to include a greater number of players from across five different Portuguese youth teams and incorporate skill variance of individual players. To reassess the influence that skeletal and sexual maturity has on the functional capacity and football specific skills, 142 boys aged between 11-14 years were measured and tested. Incidentally, Figueirdo *et al.* (2010) concluded that sexual maturity did not contribute directly to variation in performance as the gap in size and power between late and early skeletal maturers will eventually close over time; however it is important to note that the potential influence of activity levels were not actually investigated.

The importance of longitudinal research is invaluable, particularly when assessing dynamic parameters such as growth. Johnson *et al.* (2009) produced a rare study which followed the same group of young players for over six years. This Manchester based study estimated skeletal maturity using the Greulich and Pyle hand and wrist method (Greulich and Pyle, 1959), the benefit being that a radiograph of the wrist does not rely on the assessment of secondary sexual characteristics. A drawback regarding the Greulich and Pyle method is that the American reference data was found to overestimate skeletal age and maturity of the players included in their study. Radiographs are invasive with respect to the exposure of radiation and consequently have a limit as to the number of doses an individual can receive in one year which may have resulted in only 12 of the 292 boys being x-rayed for six consecutive years. Due to the fact that Johnson *et al.* (2009) investigated variables that contribute to injuries, this potentially limited the repeatability of imaging if a suspected sprain or fracture was incurred by the players during the year, as parents may have disagreed to additional exposure. Reaffirming prior research, the knee was found to be the most commonly injured site in under 14 year olds as well as being the most vulnerable site for overuse

injuries, yet due to the fact that the results are skewed by injured individuals, the skeletal and chronological ages should not be utilised to assign maturity status outwith this small population group.

Carson and Gasser (1998) found that adolescent baseball players around the age of 14 years were more prone to encountering overuse injuries at the proximal humeral epiphyses than younger players who also played continually for one year. This is likely due to the combination of an increased practice of enhanced skills and techniques at the onset of rapid growth. Another common site of injury in active baseball players is at the knee through prolonged compressive loading forces on the growing lower limbs. Liebling *et al.* (1995) reported the radiographic findings of a symptomatic 13 year old baseball catcher. Persistent chondrocytes and cartilaginous matrix surviving within the hypertrophic zone of the epiphyseal plate caused a reduced mineralisation of bone and consequently resulted in "nests of cartilage" (Liebling *et al.*, 1995) being incorporated into the metaphysis; thus leading to physeal irregularity and widening of the femoral and tibial growth plates as depicted in Figure 2.17.

2.6 Magnetic Resonance Imaging

Magnetic resonance imaging (MRI) has become the imaging modality of choice with regard to investigating growth plate morphology. MRI is a non-invasive method that can image cartilage, fibrous bridges, infection and oedema (Wardak *et al*., 2009) which are unable to be observed on computed tomography (CT) scans due to the lack of ossification (Sailhan *et al*., 2004) or can be missed on radiographs (Shih *et al.*, 1995). A small, retrospective study investigating chronic overuse knee pain was performed at an orthopaedic children's hospital between 1996 and 2002 by Laor *et al.* (2006).

Figure 2.17 – Radiograph of a 13 year old baseball player displaying 'catchers knee' which is an overuse injury that disrupts the epiphyses and results in painful widening of the growth plates.
(adapted from Liebling *et al.*, 1995)

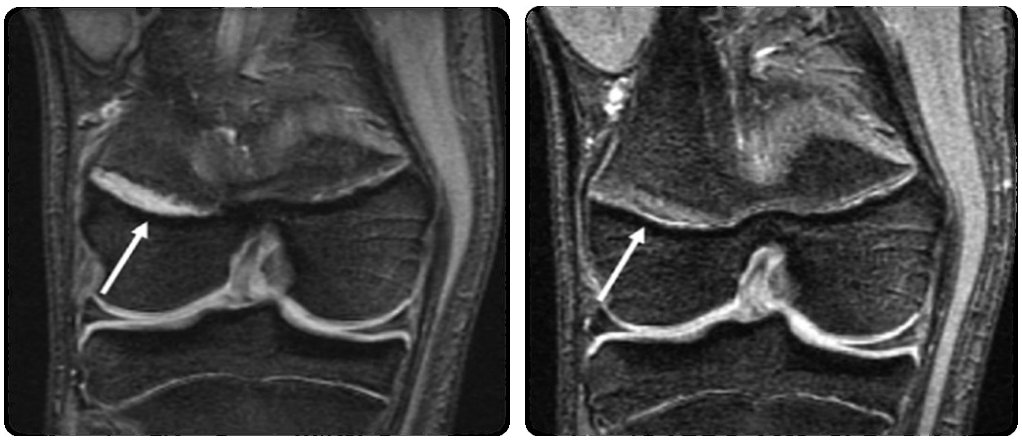

(a) (b)

Figure 2.18 – 14.5 year old football player demonstrating the maximum physeal widening, measuring 27mm, out of six patients.
(a) Physeal widening depicted by the arrow on the lateral distal femur.
(b) MRI taken after 2 months of strict rest with the arrow revealing resolution of the widening at the growth plate.
(adapted from Laor *et al.*, 2006)

Six highly competitive athletes from diverse sporting backgrounds, ranging from gymnastics to tennis, were evaluated with regard to persistent knee pain as a direct consequence of repetitive, intensive sporting activities. MRI was used to measure the extent of the physeal widening and this was aided by comparing the intensity of the emanating sclerotic signal in relation to the normal, adjacent growth plate. Of the six patients, the maximum transverse diameter of physeal widening was found in a young footballer. Figure 2.18 depicts a bright physeal extension into the dark proximal metaphysis of the right femur in addition to displaying the distal femoral growth plate from the same knee which when compared to the left has pronounced physeal widening on the lateral side. Following two months of strict rest, the enhanced quality of the growth plate elucidates the fact that measures can be taken to prevent long-term detrimental health risks.

At present there is no histological evidence regarding the nature of physeal widening; therefore the cellular site of interference and micro-trauma cannot be indicative of one specific growth plate zone and the severity of irreversible damage cannot be calculated. One case outlined by Laor *et al.* (2006) involved a young female athlete who did not adhere to medical advice and continued to play tennis intensively for two further years. Subsequent radiographs (see Figure 2.19) revealed a varus misalignment, stress fractures and development of osteochondritis dissecans in the lower limbs. These radiographic findings are supported by Caine *et al.* (2006) and Nanni *et al.* (2005) where the majority of individuals suffering from growth plate anomalies were able to return to their sport after rest and immobilisation in some circumstances.

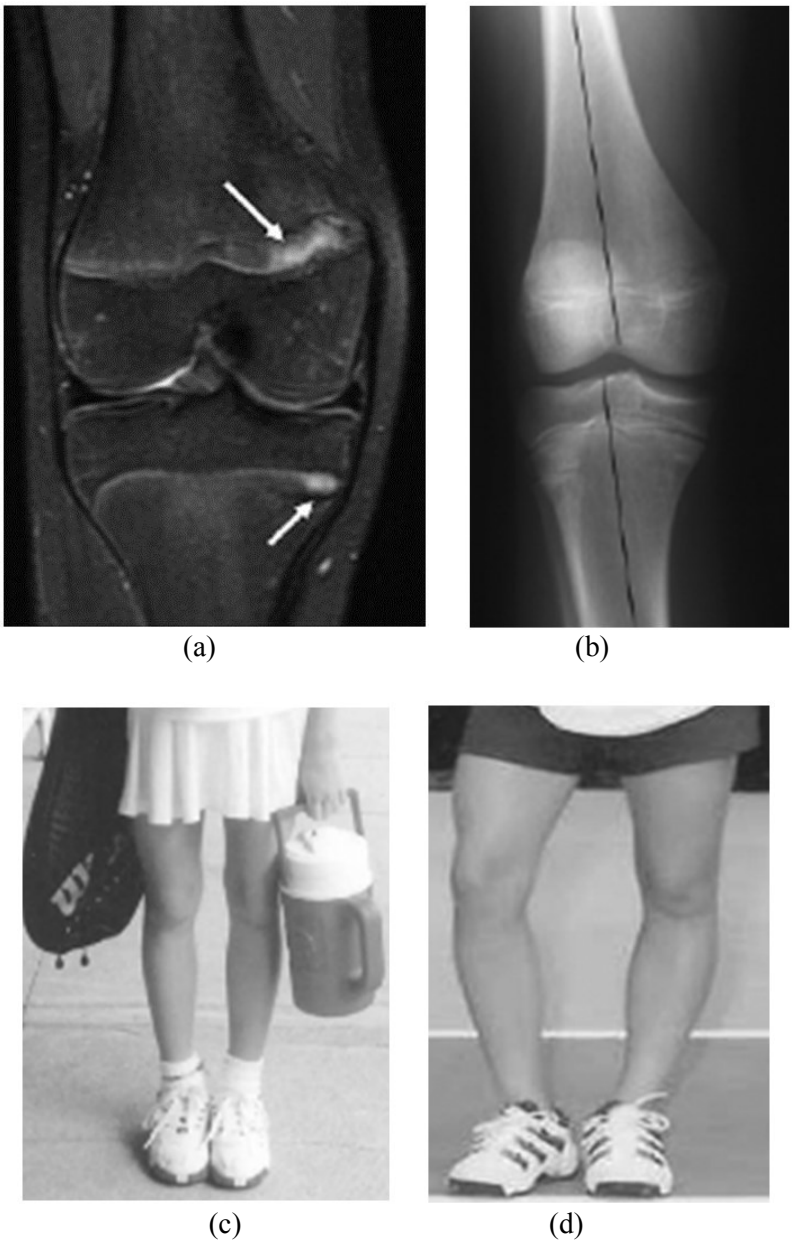

<u>Figure 2.19</u> – Case study of a young female tennis player.
(a) Two arrows on this MRI reveal widening of the medial distal femoral and medial proximal tibial epiphyseal plates respectively.
(b) Frontal radiograph of the right knee (taken while standing) after continuing to intensively playing tennis for an additional 2 years; the epiphyseal plates are beginning to fuse and both knees display relative varus alignment at 13.5 years of age as represented by the intersecting dark lines.
(c) Photograph taken at 11 years and 5 months, one month prior to the MRI scan in (a).
(d) Photograph taken after 6 years which reveals the varus effect.
(adapted from Laor *et al.* 2006)

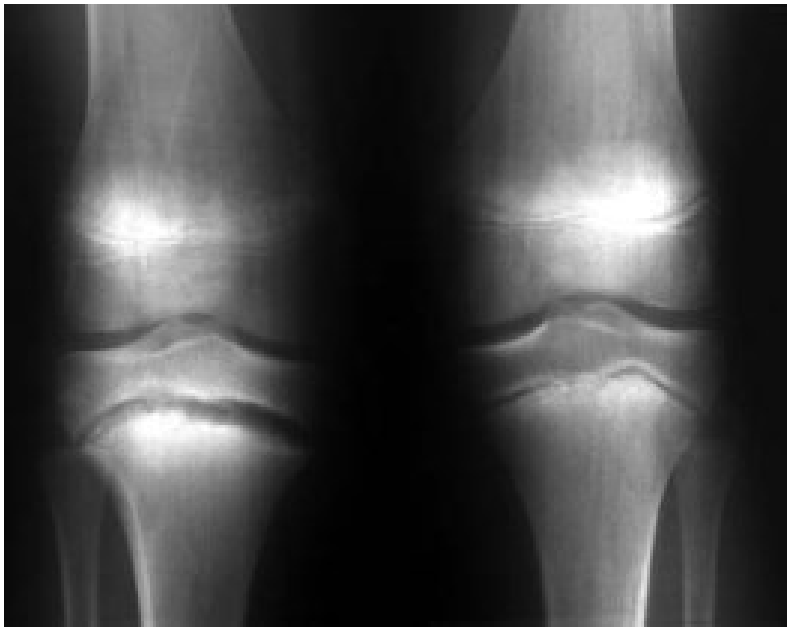

(a)

(b)

(c)

<u>Figure 2.20</u> – Case study of a 15 year old rugby player.
(a) Radiograph revealing the disruption to the tibial epiphyseal plate.
(b) MRI findings of an irregularly widened growth plate displaying nests of increased signal intensities representing metaphyseal sclerosis.
(c) Alternative MRI scan of the irregularly widened tibial epiphyseal plate.
(adapted from Nanni *et al.* 2005)

An example of an excessive stress reaction and overuse injury was highlighted in the proximal tibial epiphysis of a 15 year old rugby player who increased his daily kicking practice. The repetitive nature of the rotational pressures and forces acting on the growing bones consequently led to knee swelling, pain and physical exertion (Nanni *et al.* 2005). Figure 2.20 displays the initial radiograph that was taken and the two magnetic resonance scans clearly show the extreme sclerotic nature of the epiphyseal widening. At present there are no known studies that have biomechanically tested or measured whether disturbance of the growth plate can lead to altered joint mechanics, however, this would be expected when discrepancies in leg length and angular deformities present chronic pain while exercising.

MRI is continuously evolving and a relatively new three-dimensional technique has been utilised by Craig *et al.* (2004) and Sailhan *et al.* (2004) to facilitate the visualisation of early physeal closure and ossified bridges of bone traversing the growth plate. The technique involves the relatively simple outlining of the functional growth plate in individual coronal sections by manually using the paintbrush tool on the MRI computer workstation. Once this process is complete and repeated for isolating the bridge of bone, it is possible to quantify the volumes respectively. Surgical management and treatment of partial growth arrest is dependent on the ability to define reliably the precise area, location, nature and morphologic appearance of the disrupted region of the growth plate. Figure 2.21 provides an example of how this method can be applied with caution to investigate the pattern of damage to the underlying layers of the growth plate. The radiograph is useful in this case by clearly depicting a Harris line which is no longer parallel to the growth plate, thus demonstrating the significant extent of medial growth inhibition due to the osseous bridge of bone (Sailhan *et al*., 2004).

(a) (b)

(c) (d)

<u>Figure 2.21</u> – 12 year old female with 15° varus in the ankle and a distal tibial bony bridge.

(a) Antero-posterior plain radiograph. The Harris line is labelled by an orange arrow and the green arrow identifies the growth plate).

(b) Coronal fat-suppressed 3D spoiled MRI. The white arrow (also depicted in (a)) labels the bridge of bone that has undergone fusion.

(c) Axial 3D reconstruction of the growth plate from the MRI scans. The osseous bridge (shown as the black gap) is distinctive.

(d) Separate reconstruction of the isolated bony bar.

(adapted from Sailhan *et al*., 2004)

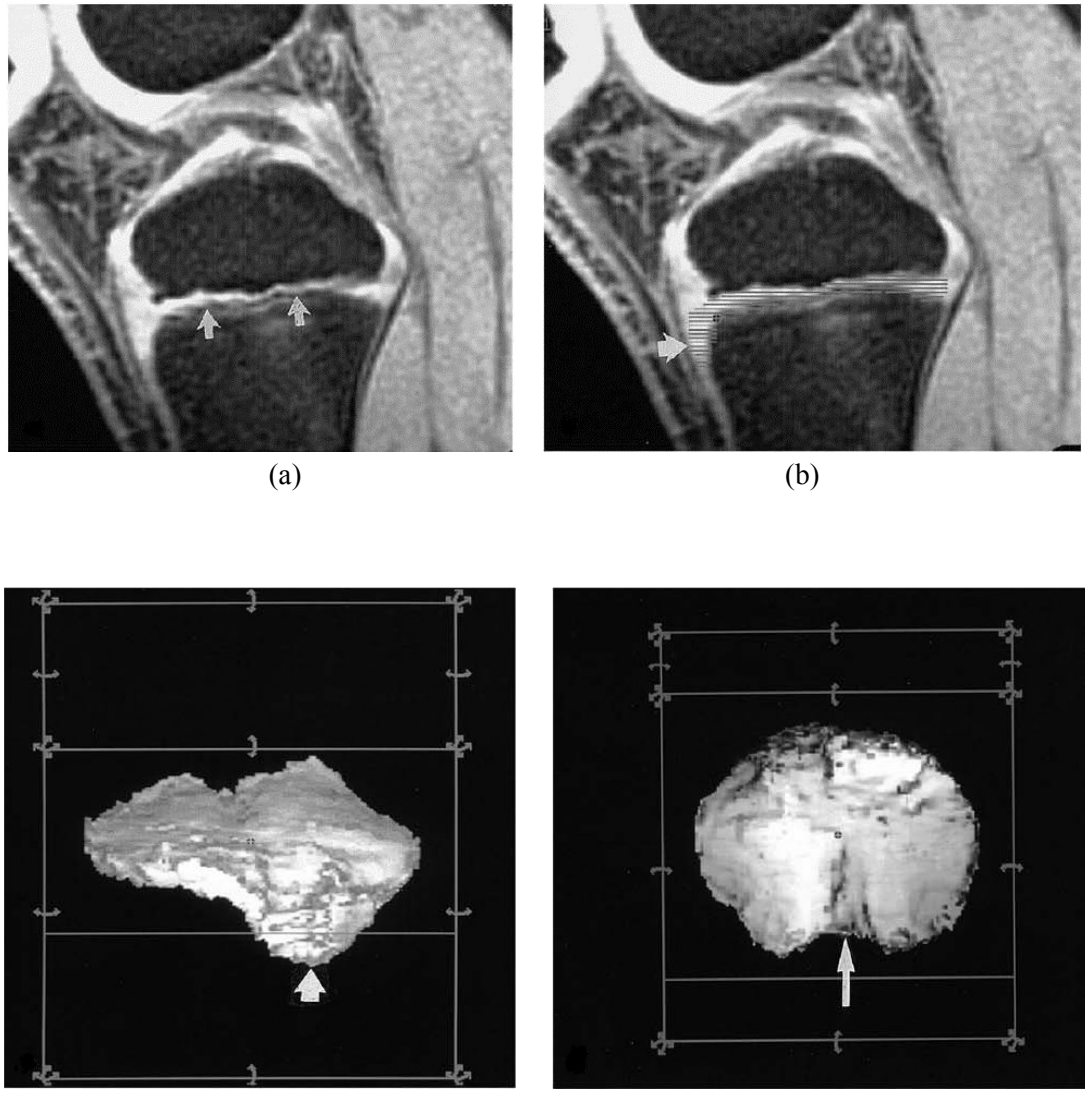

(a) (b)

(c) (d)

<u>Figure 2.22</u> – Example of Advantage windows software.

(a) Initial stages of preparing to outlining a tibial epiphyseal plate.

(b) Further outlining of the growth plate.

(c) 3D reconstruction of the superior-inferior view of the region of interest (ROI) identified by the arrow.

(d) Inferior-superior view of the same tibial growth plate.

(adapted from Craig *et al.*, 2004)

The clinical application of reconstructing anatomical structures is advancing steadily, however, there do not appear to be any standard protocols or specific programme software recommended or tested rigorously in the scientific literature. Figure 2.22 reveals an alternative workstation programme called Advantage that was used by Craig *et al.* (2004). The method is similar to that used by Sailhan *et al.* (2004) where a paintbrush tool is used to segment the epiphyseal plate as a region of interest in each slice; yet the final 3-dimensional reconstructions in Craig *et al.*'s (2004) paper appear to capture the growth plates in a smoother representation which is visually appealing and does not reveal, as readily, the discrepancies between the individual slices.

In the last nine years the scientific literature has not progressed with regards to improving and developing the techniques previously described with regards to calculating the volume of growth plates. The technological field, however, shows a stark contrast in relation to the scientific advances and software options that can be utilised to segment complex anatomical structures and calculate the total volume of a selected region of interest; as in the case of OsiriX™ (Franklin *et al*., 2012; Sicrezza *et al.*, 2011; Choudhri and Radvany, 2011).

2.7 Chapter Summary

Chapter two initially collates important background information as a context for the reader to appreciate and understand the perspective of experimental design detailed subsequently in Chapter three. Sections 2.4.3 is where Chapter two begins to explore the current scientific findings in related areas of research and the limitations encountered are addressed through a review of the literature.

Chapter 3

Experimental Design:

Materials and Methods

This research aims to investigate how intensive sports training may influence the volume and morphology of the growing epiphyseal regions of long bones. The design of this research integrated several techniques from across the fields of medical physics, biomechanics and anatomy. The potential impact that excessive pressures, forces, powers and moments may have on the volume and subsequent morphological development of the growth plate is unknown. The specialised design of this study combines the ability to capture, calculate and visualise three-dimensional data in a non-invasive environment which would otherwise remain unconnected and unexplored.

3.1 Materials

3.1.1 Participants

This study assessed fifteen young, male football players who attend Glasgow Rangers Youth Academy and were aged between 12-14 years. This active group was compared to an age-matched cohort of fifteen school boys who lead a more sedentary lifestyle in the city of Dundee and formed the control group. Previous studies (including Putti *et al.*, 2007) have calculated that, from an in-shoe pressure perspective, a minimum of ten subjects are required to ensure that results are statistically viable for an adult population. Putti *et al.* (2007) utilised the power equation described by Armitage *et al.* (2002) in '*Statistical Methods in Medical Research*' (pages 138-149) and identified the required sample size as follows:

Estimate of sample size n:

$$n > 2\left[\frac{(Z_{2\alpha} + Z_{2\beta})\sigma}{\delta}\right]^2$$

Where 2α = 0.05, $1-\beta$ = 0.8, δ = AverageX1-AverageX2, and σ represents the standard deviation. $Z_{2\alpha}$ and $Z_{2\beta}$ are fixed, e.g. in normal distribution 1.96 and 0.842, respectively.

Therefore,

$$n > 2\left[\frac{(2.802)\sigma}{\delta}\right]^2$$

Applying a significant p value of 0.05, the Type I error is 0.05 (α) when the Null hypothesis is rejected. The Type II error (β) can be calculated when the Null hypothesis is accepted and if β is taken as 0.2, the resultant power = $1-\beta$ = 0.8 (or 80%).

The standard deviation (σ) was calculated from the maximum standard deviation of peak pressure and was 83.0 kPa (Putti *et al.*, 2007). In clinical practice and at a level of significance, δ can be taken to equal 100 kPa when considering normal feet. Consequently this equation reveals $\boldsymbol{n = 10}$.

Based on the power equation for adults, the final sample size for this project exceeded the minimum and the final total of thirty subjects, comprised of fifteen active boys and fifteen more sedentary boys, can provide a statistical guide for experimental reliability. With respect to identifying the minimum number of individuals required to analyse the growth plate segmentations and overall volumes, research in the current literature has not yet determined normal or expected values that can be used to calculate a reliable standard deviation for the application of the power equation. Many research papers and studies within the wide repertoire of scientific journals available worldwide unfortunately refer back to single case studies or have limited representation for individual ages within each sex (Craig *et al.*, 2004; Panghaal *et al.*, 2012; AeRang *et al.*, 2011); therefore this project will act as a pilot study to lay a substantial foundation

for the newly developed segmentation techniques (as described in Section 3.1.4) using the volumetric data collected.

Initial contact with the parents of the Youth Academy players was orchestrated with the assistance of Rangers Football Club staff, when parents were invited to listen to a presentation given by the research team at Murray Park training grounds. The presentation, recruitment poster (Appendix A), and information sheets (Appendices B and C) provided an introductory, yet detailed, overview of the project design and aims. This environment created a friendly, dynamic opportunity for the parents to communicate directly with the researchers who were able to answer queries relating to the volunteering process. The recruitment process for the control group was more challenging with regard to the fulfilment of strict procedures prior to approaching schools. Adverts and news articles were published in local papers, in addition to the distribution of emails and posters which were placed around the University, Hospital and Scout Association Centres to invite interested individuals to respond.

The control group were permitted to participate in physical education curricular activities; however, it was important that they were not active or regular members of a sports team. Growth and development of long bones can be influenced by a variety of factors; therefore it was also necessary to recruit control subjects that were of a similar body mass index (BMI) to the intensively trained athletes in an attempt to negate the effect of weight-based factors. Activity levels for each of the sedentary volunteers was assessed when first discussing the project details with the parents and was established further by a questionnaire (Appendix D) that was completed by the subject. All participants had an opportunity to ask additional questions before completing the consent form (Appendix E) and questionnaire and understood that they could stop and

withdraw from the study at any point throughout the day without any explanation or reason. Each subject completed the forms with his parent or guardian on arrival at the laboratory. The questionnaire also confirmed that no prior involvement with clinical bone enhancing drug trials or lower limb fractures could have affected the morphology of the growth plate; consequently reducing potential variables and factors that could bias the final results. Additionally, there was a specific section in the questionnaire that only the Rangers Youth Academy players responded to, which highlighted possible sources of discrepancies between players (e.g. player position, years spent training at youth academy, type of training shoe, and type of training surface). In the case of potentially identifying an outlier within the data set, this section could later be used to help explain why an individual may follow an inconsistent trend. Table 3.1 provides a brief summary of the average group demographics and details the range of activity and frequency of weekly exercise undertaken by individuals in each group. Figure 3.1 plots the height and weight of each individual in ascending chronological age, which visually represents a clear spread of demographic data and offers a guide to gauging the percentage of body fat or body mass index (BMI) without using calculations.

Table 3.1 – Overview comparing the active and control group demographics.

ACTIVE GROUP		CONTROL GROUP	
Minimum - chronological age (months)	147	Minimum - chronological age (months)	149
Maximum - chronological age (months)	177	Maximum - chronological age (months)	179
Mean - chronological age (months)	**164.5**	Mean - chronological age (months)	**161.8**
Minimum - hours of regular weekly exercise	10	Minimum - hours of regular weekly exercise	3
Maximum - hours of regular weekly exercise	20	Maximum - hours of regular weekly exercise	13
Mean - hours of regular weekly exercise	**14**	Mean - hours of regular weekly exercise	**7**
Exertion level	**Intensive**	Exertion level	**Light**
Examples of exercise	Sprints Stretches Lunges Core (planks) Crunches Competitive Games Dribbling Shooting Running Passing Possession P.E lessons	Examples of exercise	P.E. lessons Walking (dog/school) Playing (school) Trampolining Swimming Paper round Scouts Cadets
Minimum - years at Academy	1.5		
Maximum - years at Academy	6		
Mean - years at Youth Academy	**4**		
Positions played	Defender Midfield Centre Midfield Left Midfield Centre Back Attack Striker Wing		

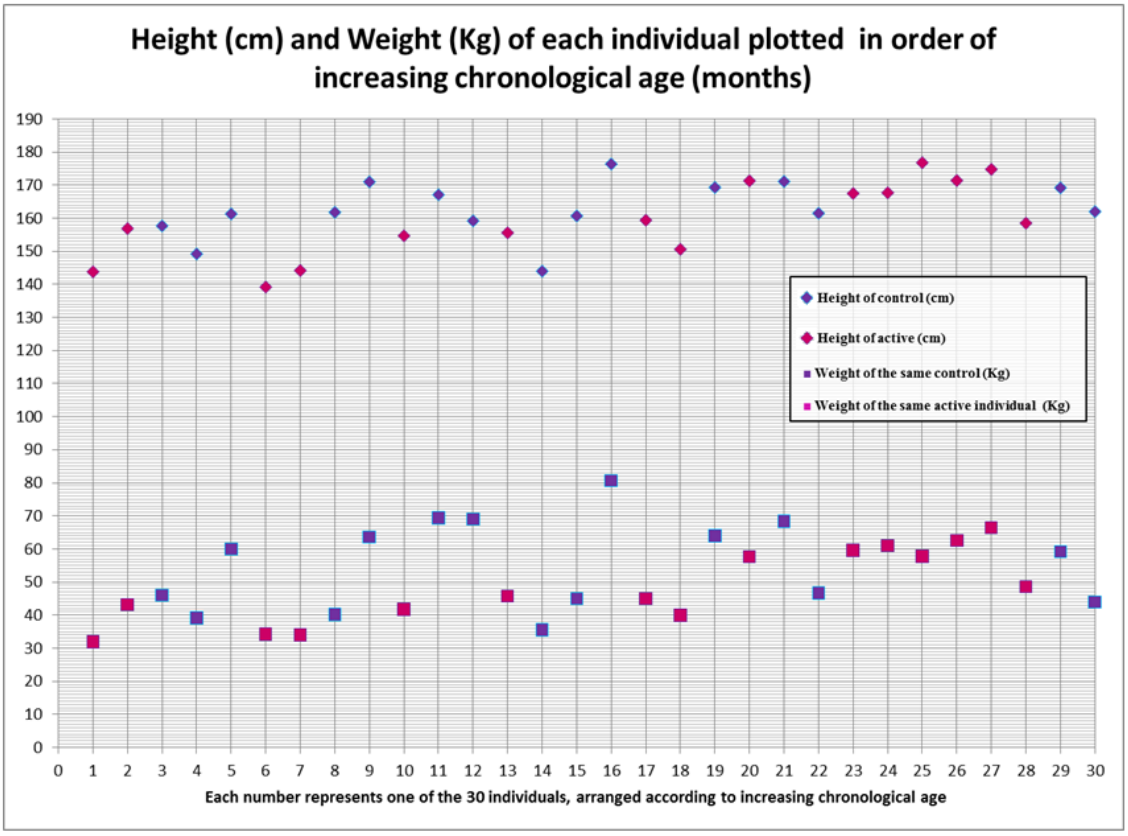

Figure 3.1 – Graphical representation of the demographic spread of height and corresponding weight of each individual organised in order of increasing chronological age. The youngest individual (number one) is an active individual (as represented by the colour pink) and the eldest individual (number thirty) is a control (as represented by the colour purple).

3.1.2 Ethical Approval

Ultimately, the future health and welfare of each participant is of the foremost importance and the East of Scotland Research Ethics Service granted favourable ethical approval. Sponsorship and insurance was governed by the Tayside Clinical Trials Unit, while Research and Development Governance was granted from NHS Tayside. Due to the sensitive nature of this project, confidentiality and anonymity were crucial and all participants were allocated a unique identifying code which was secured in a

password protected Excel database with restricted access. As with all imaging studies, there was potential to inadvertently discern 'incidental findings' or pathological anomalies through the implementation of MRI and the consent form certified that only the parent or guardian would be directly informed. The research team only sought specialist or expert advice at the discretion of the parent to ensure that confidentiality was not violated. The researcher completed a Good Clinical Practice (GCP) training course to fulfil the prerequisite of having permission to take informed consent and additionally updated the relevant disclosure through Disclosure Scotland.

3.1.3 Hardware Equipment

In terms of the equipment utilised in this project, the combination was novel with respect to applying kinematic and kinetic assessment with complementary three-dimensional imaging to determine any effects that intensive sports training may have on the dynamically developing growth plate. The Gait Analysis Laboratory is located in the Institute of Motion Analysis and Research (IMAR) and is closely linked with the Clinical Research Centre (CRC), also located at Ninewells Hospital and Medical School, where the non-invasive Magnetic Resonance Imaging scans were undertaken. The following subsections detail the fundamental elements of the applied instrumentation and software, whilst Section 3.2 addresses the comprehensive protocol, preparation and collection of data using the equipment.

3.1.3.1 Vicon Nexus®

Vicon® hardware is a complex system that has been established in the biomechanical field for over 25 years to track, measure and analyse motion accurately in a digital, three-dimensional environment. To analyse both walking and running patterns, as in the case of this project, 18 cameras were required to maximise the recording area for the Vicon® MX system. The placement and interaction of each Vicon® camera was developed and carefully orchestrated to synchronise effortlessly with many layers of innovative equipment to form the sports laboratory in IMAR. The cameras contain light-emitting diodes (LED) that transmit infra-red light and this invisible light can be recorded when the signal reflects off specialised retroflective markers. Various sizes of specialised retroflective markers are available to track the body during walking and running, with examples illustrated in Figure 3.2. This project utilised the 12mm markers which are routinely used in the clinical setting to denote the anatomical positions integral for Vicon® to reconstruct and extract clinical data.

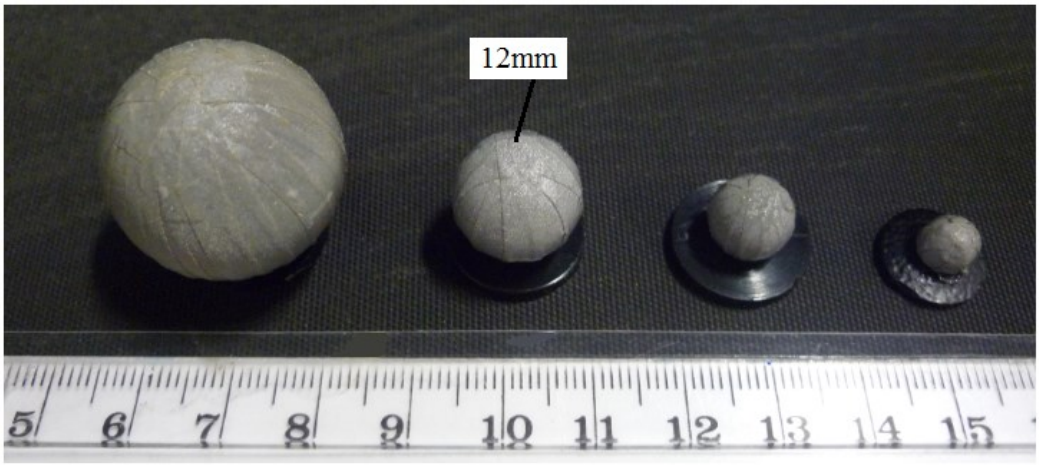

Figure 3.2 – Photograph depicting the varying sizes of retroflective markers that are commercially available.

Using the kinetic and kinematic data, the clinician is able to analyse and identify potential treatments for cerebral palsy, diabetic, or hip replacement patients with the view to improving or restoring their biomechanical function. Three-dimensional images are generated as the cameras relay the information in real time to two MX Giganets which provide power and connect the cameras, force plates, video recording devices, and Bluetooth with the PC workstation. Vicon® has a capacity to capture speeds of 2,000 frames per second through two-megapixels resolution cameras; however in the case of this project the optimum capturing rate of 100 Hz was selected. Gauging the balance between choosing a sampling frequency that is low enough to ensure the file output sizes are not too large to process, yet high enough to display and track the separate markers efficiently, was crucial. Eighteen cameras were used (twelve MX13 cameras and six T20 cameras) to generate a three-dimensional reconstruction of the participants to permit the visualisation and assessment of gait cycles by reconstructing, calibrating and calculating the angles, forces and moments incurred during walking and running.

The Sports Laboratory has two concealed AMTI® OR6 force plates which record at 1000 Hz directly into the Vicon® workstation. The force plates are mounted within the structural foundations of the laboratory in a recessed, concrete pit to minimise building and ground vibrations that could generate false signals and background noise. The importance of having camouflaged the force plates is also to prevent subjects targeting the plates, as this deliberate change of gait introduces undesirable artificial limb motion (Perry, 1992). The force plates measure three force components (Fx, Fy, and Fz) and three moment components (Mx, My, and Mz) which act along the orthogonal x, y, z-coordinate system. The strain gauges suspended within the force plates utilise the defined coordinates to calculate the vertical load, horizontal shear, vector patterns and

joint torques or rotations of the foot reacting with the ground (Perry, 1992). Figure 3.3 illustrates the design of the AMTI® force plate in addition to the respective measurement axes for the force components and the positive moment components which are displayed by the clockwise arrows rotating around the three axes.

The ability of Vicon® to simultaneously record digital video (DV) files during data collection is via two Sony DV cameras that capture movie files at a sampling frequency of 25Hz (MSDV-PAL). The video cameras are invaluable to enable the trials to be reviewed at a later date; hence the dynamic pattern of gait can be holistically visualised and a quality check of marker placement and force plate interaction can be repeated and reassessed.

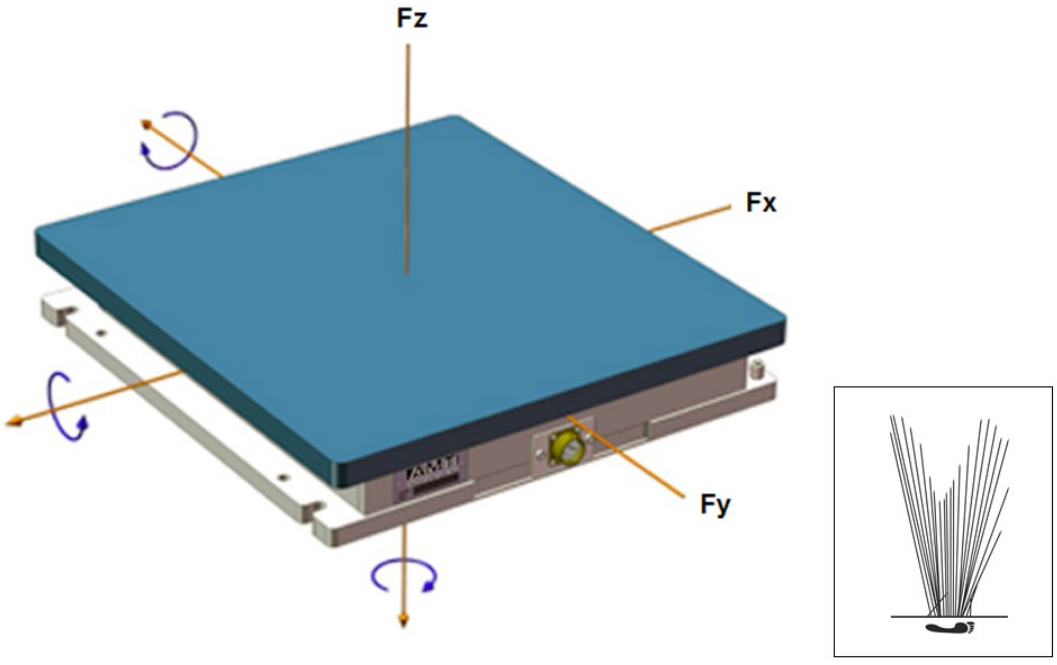

Figure 3.3 – Diagram of the AMTI® force plate and the axes of horizontal or shear (Fx and Fy) and vertical (Fz) force components. Clockwise orientation of the arrows along the axes displays the positive moment rotations and an example of the expected vertical pattern incurred during walking is presented.

(Image adapted from Advanced Mechanical Technology, Inc. (2013))

3.1.3.2 Pedar-x®

Although the force plates measure the magnitude and direction of the accumulated ground reaction force (GRF) generated underfoot, the plates were unable to reveal the specific distribution of forces located at individual anatomical points of the foot (Whittle, 2007). Pedar-x® is a mobile, in-shoe pressure distribution measurement system designed to record in-shoe pressure and was used in this research to compliment the force plate data. The Pedar-x® box connects to thin insoles, as shown in Figure 3.4, that consist of 99 capacitive pressure sensors which are evenly distributed over two layers and are separated by a soft, inner material. Electrical pulses are generated when these capacitors are forced together when a vertical load applies pressure. Individual sensors measure an area that roughly equates to 1cm^2 per sensor; ultimately providing a detailed and precise analysis of the dynamic forces across the entire foot within the shoe, which can complement the more indiscriminate ground reaction forces recorded by the AMTI® force plates.

Figure 3.4 – Photograph of the Pedar-x® box and a selection of different sized in-shoe pressure insoles (both lefts and rights).

The Pedar-x® system is repeatable and accurate (Ramanathan *et al.*, 2010; Putti *et al.*, 2007) with the capacity of recording in-shoe pressure at a sampling frequency of up to 100Hz. To enable the synchronisation of all individual recording devices, Pedar-x® was coupled with the TMSi Mobi™ which is a mobile electromyography box. A delicate fibre optic cable connects these two devices via the middle 'output' connection and the final pressure data is transferred to a workstation via a wireless Bluetooth connection. This combination of balancing synchronisation and wireless connectivity consequently resulted in sampling the pressure data at a repeatable frequency of 50Hz. Figure 3.5 illustrates the final 3-dimensional representation of the in-shoe pressure sensing system of Pedar® during walking and running respectively. The colour-coded reconstructions are invaluable visual aids to discern and interpret the ensuing statistical data of peak pressures and forces, with the black colour representing low pressure and pink displaying an excessively large pressure.

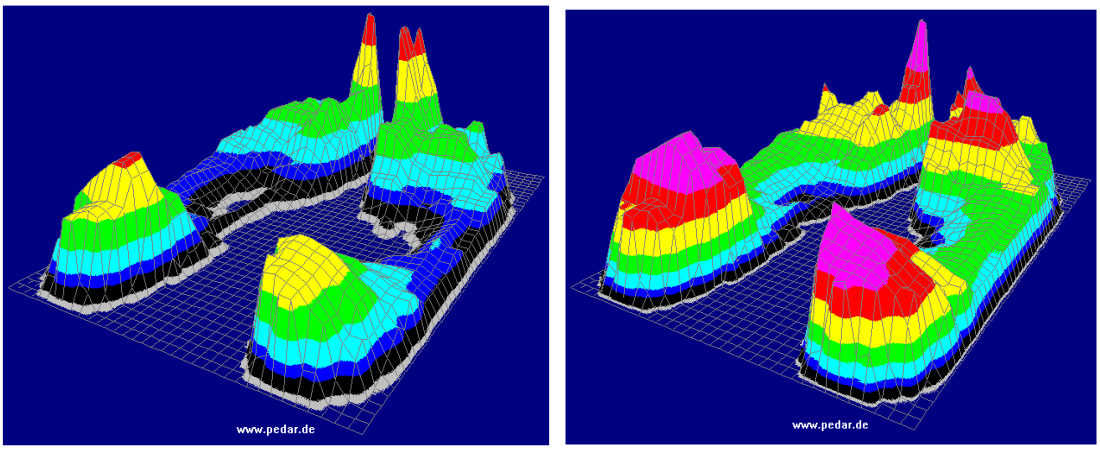

(a) (b)

<u>Figure 3.5</u> – A comprehensive representation of the overall peak forces detected by Pedar-x® through the 99 in-shoe pressure sensors.

(a) Walking

(b) Running.

3.1.3.3 Electromyography measured using TMSi Mobi™

Electromyography (EMG) is defined as "the study of muscle function through the inquiry of the electrical signal the muscles emanate" (Basmajian and Deluca, 1985) and the bioelectrical feedback design of the human motor system regulates the power, force, and actions necessary for locomotion (Moritani *et al.*, 2004). During walking and running, joint stability is provided by muscular action and the importance of EMG to calculate the dynamic effort generated by each muscle at the correct time is vital to recognise if the muscle has been damaged (Cifrek *et al*., 2009). Muscle tissue can have between 100 to +1000 motor units (MU), which in turn contain an α-motoneuron. The α-motoneuron in each motor unit generates the electro-physiological firing pattern when the muscles contract at the sacromeres (Hogrel, 2005) and this action can be measured either by needles or by surface electrodes placed on the skin. The analogous position of each electrode is of critical importance with regard to the signal strength that is obtained and for repeatability; therefore between 1996 and 1999 the Biomedical Health and Research Program developed a European SENIAM (surface EMG for non-invasive assessment of muscles) project to establish a peer-reviewed protocol.

Figure 3.6 – Image of the portable TMSi Mobi™ and example of the Noraxon™ surface electrodes.

Noraxon™ dual electrodes are disposable, self-adhesive Ag/AgCl snap electrodes which are non-invasive and are pictured in Figure 3.6 with the TMSi Mobi™. The surface electrodes spaced at 2.0 cm were selected for this study as the advantages far out-weighed the disadvantages that would have been encountered using the invasive, needle method. The wire-electrode method is not child friendly, introduces the risk of infection, and only detects a selected number of motor units which would record inconsistent signals, particularly during running. The key disadvantages that may be encountered when sampling surface measurements is that there is an increased risk of interference or 'cross talk' from surrounding muscles, tissue filtering (through skin and fat) can result in a diminished signal quality, and poor skin conditions (such as dry skin or excessive hair growth) may cause complications when attempting to acquire a good quality signal (Koh and Grabiner, 1992; Goryachev *et al*., 2011; Cram, 2003). To minimise and limit skin impedance, the area of skin is prepared using NūPrep abrasive gel to remove gently any dry, dead skin cells prior to the application of the electrodes. The small layer of conductive gel on the base of the surface electrodes significantly facilitates the clean transmission of signals.

The TMSi Mobi™ is able to assist with synchronising all of the data collected within the Gait Analysis Laboratory; therefore the opportunity to record the muscular activity of lower limb muscles was presented at this stage in the research and is why the EMG data was collected yet not analysed. The TMSi Mobi™ is limited to four active ports (labelled A/B and C/D) where two electrode cables attach to connect the recording box with four individual muscles. The impracticalities of assessing all of the lower limb muscles resulted in the final selection of the following four muscles: *Tibialis anterior*, *Peroneus longus*, *Lateral gastrocnemius* and *Vastus lateralis*. The anatomical position of each selected muscles is ideally suited for surface electrode placement and the

combined activation patterns at various points while walking or running ultimately provides an optimal range of information for the interpretation of gait.

The wires from the portable pack connect via a clip/snap action onto the surface electrodes and the subsequent signals generated by the effort of each muscle is sent via Bluetooth® to the computer workstation. As a consequence of EMG signals being very small and ranging from 300uv to 5mv (Perry,1992), the signals are unable to be analysed directly without amplification. There is a green wire with only one wire connection, which acts to earth the signal by attaching to a bony prominence instead of muscle and this is vital for recording clean data. The TMSi Mobi™ has two additional ports, labelled E and F, to allow synchronisation of alternative software and devices. The port which is labelled E can provide an integrated link for the attachment of a small aerial that receives the Bluetooth® radio synchronisation pulse into the Mobi™ EMG measurements. A uniquely designed box was developed in-house to signal the reference synchronisation point to both the TMSi Mobi™ and Vicon® systems by pressing the radio synchronisation button. The cable which feeds directly into the Vicon® system captures at a frequency of 1000 Hz and the final port (labelled F) provides a connection to synchronise the 50 Hz pulse outputs from Pedar® with the real-time recording of the 1024 Hz capturing rate of EMG output.

3.1.4 Software Equipment

3.1.4.1 Vicon® Polygon®

Quantitative data that is generated from Vicon® can be imported into this complementary software used to report and interpret the kinetic and kinematic graphical data compared against a database of normal average values. Polygon® also offers a professional presentation platform to format and analyse the complex data in addition to being able to apply full skeletal templates in the form of movie files, as displayed in Figure 3.7 which highlights the GRF during walking and running respectively.

3.1.4.2 MATLAB®

MATLAB® is a specialised computer programming language which uses matrices to develop an interactive environment to solve technical computational tasks. The interactive system of MATLAB® has been used to code (Appendix N) a key program for the analysis of MRI data included as part of this research project. The MATLAB® program enables the creation of T2 images from two-dimensional multi-echo MRI sequence data. Complex algorithms sort and organise the DICOM (Digital Imaging and Communications in Medicine) files to display a transparent colour T2 map which is overlaid onto the original gray scale image data. The program enables the threshold frequency to be altered and through experimentation in this project group, the optimal frequency across all individuals was found to be approximately 80Hz. The minimum and maximum frequency acts to alter the number of T2 pixels that are visible; for example in Figure 3.7 the 20-30 Hz pixels are depicted as light blue and the 100-110 Hz pixels are pink.

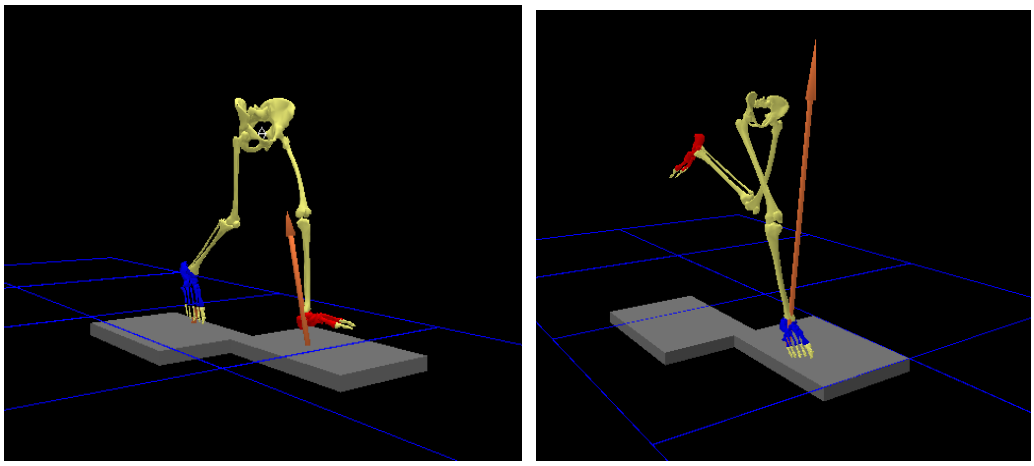

(a) (b)

Figure 3.7 – Examples of a reconstructed trial using Polygon® technology. The red arrow represents the direction and magnitude of the GRF.

(a) Active individual walking.

(b) Same active individual running.

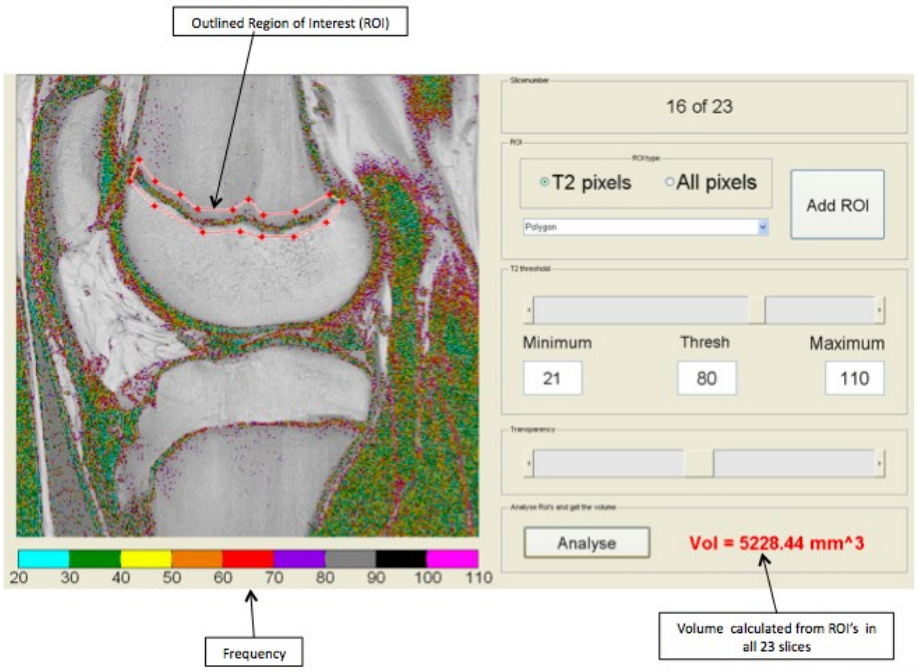

Figure 3.8 – T2 mapping software depicting the outline of the region of interest. In this case it is of the femoral growth plate and the final calculation of the volume, of all the T2 epiphyseal plate pixels across 23 slices, is presented in the lower right corner.

The transparency of the original T2 scan can be altered and this aids greatly in identifying the anterior and posterior delimited edge of the epiphyseal plate, which is more difficult to determine when only the coloured T2 pixels are presented. The programme facilitates simple calculation of volumes from different T2 thresholds in a reproducible manner by drawing regions of interest (ROIs) in a planar image which can be exported and saved in a selection of image formats.

3.1.4.3 OsiriX™

OsiriX™ is a Picture Archiving and Communications System (PACS) workstation that processes DICOM files to permit the visualisation, reconstruction and navigation of multidimensional MRI pictures, as featured in Figure 3.9. The first version of OsiriX™ was released in 2003 (Rosset *et al.*, 2004) and was written and developed using a free open-source format; thus resulting in the software having the unconstrained ability to progress with ever-evolving updates, versions, and plugins which automatically keep the user at the forefront of current technological advances (Ratib and Rosset, 2006). The only disadvantage encountered while using OsiriX™ to calculate growth plate volumes, was the fact that the tools available to outline the borders are intricate as well as extremely difficult to define accurately by eye; therefore the segmentations are traced by hand without the guidance of a semi-automatic segmentation technique.

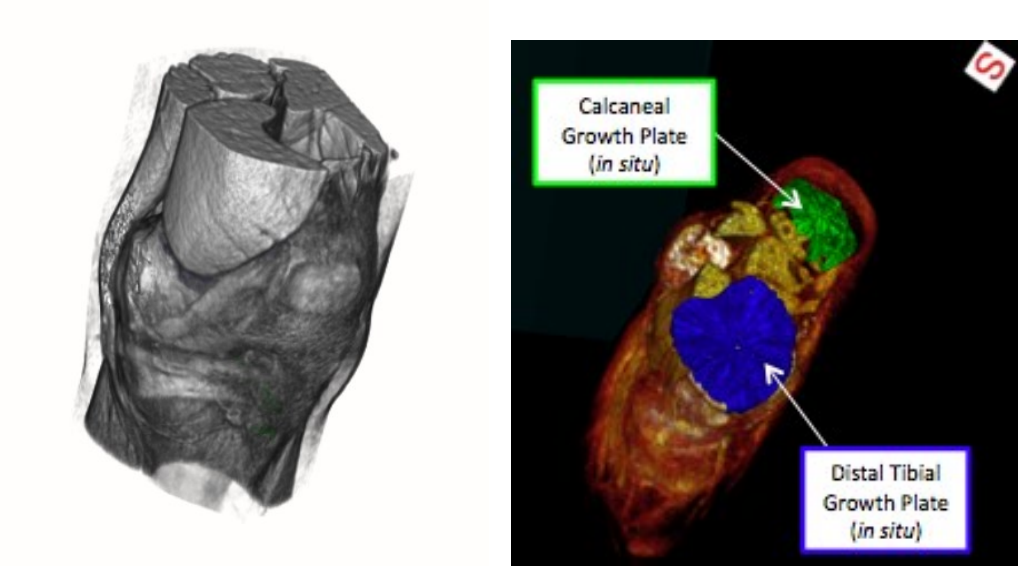

(a) (b)

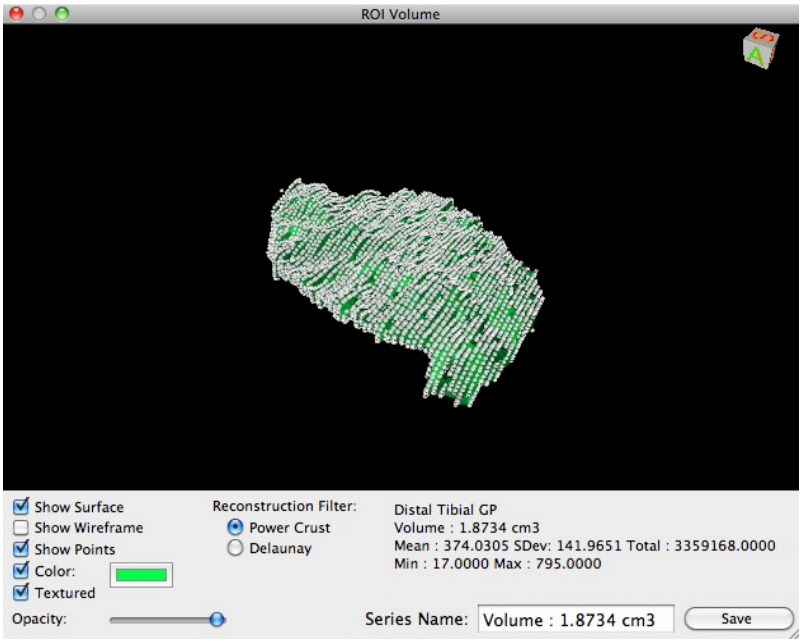

(c)

Figures 3.9 – Illustrations of the OsiriX™ software reconstructed MRI data.

(a) 3D surface rendered reconstruction of the knee.

(b) Superior view of the ankle and foot showing the distal epiphyseal plate and calcaneal traction growth plate.

(c) Distal tibial epiphyseal plate using the Power Crust Reconstruction Filter to show the morphological shape in addition to calculating the overall volume.

3.1.4.4 Endpoint

Acquisition of an old version of Endpoint software (developed in 2001) was discovered during the extensive search for a software with a suitably sensitive algorithm to balance and combine the efficacy of automated and manual segmentation methods, without the disadvantages associated with each type of method respectively (Poon *et al*., 2008). Endpoint has a 'livewire' tool that is depicted by the red, closely associated outline in Figure 3.10. Livewire uses built-in algorithms to decipher and outline the region of interest semi-automatically by performing a clinging action when the mouse is guided close to where the edges of the epiphyseal plate occur. Thus, when this action is repeated across all of the growth plate slices, the epiphyseal plate volume is calculated once the view measurements button is clicked. The DICOM files must first be converted into an ANALYSE file format and compressed further to result in 160 DESS slices reducing down to approximately 80 DESS slices per individual while maintaining the volumetric dimensions.

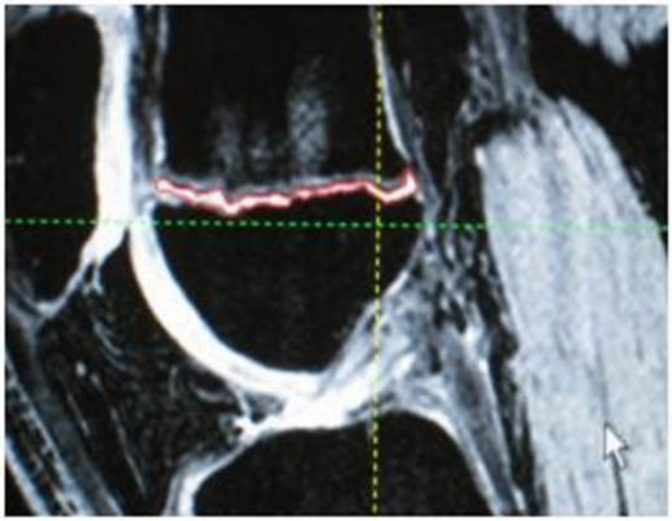

Figure 3.10 – A screen shot of Endpoint software with the red outline demonstrating the accuracy of the livewire function outlining the borders of the femoral epiphyseal plate.

3.2 Methods

3.2.1 Imaging of the epiphyseal plate

The primary focus of the MRI scans was to generate images of the internal anatomical structures of the knee, foot and ankle; thus enabling metaphyseal dimensions to be recorded and quantified for each epiphyseal plate. The initial scanning protocol centred on the knee region where the scanning sequences were set to discern and concentrate on the distal femoral, proximal tibial, and proximal fibular epiphyseal plates. The sequence of scans was then repeated for the foot and ankle region with the focus now centred on the distal tibial growth plate, distal fibular growth plate, and the traction epiphysis of the calcaneus.

On arrival at the laboratory, the subjects and parents were greeted and had time to take a seat while the project information was re-discussed to guarantee that they were clear on the activities for the day and that the boys could withdraw from the study at any time. After completing the consent form and questionnaire together, the naturally dominant leg was determined independently by asking each subject to kick a small ball into the centre of the room and this action established which leg would undergo analysis. A Siemens MAGNETOM Trio, A Tim 3T MRI scanner was utilised by NHS radiographers at the Clinical Research Centre with the expertise and guidance of NHS medical physicists. Within the MRI area, the NHS staff additionally completed a safety checklist for each subject (Appendix F) before measuring the subject's height and weight to input into the scanner. The participant changed into light gowns with no metal objects attached and was introduced to the MRI scanner before lying down with toes and feet pointing in towards the machine as depicted in Figure 3.11. This position

did not require the head to be fully enclosed within the scanner; therefore reducing any claustrophobic feelings that may have incurred.

As the knee was the first joint to be scanned, the CP Extremity coil was positioned to surround the entire anatomical area and subsequently packed with a combination of support bags/foam to prevent any movement of the knee and enhance the localised magnetic field. Initially, three standard 2-dimensional reporting scans were taken for a clinical radiologist to conduct a compulsory report; thus ensuring that any significant incidental findings relating to an individual's health were recognised and handled in an ethical and professional manner. The first investigative scan at the knee is named the T_1-weighted Dual Echo Steady State (DESS) scan and consists of 160 slices. The DESS images are acquired with isotropic voxels, which is imperative for the generation of three-dimensional reconstructions and for accurate volumes to be calculated.

Figure 3.11 – Photograph of the Siemens MAGNETOM Trio, A Tim 3T Magnetic Resonance scanner at the CRC set up for an ankle scan.

The second investigative scan of the knee differed from the DESS as it was a T_2-weighted scan and involved 23 scans taken at eight different frequency thresholds. T_1 and T_2 sequenced images alter the appearance of certain tissues; with fluid (including bone marrow and fat) characteristically appearing bright in T_2-weighted scans compared to the darker characteristic appearance in T_1-weighted images. Specialised algorithms were applied mathematically to determine the properties of the material by overlaying the different threshold frequencies. Table 3.2 details a selected number of variable settings used to highlight the differences between the DESS and T_2 MRI scans. The total acquisition time for scanning the knee was approximately 30 minutes and once this was complete, the volunteer changed position so that the same processes and sequences could be repeated for the foot and ankle.

Table 3.2 – Settings for some of the variable fields for the DESS and T_2 scans for MRI acquisition at the knee.

Field Name	Value for DESS	Value for T_2
Pixel Spacing (mm)	0.59 by 0.59	0.31 by 0.31
Slice Thickness (mm)	0.59	3.0
Spacing Between Slices (mm)	0	3.6
Samples per Pixel	1	1
Echo Number	1	1
Echo Time (s)	4.91	10.0
Repetition	14	2000

Analysis of the DICOM data was undertaken using the three different software programmes described earlier in Section 3.1.4; OsiriX™, Endpoint and a specially developed programme written in-house on MATLAB®. OsiriX™ is ideal for presenting an attractive 3-dimensional visual representation of the growth plates by outlining the region of interest in each slice of the DESS scans as demonstrated by the simple steps shown in Figure 3.12. Although there are tools available to calculate the surface area and volume of the epiphyseal plates using OsiriX™, the 'livewire' tool in Endpoint is more user friendly than the 'paintbrush' tool in OsiriX™. The livewire tool enables the user to outline the epiphyseal plate semi-automatically and this recognition of the outline is a beneficial aid for investigators in the rather subjective nature of epiphyseal plate borders.

A comparison of epiphyseal plate volumes calculated from the DESS images was then used to complement the calculated volumes from the T_2 images. T_2-weighted scans depict fat as having a darker composition and water is represented as having a lighter greyscale colour than in the DESS scans. A region of interest (ROI) was outlined in each of the 23 slices using the polygon setting and the 'analyse' function calculated the total volume of T_2 pixels of the growth plate across all of the ROIs; therefore generating the final growth plate volume. The benefit of the T_2 technique is that the process is not as time consuming with respect to outlining the ROIs on each individual slice, which can be demanding with regard to the time and concentration required to fully process one epiphyseal plate volume.

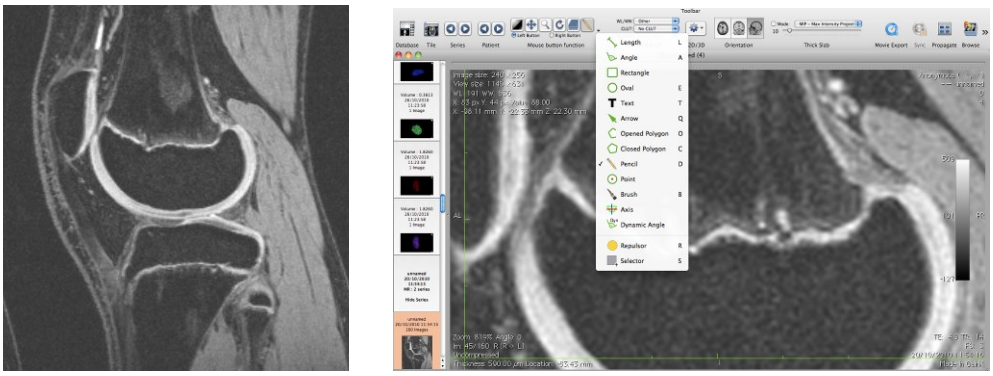

(a) (b)

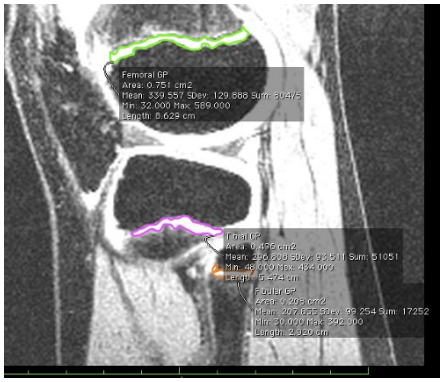

(c)

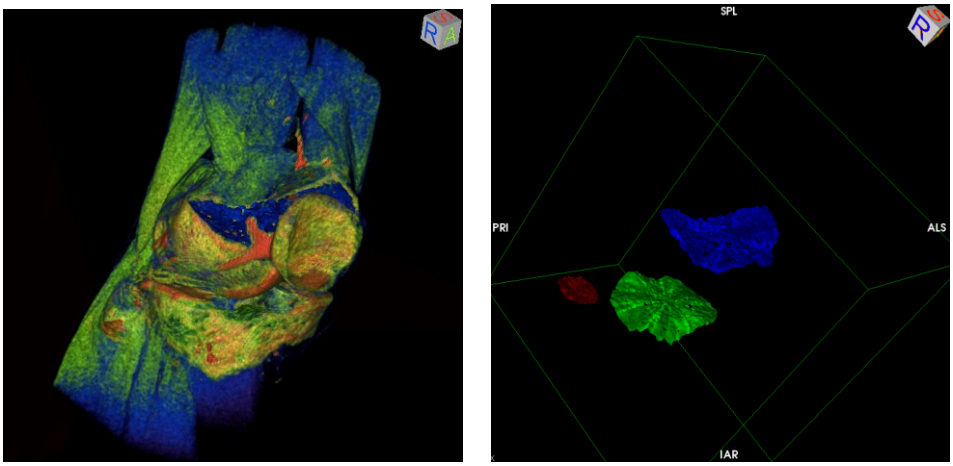

(d) (e)

Figure 3.12 – Summary of steps taken to calculate the volume of a growth plate from DESS scans using OsiriX™.

(a) Sagittal orientation before magnification to the desired view.

(b) Paintbrush tool enabling the mouse to outline a desired ROI individually on each slice.

(c) Three completed growth plate ROIs ready to undergo 3D reconstruction.

(d) 3D volume rendered view of the knee with rainbow colours selected.

(e) Resultant ROIs remaining *in situ* after the 'window level' is reduced to remove the surrounding anatomical structures.

3.2.2 Gait Analysis

To investigate the potential reason for any morphological differences found across the epiphyseal plates, it was necessary to compare the pressures and forces transmitted through the lower limbs in each participant. The gait analysis and sports laboratory provided an ideal setting for the second phase of data collection.

3.2.2.1 Calibration

Prior to the subject's arrival at IMAR's Sports Laboratory, all of the Vicon® cameras were switched to 'live' mode and left to warm for a few hours to prevent additional 'ghost' markers from interfering with the smooth collection of the kinematic data. Temperature fluctuations can cause each camera to sometimes 'drift' and this results in false, sparkling markers that can be hidden or tweaked by implementing camera masks; camera masks will conceal this area and prevent markers being tracked which is an additional reason to warm the cameras and ensure that the threshold and strobe intensities are set within the optimal values (<0.5 and between 0.8-1.0 respectively) with as much as possible of the capture volume being clearly visible. Calibration is vital for measurements of distance to be calculated accurately (Whittle, 2007) and the sports laboratory cameras are calibrated using a 5 marker L-shaped wand as pictured in Figure 3.13(a). The calibration wand is first waved in circular motions for the cameras to acquire a minimum of 1000 frames whilst covering as much of the capture volume as possible. Once Vicon® completed the image error feedback process, the final error values should be less than 0.2 and the onscreen boxes should remain green in colour; consequently guaranteeing that each camera is recording clear marker trajectories. The wand is then positioned precisely over the far left hand corner of force plate one, with the spirit levels on the frame assuring that the origin is set on a level plane.

Figure 3.13(b) demonstrates the importance of taking time to position and construct a long, straight walkway of at least 9m (Orlin and McPoil, 2000) to provide adequate space to preserve the quality of data collection by adequately dividing the laboratory into three recommended divisions; a preparation area, a central recording area to collect a natural gait, and thirdly a deceleration area. A further quality assurance check is conducted by capturing a calibration check trial in Vicon® and comparing the resultant trajectory values of the markers against the X, Y, and Z components of pre-defined limits.

Calibration of each Pedar insole is achieved using a Trublu® calibration device. The insoles are calibrated every month using constant air pressure and the final calibration curves of individual sensors can be checked at any time.

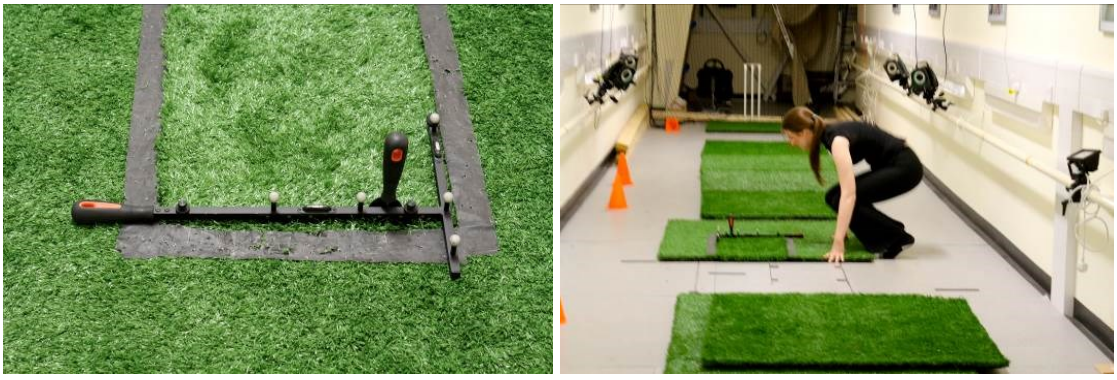

(a) (b)

Figures 3.13 – Calibration process of the Vicon® cameras in relation to the force plates.
(a) The 5 marker L-shaped calibration wand for Vicon®.
(b) Central position of force plate one in relation to the length of the walkway.

3.2.2.2 Preparation

A total of sixteen anthropometric measurements were recorded on the final section of the questionnaire and the following protocol within Table 3.3 was completed by the

researcher prior to marker placement. Thirty-five reflective markers were adhered to the skin via double sided tape and were positioned at the anatomical landmarks highlighted in Figure 3.14, with the most important lower limb marker positions detailed in Table 3.4. The markers were positioned according to the placement protocol developed in-house for clinical services and accredited by the Clinical Movement Analysis Society (CMAS). The position and anthropometric measurements correlate distinctively to the algorithms programmed within Vicon® to reconstruct reliably predefined PlugInGait models, as observed in Figure 3.15.

Table 3.3 – Anthropometric measuring protocol.

Anthropometric Measurement	Measuring Instrument	Definition
Height (cm)	Combined digital weighing scale and height rod	Standing in the centre of the weighing scales in an anatomical position the subject is measured from soles of feet to the corresponding height value when the rod rests on top of the head.
Weight (Kg)	Combined digital weighing scale and height rod	Standing in the centre of the weighing scales and the weight read of the digital display.
Shoe Size (UK)	Wooden measuring stick 	The outer size for the total length of the sole of the shoe.
Foot Size (UK)	Wooden measuring stick	From toe to heel when standing with feet flat.
Foot Width (cm)	Outside measuring calliper and a solid ruler attached to a desk 	Width of foot from medial aspect to lateral aspect from widest point at the level of the first metatarsal head.

Ankle Width (cm)	Outside measuring calliper and a ruler	From the medial malleolus of the tibia to the lateral malleolus of the fibula.
Knee Width (cm)	Outside measuring calliper and a ruler	The distance from the medial epicondyle to the lateral epicondyle of the femur.
Thigh/Leg Girth (cm)	Flexible measuring tape 	The circumference of the thigh 30% above the knee. 
Total Leg Length (cm)	Flexible measuring tape	From the bony prominence of the ASIS to the medial malleolus of the tibia when the leg is relaxed. 
Thigh Length (cm)	Flexible measuring tape	From bony prominence of the ASIS to the anterior aspect of the medial epicondyle of the femur. 
Lower Leg Length (cm)	Flexible measuring tape	From the anterior aspect of the lateral epicondyle of the femur to the medial malleolus of the tibia.
Tibial Torsion (-°)	'Jig' or Torsiometer with protractor scale	Leg is supported in the two U-shaped cushions with the patella and tibial tuberosity facing directly in the frontal plane. The two pointers are aligned with the midpoint of the medial malleolus and the apex of the lateral malleolus before the angle is measured on the protractor. 

Shoulder Offset (cm)	Outside measuring calliper and a ruler	After observing the arm rotating and slowing swinging backwards over the subject's head, place finger on the position of the humeral head centre and measure distance to the bony prominence at the acromioclavicular joint.
Elbow Width (cm)	Outside measuring calliper and a ruler	From the medial epicondyle to the lateral epicondyle of the humerus.
Wrist Width/ Thickness (cm)	Outside measuring calliper and a ruler	Measuring the thickness of the wrist at the midpoint at the level between the styloid process of the ulna to the styloid process of the radius.
Hand Thickness (cm)	Outside measuring calliper and a ruler	Thickness at the midpoint of the third metacarpal at the level just proximal to the third metacarpal head.

Table 3.4 – Description of the standard definitions for the marker positions of the lower limb.

Anatomical Location	Considerations to ensure correct placement for the lower limb markers
Anterior Superior Iliac Spines (ASIS)	Palpated by running thumb from a distal position upward to a proximal position until the thumb pushes up against the bony prominence. Keeping the thumb on this spot, place the marker directly above.
Posterior Superior Iliac Spines (PSIS)	Place a marker on each dimple which indicates the location of the two PSIS.
Knee	Palpate the lateral side of the distal femur and place the marker on the anterior aspect of the epicondyle.
Ankle	Place marker on the apex of the lateral malleolus of the fibula.
Forefoot	Placed anywhere along the length between the 2nd and 3rd metatarsals.
Heel	Marker is placed to align with the forefoot marker to 1) define the long axis of the foot and 2) ensure that the markers are parallel with the plantar surface of the foot. Positioning the head close to the floor and using a steel ruler to view the correct plane is the ideal method.  
Thigh	Wand is positioned on the lower lateral third of the femur ensuring that arm swing will not interfere or knock the wand.
Lower Leg *(Termed as Shank in Vicon)*	Wand is placed on the lower lateral third of the leg ensuring that it avoids the main bulk of the calf muscles which could induce unwanted movement.

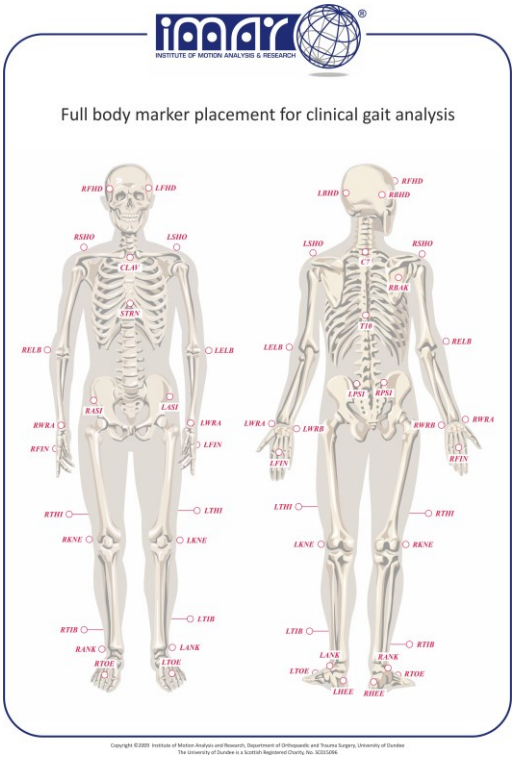

Figure 3.14 – Anatomical landmarks for full body marker placement (adapted from Institute of Motion Analysis and Research, 2013).

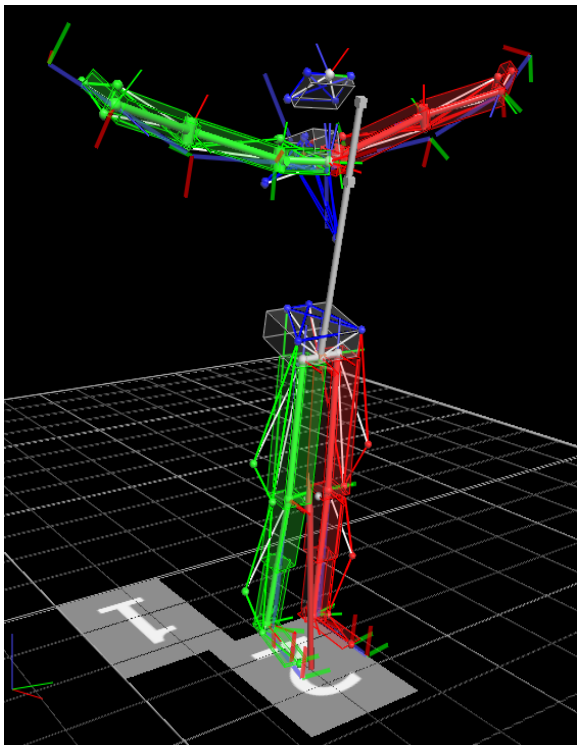

Figure 3.15 – Vicon® reconstruction of a static trial after labelling.

The importance of the thigh and lower leg markers being positioned on a stick/wand is to aid with defining the third plane (or z-axis) by creating a triangular segment. The correct alignment of these wand markers is imperative to the collection of viable data and is achieved by following the Dundee Mirror Technique as pictured in Figure 3.16. Firstly, the participant is positioned at a 90° angle parallel to a full length mirror with a walking frame available to provide support if required. The suject was asked to look straight ahead with their toes pointing directly anteriorly while maintaining a slight gap between both feet flat on the floor. The investigator ensures that the lower limbs are correctly positioned by asking the subject to flex both knees with the resultant movement only occuring in the sagittal plane when observing the subject from behind. The researcher repositions to sit on the floor facing the mirror, with the participant inbetween, and by viewing the reflection a steel ruler can be used as a guide to create a straight line. The 'visual line' observed in the reflection of the mirror is used to connect the surface point of where the greater trochanter of the femur is positioned with the lateral marker of the knee. The thigh wand is then adjusted to align with this straight line.

Figure 3.16 – Dundee Mirror Technique used to align the thigh and shank wand markers.

The process is repeated for the lower leg (or shank) wand which is aligned using the straight line visualised through the use of the ruler to connect the lateral knee marker with the ankle marker while the knee remains in a flexed position. Once the wand's markers have been aligned on both left and right legs, it is vital that the subject does not accidently knock or alter the correct position. If the markers become misaligned at any time, the mirror technique simply has to be repeated.

Following marker placement, the dominant leg was prepared for EMG using NūPrep abrasive gel, which was applied gently with a cotton bud, to remove dead skin cells that could introduce signal artefact. Surface EMG sensors are placed at specific anatomical points to limit 'cross talk' from nearby muscles and is standardised using the European SENIAM guide. Table 3.5 presents the protocol that was employed to ensure that the EMG data from all individuals remained constant to avoid subsequent confusion when analysing the results. Figure 3.17 provides an illustration of the correct electrode placement as described in Table 3.5.

To prevent the wires from moving and disconnecting with the box, all cables and wires were taped down to the leg using hypoallergenic transpore tape, which is highly adhesive yet gentle to skin. Care was taken to secure the wires and equipment at the preparation stage to ensure that, once the process of data collection was underway, there would be no disruptions, for example reprogramming the TMSi Mobi™ or Pedar-x® box if they became disconnected through the vigorous movements incurred during running.

Table 3.5 – Protocol developed for EMG connections in this study.

EMG Wire Connections	Channel	Attachment/Muscle	Electrode Position (*Black* = Top, *Red* = Bottom)
A/B	Channel One	Tibialis Anterior (TA)	25% from fibular head with the proximal electrode below the 25% line and in the direction of muscle fibres.
A/B	Channel Two	Peroneus Longus (PL)	25% from fibular head and placed anterior to the fibula with the proximal electrode below the 25% line.
C/D	Channel One	Lateral Gastrocnemius (LG)	On the lateral muscle belly at the same level as peroneus longus electrode (25% line).
C/D	Channel Two	Vastus Lateralis (VL)	24% from the tibial tubercle to the ASIS with the distal electrode on the 24% line.
Earth (Green Wire)	Reference	Clavicle (Bony prominence)	On the anterior surface.

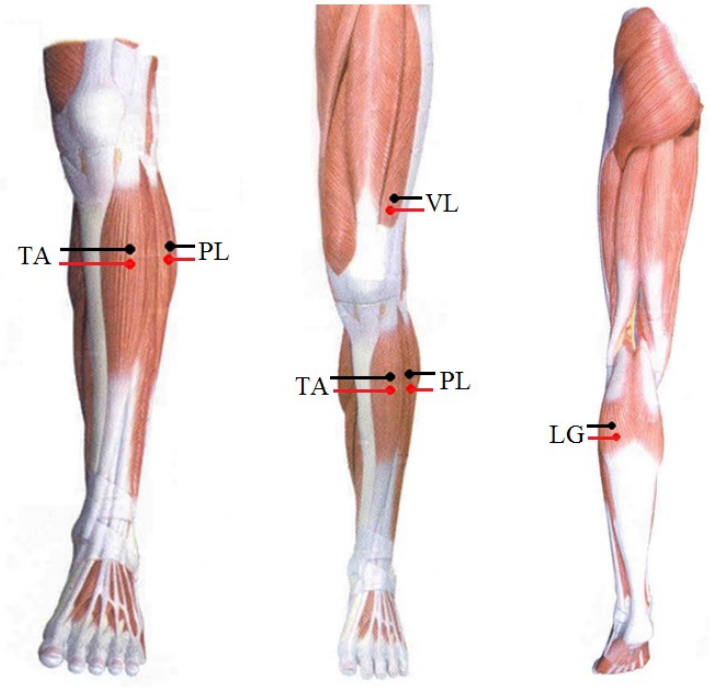

Figure 3.17 – EMG surface electrode placement (adapted from Saul (2013)).

All participants wore the same Nike Tiempo brand of shoe which are pictured in Figure 3.18 and wore the same style of black cotton socks. Different types of footwear attenuate peak ground reaction forces during the gait cycle and this highlights the importance of limiting and controlling all possible variables, including lacing of the shoes by the investigator (Fiedler *et al.,* 2011). The behaviour of the forefoot in particular is modified by wearing shoes as the overall contact time of the toes during the gait cycle is increased as a consequence of altered pressure distribution across the heads of the metatarsals (Soames, 1985). Pedar® insoles of the correct size were inserted into the shoe and connected to the Pedar-x® box port via specially designed cables. Once all of the wires were connected correctly and taped into place, the different components of the equipment were tested individually. The 'test connection' function of the Pedar® system was initiated and tested against the Bluetooth® link, and once this was recognised the insoles were individually set to zero when the relevant

Figure 3.18 – Photograph demonstrating the style and make of indoor football boots used as a standard in the study with sizes ranging from UK size 4 to UK size 10.

foot was confirmed as being lifted from the ground. To test the quality of the EMG signals, a practice sample was collected where the subject was instructed to tap the dominant foot five times and then perform specific movements (stand on tip toe, evert the foot, squat low to the ground, and extend the leg against a resisting downward force) to judge the action of the four respective muscles.

The equipment is fairly cumbersome for children as the general design is aimed for adult use, however, a specially adapted backpack carefully segregated the individual sections of equipment while at the same time providing a supportive structure for children to carry the contents without any difficulty. Figure 3.19(a) shows how all of the equipment and components connect together and Figure 3.19(b) demonstrates the bag in use.

(a) (b)

Figure 3.19 – Photograph of the equipment carried in modified back pack.
(a) EMG, Pedar-x®, Pedar® battery and radio sync box connected together with the insoles and EMG wires.
(b) Volunteer in the sports lab with markers and kit attached.

3.2.2.3 Trials

The floor of the Sports Laboratory was covered with astroturf® to recreate appropriate conditions that simulate football training, as Girard *et al.* (2007) established the importance of how surfaces can affect in-shoe pressure data. The astroturf® also acts to conceal the force plates further and orange cones were used to indicate the starting positions. The workstation layout of the integrated systems is pictured in Figures 3.20(a) and (b) and is positioned according to the protocol of collecting the trial data.

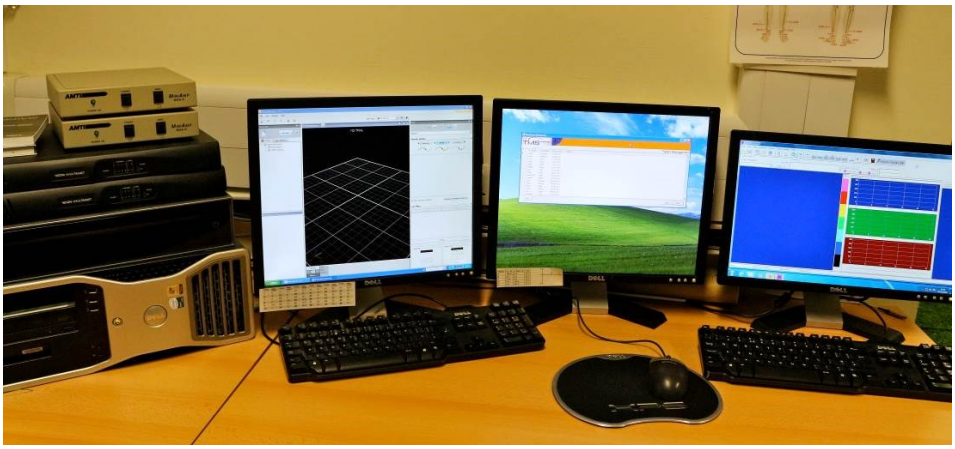

(a)

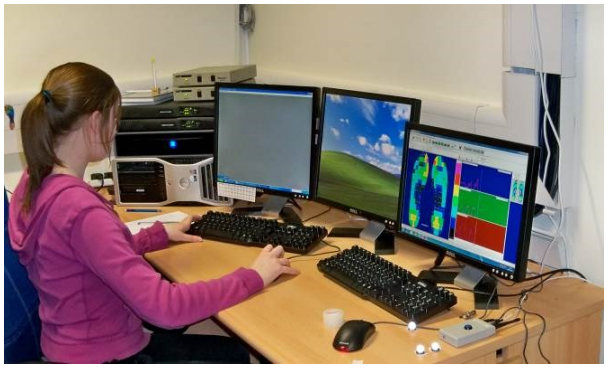

(b)

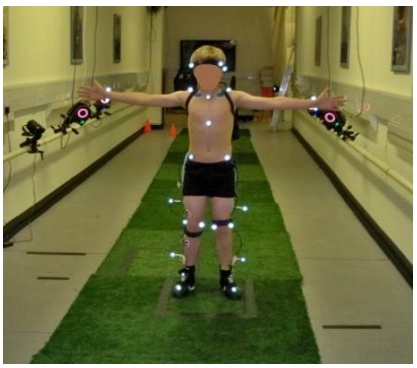

(c)

Figure 3.20 – Workstation layout positioned according to the protocol of data collection.

(a) Vicon®, Portilab™ and Pedar®.

(b) Preparing workstations for static trial.

(c) Correct static position conducted prior to the dynamic trials.

Starting from the left hand side the two ATMI® force plate zero boxes sit above two black MX Giganets that are placed upon the Vicon® workstation hard drive. The first two computer screens connect to the same hard drive and display the Vicon® software and EMG Portilab™ software respectively. The third computer screen is connected to a separate hard drive and is responsible for displaying the Pedar® software. A small grey box, located to the far right of the work space and which connects to the mains power supply, houses a blue button which initiates the radio pulse signal via Bluetooth® and simultaneously synchronises an identical pulse in Vicon®.

Initially the force plates are reset to zero and the participant is instructed to stand with both feet on force plate two, facing anteriorly with both arms held out to the side and thumbs pointing up towards the ceiling. The static position is represented by Figure 3.20(c) and is captured for 3 seconds before being reconstructed in Vicon® to act as a check and ensure that all markers are visible and correctly placed. Due to the size of the bag in relation to the overall size of some of the subjects, it was necessary in the case of smaller individuals to wear two additional markers at the same level as the PSIS markers. During running trials particularly, the bag occasionally concealed the PSIS markers; therefore it was deemed permissible to position extra markers on the same line in order to define and represent the location of these PSIS markers. The ASIS markers create the frontal plane of the pelvis and these are the influencing points utilised by the algorithms within Vicon® to calculate the kinetic and kinematic data. An additional static trial was then repeated on force plate one to affirm the quality assurance once again.

Prior to recording the active trials, the participants acquainted themselves with the equipment by walking in a normal fashion along the walkway to help adopt their

natural gait. The practice walks also aided the investigator by helping to position where the start line would be so that the force plates fell within the correct location for collecting data of the entire foot at the centre of the plates. For dynamic trials, the researcher indicated when to begin the trial by shouting, "On your marks, get set, on you go." While shouting out the starting instructions, the simultaneous protocol of starting the recording of all of the equipment began with zeroing the force plate, starting the dynamic trial of Vicon®, clicking the EMG Portilab™ start button, followed by initiating Pedar® with the start button before finalising the radio sync pulse to coincide approximately when the subject reaches the concealed force plates. This process was reversed to stop each component in a mirrored pattern, firstly stopping Pedar® and following this by the cessation of EMG and then Vicon®.

The participants were instructed to walk at a self-selected velocity to represent walking function as a whole. If an individual is forced to walk at an unnatural pace from what is typically experienced day-to-day, this has been found to increase gait asymmetry in children (Bosch and Rosenbaum, 2010); ultimately negating normal function and modifying the resultant gait pattern. A minimum number of three clear walking trials displaying both right and left force plate data were required for each subject, therefore multiple walking trials were recorded to guarantee the quality of data acquired. Once the walking trials were complete, the volunteer was instructed to run at a self-selected running speed with the only guide of "not quite sprinting but running at a speed that you are able to maintain over several trials and that you might usually encounter during sports training/P.E. lessons." Standardising the running speed has not been found to significantly affect the reproducibility of kinetic and kinematic data (Queen *et al.*, 2006) and ensured that participants did not feel any pressure to exert an uncomfortable level of physical activity during the collection of data.

3.3 Chapter Summary

To summarise the content of chapter three, qualitative and quantitative analysis of bone growth through the use of MRI can aid with the holistic interpretation of biomechanical effects upon the ossification and subsequent development of the long bones in a revolutionary way. The incorporation and synchronisation of numerous systems and specialised equipment further reveals the convoluted interaction of the underlying skeletal, muscular, and neurological components of gait, which must be understood collectively before assessment can be made on individual parameters.

Chapter 4

Experimental Results and Statistical Analysis

4.1 Preparation of the Primary data

Following the completion of data collection as described in Chapter 3, the raw data was converted and prepared into the formats suitable for subsequent analysis.

4.1.1 MRI Scans

The MR images are automatically stored on the NHS PAC system in a DICOM format for safe, secure storage and to allow the clinical radiologist to blind report medical findings. The DICOM files were copied anonymously from the PACS system onto a CD which was then stored in a secure locker only accessible by the researcher. The T2 program developed within MATLAB® has built-in code to execute the handling of DICOM files and a function to sort and prepare the overlay of the individual images automatically. OsiriX™ is an advanced DICOM software reader and therefore is exceptionally easy and straightforward to navigate once the data is loaded. The Endpoint software differs from the other two programs in that the DICOM files must be converted to an Analyze format prior to recognition and becoming accepted. The Analyze file size introduced one or two minor malware bugs to the software which temporarily crashed the program. Subsequently this `was overcome by reducing the file size by 50% while maintaining the isotropic dimensions necessary for segmenting the three dimensional structure and nature of the ROI.

4.1.2 Pedar® Files

The raw SOL file of each trial was required to be exported into an ASCII format. Once a folder was created with copies of clean, clear trials; the Group Editor package of Novel® was used to process the selected files and save the trial data in a new group in the required parity archive (PAR) file format. The Novel® Groupmask Evaluation

function package selects the relevant group to undergo assessment and the IMAR mask segregates the in-shoe pressure data of each foot into 10 smaller defined regions. The option of analysing 'statistics over the steps' in each individual trial was selected to generate the resultant output of final data.

4.1.3 Vicon® Files

The Vicon® files were reconstructed by running the "Reconstruct" pipeline and labelled according the full body anatomical landmarks previously described in Chapter 3. The process was conducted manually by selecting a marker to label which proceeded to automatically advance to the next unlabelled trajectory label until all 35 markers were labelled in a single frame. Once labelled, any gaps or small breaks in the trajectory between sequential frames were filled using the 'pick source pattern fill' tool if less than three frames were missing a marker. Occasionally the tracking algorithm was affected by small, undetectable breaks which caused the label of one marker to 'jump' onto an adjacent, erroneous trajectory. This occurred most commonly between the ankle and heel markers, which are closely associated, and could easily be identified and rectified if each frame was individually checked. A single walking trial in the sports laboratory can typically span approximately 285 frames, therefore the quality assurance process of the data can be substantially lengthy.

A static Plug-in Gait pipeline was run on a labelled three second static trial of the individual. This utilises the calibrated measurements of the 5 marker L-shaped calibration wand to correctly orientate and calculate subsequent algorithms generated by the full body markers in relation to the camera positions within the laboratory. The dynamic Plug-in Gait pipeline was then run for all dynamic trials and this function incorporates the processed static trial calibration measurements. Once the dynamic

Plug-in Gait pipeline has been selected, the gait cycle events are detected, the Woltring filtering routine is applied, events are autocorrelated, a Virtual Path Identifier (VPI) Compatibility package is run for the dynamic gait model and finally the output data is exported as a C3D file which is a compatible format to open the data within Polygon®. Due to the fast nature of the running trials, the 'foot strike' and 'foot off' events were not detected automatically for the cycles when the foot did not contact the force plates; this resulted in the researcher inserting the events manually by synchronising the Vicon® and Pedar® data to check for accuracy in the final placement. One of the main functions of Polygon® was to check the quality of the numerical data within Vicon® by using the normalised average graphs to ensure that alignment of the thigh and lower leg wands were correct. Tibial torsion, shank rotation and tibial rotation were also checked in reference to a normal averaged database. On completion, three good trials were exported for each foot (left and right) to an ASCII advanced, tab delimited format. The marker file was selected and the following variables were chosen to undergo statistical analysis:

- Angles (Pelvis, Hip, Knee, Ankle)
- Forces (Waist, Hip, Knee, Ankle)
- Moment (Waist, Hip, Knee, Ankle)
- Power (Waist, Hip, Knee, Ankle)
- Centre of Mass

4.2 Statistical Analysis

4.2.1 Intra and Inter-observer Error

The primary investigator and an MRI expert worked together to define the ROI and boundaries for measuring each of the growth plate volumes of the knee and ankle. Inter-observer error was tested using the Endpoint software due to the semi-automatic recognition of the epiphyseal outline which was thought to consequently be more repeatable and less subjective in nature. The observers outlined, measured and calculated each growth plate volume twice for the distal femur, proximal tibia, distal tibia and calcaneus which were then assessed using the Intraclass Correlation Coefficient as summarised in Table 4.1.

The nature of the compositionally 'layered' appearance of the growth plate only displays an observable tri-laminar appearance in the distal femoral epiphyseal plate and distal tibial epiphyseal plate; consequently resulting in a slightly different approach being applied to define and measure the total segment. The three layers are evident in Figure 4.1 where the main physis of the growth plate is clearly the brightest band and separated from another bright line (the primary spongiosa) by a dark line which denotes the zone of cartilage transformation. The bright physis was measured initially and the total segmented volume calculated, however a second measurement then calculated the TOTAL growth plate boundary as defined by the occasionally difficult to delineate layer of the primary spongiosa representing mineralisation of the cartilage. All other growth plates of the lower limb only displayed two visual layers and failed to represent clearly the primary layer of spongiosa. Therefore, the proximal tibial growth plate and traction growth plate of the calcaneus were unable to have a TOTAL volume calculated

Table 4.1 – Intraclass Correlation Coefficient comparing the measurements of the primary investigator and measurements of a medical physics expert.

	Intraclass Correlation[a]	*95% Confidence Interval*		F Test with True Value 0			
		Lower Bound	*Upper Bound*	Value	Degrees of Freedom 1	Degrees of Freedom 2	**Significance**
Single Measures	0.949[b]	0.908	0.975	75.697	23	69	0.000
Average Measures	0.987[c]	0.975	0.994	75.697	23	69	0.000

****Two-way mixed effects model where people effects are random and measures effects are fixed.*

a – Type C intraclass correlation coefficients using a consistency definition. The between measure variance is excluded from the denominator variance.

b – The estimator is the same, whether the interaction effect is present or not.

c – This estimate is computed assuming the interaction effect is absent, because it is not estimable otherwise.

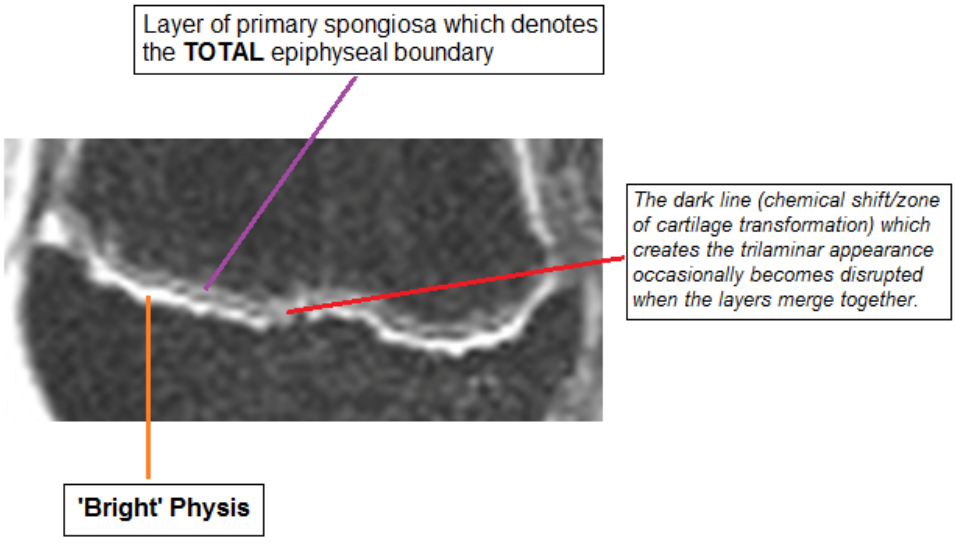

Figure 4.1 – Visualisation of the distal femoral growth plate and the two different superior boundaries. The first boundary is the bright band of the physis outlined as far as the dark line and the second boundary is the TOTAL measurement, which includes the additional layer of the primary spongiosa. The red line illustrates a small area where disruption has occurred which can make measuring difficult for the observer.

as a supplement to the typical physeal layer. The inter-observer correlation results for the calculation of the distal femoral, proximal tibial and distal tibial growth plate volumes were found to be very highly significant ($p < 0.001$) for both single and average measurements of the two observers. No significant differences were encountered when assessing the errors in the inter-observer data and this positive result was similar for the calculation of single and average measurements of intra-observer errors, which was also not found to be significantly different.

4.2.2 Growth Plate Volumetric Data

The dataset for all of the growth plate volumes was shown to follow a normal distribution as calculated by the One-Sample Kolmogorov-Smirnov Test for both the control and active groups. Levene's Test for Equality of Variances was then applied to the data to ensure that the variance of the group samples were equal which is the second assumption required before applying an Independent Samples T-Test. Table 4.2 summarises the results of the T-Test which measures the Equality of Means between the active and control group.

A significance level of $p \leq 0.01$ was selected to mark the minimal level of significance required for the T-Test results due to the small sample size. Consequently, the results of the T-Test do not highlight any significant differences between the active and control groups. Although the growth plate volumes do not show any significant statistical differences, there is clearly a definite trend and relationship within the individual groups when the correlations of the active and control groups are analysed separately (refer to correlation tables in Appendix O).

Table 4.2 – Independent Samples T-Test for the equality of means to show differences in the growth plate volumes of the active and control groups.

Independent Samples	$\bar{x}$	σ	Levene's Test		T-Test		
			F Value	p	t	Degrees of Freedom	p
Endpoint Femoral (cm^3) *Control* *Active*	 *4.73* *4.40*	 *0.72* *1.41*	1.563	0.222	0.807[a]	28[a]	0.427[a]
Endpoint TOTAL Femoral (cm^3) *Control* *Active*	*8.49* *7.74*	*1.61* *3.06*	2.166	0.152	0.839[a]	28[a]	0.408[a]
T2 Map Femoral (cm^3) *Control* *Active*	 *4.51* *4.63*	 *0.88* *1.90*	4.848	0.038	-0.221[a]	24[a]	0.827[a]
Endpoint Proximal Tibial (cm^3) *Control* *Active*	*4.71* *3.76*	*0.99* *1.76*	4.507	0.043	1.829[a]	28[a]	0.078[a]
T2 Map Proximal Tibial (cm^3) *Control* *Active*	 *3.60* *3.42*	 *0.80* *1.98*	15.738	*0.001*	0.296[b]	14.061[b]	0.772[b]
Endpoint Distal Tibial (cm^3) *Control* *Active*	*2.33* *1.96*	*0.33* *1.10*	11.863	*0.002*	1.248[b]	16.487[b]	0.229[b]
Endpoint TOTAL Distal Tibial (cm^3) *Control* *Active*	 *3.69* *3.39*	 *0.90* *2.01*	6.019	0.021	0.517[a]	28[a]	0.609[a]
T2 Map Distal Tibial (cm^3) *Control* *Active*	 *2.28* *2.42*	 *0.72* *1.45*	6.507	0.017	-0.341[a]	25[a]	0.736[a]
Endpoint Calcaneal (cm^3) *Control* *Active*	 *1.83* *1.55*	 *0.67* *1.13*	7.983	*0.009*	0.833[b]	22.695[b]	0.414[b]
T2 Map Calcaneal (cm^3) *Control* *Active*	 *1.29* *1.20*	 *0.74* *0.87*	0.929	0.344	0.316[a]	25[a]	0.754[a]

[a]Equal variances assumed – F value defined at level of ≤ 0.01 significance.
[b]Equal variances not assumed – F value defined at level of ≤ 0.01 significance.

The volumetric measurements of the active group growth plates in the dominant lower limb were found to have stronger relationships overall, compared to the growth plate volumes within the control group. Tables 4.3, 4.5 and 4.7 display the significance of the relationships within the active group when assessing the different growth plates as measured by the same technique. The correlations can be compared to the control group where the significance of the relationships are described in Tables 4.4, 4.6 and 4.8.

The different trend of each relationship between the two groups is evident when considering the Endpoint volumes for the growth plates of the tibia (proximal tibial and distal tibial) in addition to the Endpoint volumes of the knee and foot (proximal tibial and calcaneal). The relationships overall are significantly stronger in the active group for the Endpoint measurements of the proximal and distal tibia ($p < 0.001$ and $p = 0.328$ for the active and control groups respectively) and the Endpoint measurements of the proximal tibia and calcaneus ($p = 0.006$ and $p = 0.998$ for the active and control groups respectively). Interestingly, the TOTAL growth plate volumes measured within Endpoint prove to have equally significant correlation $p < 0.001$ for both the active and control groups. This stark difference of the Endpoint and TOTAL Endpoint volumes suggests that the outline of the growth plates are perhaps more difficult to define reliably when the tri-laminar form appears disrupted, even with the aid of the semi-automatic outlining 'livewire' tool.

The T2 mapping method is not only faster in permitting the calculation of growth plate volumes; however the resultant correlations illustrate the T2 mapping method also shows a greater degree of concordance when comparing the active and control groups. The majority of volumetric relationships within both the active and control groups are

at a very highly significant level ($p \leq 0.001$); however, the underlying trend is still largely stronger within the active group. The fact that the T2 map method relies on algorithmic delineation of the cut-off threshold for growth plate cartilage may explain the increased statistical significance compared to the Endpoint measurements, which are more dependent on the subjectivity of the observer.

Table 4.3 – Relationship of the growth plate volumes within the active group measured by Endpoint and the bright layer of the physis.

Active Group Variables *Endpoint Growth Plate Volumes*	Pearson Correlation (r)	R^2	Significance (p)
Endpoint Distal Femoral (AES01) vs Endpoint Proximal Tibial (AES01)	0.681	0.464	0.005
Endpoint Distal Femoral (AES01) vs Endpoint Distal Tibial (AES01)	0.624	0.389	0.013
Endpoint Distal Femoral (AES01) vs Endpoint Calcaneal (AES01)	0.460	0.212	0.085
Endpoint Proximal Tibial (AES01) vs Endpoint Distal Tibial (AES01)	0.853	0.728	0.000
Endpoint Proximal Tibial (AES01) vs Endpoint Calcaneal (AES01)	0.673	0.453	0.006
Endpoint Distal Tibial (AES01) vs Endpoint Calcaneal (AES01)	0.818	0.669	0.000

***Green denotes p value is very highly significant (0.000-0.001), yellow denotes p value is highly significant (0.001-0.01) and orange denotes p value is significant (0.01-0.05).

Table 4.4 – Relationship of the growth plate volumes within the control group measured by Endpoint and the bright layer of the physis.

Control Group Variables *Endpoint Growth Plate Volumes*	Pearson Correlation (r)	R^2	Significance (p)
Endpoint Distal Femoral (AES01) vs Endpoint Proximal Tibial (AES01)	0.572	0.327	0.026
Endpoint Distal Femoral (AES01) vs Endpoint Distal Tibial (AES01)	0.732	0.536	0.002
Endpoint Distal Femoral (AES01) vs Endpoint Calcaneal (AES01)	0.043	0.002	0.879
Endpoint Proximal Tibial (AES01) vs Endpoint Distal Tibial (AES01)	0.271	0.073	0.328
Endpoint Proximal Tibial (AES01) vs Endpoint Calcaneal (AES01)	0.001	0.000	0.998
Endpoint Distal Tibial (AES01) vs Endpoint Calcaneal (AES01)	0.623	0.388	0.013

***Green denotes p value is very highly significant (0.000-0.001), yellow denotes p value is highly significant (0.001-0.01) and orange denotes p value is significant (0.01-0.05).

Table 4.5 – Relationship of the growth plate volumes within the active group measured by the TOTAL Endpoint definition of layer.

Active Group Variables *Endpoint TOTAL Growth Plate Volumes*	Pearson Correlation (r)	R^2	Significance (p)
Endpoint TOTAL Distal Femoral (AES01) vs Endpoint TOTAL Distal Tibial (AES01)	0.814	0.663	0.000

***Green denotes p value is very highly significant (0.000-0.001), yellow denotes p value is highly significant (0.001-0.01) and orange denotes p value is significant (0.01-0.05).

Table 4.6 – Relationship of the growth plate volumes within the control group measured by the TOTAL Endpoint definition of layer.

Control Group Variables *Endpoint TOTAL Growth Plate Volumes*	Pearson Correlation (r)	R^2	Significance (p)
Endpoint TOTAL Distal Femoral (AES01) vs Endpoint TOTAL Distal Tibial (AES01)	0.796	0.634	0.000

***Green denotes p value is very highly significant (0.000-0.001), yellow denotes p value is highly significant (0.001-0.01) and orange denotes p value is significant (0.01-0.05).

Table 4.7 – Relationship of growth plate volumes in the active group as measured by T2 mapping.

Active Group Variables *T2map Growth Plate Volumes*	Pearson Correlation (r)	R^2	Significance (p)
T2map Distal Femoral (AES01) vs T2map Distal Tibial (AES01)	0.900	0.81	0.000
T2map Distal Femoral (AES01) vs T2map Proximal Tibial (AES01)	0.915	0.837	0.000
T2map Distal Femoral (AES01) vs T2map Calcaneal (AES01)	0.746	0.557	0.005
T2map Proximal Tibial (AES01) vs T2map Distal Tibial (AES01)	0.912	0.832	0.000
T2map Proximal Tibial (AES01) vs T2map Calcaneal (AES01)	0.685	0.469	0.014
T2map Distal Tibial (AES01) vs T2map Calcaneal (AES01)	0.875	0.766	0.000

***Green denotes p value is very highly significant (0.000-0.001), yellow denotes p value is highly significant (0.001-0.01) and orange denotes p value is significant (0.01-0.05).

Table 4.8 – Relationship of the growth plate volumes within the control group measured by the T2 map.

Control Group Variables *T2map Growth Plate Volumes*	Pearson Correlation (r)	R^2	Significance (p)
T2map Distal Femoral (AES01) vs T2map Distal Tibial (AES01)	0.898	0.806	0.000
T2map Distal Femoral (AES01) vs T2map Proximal Tibial (AES01)	0.732	0.536	0.003
T2map Distal Femoral (AES01) vs T2map Calcaneal (AES01)	0.730	0.533	0.003
T2map Proximal Tibial (AES01) vs T2map Distal Tibial (AES01)	0.836	0.699	0.000
T2map Proximal Tibial (AES01) vs T2map Calcaneal (AES01)	0.741	0.549	0.002
T2map Distal Tibial (AES01) vs T2map Calcaneal (AES01)	0.793	0.629	0.000

***Green denotes p value is very highly significant (0.000-0.001), yellow denotes p value is highly significant (0.001-0.01) and orange denotes p value is significant (0.01-0.05).

4.2.3 Magnetic Resonance Imaging 'Incidental' Findings

Visualising the morphological form of anatomical structures in MR images, through the use of OsiriX®, was valuable in attaining the necessary understanding of the functional interactions within each individual; particularly when ascertaining whether the relationship of the growth plate volumes supported the final statistical results. The ability to determine the fusion pattern of a growth plate, or identify damage to the growth plate by the presence of an intersecting bridge of bone, can be used tentatively as evidence to support potential findings of biomechanical discrepancies encountered between different individuals.

A clinical radiologist, who was blind to the activity status of each participant, identified the MRI findings of this research which are detailed in Tables 4.9 and 4.10. Approximately 80 percent of the active group (12 out of 15 individuals) displayed an incidental anomaly at the knee which was also true for the percentage of incidental findings at the foot and ankle. Conversely, approximately 47 percent of the control group encountered an incidental anomaly at the knee while at the foot and ankle this percentage increases to 67 percent of the group.

One of the most interesting observations was that nineteen instances of oedema-like signal were identified in the bone marrow of the active group (ratio of 0.9:1 for the knee to foot) which signifies the existence of bruising to the bone. This observation differs from the control group, where ten occurrences of oedema-like signal were found in the bone marrow (ratio of 1:4 for the knee to foot). Figures 4.2 to 4.5 illustrate a selection of the asymptomatic anomalies encountered during this research.

Table 4.9 – Observation of MRI incidental findings in the active and control group for the knee.

Observation of Anomalies in Knee	Active Group *Number and % of Incidences*		Control Group *Number and % of Incidences*	
Bone Marrow Oedema	9	*60%*	2	*13%*
Focal Tendinosis	2	*13%*	2	*13%*
Subchondral Bone Irregularity	3	*20%*	3	*20%*
Osteochondrial Signal Abnormality	1	*7%*	-	-
Baker's Cyst	1	*7%*	-	-
Pedunalated Osteochondroma *(Developmental)*	1	*7%*	-	-
Osgood Schlatters	1	*7%*	-	-
Oedema in Vastus Lateralis Muscle (relating to Baker's Cyst)	1	*7%*	-	-
Lesion Projecting into Hoffa's Fat Space	1	*7%*	-	-
Joint ganglion	2	*13%*	1	*7%*
Lateral patellar tilt	-	-	1	*7%*
Bipartite patella (normal variant)	2	*13%*	-	-
OCD style osteochondral lesion	-	-	1	*7%*
Partially discoid lateral meniscus	-	-	1	*7%*
Total	**24**		**11**	

***No abnormalities detected in 3 of the active boys and 7 control boys.

Table 4.10 – Observation of MRI incidental findings in the active and control group for the foot.

Observation of Anomalies in Foot	Active Group *Number and % of Incidences*		Control Group *Number and % of Incidences*	
Bone Marrow Oedema	10	*67%*	8	*53%*
Os trigonum	3	*20%*	1	*7%*
Subchondral Bone Irregularity	2	*13%*	1	*7%*
Osteochondrial Signal Abnormality	2	*13%*	2	*13%*
Separated Bone Fragment	1	*7%*	-	-
Bony Impaction	9	*60%*	4	*27%*
Synovitis	1	*7%*	-	-
Tenosynovitis in Flexor Hallucis Longus Tendon Sheath	1	*7%*	-	-
Loculated fluid collection	-	-	1	*7%*
Increased Signal at Plantar Fascial Insertion	1	*7%*	-	-
Total	**30**		**17**	

***No abnormalities detected in 3 of the active boys and 5 control boys.

(a)

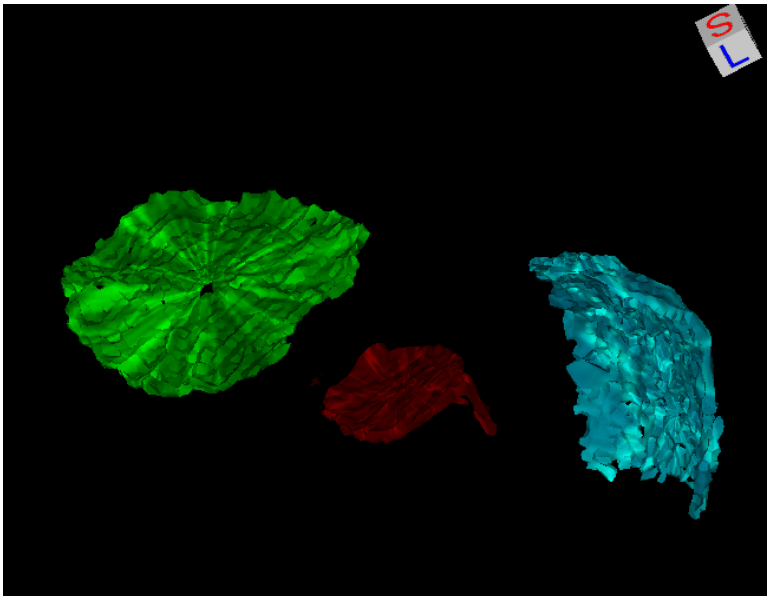

(b)

<u>Figure 4.2</u> – MR image of a prior injury on the superior surface of the calcaneus discovered as an incidental finding in one of the controls.

(a) Purple arrow denotes site of bony impaction.

(b) 3D reconstructions of the distal tibial (green), distal fibular (red) and calcaneal (light blue) epiphyses in the same ankle.

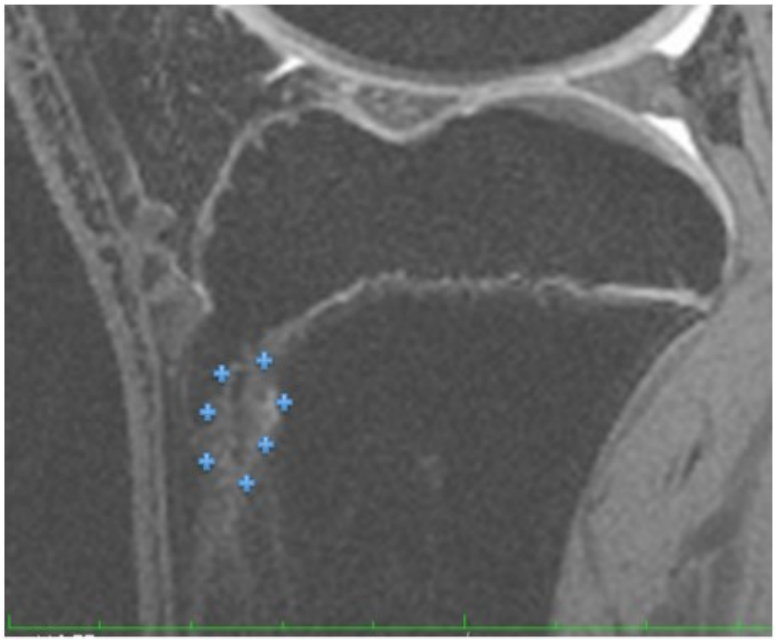

(a)

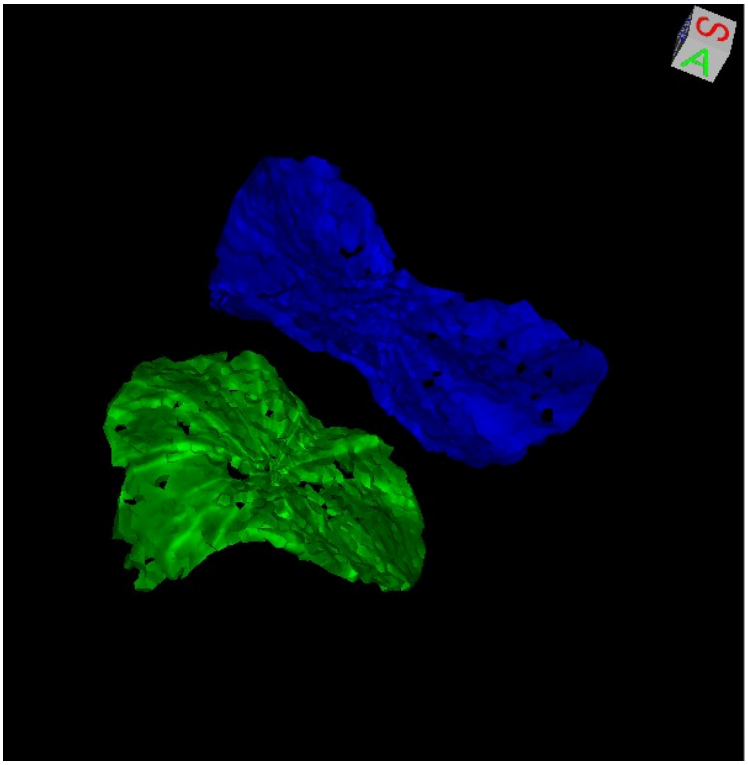

(b)

<u>Figure 4.3</u> – MR image displaying a traction reaction of the tibial apophysis in an active individual.

(a) Area of tibial apophysis outlined by blue markers.

(b) 3D reconstructions of the femoral (dark blue) and proximal tibial (green) epiphyses in the same individual.

(a)

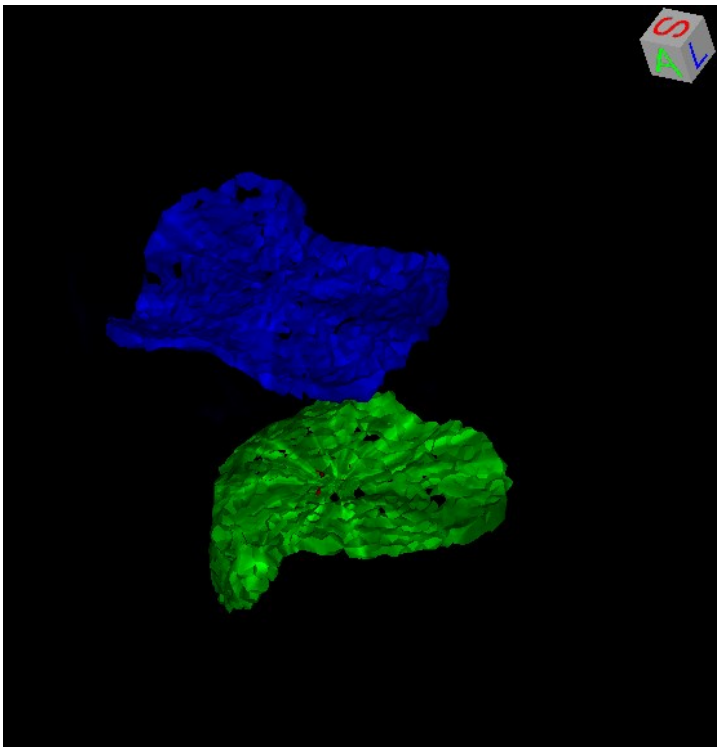

(b)

<u>Figure 4.4</u> – MR image revealing longitudinal extensions of the epiphyseal cartilage signal into the metaphysis which was reported as likely bone bruising of the femoral lateral metaphysis in an active individual.

(a) Yellow arrows highlight sites of disrupted growth.

(b) 3D reconstructions of the femoral (dark blue), proximal tibial (green) and obscured proximal fibular (red) growth plates of the same individual.

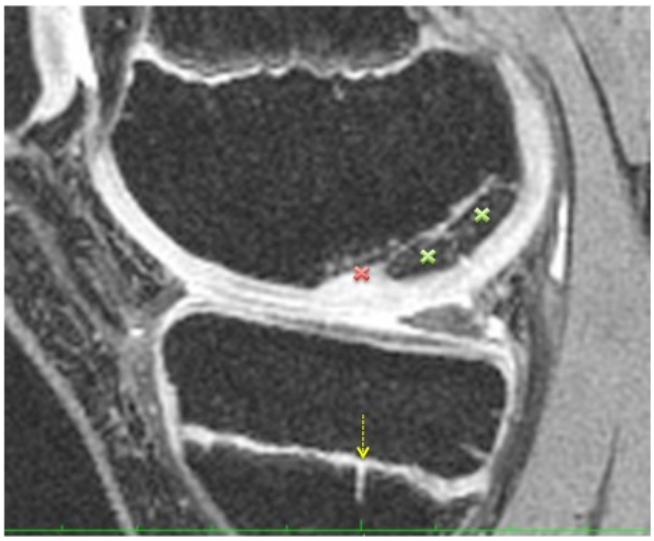

(a)

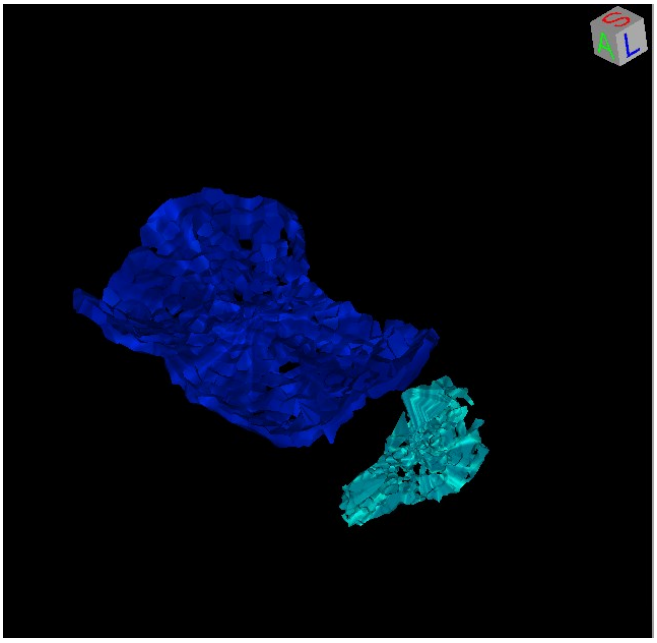

(b)

<u>Figure 4.5</u> – MR image displaying a large osteochondral style lesion on the posterior aspect of the femur in a control individual.

(a) Two green markers reveal fragments of bone separated by the osteochondral style lesion which has severely damaged the area of bone that should be located at the red marker. Although the individual had not participated in any team sports for some time, he previously played hockey occasionally during school intervals. The dotted yellow arrow highlights a longitudinal extension of the epiphyseal cartilage signal into the tibial metaphysis.

(b) 3D femoral growth plate (dark blue) reconstruction in relation to the osteochondral style lesion (light blue) that was also outlined in OsiriX™.

As a separate consideration to this research, the ability to further extract information from the MRI scans with regard to observing incidental findings, such as bone marrow oedema, may be achieved by enhancing subtle signal differences through the transformation of greyscale pixels into another range of colours. The MR images in this research did not have a set window to lock each scan at the same greyscale level, therefore Figures 4.6 and 4.7 are unable to be compared with any scientific reliability. Nevertheless, simply changing the colour look-up table (CLUT) from 'No CLUT' to 'Flow' illustrates that it may be possible for bone marrow oedema signal changes in the DESS scans to be perceived using gradient map tools. This technique has the potential to be further investigated as it may be interesting to note that in the fully fused example of the knee, Figure 4.7, there are no signal anomalies or disruptive patterns evident.

Figure 4.6 – DESS scan of the knee of an active individual with the colour look-up table (CLUT) set as 'Flow'.

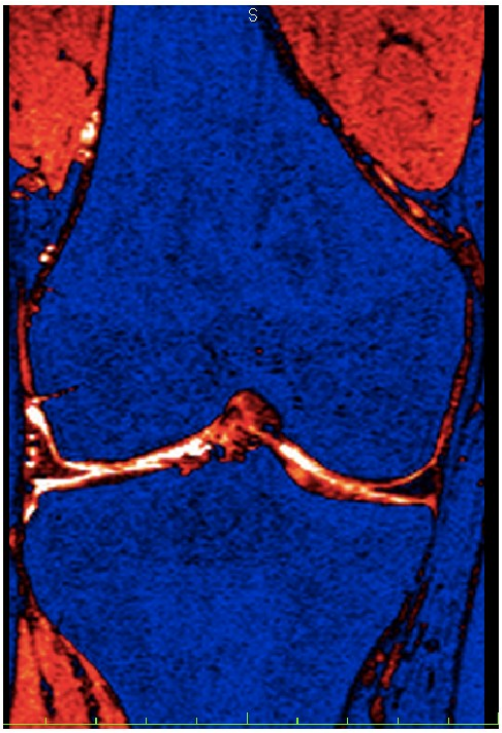

<u>Figure 4.7</u> – Active individual with fully fused distal femoral and proximal tibial epiphyses at 14 years with no disruption or darkening indicated when the CLUT is set to 'Flow'.

4.2.4 In-Shoe Pressure

Once the raw ASCII pressure data for each individual was separated into the relevant group (active or control) by using the Novel® Group Editor application, the Novel® Groupmask Evaluation tool was run to process and extract thirteen dependant variables for the right and left feet respectively. Each dependent variable was further divided into ten regional masks which are outlined in Figure 4.8 to define accurately the path of plantar pressure distribution across anatomical load bearing points of the foot. Due to the complexity of the data, a General Linear Model was run to calculate between-subject factors to summarise the mean of each variable descriptively. The Estimated Marginal Mean for each variable was also run to check the dependence of the individual variables for each group, prior to running Pairwise Comparisons tests for both walking and running.

The significance of the resultant mean differences between the active and control group for each of the Pairwise Comparisons that are most relevant for discussion are presented in Tables 4.11 to 4.20 and further detailed in Appendix H. On a statistical level, some of the masks on the right foot which are paired with a mirrored mask on the left were found to differ significantly; therefore it is for this reason that the left and right in-shoe pressure data were not combined. An example of a paired statistical difference between the left and right feet is highlighted in Table 4.17 which summarises the mean differences between the active group and control group for each mask with regard to the Maximum Force Totals. Mask 7 (left foot) and Mask 17 (right foot) differ in their level of significance between the active and control groups. The Maximum Force Total when walking with the right foot showed a p value of 0.001 however the left foot p value is not significant at 0.815. Although one or two individual masks were

shown to differ significantly across the left and right feet, once the data was normalised for a single, average gait cycle and plotted in Excel, the graphical presentation of the data clearly showed that a similar path of pressure distribution was being followed; albeit not at a highly significant level. A possible explanation for some mask differences, as in the case of mask 7, may be a consequence of collecting a wide range of pressure distribution due to the size and weight differences of this age cohort. The smaller 12 year old individuals, who had not yet attained the peak of their adolescent growth spurt, when compared with some of the older 14 year olds, who were close to having attained full adult height, consequently displayed an extremely large range of pressure. Mask 7 is only one cell wide and located at the edge of the shoe and as some of the boys had narrow feet, this may explain the reason for occasional significant differences in a diminutive area.

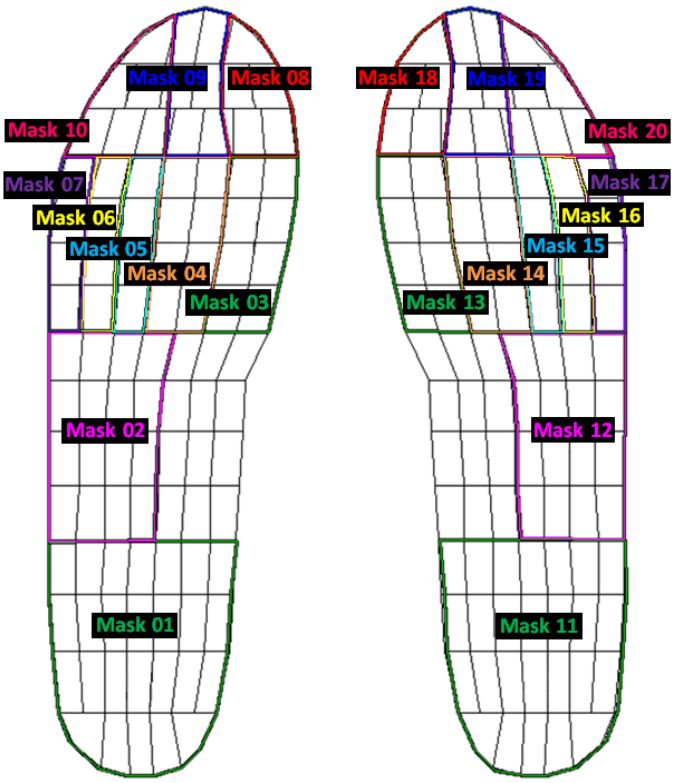

Figure 4.8 – Illustration of the ten regional Pedar masks developed within IMAR to analyse the left and right foot in-shoe pressures respectively.

Table 4.11 – Pairwise Comparisons comparing the active and control group contact areas total (cm^2) while running.

Mask (Left foot)	Mean Difference (Active minus Control)	$\bar{x}$	σ	p
Contact Areas M1	-9	31	10	0.000
Contact Areas M2	-3	23	5	0.008
Contact Areas M3	-1	13	2	0.004
Contact Areas M4	-1	12	2	0.007
Contact Areas M5	-1	7	1	0.001
Contact Areas M6	0	6	1	0.068
Contact Areas M7	0	6	1	0.006
Contact Areas M8	-1	8	1	0.000
Contact Areas M9	-1	8	1	0.002
Contact Areas M10	-1	9	1	0.002

Mask (Right foot)	Mean Difference (Active minus Control)	$\bar{x}$	σ	p
Contact Areas M11	-10	32	10	0.000
Contact Areas M12	-3	24	4	0.000
Contact Areas M13	-1	12	2	0.001
Contact Areas M14	-1	13	2	0.001
Contact Areas M15	-1	6	1	0.002
Contact Areas M16	0	6	1	0.04
Contact Areas M17	-1	6	1	0.000
Contact Areas M18	-1	7	1	0.001
Contact Areas M19	-1	8	1	0.001
Contact Areas M20	-1	8	2	0.005

****Green* denotes p value is very highly significant (0.000-0.001), *yellow* denotes p value is highly significant (0.001-0.01) and *orange* denotes p value is significant (0.01-0.05). The mean difference values are rounded to the nearest whole number.*

Table 4.12 – Pairwise Comparisons comparing the active and control group maximum force total (N) while running.

Mask (Left foot)	Mean Difference (Active minus Control)	$\bar{x}$	σ	p
Maximum Force M1	-169	410	193	0.000
Maximum Force M2	-36	189	79	0.034
Maximum Force M3	-13	199	61	0.309
Maximum Force M4	8	181	57	0.497
Maximum Force M5	4	92	29	0.518
Maximum Force M6	0	76	24	0.955
Maximum Force M7	2	62	24	0.720
Maximum Force M8	-13	172	61	0.340
Maximum Force M9	12	83	20	0.006
Maximum Force M10	13	84	25	0.011

Mask (Right foot)	Mean Difference (Active minus Control)	$\bar{x}$	σ	p
Maximum Force M11	-215	421	198	0.000
Maximum Force M12	-40	191	66	0.004
Maximum Force M13	-4	215	77	0.814
Maximum Force M14	6	188	57	0.648
Maximum Force M15	5	90	25	0.349
Maximum Force M16	1	73	20	0.722
Maximum Force M17	-6	64	21	0.201
Maximum Force M18	14	166	53	0.230
Maximum Force M19	21	80	19	0.000
Maximum Force M20	12	80	25	0.029

****Green* denotes p value is very highly significant (0.000-0.001), *yellow* denotes p value is highly significant (0.001-0.01) and *orange* denotes p value is significant (0.01-0.05). The mean difference values are rounded to the nearest whole number.*

Table 4.13 – Pairwise Comparisons comparing the active and control group peak pressure total (kPa) while running.

Mask (Left foot)	Mean Difference (Active minus Control)	$\bar{x}$	σ	p
Peak Pressure M1	-56.02	197	79	0.001
Peak Pressure M2	-5.69	113	35	0.454
Peak Pressure M3	10.45	253	87	0.577
Peak Pressure M4	42.09	214	48	0.000
Peak Pressure M5	37.20	193	52	0.001
Peak Pressure M6	18.44	159	42	0.039
Peak Pressure M7	10.79	139	46	0.275
Peak Pressure M8	5.70	350	112	0.814
Peak Pressure M9	34.99	158	44	0.000
Peak Pressure M10	34.13	158	39	0.000

Mask (Right foot)	Mean Difference (Active minus Control)	$\bar{x}$	σ	p
Peak Pressure M11	-83.95	203	85	0.000
Peak Pressure M12	-6.28	113	28	0.292
Peak Pressure M13	42.96	267	97	0.038
Peak Pressure M14	36.43	213	54	0.001
Peak Pressure M15	41.39	185	45	0.000
Peak Pressure M16	18.74	153	33	0.007
Peak Pressure M17	-8.49	140	41	0.337
Peak Pressure M18	82.13	352	107	0.000
Peak Pressure M19	50.90	195	59	0.000
Peak Pressure M20	34.37	155	41	0.000

****Green* denotes p value is very highly significant (0.000-0.001), *yellow* denotes p value is highly significant (0.001-0.01) and *orange* denotes p value is significant (0.01-0.05).*

Table 4.14 – Pairwise Comparisons comparing the active and control group maximum mean pressure (kPa) while running.

Mask (Left foot)	Mean Difference (Active minus Control)	$\bar{x}$	σ	p
Mean Pressure M1	-28.55	109	40	0.001
Mean Pressure M2	-5.50	77	22	0.244
Mean Pressure M3	-1.43	160	37	0.856
Mean Pressure M4	19.07	148	30	0.002
Mean Pressure M5	18.37	139	35	0.013
Mean Pressure M6	7.74	121	29	0.220
Mean Pressure M7	11.18	104	31	0.94
Mean Pressure M8	6.24	209	60	0.629
Mean Pressure M9	23.05	103	26	0.000
Mean Pressure M10	24.15	98	24	0.000

Mask (Right foot)	Mean Difference (Active minus Control)	$\bar{x}$	σ	p
Mean Pressure M11	-38.91	113	40	0.000
Mean Pressure M12	-8.07	78	18	0.032
Mean Pressure M13	14.98	170	49	0.152
Mean Pressure M14	19.48	149	36	0.010
Mean Pressure M15	19.02	141	31	0.003
Mean Pressure M16	9.90	121	22	0.036
Mean Pressure M17	2.26	102	26	0.686
Mean Pressure M18	37.28	219	58	0.002
Mean Pressure M19	32.26	97	24	0.000
Mean Pressure M20	23.04	101	28	0.000

****Green* denotes p value is very highly significant (0.000-0.001), *yellow* denotes p value is highly significant (0.001-0.01) and *orange* denotes p value is significant (0.01-0.05).*

Table 4.15 – Pairwise Comparisons comparing the active and control group pressure-time integral (PTI) total while running.

Mask (Left foot)	Mean Difference (Active minus Control)	$\bar{x}$	σ	p
PTI Mask 1	-7.90	15	8	0.000
PTI Mask 2	-5.01	14	6	0.000
PTI Mask 3	-6.58	34	11	0.004
PTI Mask 4	-1.38	30	6	0.318
PTI Mask 5	-1.33	27	7	0.389
PTI Mask 6	-2.30	23	6	0.087
PTI Mask 7	-2.20	19	7	0.136
PTI Mask 8	-7.17	43	14	0.016
PTI Mask 9	0.84	22	6	0.530
PTI Mask 10	0.56	22	5	0.599

Mask (Right foot)	Mean Difference (Active minus Control)	$\bar{x}$	σ	p
PTI Mask 11	-10.84	16	9	0.000
PTI Mask 12	-5.05	15	5	0.000
PTI Mask 13	-3.76	37	12	0.156
PTI Mask 14	-1.94	31	7	0.218
PTI Mask 15	-0.14	27	6	0.912
PTI Mask 16	-1.93	22	5	0.081
PTI Mask 17	-5.28	20	7	0.000
PTI Mask 18	3.08	44	13	0.256
PTI Mask 19	3.73	27	8	0.021
PTI Mask 20	1.71	22	6	0.192

****Green* denotes p value is very highly significant (0.000-0.001), *yellow* denotes p value is highly significant (0.001-0.01) and *orange* denotes p value is significant (0.01-0.05).*

Table 4.16 – Pairwise Comparisons comparing the active and control group contact areas total (cm^2) while walking.

Mask (Left foot)	Mean Difference (Active minus Control)	$\bar{x}$	σ	p
Contact Areas M1	-3	38	6	0.004
Contact Areas M2	-3	22	4	0.000
Contact Areas M3	-2	12	2	0.000
Contact Areas M4	-2	12	2	0.001
Contact Areas M5	-1	7	1	0.001
Contact Areas M6	0	6	1	0.065
Contact Areas M7	0	6	1	0.115
Contact Areas M8	-1	8	1	0.000
Contact Areas M9	-1	8	1	0.002
Contact Areas M10	-1	9	1	0.040

Mask (Right foot)	Mean Difference (Active minus Control)	$\bar{x}$	σ	p
Contact Areas M11	-6	38	7	0.000
Contact Areas M12	-4	23	5	0.000
Contact Areas M13	-2	12	3	0.000
Contact Areas M14	-2	12	2	0.000
Contact Areas M15	-1	6	1	0.001
Contact Areas M16	-1	6	1	0.022
Contact Areas M17	-1	6	1	0.000
Contact Areas M18	-1	7	1	0.000
Contact Areas M19	-1	8	1	0.001
Contact Areas M20	-1	8	2	0.002

****Green* denotes p value is very highly significant (0.000-0.001), *yellow* denotes p value is highly significant (0.001-0.01) and *orange* denotes p value is significant (0.01-0.05). The mean difference values are rounded to the nearest whole number.*

Table 4.17 – Pairwise Comparisons comparing the active and control maximum force total (N) while walking.

Mask (Left foot)	Mean Difference (Active minus Control)	$\bar{x}$	σ	p
Maximum Force M1	-43	461	133	0.131
Maximum Force M2	-24	97	41	0.006
Maximum Force M3	-50	116	44	0.000
Maximum Force M4	-16	112	36	0.015
Maximum Force M5	-4	62	19	0.313
Maximum Force M6	-1	51	17	0.687
Maximum Force M7	1	38	14	0.815
Maximum Force M8	-31	120	50	0.003
Maximum Force M9	-2	60	17	0.643
Maximum Force M10	-3	57	21	0.549

Mask (Right foot)	Mean Difference (Active minus Control)	$\bar{x}$	σ	p
Maximum Force M11	-86	446	134	0.002
Maximum Force M12	-30	100	40	0.000
Maximum Force M13	-45	125	55	0.000
Maximum Force M14	-30	119	42	0.000
Maximum Force M15	-11	62	19	0.009
Maximum Force M16	-8	50	16	0.026
Maximum Force M17	-11	41	16	0.001
Maximum Force M18	-13	117	50	0.201
Maximum Force M19	3	57	17	0.433
Maximum Force M20	-4	53	20	0.407

****Green* denotes p value is very highly significant (0.000-0.001), *yellow* denotes p value is highly significant (0.001-0.01) and *orange* denotes p value is significant (0.01-0.05). The mean difference values are rounded to the nearest whole number.*

Table 4.18 – Pairwise Comparisons comparing the active and control group peak pressure total (kPa) while walking.

Mask (Left foot)	Mean Difference (Active minus Control)	$\bar{x}$	σ	p
Peak Pressure M1	17.83	233	55	0.128
Peak Pressure M2	-1.89	71	19	0.641
Peak Pressure M3	-41.63	156	45	0.000
Peak Pressure M4	1.13	145	27	0.843
Peak Pressure M5	11.77	135	32	0.086
Peak Pressure M6	12.32	110	29	0.44
Peak Pressure M7	9.71	87	28	0.096
Peak Pressure M8	-31.80	246	86	0.079
Peak Pressure M9	9.08	119	31	0.171
Peak Pressure M10	7.61	113	32	0.267

Mask (Right foot)	Mean Difference (Active minus Control)	$\bar{x}$	σ	p
Peak Pressure M11	-12.54	224	51	0.247
Peak Pressure M12	-9.56	73	19	0.019
Peak Pressure M13	-31.15	156	45	0.001
Peak Pressure M14	-6.07	144	32	0.372
Peak Pressure M15	0.80	132	33	0.909
Peak Pressure M16	-0.23	112	31	0.972
Peak Pressure M17	-21.61	94	33	0.002
Peak Pressure M18	14.65	240	91	0.450
Peak Pressure M19	0.58	159	61	0.964
Peak Pressure M20	9.11	108	33	0.192

****Green* denotes p value is very highly significant (0.000-0.001), *yellow* denotes p value is highly significant (0.001-0.01) and *orange* denotes p value is significant (0.01-0.05).*

Table 4.19 – Pairwise Comparisons comparing the active and control group maximum mean pressure (kPa) while walking.

Mask (Left foot)	Mean Difference (Active minus Control)	$\bar{x}$	σ	p
Mean Pressure M1	1.84	121	23	0.705
Mean Pressure M2	-2.61	46	11	0.280
Mean Pressure M3	-29.39	101	26	0.000
Mean Pressure M4	-2.43	99	17	0.511
Mean Pressure M5	4.07	96	22	0.391
Mean Pressure M6	4.04	83	21	0.364
Mean Pressure M7	5.67	66	19	0.155
Mean Pressure M8	-16.21	148	43	0.077
Mean Pressure M9	6.10	77	18	0.107
Mean Pressure M10	4.68	69	18	0.220

Mask (Right foot)	Mean Difference (Active minus Control)	$\bar{x}$	σ	p
Mean Pressure M11	-10.58	120	26	0.056
Mean Pressure M12	-5.79	45	11	0.011
Mean Pressure M13	-20.87	101	30	0.001
Mean Pressure M14	-10.04	98	22	0.029
Mean Pressure M15	-5.33	98	24	0.288
Mean Pressure M16	-7.74	83	21	0.083
Mean Pressure M17	-10.23	67	22	0.027
Mean Pressure M18	-0.33	154	51	0.976
Mean Pressure M19	11.86	73	18	0.002
Mean Pressure M20	-0.88	67	19	0.830

****Green* denotes p value is very highly significant (0.000-0.001), *yellow* denotes p value is highly significant (0.001-0.01) and *orange* denotes p value is significant (0.01-0.05).*

Table 4.20 – Pairwise Comparisons comparing the active and control group pressure time integral (PTI) total while walking.

Mask (Left foot)	Mean Difference (Active minus Control)	$\bar{x}$	σ	p
PTI Mask 1	0.39	52	17	0.915
PTI Mask 2	-1.96	28	9	0.314
PTI Mask 3	-12.58	47	15	0.000
PTI Mask 4	-2.70	44	9	0.145
PTI Mask 5	-0.21	42	10	0.923
PTI Mask 6	-1.15	37	11	0.608
PTI Mask 7	-1.01	30	11	0.670
PTI Mask 8	-10.73	57	19	0.006
PTI Mask 9	-0.09	29	11	0.970
PTI Mask 10	0.93	27	11	0.678

Mask (Right foot)	Mean Difference (Active minus Control)	$\bar{x}$	σ	p
PTI Mask 11	-9.95	53	20	0.018
PTI Mask 12	-5.51	29	9	0.002
PTI Mask 13	-9.67	47	14	0.001
PTI Mask 14	-4.25	44	11	0.080
PTI Mask 15	-2.97	42	11	0.201
PTI Mask 16	-4.15	38	11	0.074
PTI Mask 17	-9.33	33	13	0.001
PTI Mask 18	-2.65	54	18	0.485
PTI Mask 19	-2.52	38	15	0.416
PTI Mask 20	1.15	24	9	0.556

****Green* denotes p value is very highly significant (0.000-0.001), *yellow* denotes p value is highly significant (0.001-0.01) and *orange* denotes p value is significant (0.01-0.05).*

Averaged Excel graphs were created for each group separately to visualise the Contact Areas (cm^2), Maximum Forces (N), Peak Pressures (kPa) and Mean Pressures (kPa) while walking and running. As the graphs for right and left foot data follow extremely similar distribution paths, only the right foot data is displayed in Figures 4.9, 4.10, 4.11, 4.12 for the active group and Figures 4.13, 4.14, 4.15 and 4.16 for the control group. The graphs are arranged to highlight the large differences of in-shoe pressure distribution when individuals within the same group are recorded walking and then compared with the recorded data when running. This organisation provides an optimal presentation of the data to recognise that the control group walk and run in a similar manner to the way in which the active group walk. However, when comparing the graphs of active individuals running, the pattern dramatically contrasts.

The pairwise comparisons also confirm that the active group tend to adopt a toe-running technique and this dramatically contrasts the heel-strike running of the control group which is confirmed by the following summary of results using the right foot as an example:

- active group contact area for the heel was smaller by $10cm^2$ ($p < 0.001$),
- maximum force at the heel of the active group was lower by 215N ($p < 0.001$)
- maximum force at the toes of the active group was 21N greater for the 2^{nd} toe and 12N greater between the 3^{rd} to 5^{th} toes ($p < 0.001$ and 0.029 respectively),
- active group peak pressure of the hallux was greater by 82kPa and the heel was 84kPa lower ($p < 0.001$).

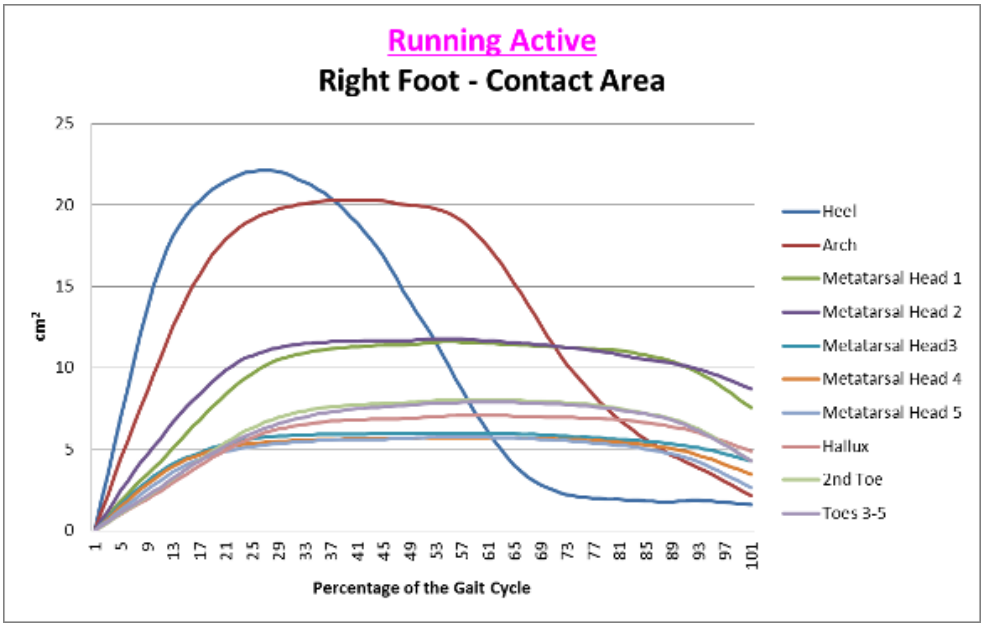

(a)

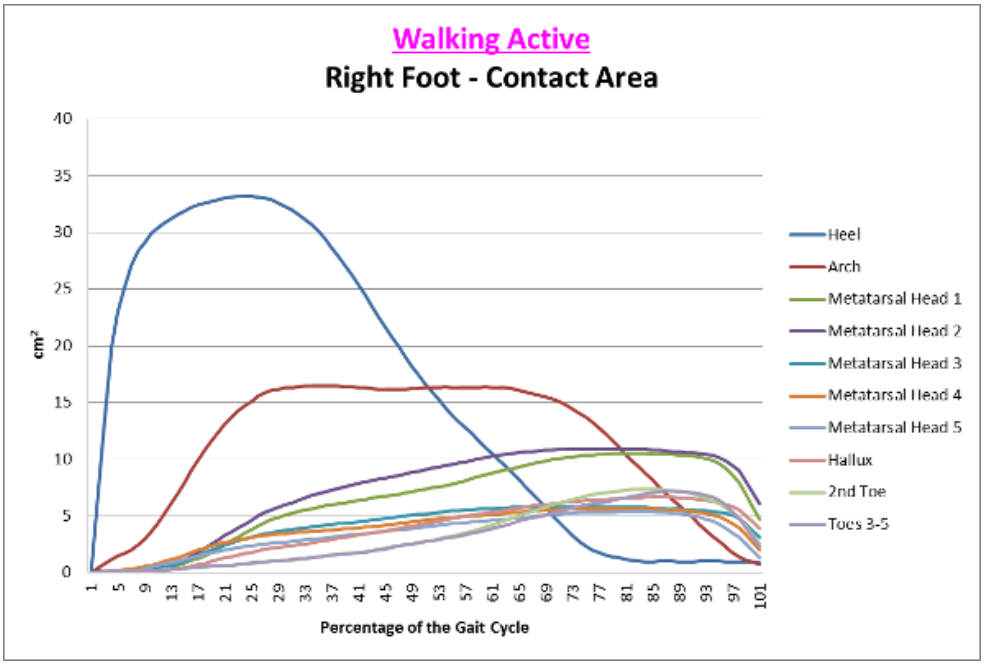

(b)

Figure 4.9 – Graphical depiction of the normalised in-shoe data comparing the right foot contact areas of the active group revealing a dramatic decrease in the heel contact area is evident during running compared to walking.

(a) Running.

(b) Walking.

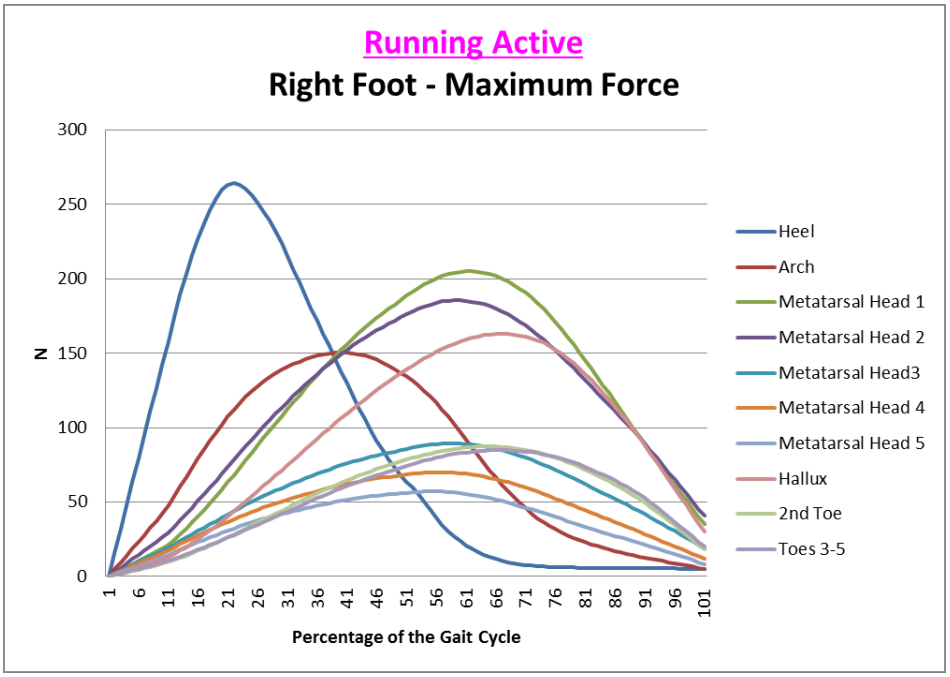

(a)

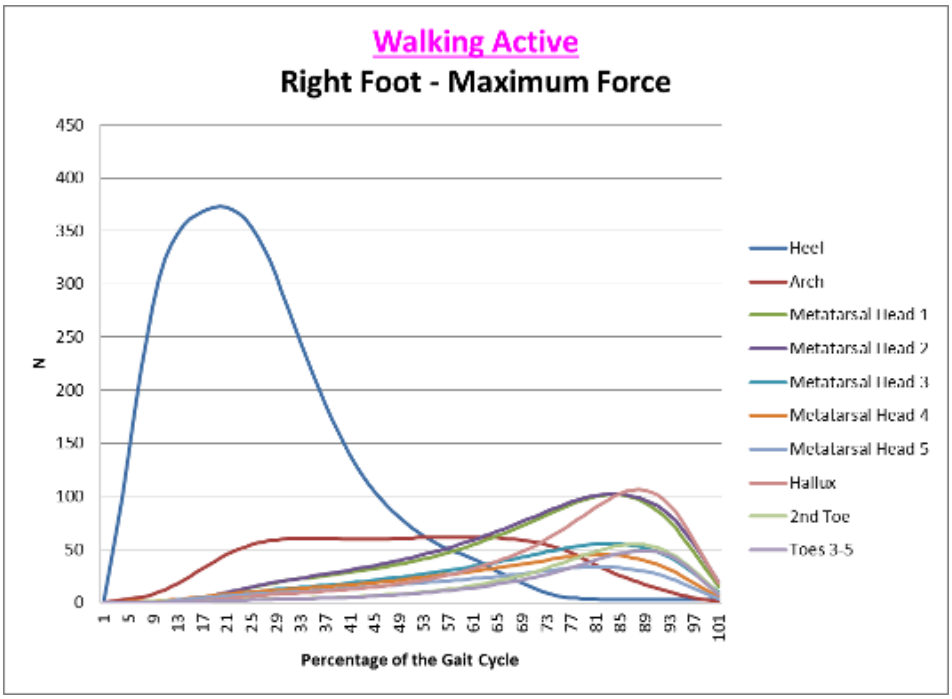

(b)

Figure 4.10 – Graphical depiction of the normalised in-shoe data comparing the right foot maximum force of the active group.

(a) Running.

(b) Walking.

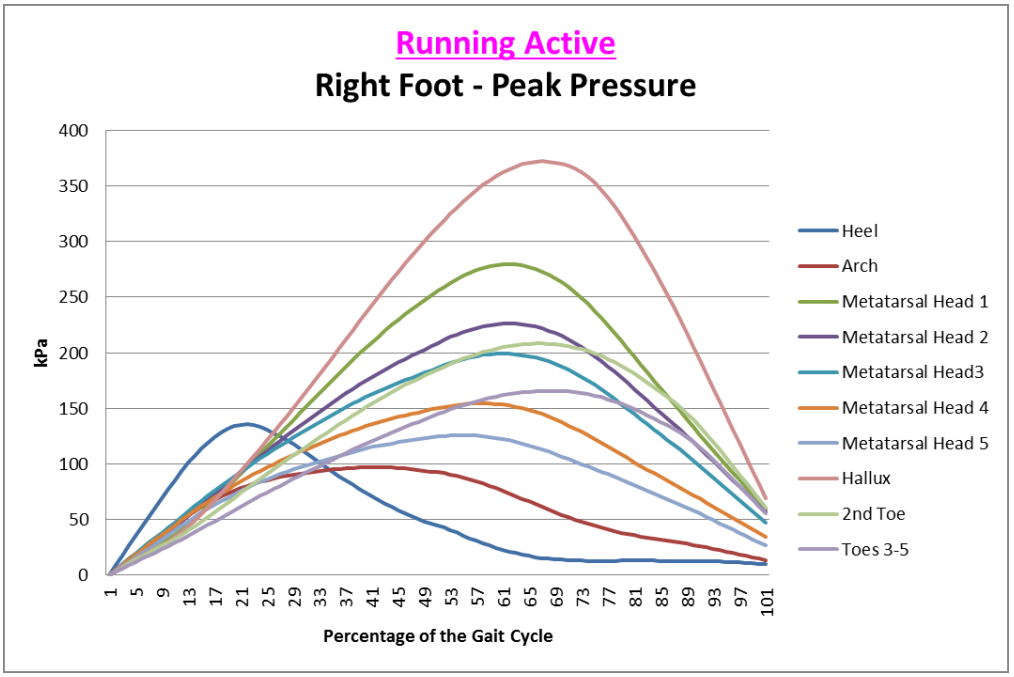

(a)

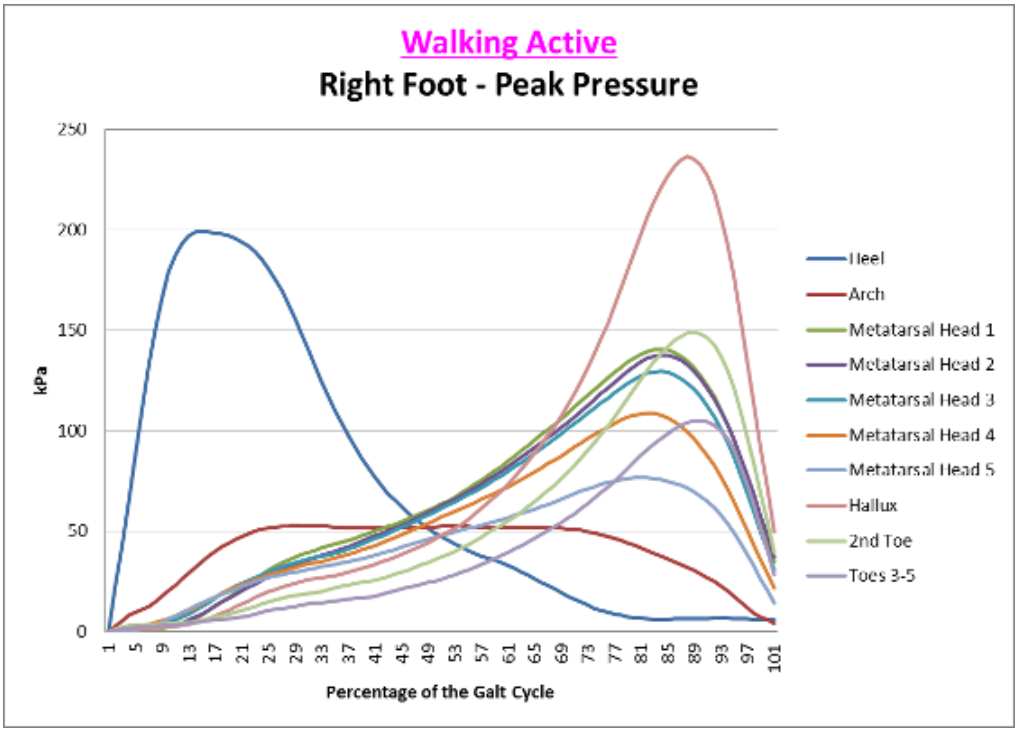

(b)

Figure 4.11 – Graphical depiction of the normalised in-shoe data comparing the right foot peak pressure of the active group.

(a) Running.

(b) Walking.

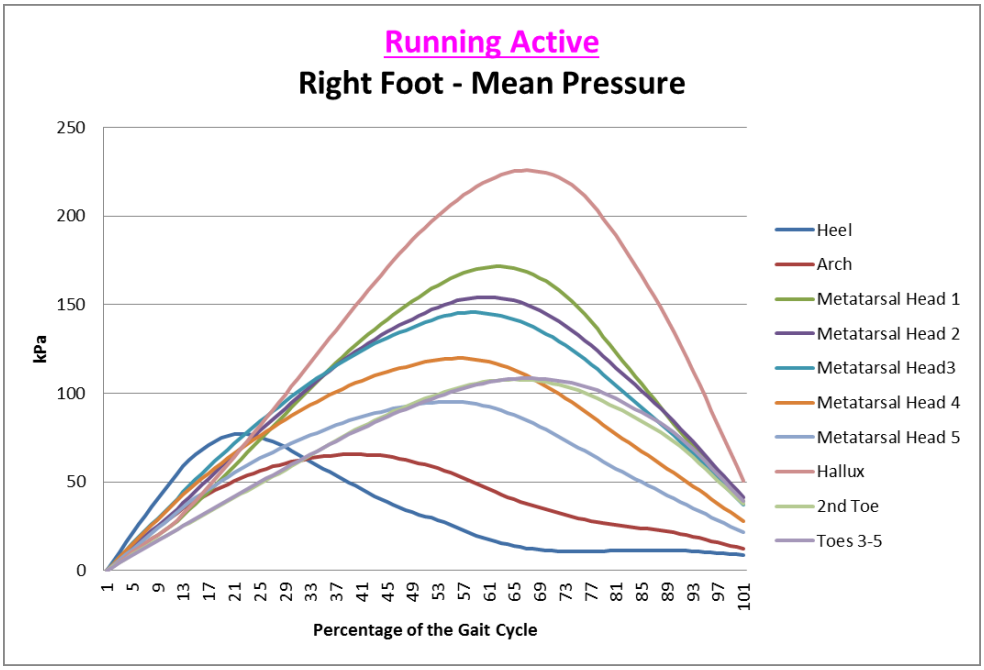

(a)

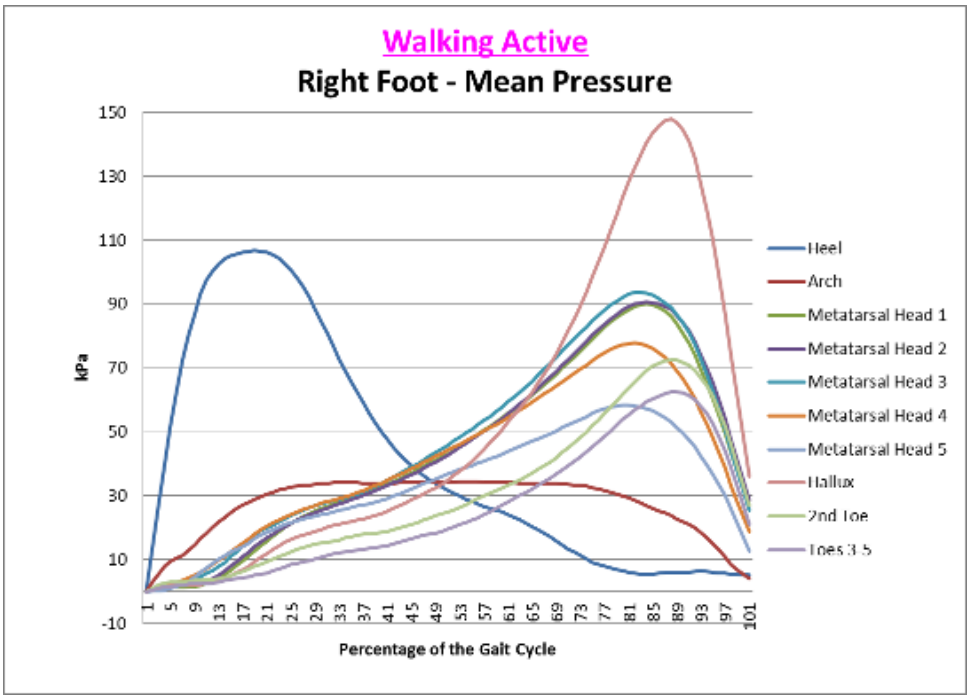

(b)

Figure 4.12 – Graphical depiction of the normalised in-shoe data comparing the right foot mean pressures of the active group, demonstrating that the overall pressure distribution is altered to adopt a biomechanically efficient running technique.

(a) Running.

(b) Walking.

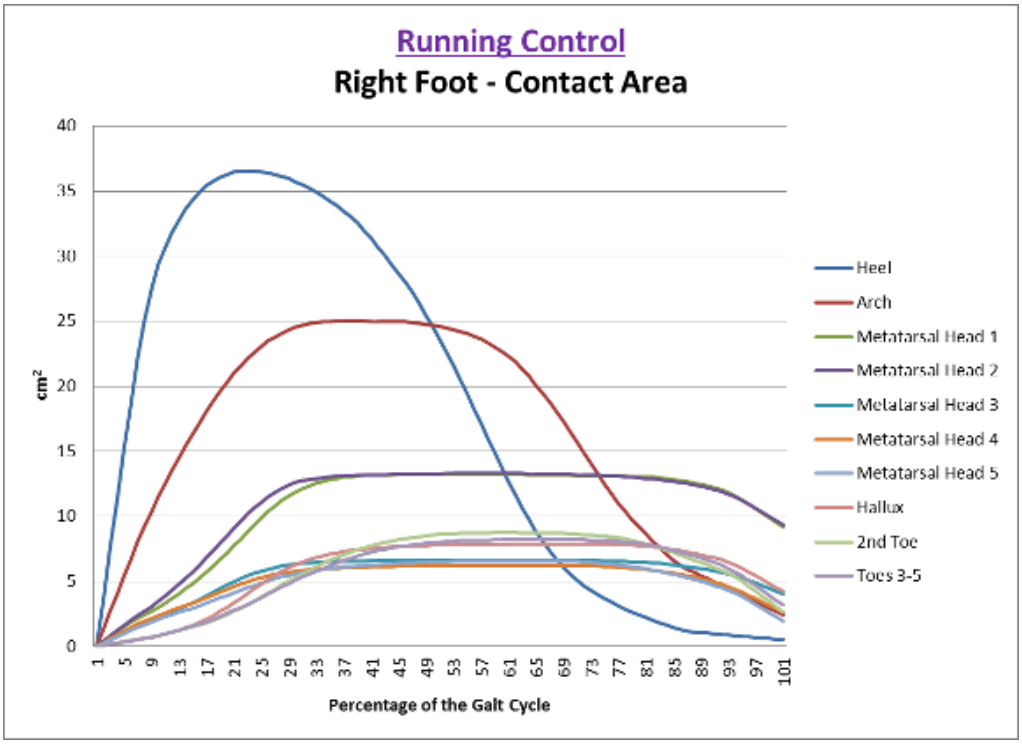

(a)

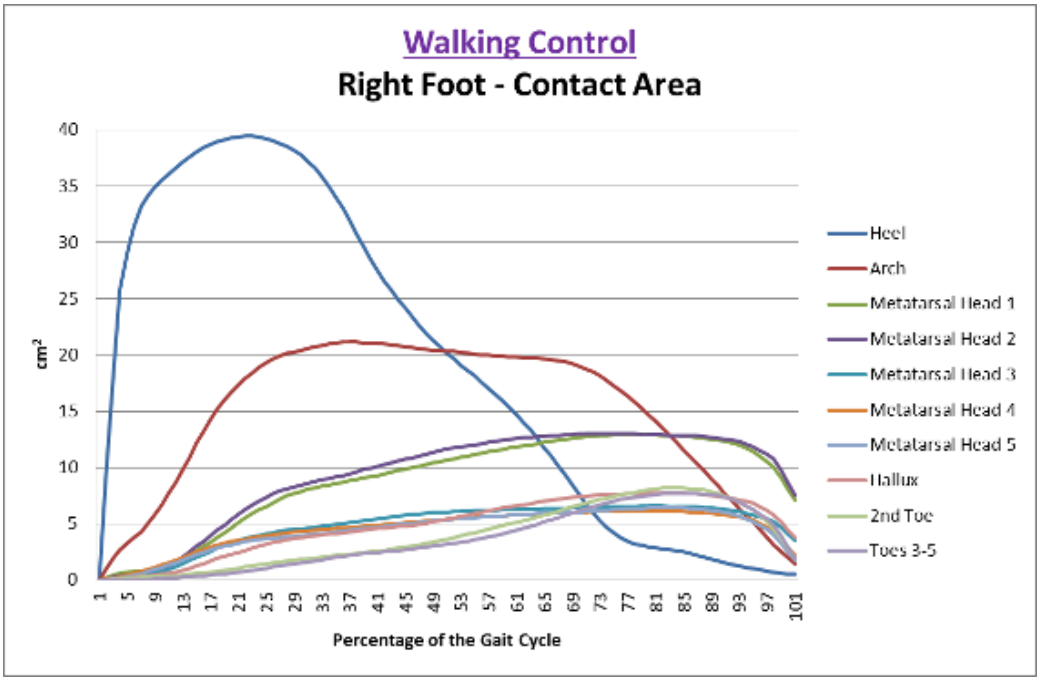

(b)

Figure 4.13 – Graphical depiction of the normalised in-shoe data comparing the right foot contact areas of the control group.

(a) Running.

(b) Walking.

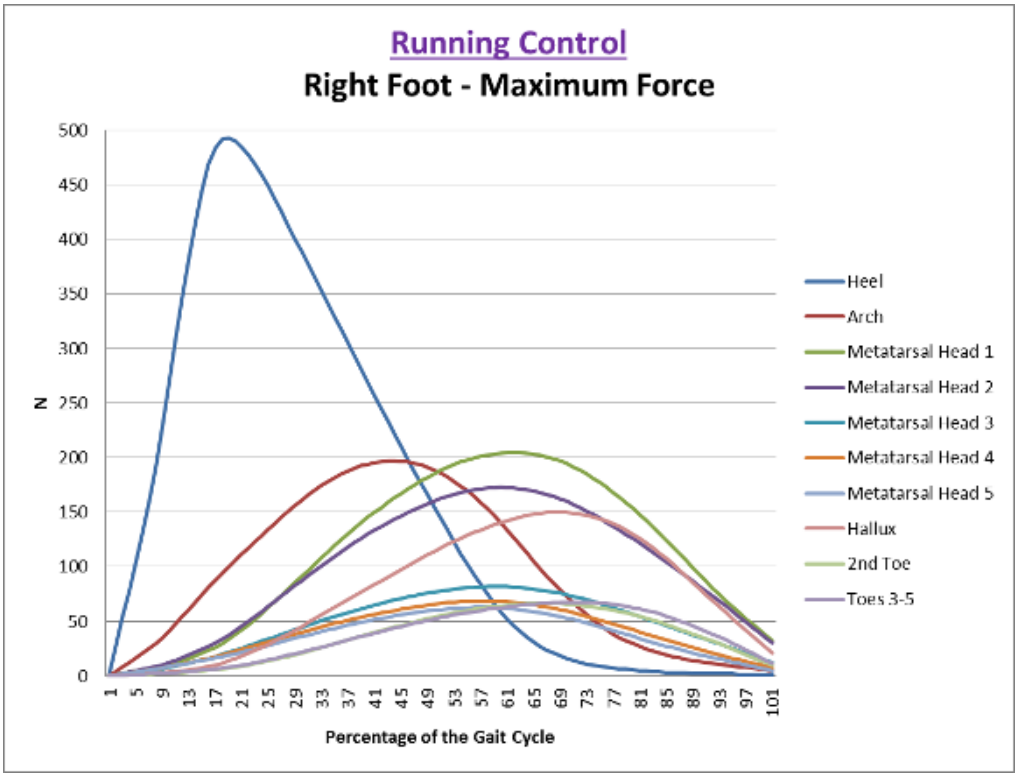

(a)

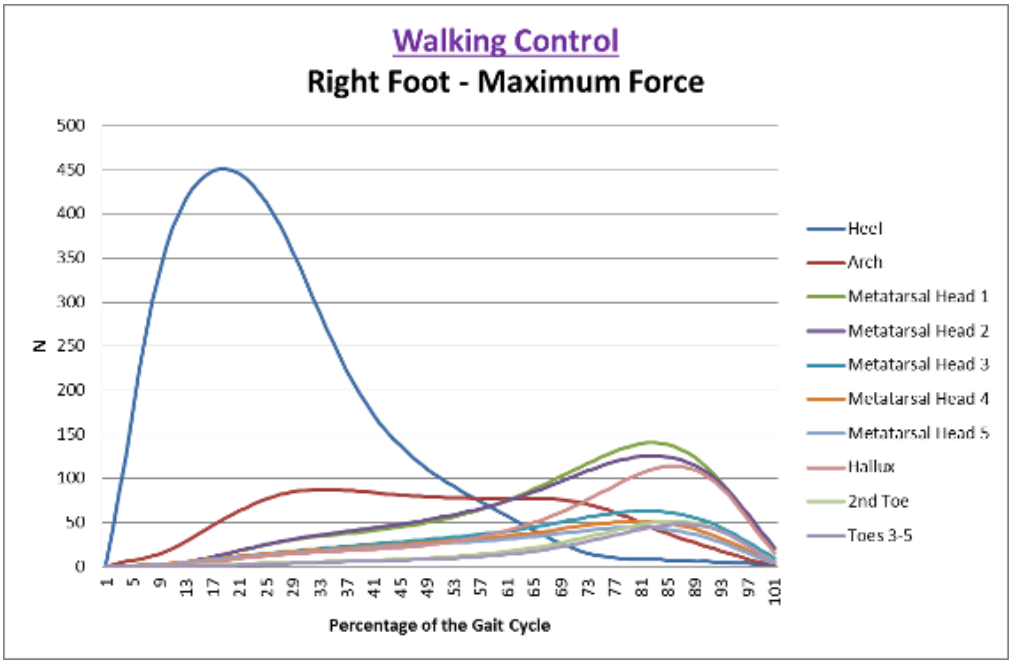

(b)

Figure 4.14 – Graphical depiction of the normalised in-shoe data comparing the right foot maximum force of the control group.

(a) Running.

(b) Walking.

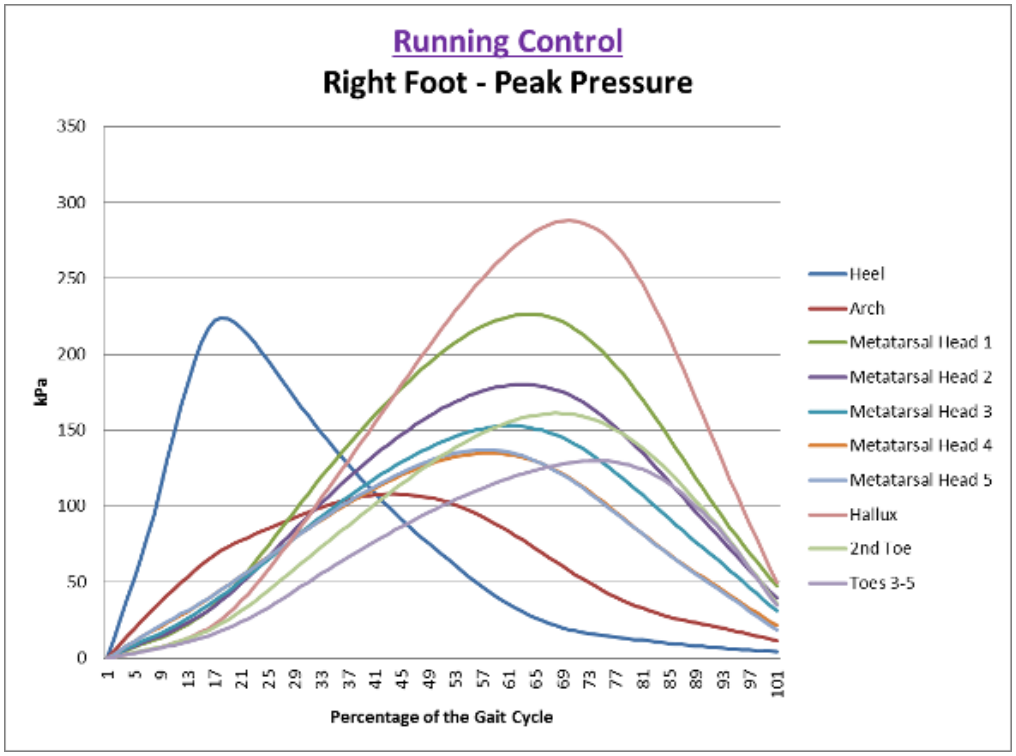

(a)

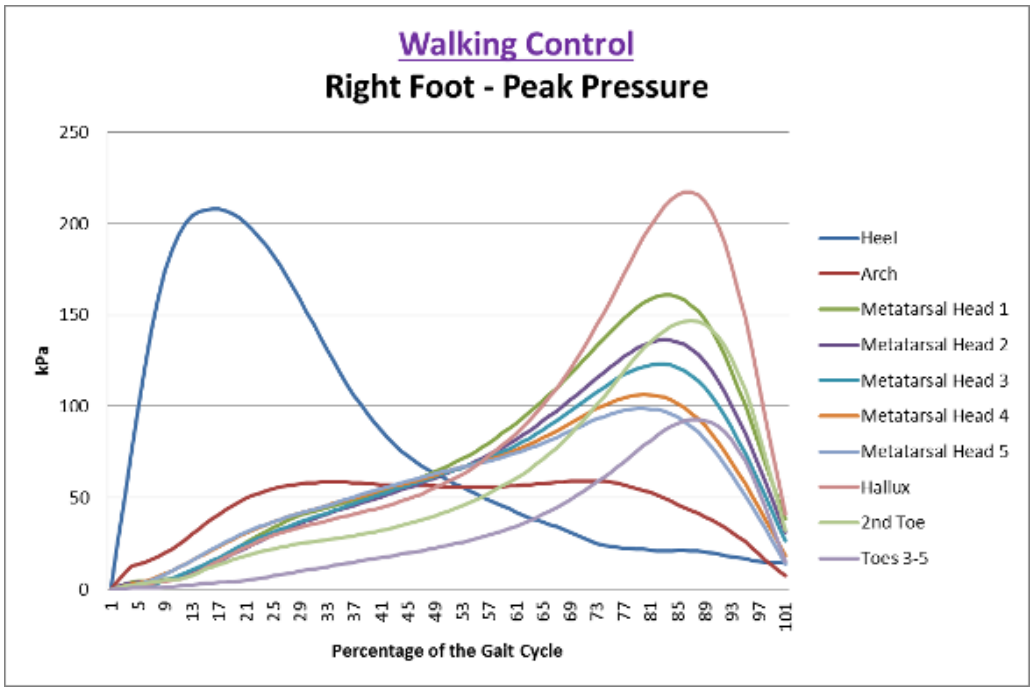

(b)

Figure 4.15 – Graphical depiction of the normalised in-shoe data comparing the right foot peak pressure of the control group.

(a) Running.

(b) Walking.

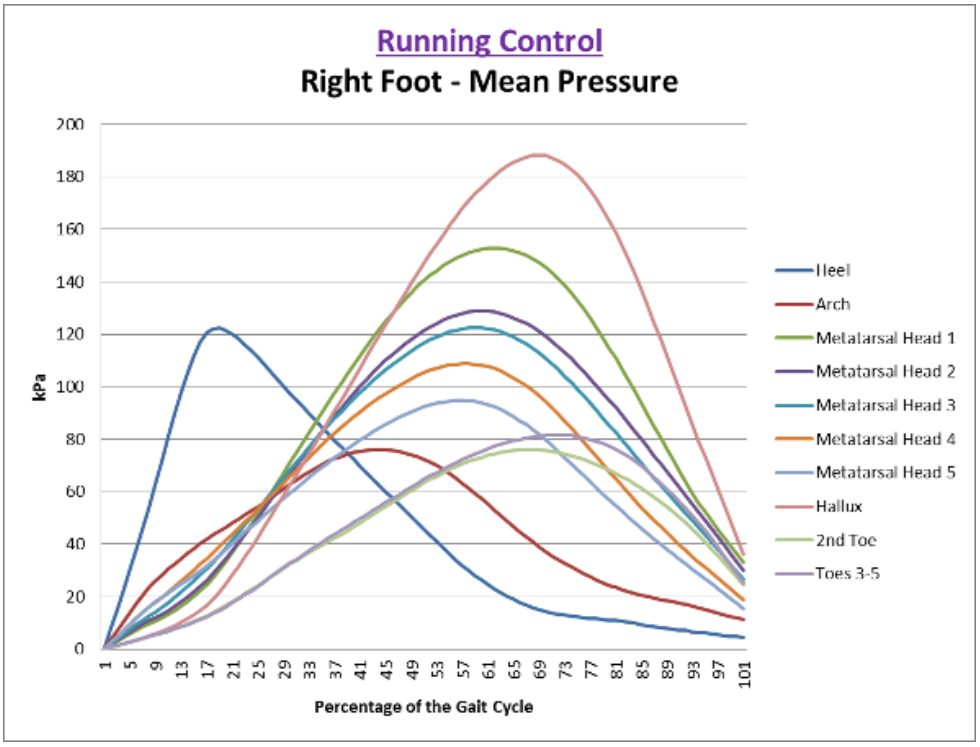

(a)

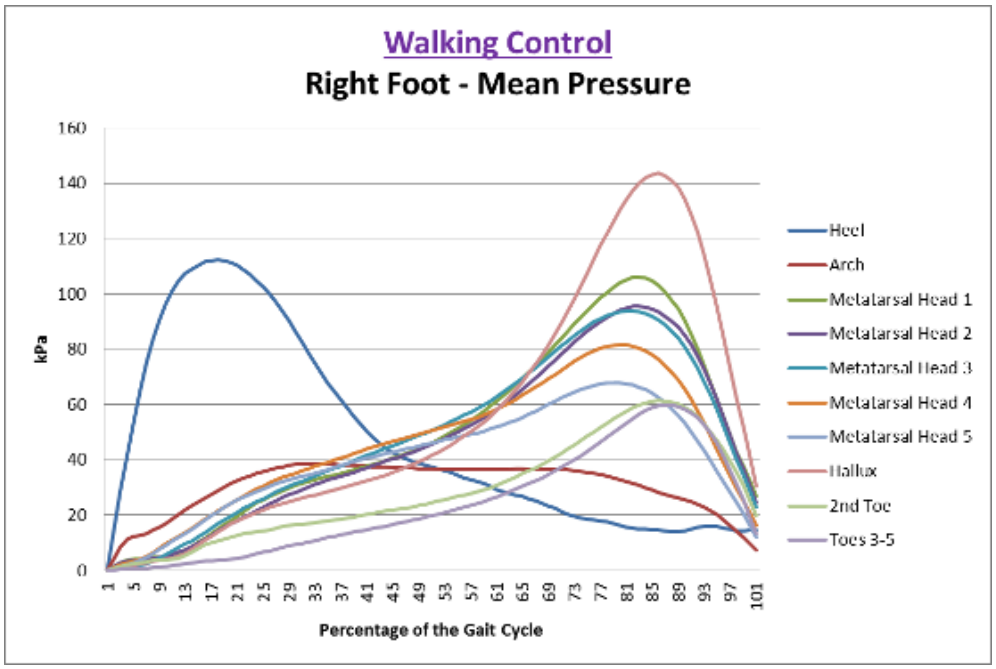

(b)

Figure 4.16 – Graphical depiction of the normalised in-shoe data comparing the right foot mean pressure of the control group showing that overall the running graphs still follow the same pattern when compared to walking.

(a) Running.

(b) Walking.

A non-parametric one-sample Kolmogorov-Smirnov Test revealed that the in-shoe pressure dataset within a group did not follow normal distribution; therefore a Student's T-Test would be inappropriate to test the statistical significance of gait within each group based on this assumption. To compare the significance of walking and running of the right foot within a group, the 2 Independent Samples Mann-Whitney Test was applied to the group data. Tables 4.21 and 4.22 display the results of significance for the contact area, maximum force, peak pressure and mean pressures for within the control group and active group respectively.

The Mann-Whitney Tests highlight that the control group does not have a significant difference when comparing the contact area of the heel during walking and running ($p = 0.251$); thereby highlighting that individuals in the control group do not noticeably alter the biomechanical technique of striking the ground with their heel when changing from a walking gait to running gait. Interestingly, the active group do however demonstrate a significant difference in the heel contact area when walking and running ($p = 0.026$) which, when combined with the significant Pairwise Comparison differences, provides a clear indication that intensive training positively influences the biomechanical function of running. This means that the active group significantly changes the way that the heel ($p=0.026$) and arch ($p=0.005$) of their right feet interact with the ground, with respect to the contact area, when walking and running. Through the comparison of active data and control data, the Mann-Whitney results test the significance of the patterns observed in Figures 4.9 through to 4.16 and emphasise that biomechanical changes occur as a result of intensive sports training.

Table 4.21 – Control group Mann-Whitney Test of the regions of right foot when walking compared with the same regions of the right foot when running.

Region of Right Foot	Contact Area (cm^2)			Maximum Force (N)			Peak Pressure (kPa)			Mean Pressure (kPa)		
	$\bar{x}$	σ	p	$\bar{x}$	σ	p	$\bar{x}$	σ	p	$\bar{x}$	σ	p
Heel	18.72	14.23	0.251	159.47	164.71	0.781	79.97	69.82	0.163	47.60	37.05	0.189
Arch	15.42	7.49	0.031	74.96	56.57	0.001	54.30	27.90	0.000	36.43	18.38	0.000
Metatarsal Head 1	9.72	4.07	0.000	86.44	64.20	0.000	100.27	69.02	0.000	67.84	46.02	0.000
Metatarsal Head 2	10.07	4.07	0.000	78.29	53.31	0.000	84.57	54.70	0.000	61.01	38.42	0.000
Metatarsal Head 3	5.14	1.93	0.000	36.75	24.82	0.000	75.55	45.43	0.000	60.21	35.71	0.000
Metatarsal Head 4	4.76	1.69	0.000	32.37	20.16	0.000	68.60	38.27	0.000	54.54	30.09	0.000
Metatarsal Head 5	4.70	1.86	0.000	28.84	18.24	0.000	67.57	38.23	0.000	47.80	25.52	0.000
Hallux	5.34	2.59	0.000	58.73	48.81	0.000	114.91	91.17	0.000	77.40	59.33	0.000
Toe 2	4.85	2.99	0.000	26.26	22.10	0.000	74.14	52.81	0.000	36.45	23.21	0.000
Toes 3-5	4.61	2.89	0.000	26.06	22.63	0.000	53.67	42.68	0.000	35.58	26.12	0.000

****Green* denotes p value is very highly significant (0.000-0.001), *yellow* denotes p value is highly significant (0.001-0.01) and *orange* denotes p value is significant (0.01-0.05).*

Table 4.22 – Active group Mann-Whitney Test of the regions of right foot when walking compared with the same regions of the right foot when running.

Region of Right Foot	**Contact Area** (cm^2)			**Maximum Force** (N)			**Peak Pressure** (kPa)			**Mean Pressure** (kPa)		
	$\bar{x}$	σ	p	$\bar{x}$	σ	p	$\bar{x}$	σ	p	$\bar{x}$	σ	p
Heel	13.26	10.99	0.026	106.51	116.82	0.50	61.74	58.70	0.506	37.48	31.10	0.469
Arch	12.13	6.27	0.005	57.90	44.33	0.000	50.07	25.65	0.000	33.60	16.02	0.000
Metatarsal Head 1	7.93	3.61	0.000	80.56	64.55	0.000	114.47	84.50	0.000	72.50	51.40	0.000
Metatarsal Head 2	8.60	3.54	0.000	79.60	56.14	0.000	102.29	68.14	0.000	70.82	46.34	0.000
Metatarsal Head 3	4.63	1.74	0.000	40.92	27.44	0.000	94.26	59.27	0.000	70.24	43.16	0.000
Metatarsal Head 4	4.38	1.59	0.000	32.81	21.15	0.000	76.99	45.23	0.000	59.36	34.30	0.000
Metatarsal Head 5	4.06	1.67	0.000	25.86	17.20	0.000	62.60	36.13	0.000	47.07	26.78	0.000
Hallux	4.78	2.30	0.000	63.52	54.10	0.000	144.29	120.49	0.000	92.63	72.64	0.000
Toe 2	4.80	2.83	0.000	34.92	29.54	0.000	92.71	68.25	0.000	49.93	33.61	0.000
Toes 3-5	4.67	2.74	0.000	33.44	28.75	0.000	72.49	54.51	0.000	47.95	34.94	0.000

****Green* denotes p value is very highly significant (0.000-0.001), *yellow* denotes p value is highly significant (0.001-0.01) and *orange* denotes p value is significant (0.01-0.05).*

4.2.5.1 Kinematic Data - Walking

The kinematic data for each individual was first checked against a standard, normalised database that was created in the same gait analysis laboratory by a senior clinical scientist. A total of three trials were selected which best represented the gait cycle for each individual, and the process of creating an average database for both groups was developed to compare an individuals' data within the appropriate normal ranges for the respective group. This resulted in the creation and development of six databases:

- Walking Control (Both Right and Left)
- Walking Active (Both Right and Left)
- Running Control (Right Feet)
- Running Control (Left Feet)
- Running Active (Right Feet)
- Running Active (Left Feet)

The running databases were divided into right and left feet as a consequence of the increased stride length and velocity of many of the individuals, which resulted in only one foot interacting with a concealed force plate. Polygon® requires the gait cycle to be defined from 'foot strike' to 'foot strike' before the graphs are able to be normalised into a percentage of the gait cycle. The function to automatically detect gait cycle events for the running trials was not entirely successful when using the Vicon® software; therefore it was necessary to manually create a consecutive event in certain trials where the 'foot strike' and 'foot off' of the successive cycle were not routinely recognised.

Figures 4.17(a) through to (j) display the kinematic graphs of motion from one individual in the control group. The right and left feet can be compared in relation to the average database of walking averages for the control group, as signified by the grey shaded area and green line, which reflect the group pattern as a whole. Figures 4.18(a) through to (j) display the kinematic graphs for an active individual; in this case the average walking database for the active group provides the relevant range of motion and pattern of the group as a whole via the delimitation of the grey shaded area and average green line. On a visual level, there is no perceivable difference between the normalised walking graphs of the control database and the active database with respect to the kinematic data. Although the kinematic data does not reveal any observable differences in relation to the normalised data of the average active and control groups during the walking cycle, the possibility of exploring the kinetic data further may unearth otherwise hidden differences.

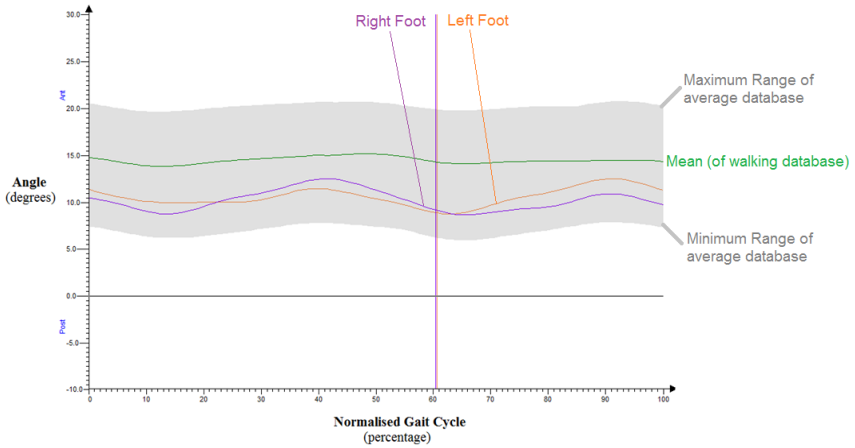

(a) Pelvic Tilt

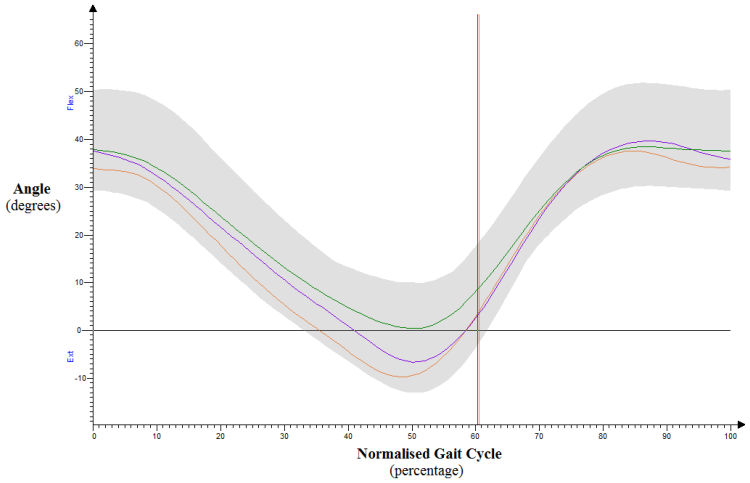

(b) Hip Flexion/Extension

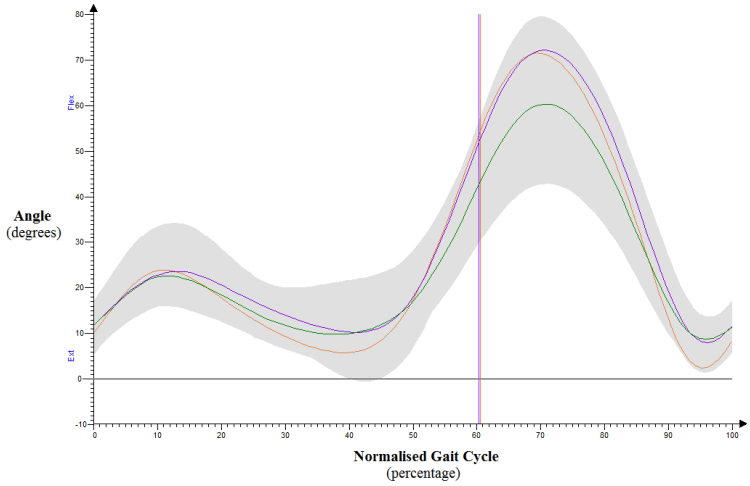

(c) Knee Flexion/Extension

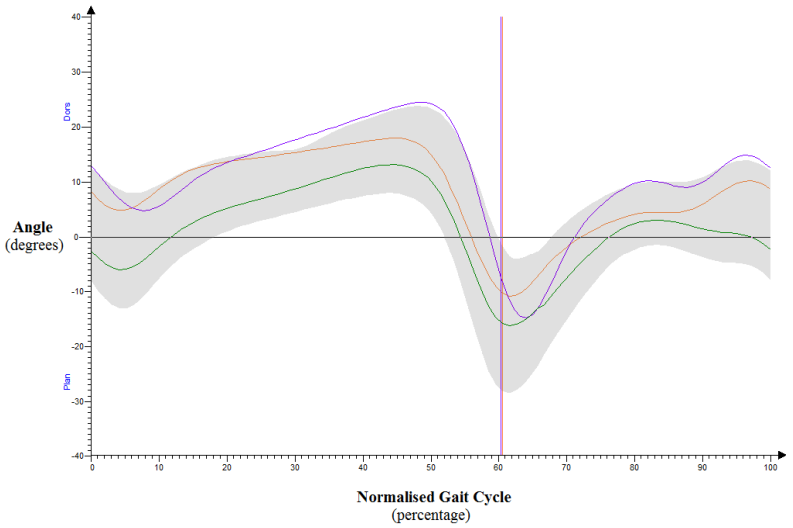

(d) Ankle Dorsiflexion/Plantarflexion

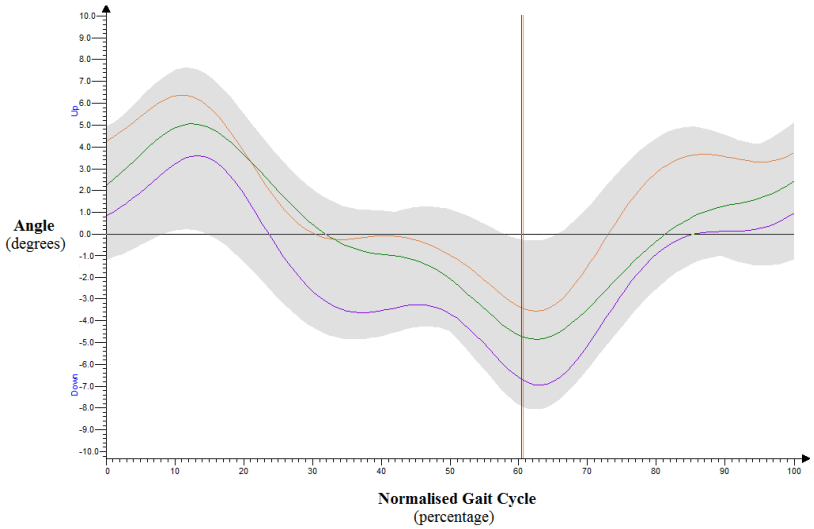

(e) Pelvic Obliquity

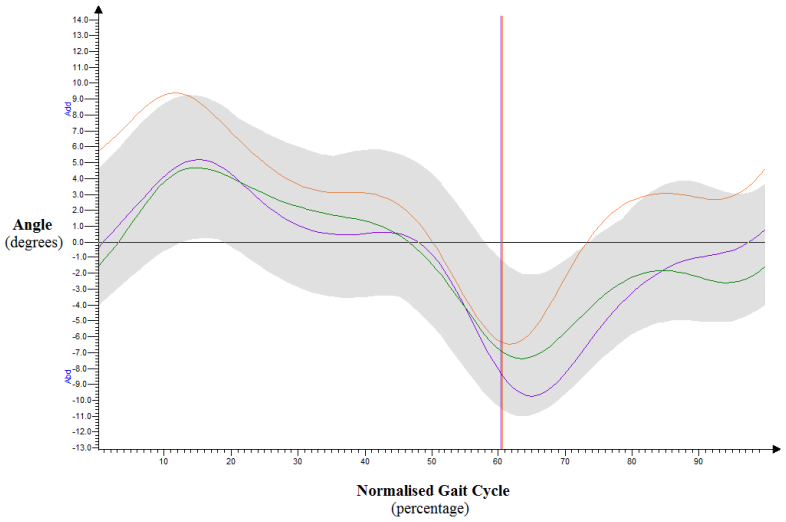

(f) Hip Abduction/Adduction

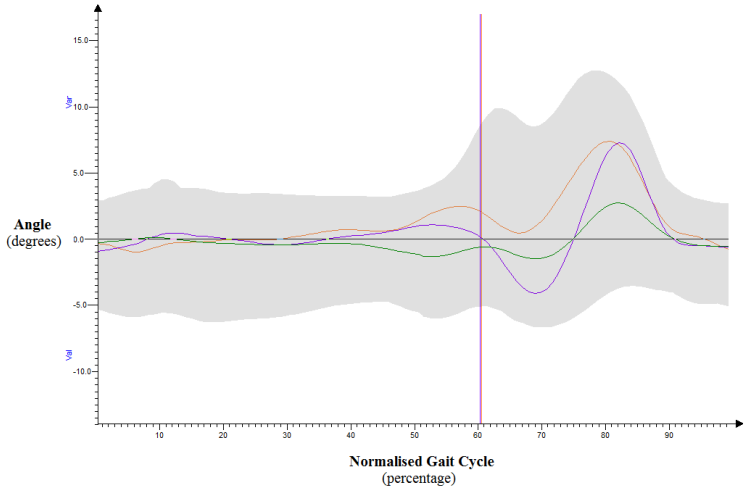

(g) Knee Abduction/Adduction

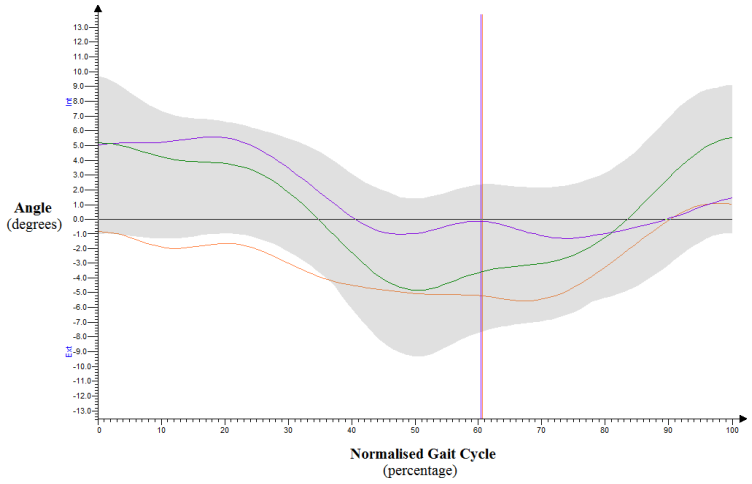

(h) Pelvic Rotation

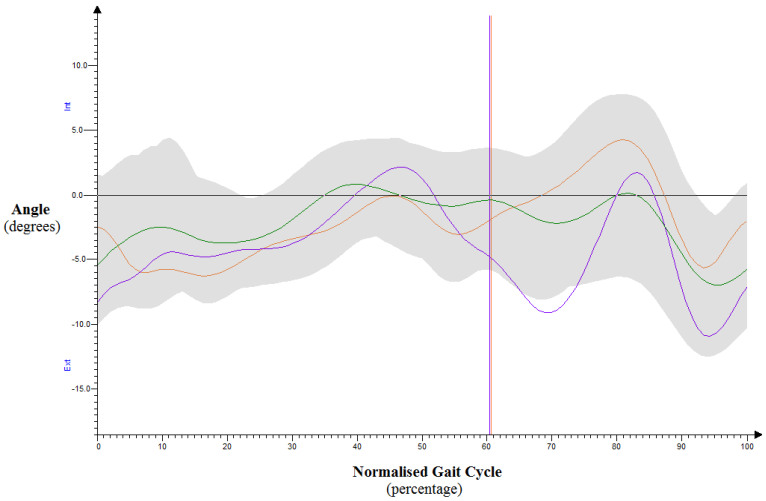

(i) Hip Rotation

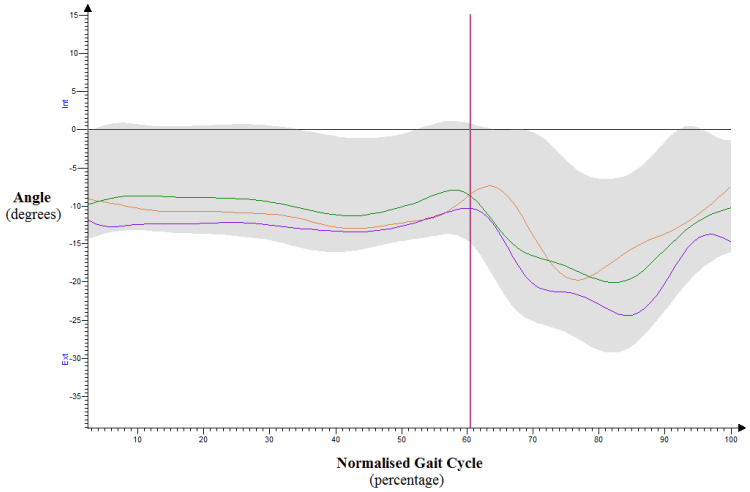

(j) Foot Progression

<u>Figures 4.17(a) to (j)</u> – Examples of the graphical kinematic outputs from Polygon® of one individual's walking trial from the control group. The walking average database for all controls is depicted by the grey shaded areas. The green line represents the normalised average for the group, the orange line highlights the left foot and the purple line represents the right foot.

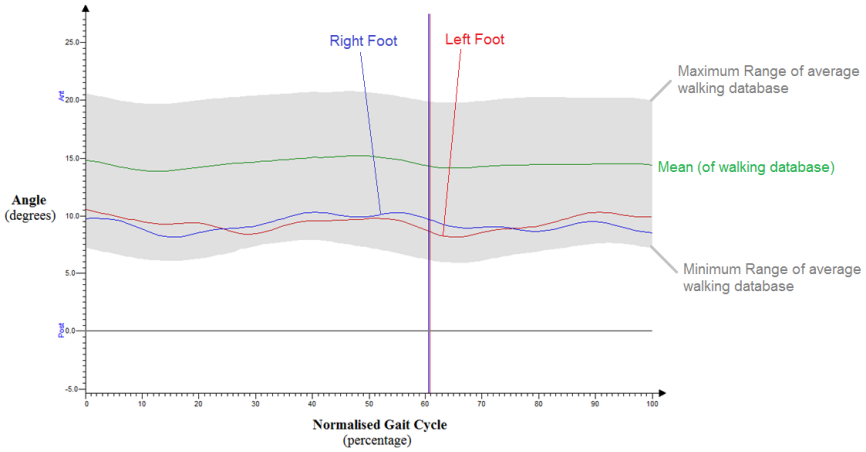

(a) Pelvic Tilt

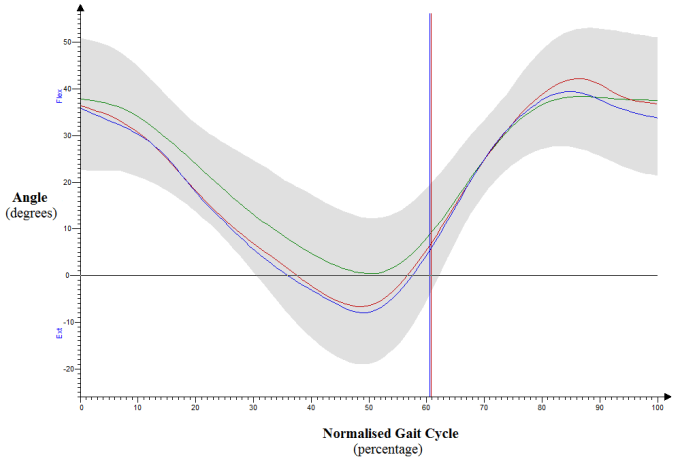

(b) Hip Flexion/Extension

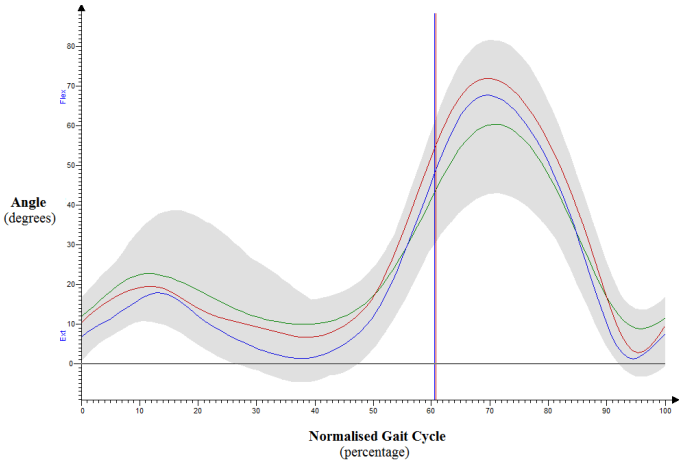

(c) Knee Flexion/Extension

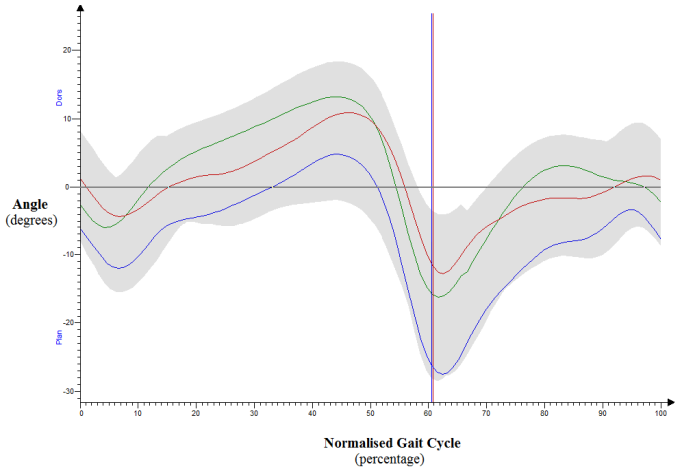

(d) Ankle Dorsiflexion/Plantarflexion

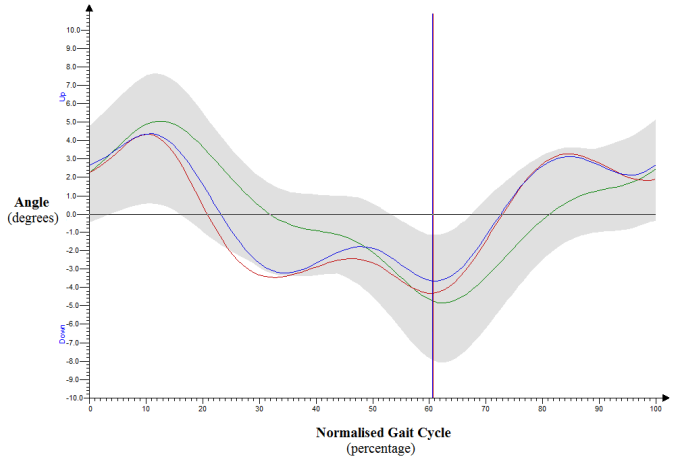

(e) Pelvic Obliquity

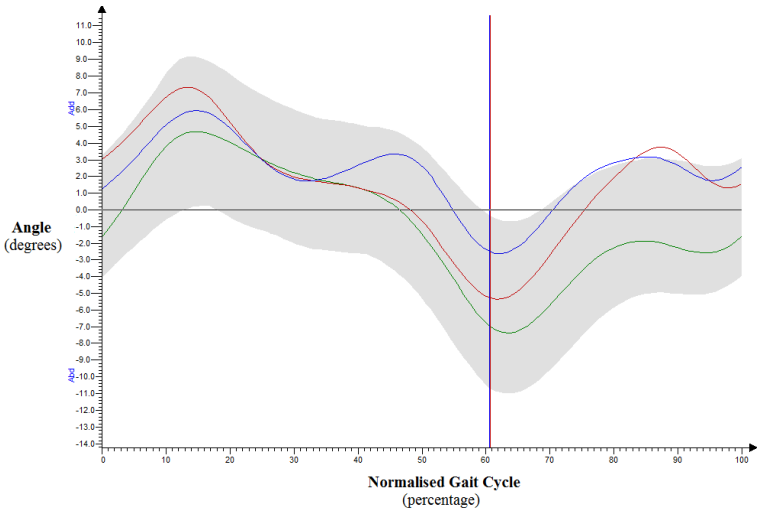

(f) Hip Abduction/Adduction

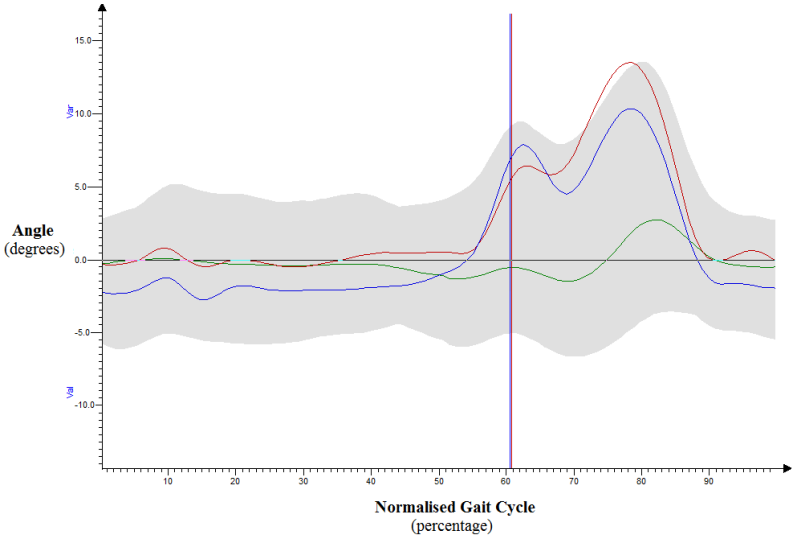

(g) Knee Abduction/Adduction

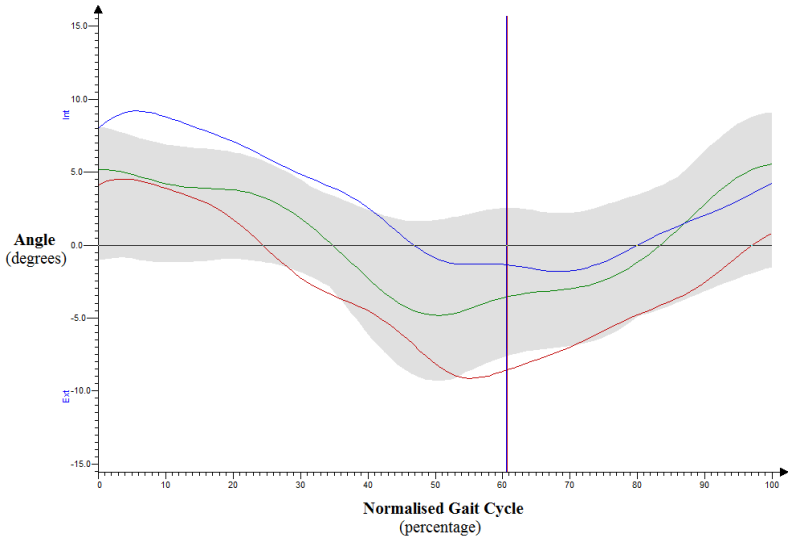

(h) Pelvic Rotation

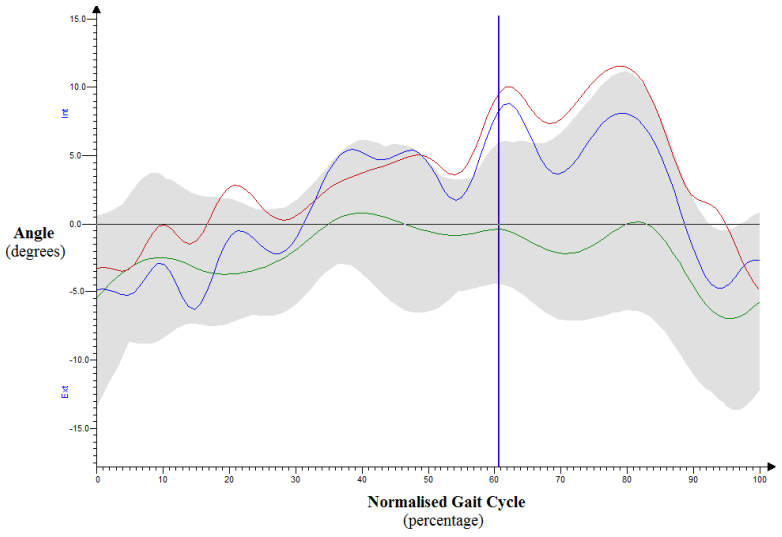

(i) Hip Rotation

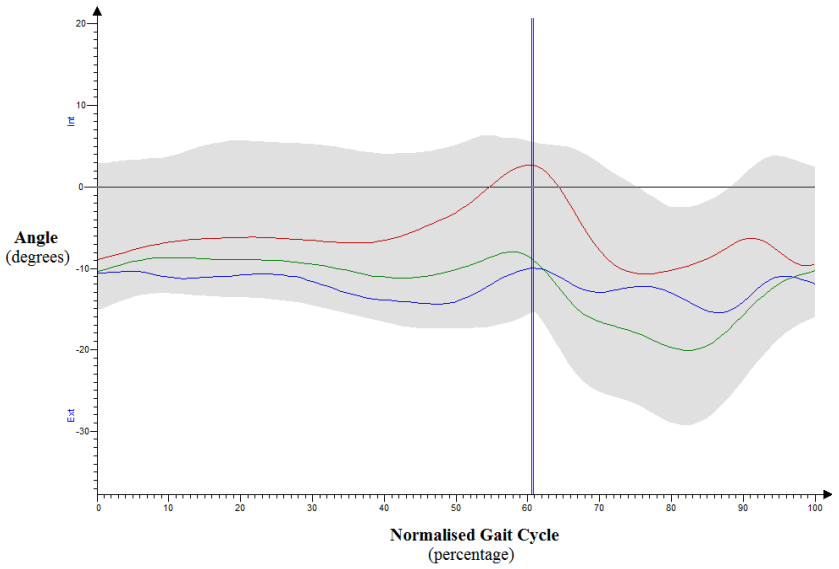

(j) Foot Progression

<u>Figures 4.18(a) to (j)</u> – Examples of the graphical kinematic outputs from Polygon® of one individual's walking trial from the active group. The walking average database for all actives is depicted by the grey shaded areas. The red line highlights the left foot and the blue line represents the right foot, while the green line represents the normalised mean /average for the group.

4.2.5.2 Kinematic Data - Running

Capturing clean trajectories and acquiring smooth kinematic data during running trials was found to be slightly more difficult in active individuals, typically due to the active group preferring to adopt a naturally faster approach to running. The increased velocity, which for some of the older individuals in the active group was close to sprinting, caused greater displacement of the bag carrying the equipment and ultimately increased the likelihood of markers becoming detached or wires disconnecting from the equipment. Overall 20% (3 individuals out of 15) of the active group adopted a heel-strike method of running while 73% (11 individuals out of 15) of the control group ran in an identical manner with the heel first contacting the ground. Exclusive toe-running was performed by 7 individuals from the active group (47%) whereas only 1 individual from the control group adopted this technique. A total of 5 active individuals, who represent approximately 33% of the group, briefly contacted the ground with the heel initially; however the majority of the ground reaction force and body weight diverted to the forefoot and toes quickly. Although this is not strictly toe running, this midfoot pressure pattern significantly reduces the heel contact area and additionally improves the efficacy of biomechanical function in the lower limb. The midfoot running style was only evident in 20% the control group in comparison to the majority of the group (73%) who ran using the heel strike method of running.

The kinematic data for running clearly displays a large difference with regard to the style implemented by the individuals in the control and active groups, which is supported by the results obtained from the in-shoe pressure data. The control group typically follow the same pattern for the graphical curves, however as expected the peaks are larger in comparison to the walking data. Figure 4.19 depicts the right foot

Polygon® data of one of the control group when compared against the average database of running averages for the right feet. Figures 4.20 and 4.21, on the other hand, provide two examples of a Polygon® report demonstrating an active individual running on his toes and another active individual running on the heel respectively. Both the control and active groups display a clear increase in the anterior tilt of the pelvis when running, which is supported by the findings of Dugan and Bhat (2005).

Comparing the normalised kinematical data, anterior pelvic tilt is found to be most extreme in the active group, occurring as a direct result of an increased running velocity being selected by the majority of the active individuals. Ultimately, lowering the head and dropping the body forwards attempts to counteract, drive and balance the propulsive forces while running and Figures 4.22, 4.23, 4.24 and 4.25 illustrate examples of the different style the running techniques of the active and control group individuals. A particularly predominant range of dorsiflexion and plantarflexion of the ankle can be observed for the average active database in Figure 4.25, which unmistakably represents the most diverse pattern for the average database, even when all of the trials are normalised. This diverse variation of the average trials displaying a far greater range of plantarflexion, demonstrates how the naturally faster running styles of the active group promotes adoption of the more efficient biomechanical barefoot running style (on the toes). Ultimately, the active group evolve and develop to automatically adopt a running technique which no longer mimics the patterns of walking, unlike the control group.

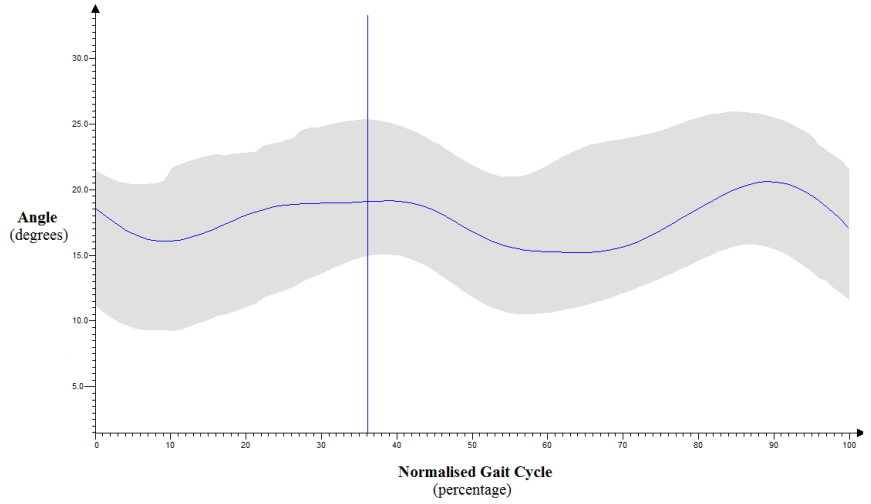

(a) Pelvic Tilt

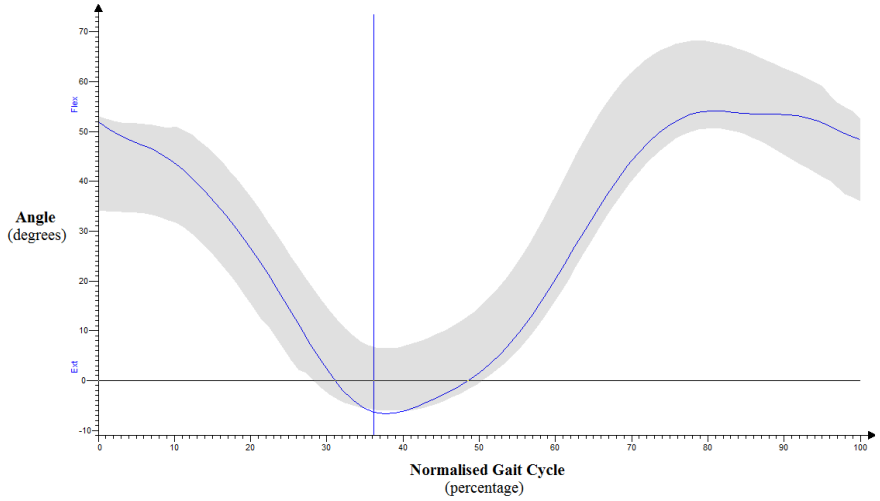

(b) Hip Flexion/Extension

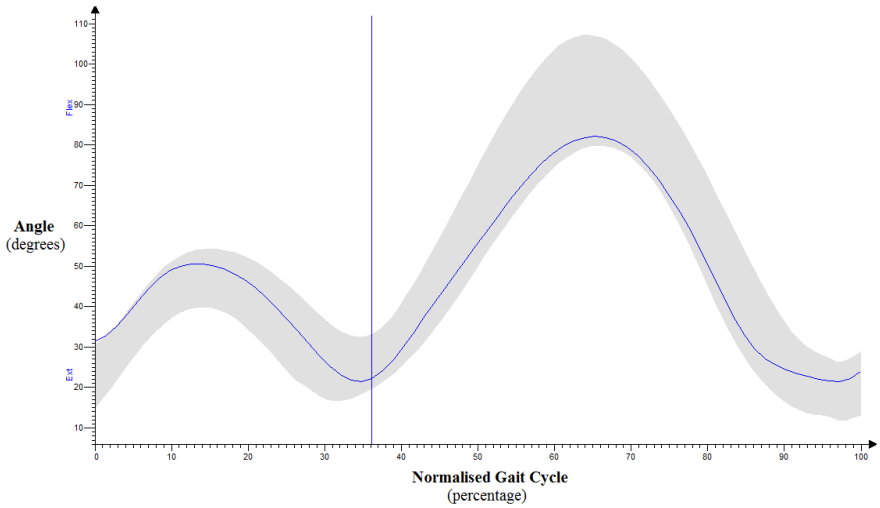

(c) Knee Flexion/Extension

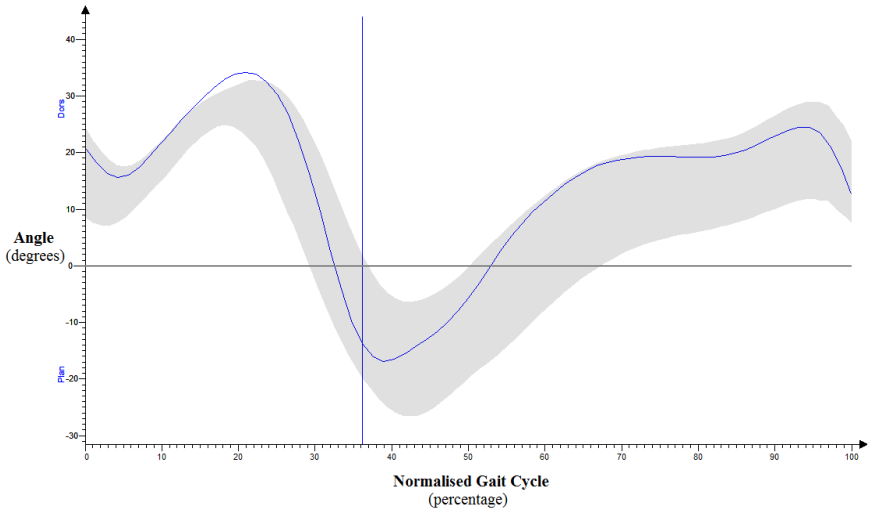

(d) Ankle Dorsiflexion/Plantarflexion

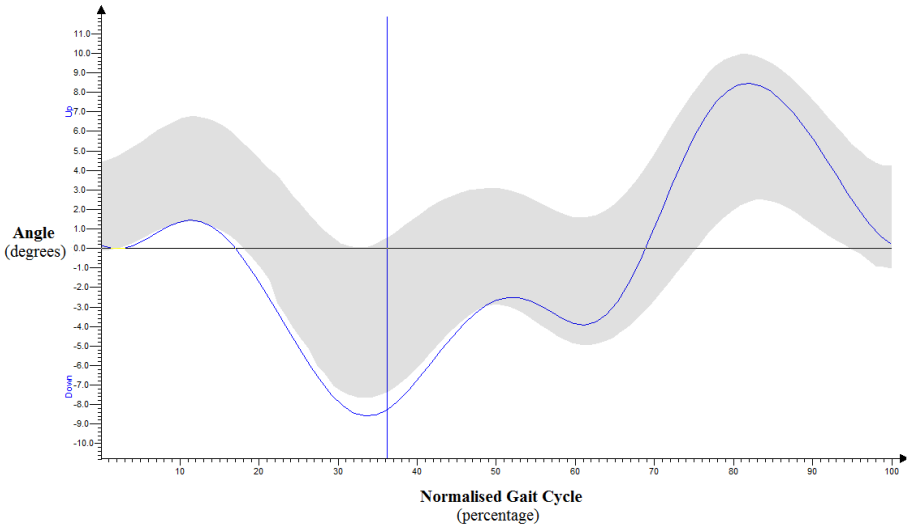

(e) Pelvic Obliquity

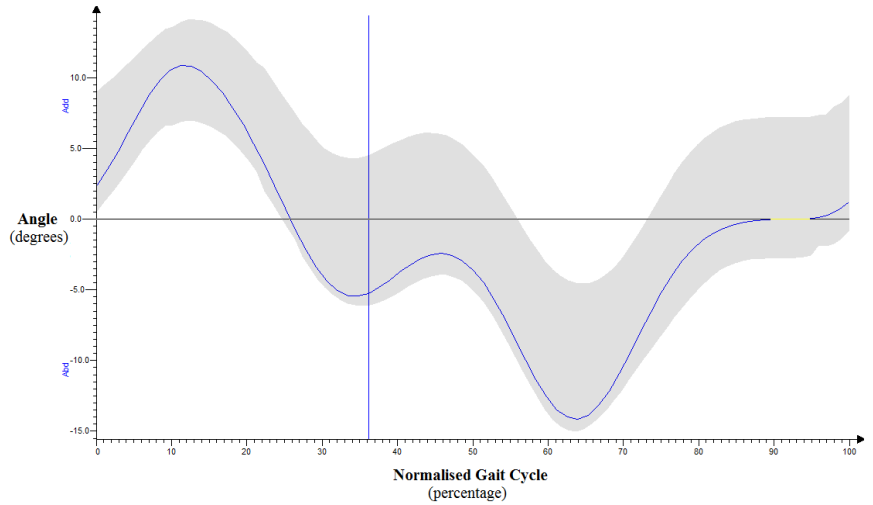

(f) Hip Abduction/Adduction

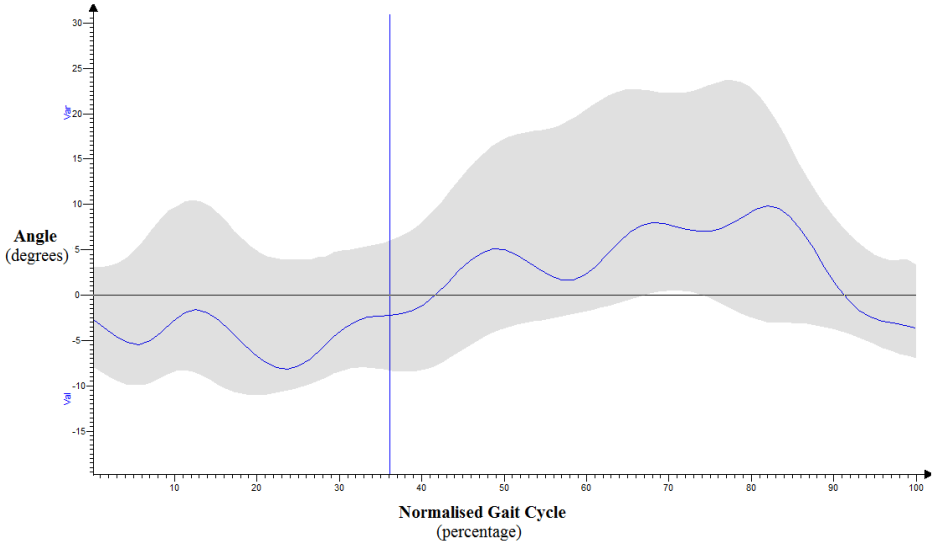

(g) Knee Abduction/Adduction

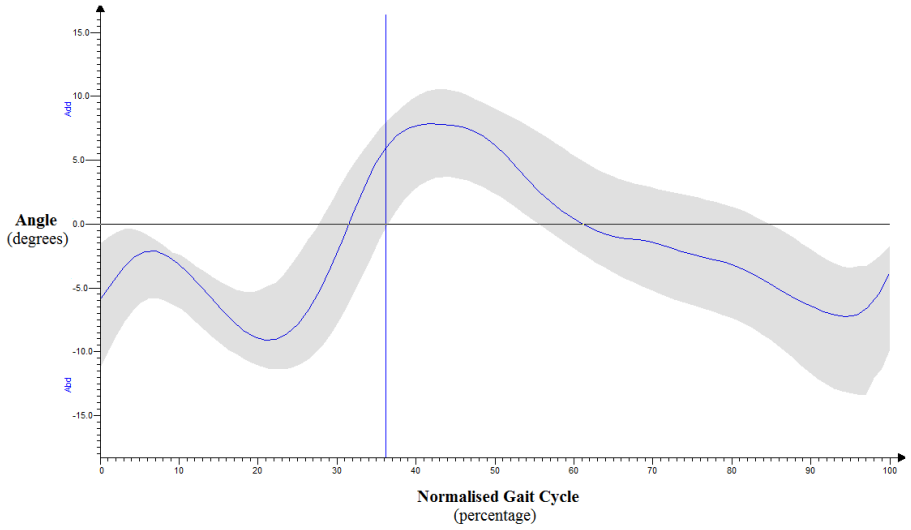

(h) Ankle Abduction/Adduction

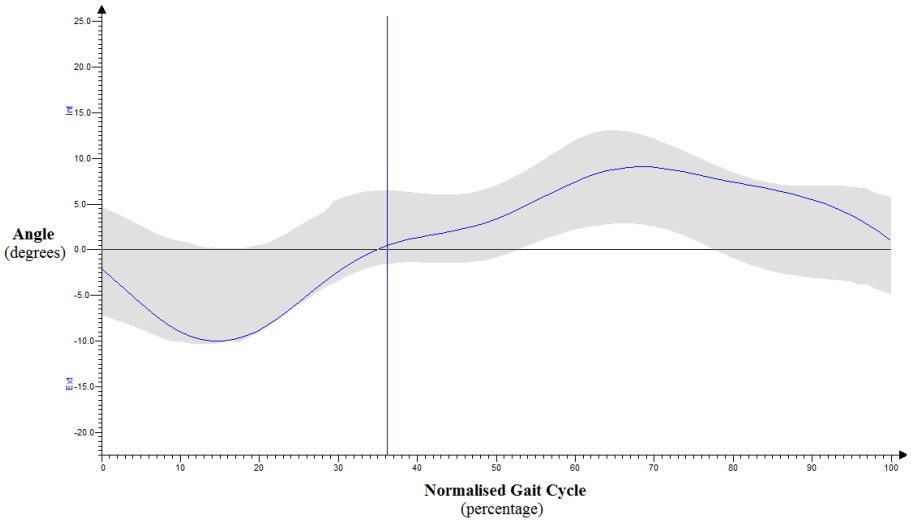

(i) Pelvic Rotation

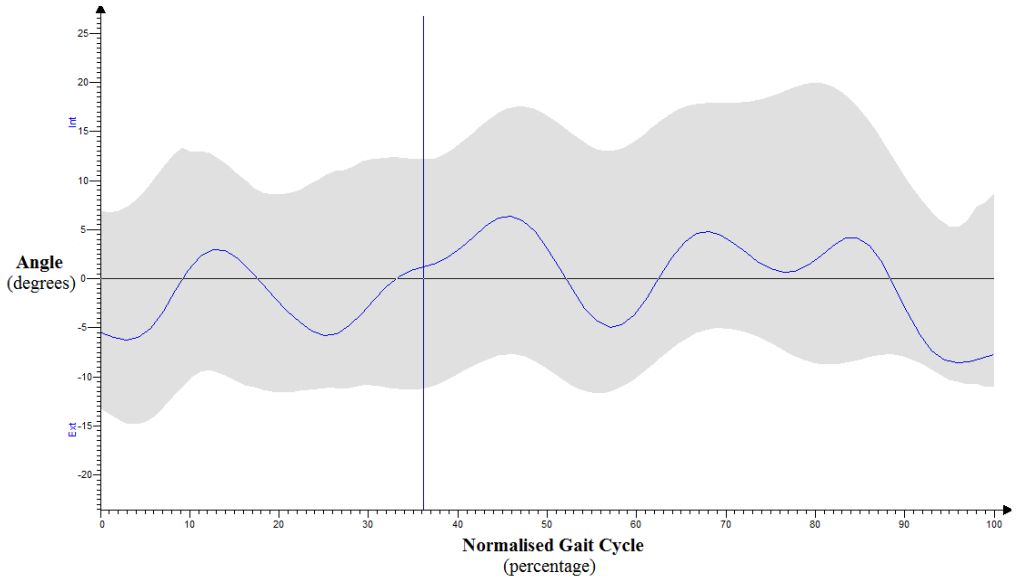

(j) Hip Rotation

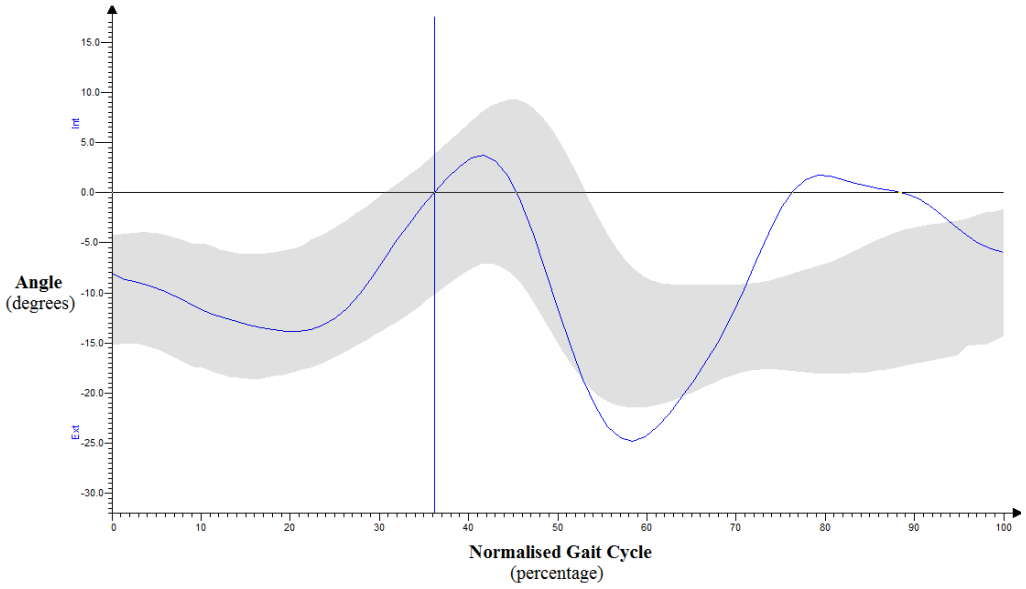

(k) Foot Progression

<u>Figure 4.19(a) through to (k)</u> – Polygon® kinematic graphs for a heel running control individual. The blue line depicts the pattern of the right foot while running with the average range of the running control database shown as the grey shaded area.

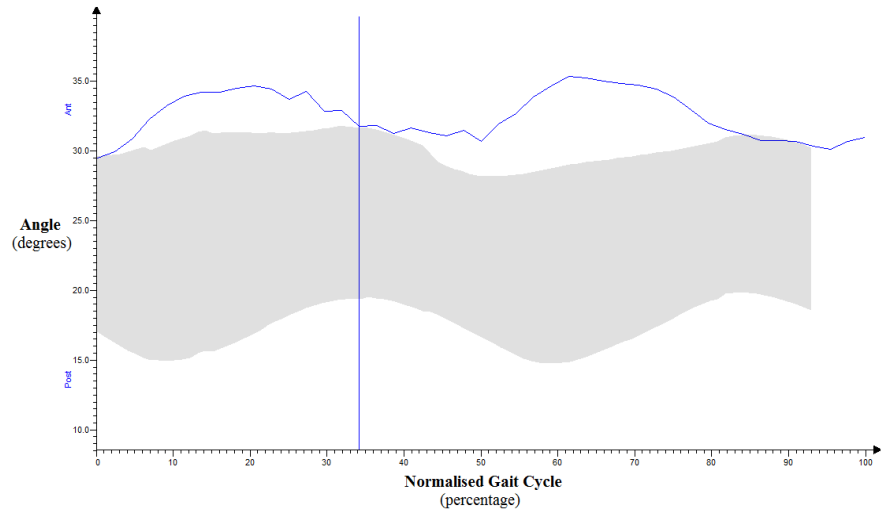

(a) Pelvic Tilt

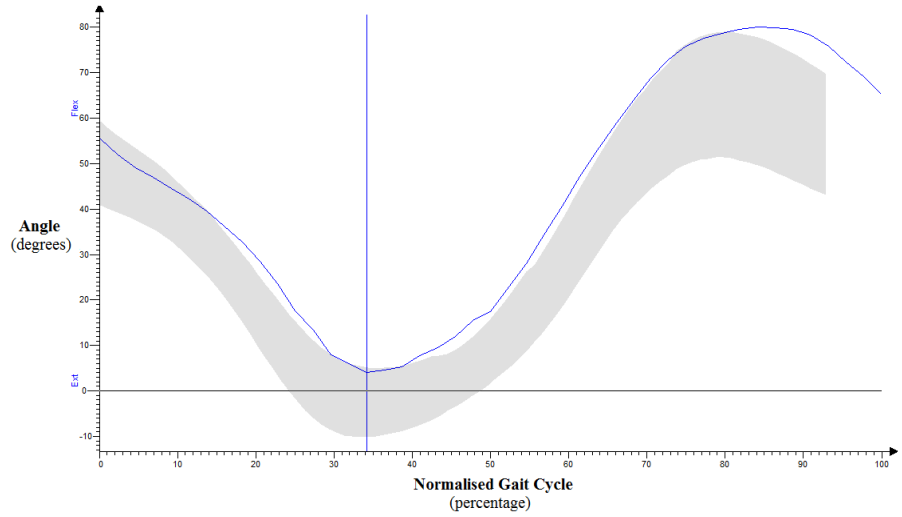

(b) Hip Flexion/Extension

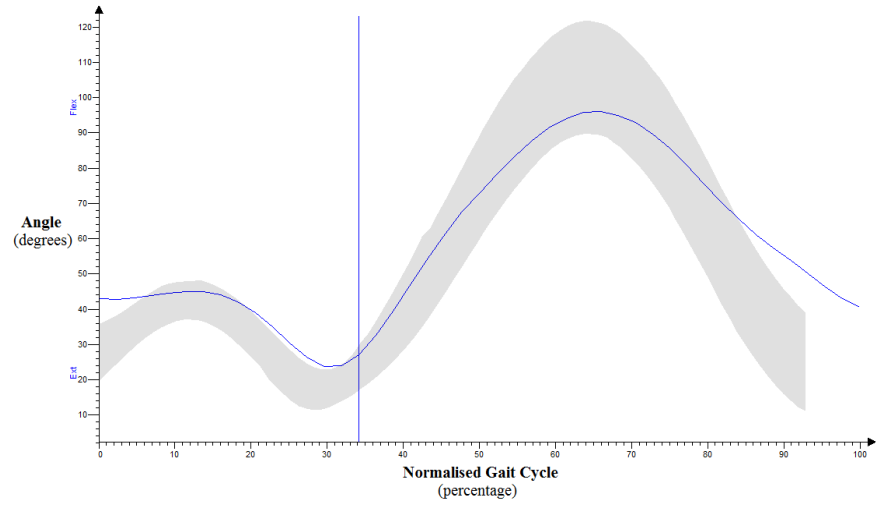

(c) Knee Flexion/Extension

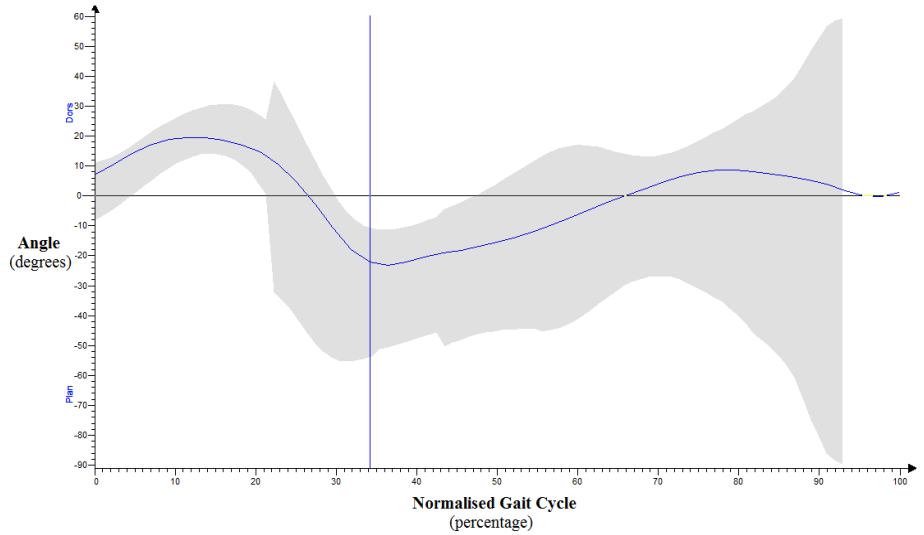

(d) Ankle Dorsiflexion/Plantarflexion

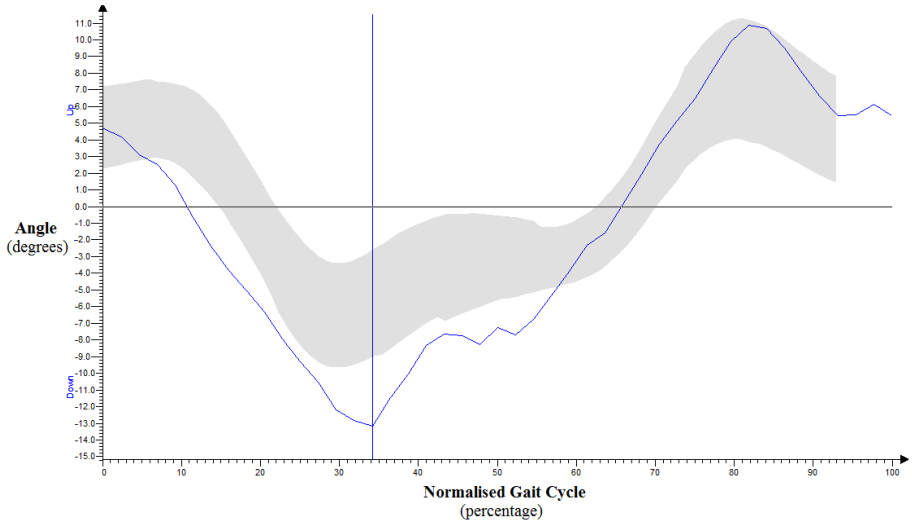

(e) Pelvic Obliquity

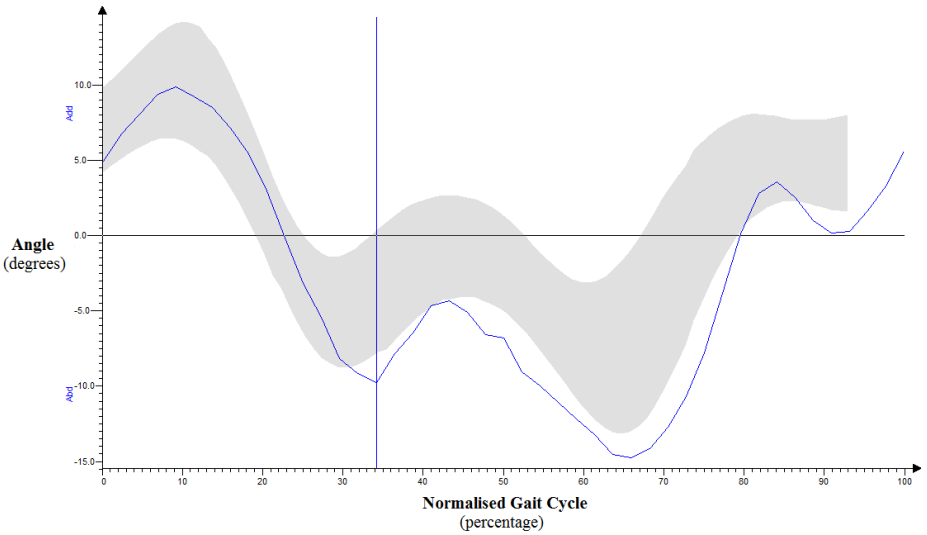

(f) Hip Abduction/Adduction

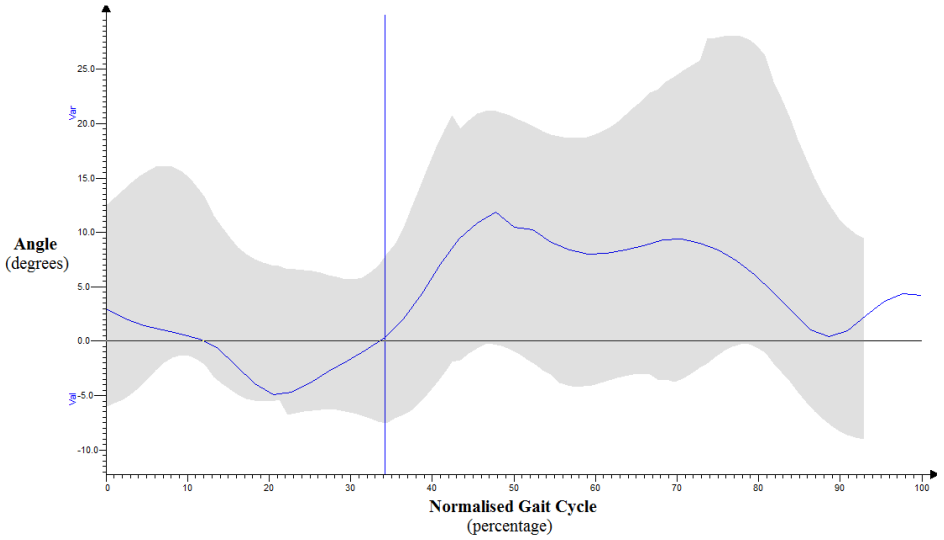

(g) Knee Abduction/Adduction

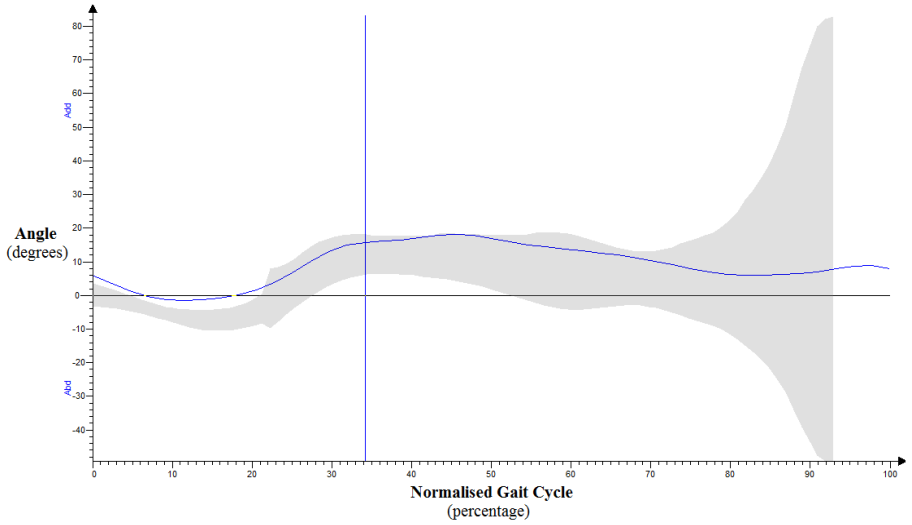

(h) Ankle Abduction/Adduction

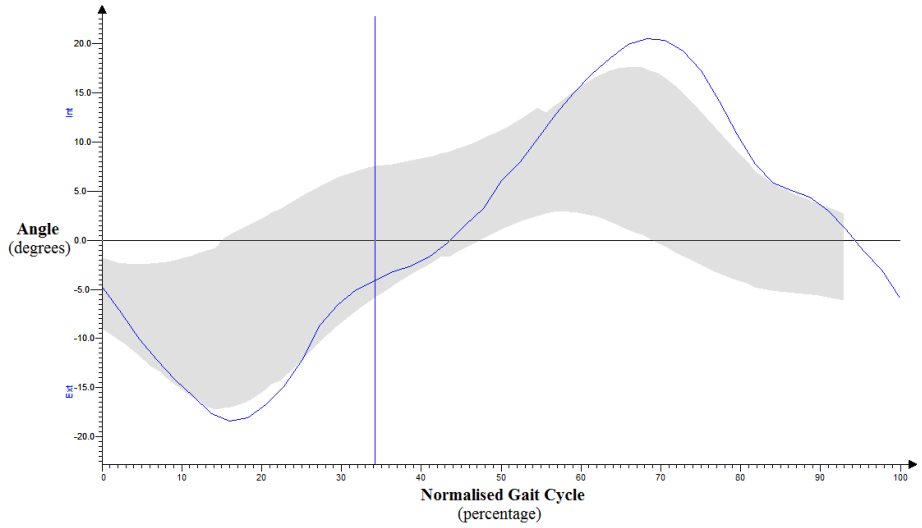

(i) Pelvic Rotation

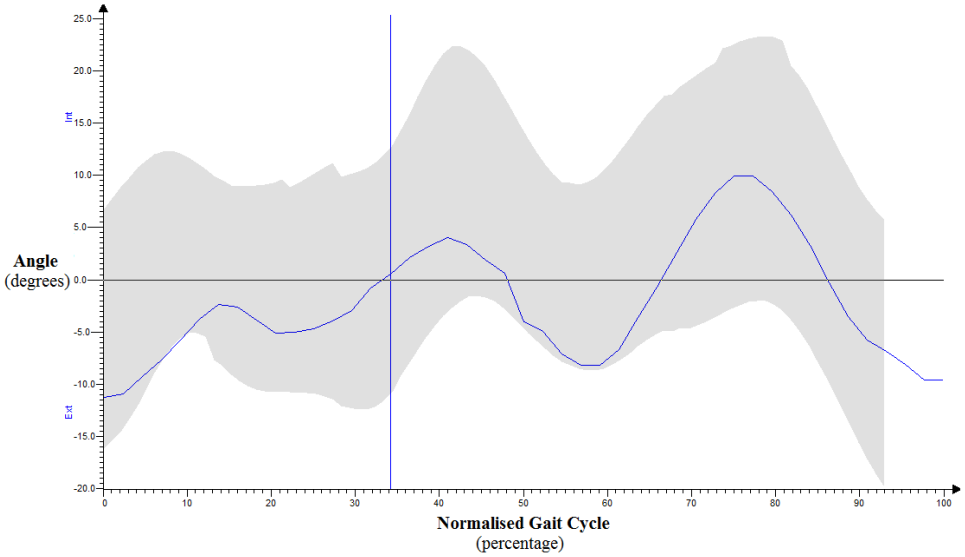

(j) Hip Rotation

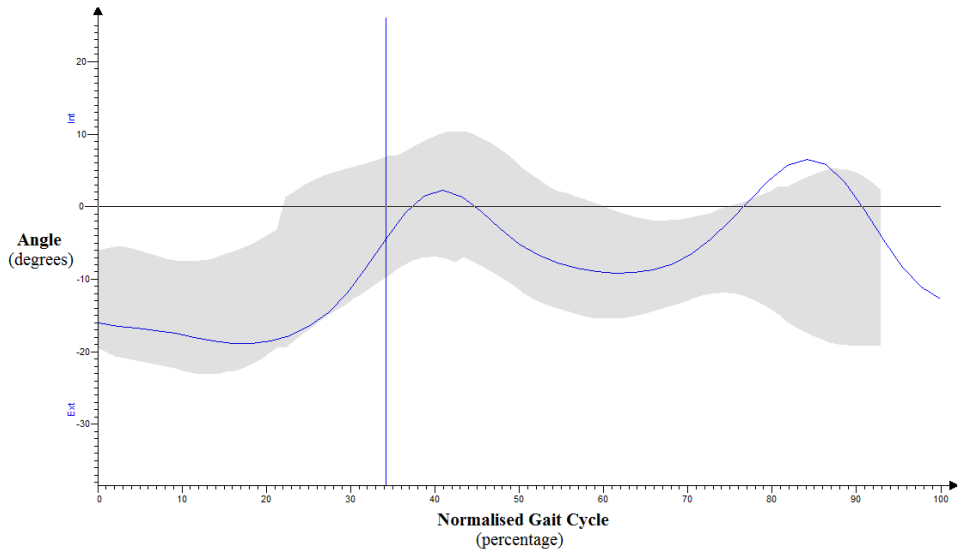

(k) Foot Progression

<u>Figure 4.20(a) to (k)</u> – Polygon® kinematic graphs for a toe running active individual. The blue line depicts the pattern of the right foot while running and the average range of the running control database is shown as the grey shaded area.

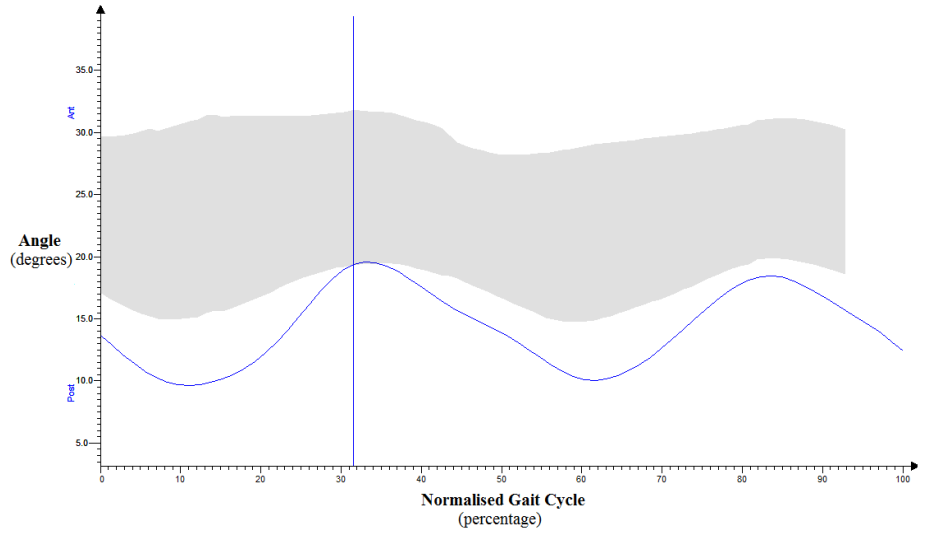

(a) Pelvic Tilt

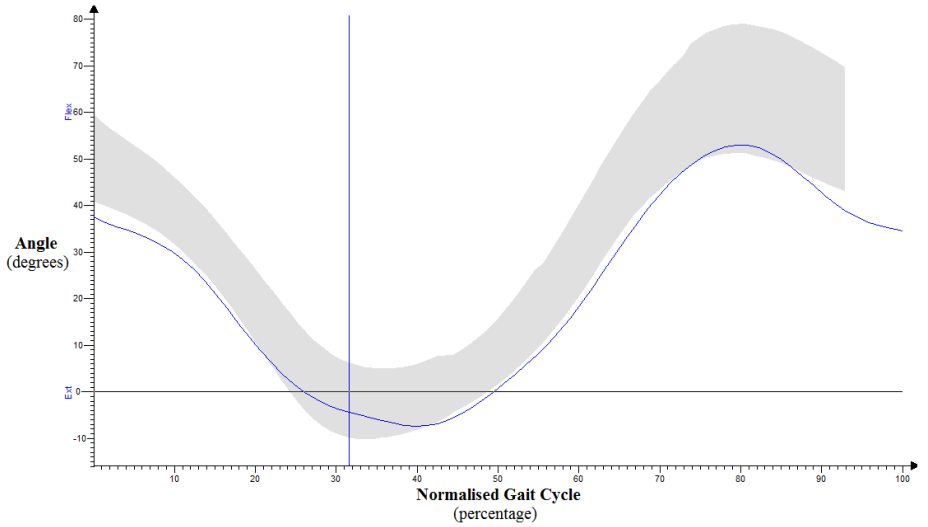

(b) Hip Flexion/Extension

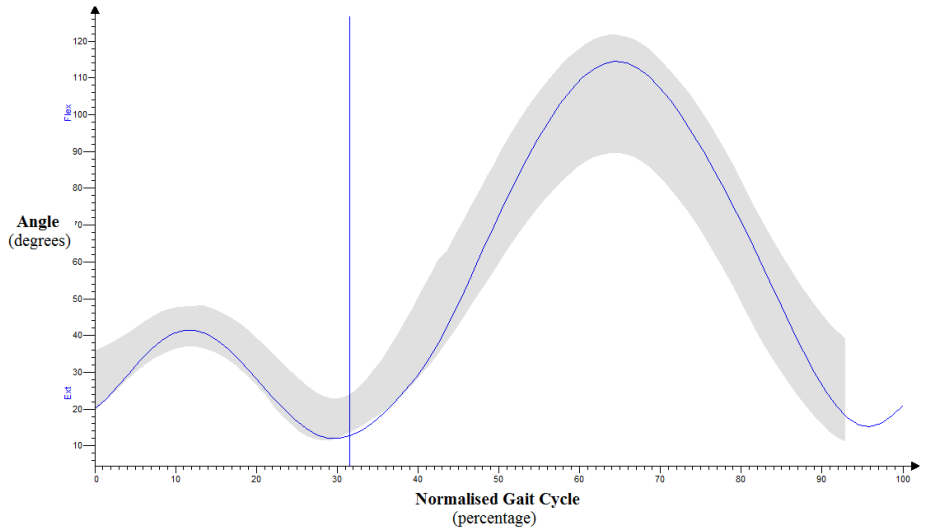

(c) Knee Flexion/Extension

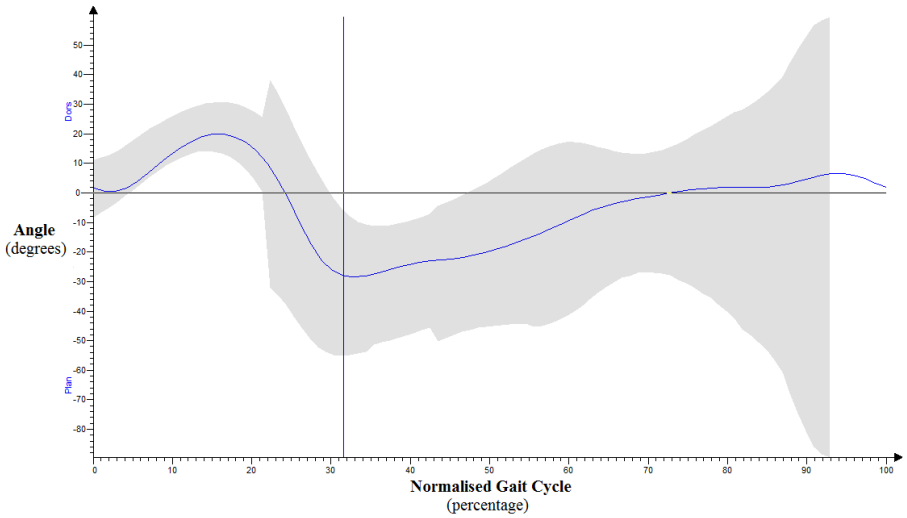

(d) Ankle Dorsiflexion/Plantarflexion

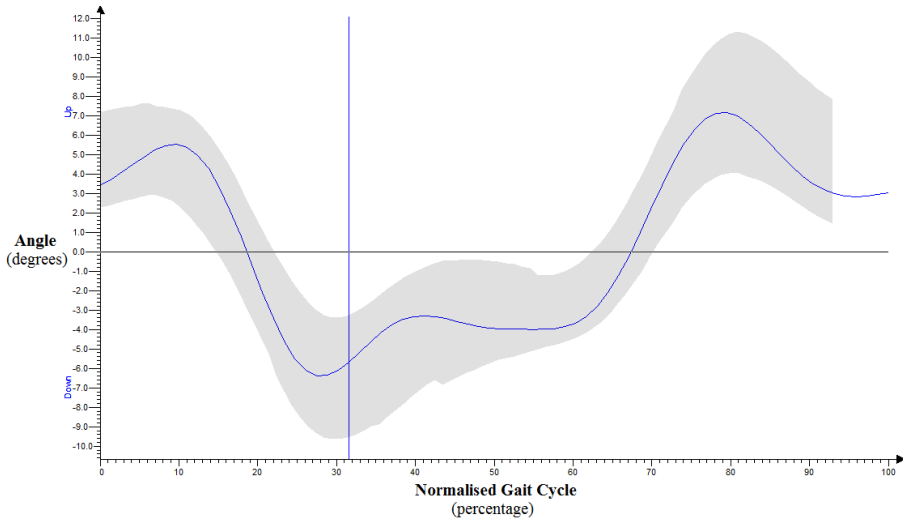

(e) Pelvic Obliquity

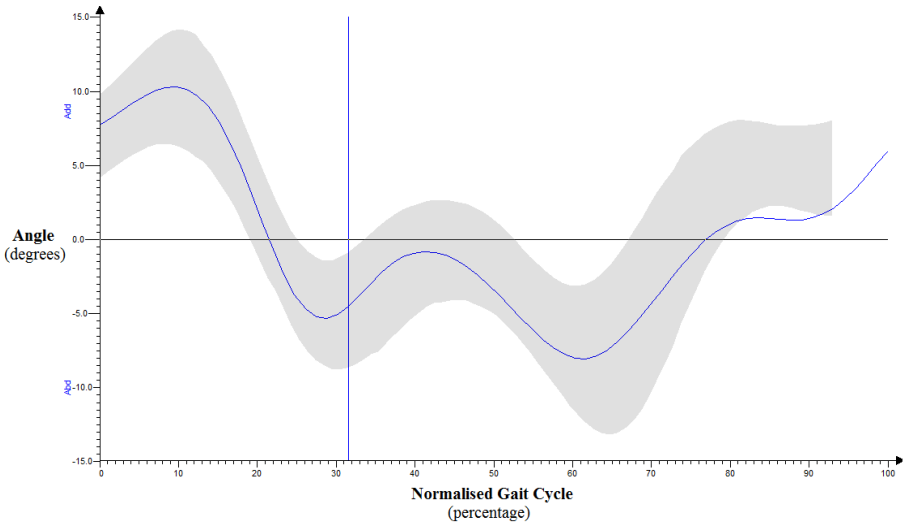

(f) Hip Abduction/Adduction

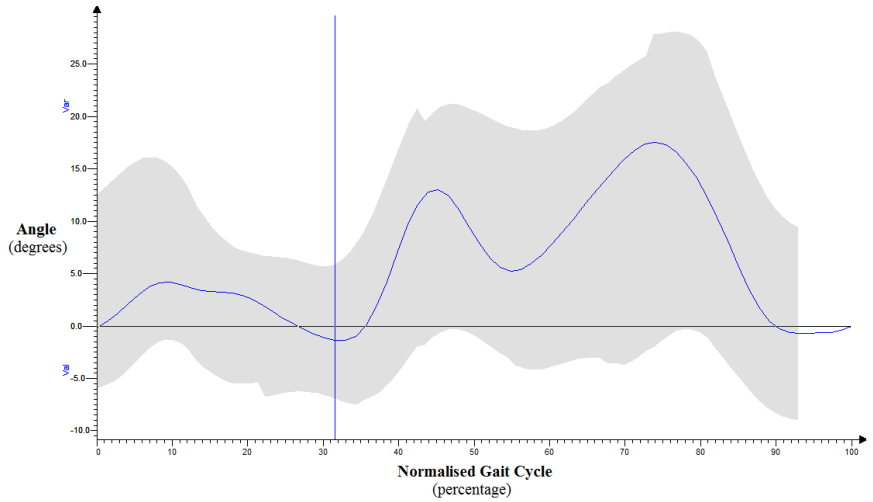

(g) Knee Abduction/Adduction

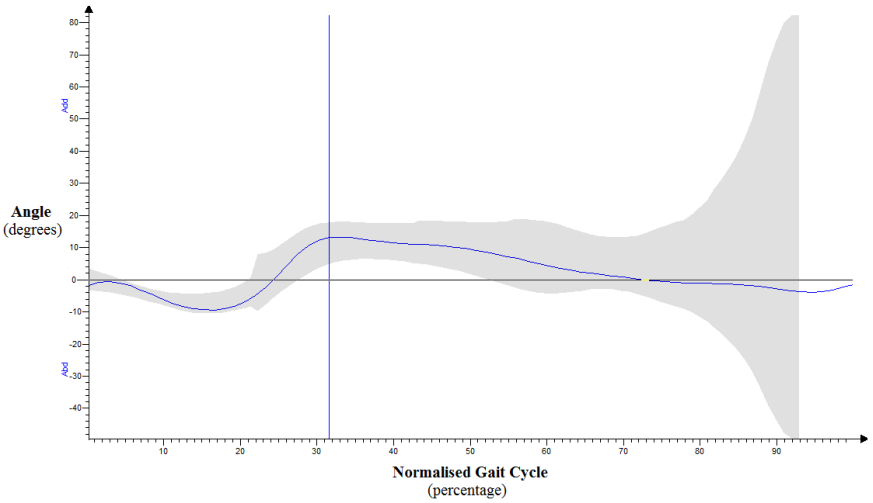

(h) Ankle Abduction/Adduction

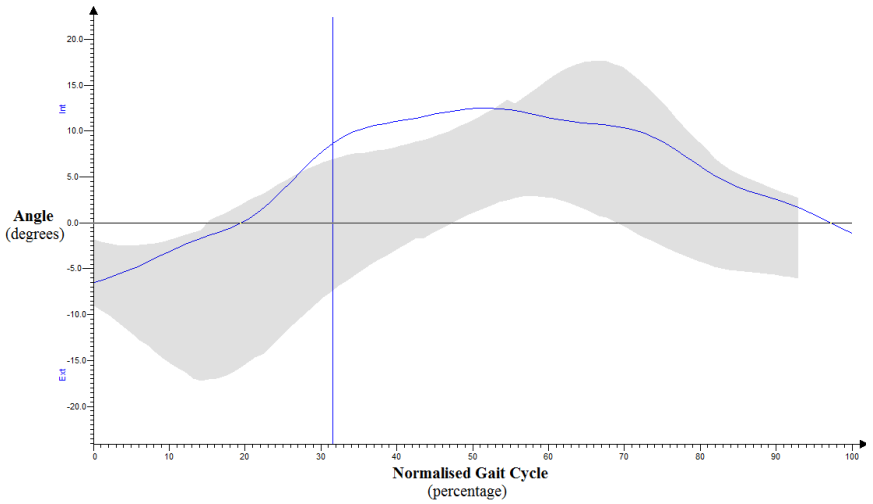

(i) Pelvic Rotation

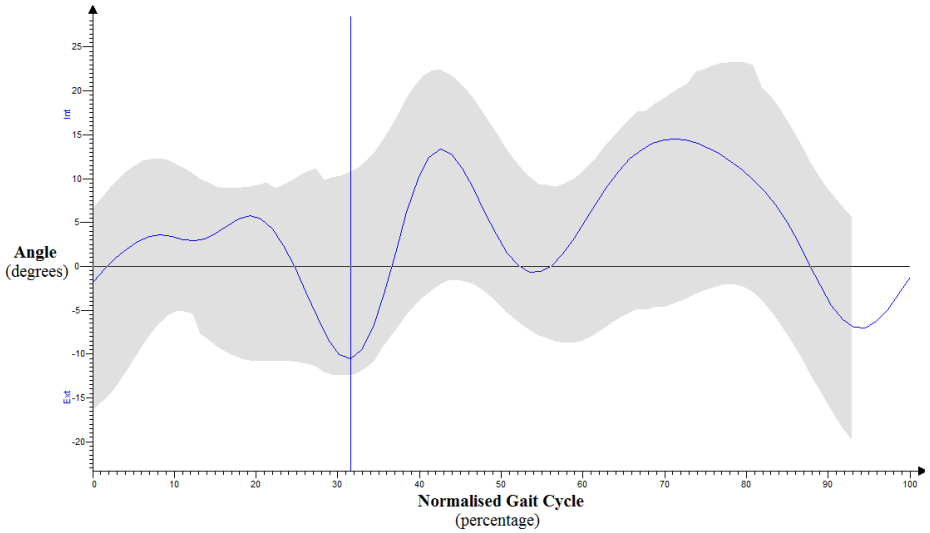

(j) Hip Rotation

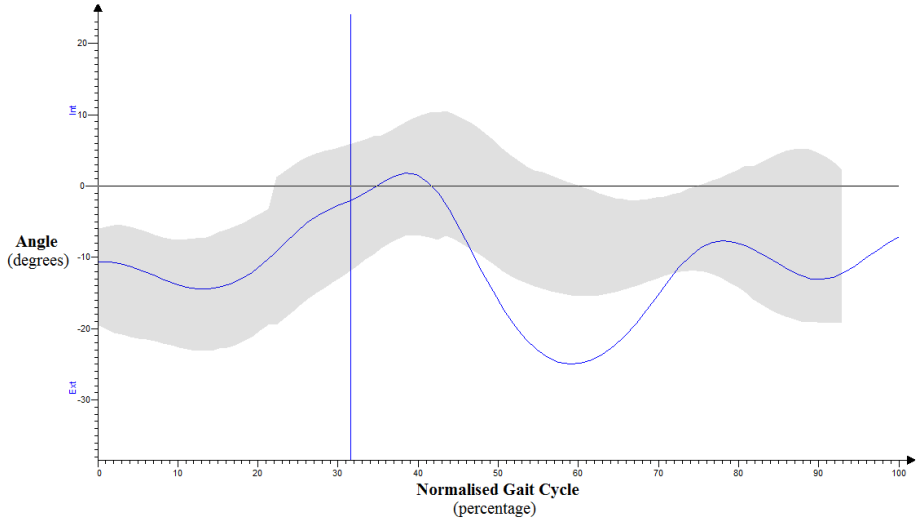

(k) Foot Progression

<u>Figure 4.21(a) to (k)</u> – Polygon® kinematic graphs for a midfoot running active individual. The blue line depicts the pattern of the right foot while running and the average range of the running control database is depicted as the grey shaded area.

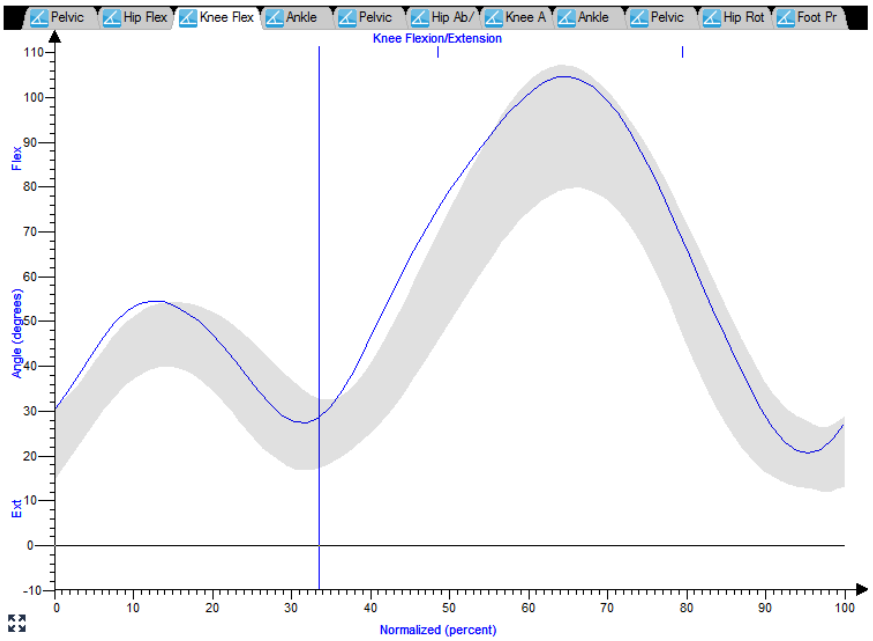

Figure 4.22 – Average control running database for the right feet represented by the grey region with one individual's data for knee flexion and extension (blue line). Notice the average maximum peak flexion falls short of reaching 110 degrees (with a minimum peak of 80 degrees) normalised to 65% of the gait cycle.

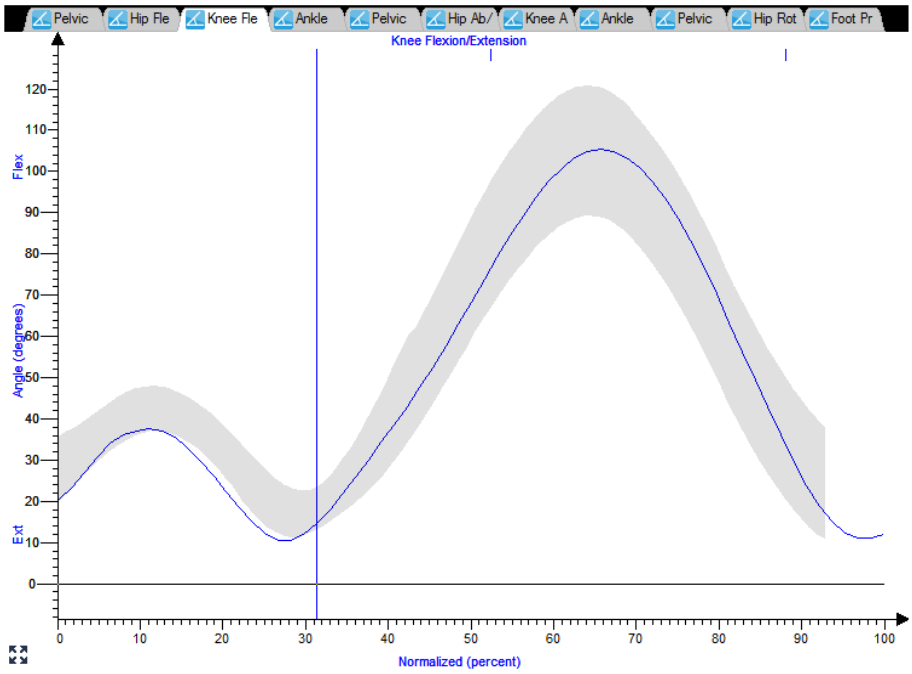

Figure 4.23 – Average active running database for the right feet represented by the grey region to show the average range behind one individual's data for knee flexion and extension (blue line). Notice the average maximum peak flexion reaches greater than 120 degrees (with a minimum peak of 90 degrees) normalised to 65% of the gait cycle.

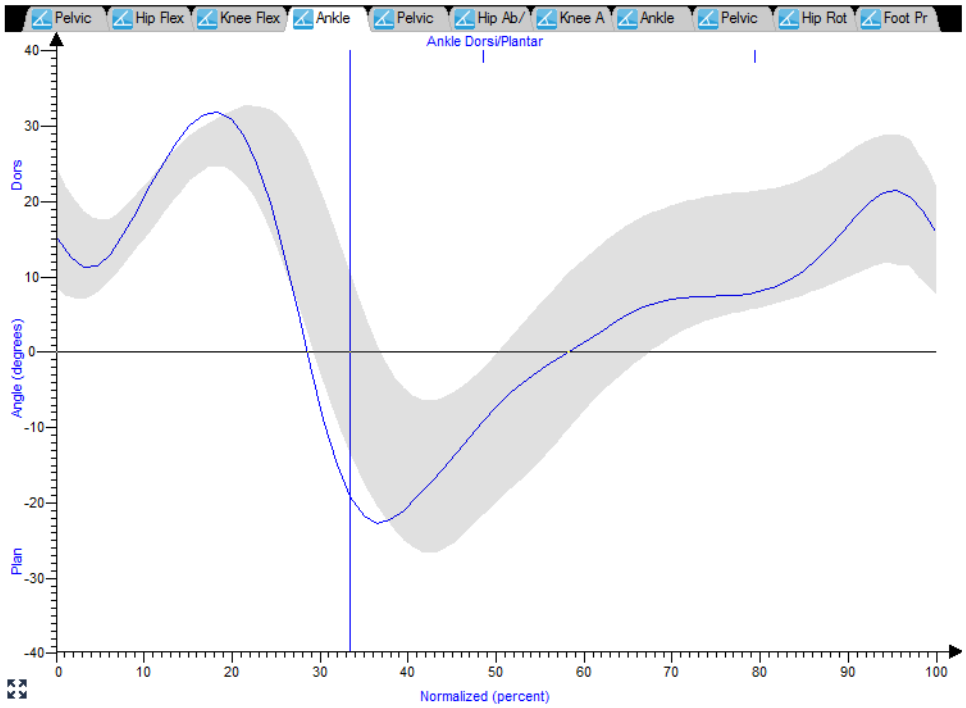

Figure 4.24 – Average control running database for the right feet with the average range for the group represented by the grey region behind one individual's data for ankle dorisflexion and plantarflexion (blue line).

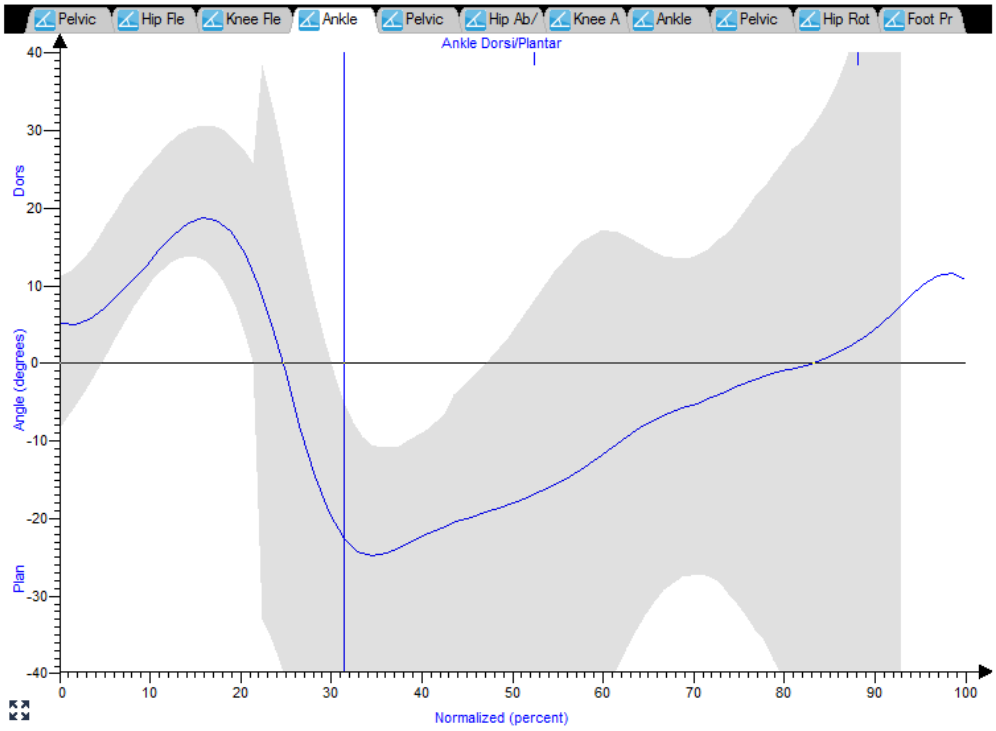

Figure 4.25 – Average active running database for the right feet with the group average range represented by the grey region, with one individual's data for ankle dorisflexion and plantarflexion depicted by the blue line.

4.2.6 Kinetic Data

The raw kinetic data recorded in Vicon® was exported and checked within Polygon® using normalised, average database graphs to assess the reliability of the numerical data. Figures 4.26, 4.27, 4.28 and 4.29 provide examples of the graphical visualisation of the kinetic output data for both walking and running, in the control and active groups respectively, which are referenced and can be compared with the expected average walking pattern (represented by the green line). The self selected speed each individual chose to repeat across all of the running trials ultimately coincided and supported the literature which also found that as the running velocity increases, the greater and more dramatic the range of motion (or excursion) at the joints in the sagittal plane (Õunpuu, 1994; Zackowski *et al.*, 2004).

The graphical representation of kinetic data during walking and running is helpful when analysing the gait of single individuals; however to compare the kinetic differences between groups it is necessary to export the raw data directly from Vicon®. The exported advanced ASCII file creates an output file detailing the maximum and minimum values for the range of motion during each gait cycle. A non-parametric one-sample Kolmogorov-Smirnov Test revealed that the range of motion for each variable did not follow normal distribution; therefore the Mann-Whitney Test was applied to compare the minimum and maximum range of motion values of the active group and control group.

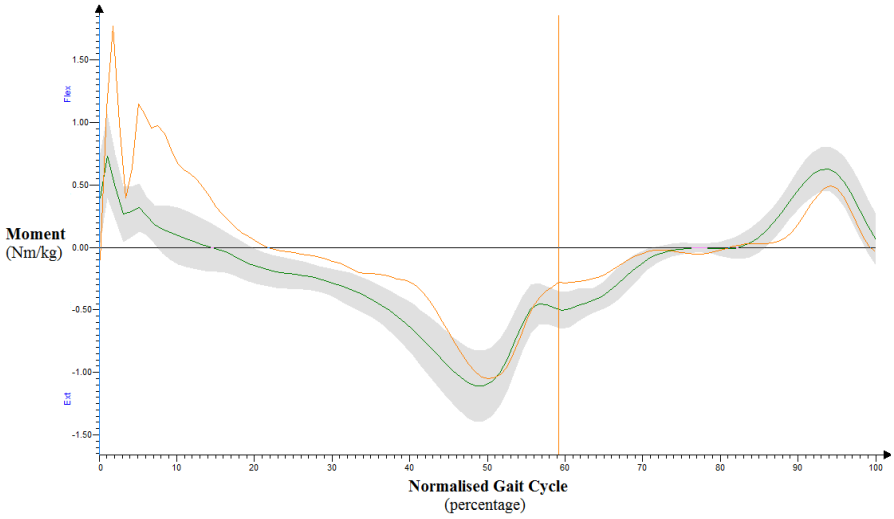

(a) Hip Flexion/Extension

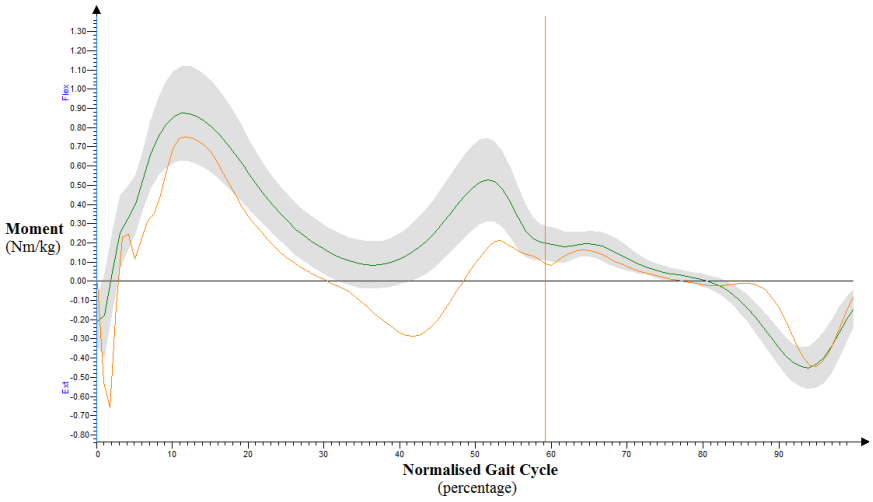

(b) Knee Flexion/Extension

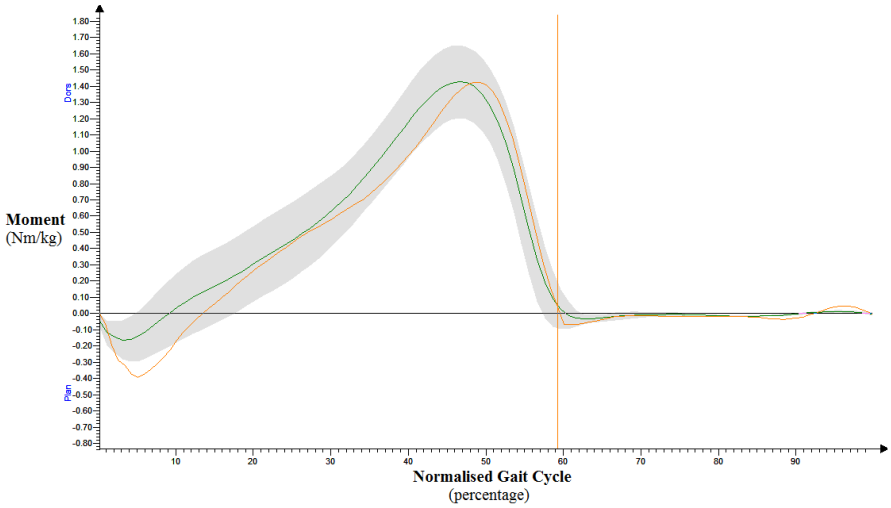

(c) Ankle Dorsiflexion/Plantarflexion

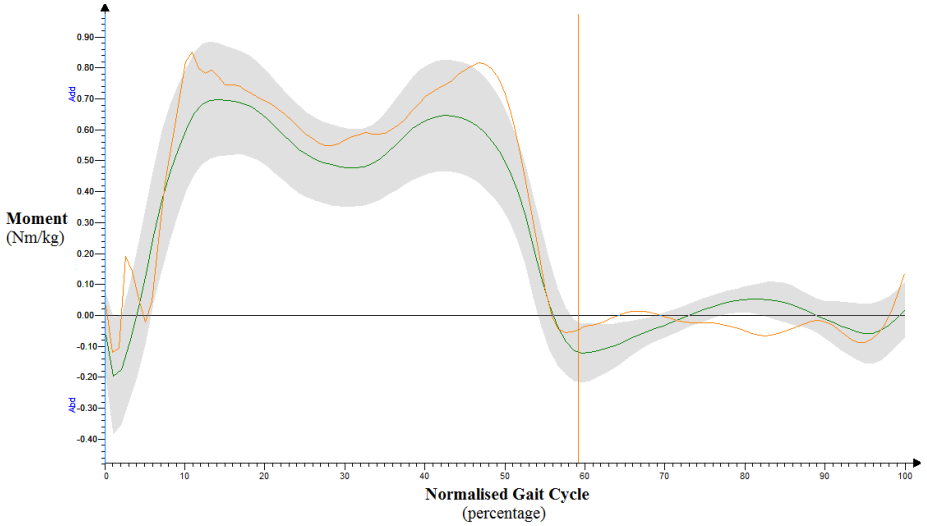

(d) Hip Abduction/Adduction

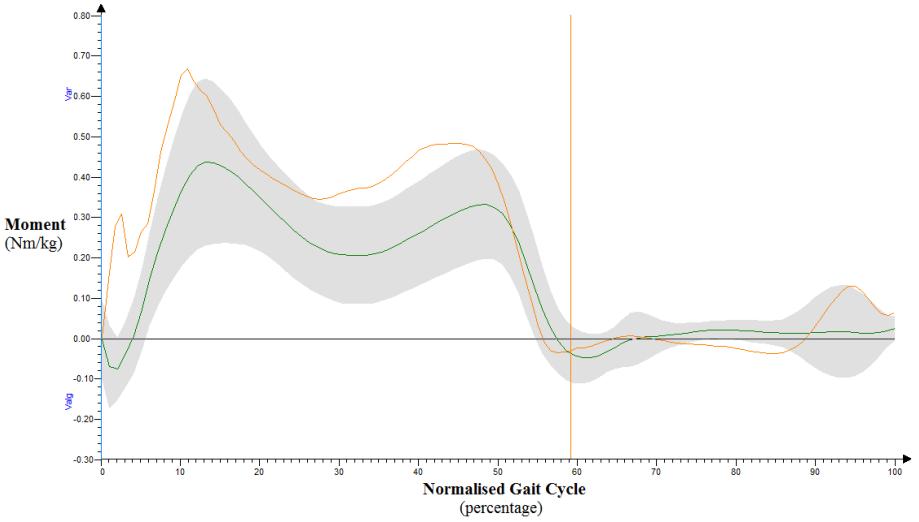

(e) Knee Valgus/Varus

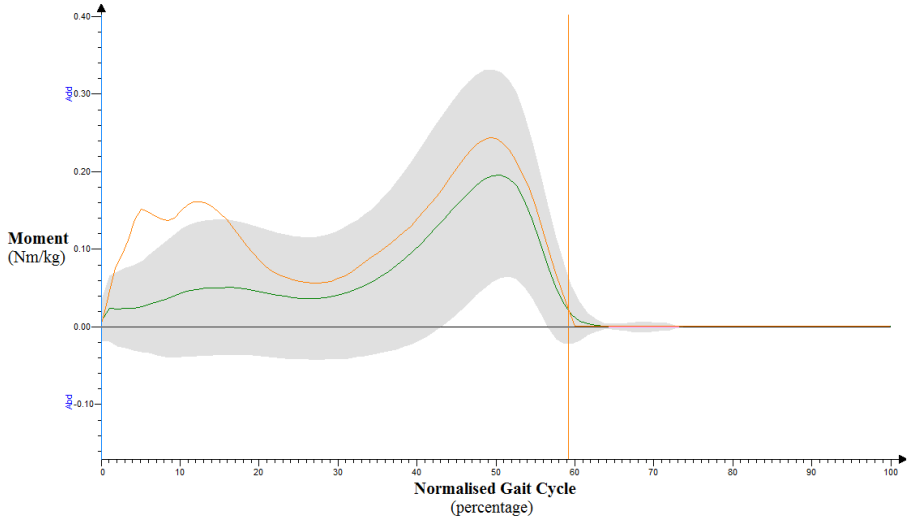

(f) Ankle Abduction/Adduction

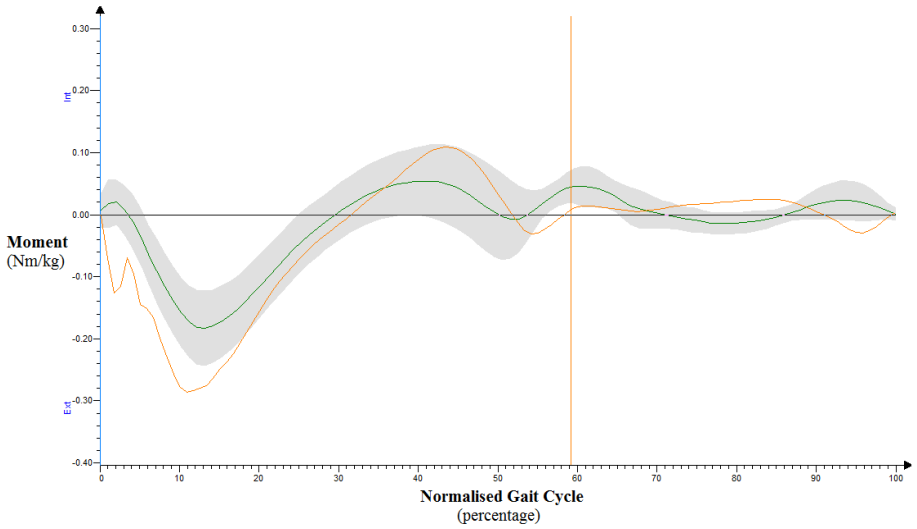

(g) Hip Rotation

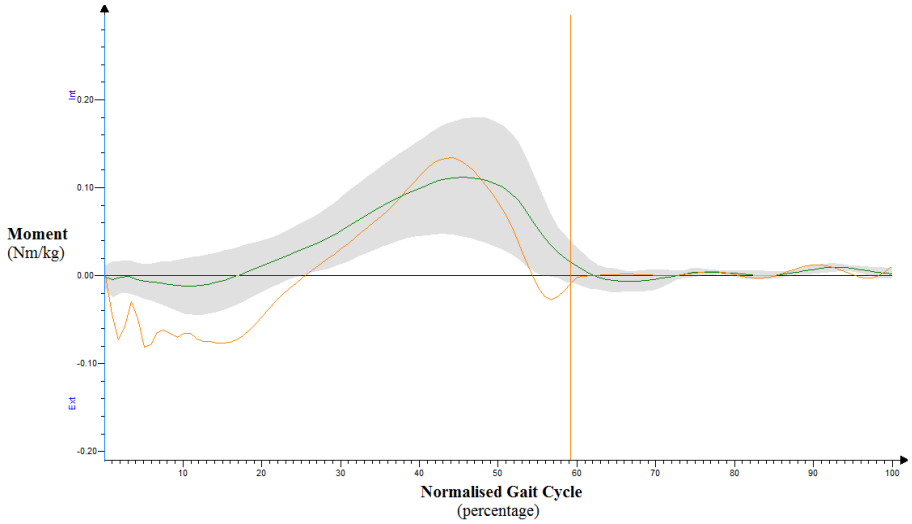

(h) Knee Rotation

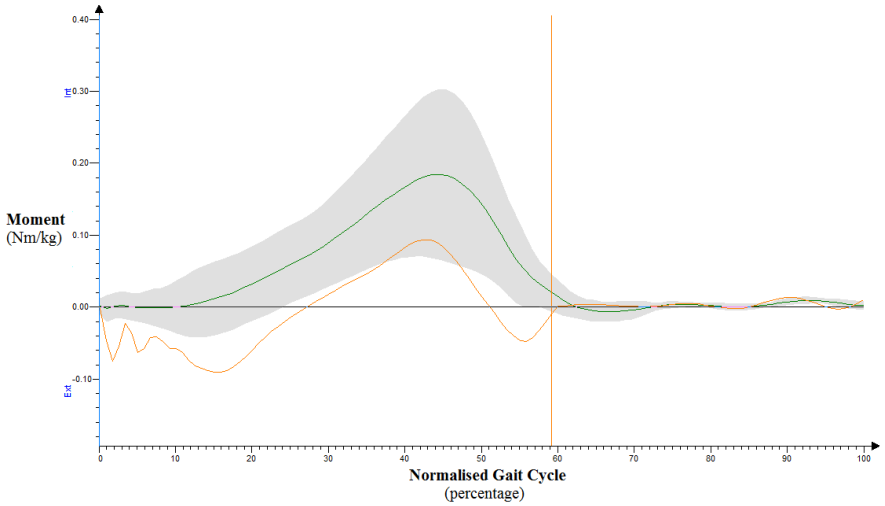

(i) Ankle Rotation

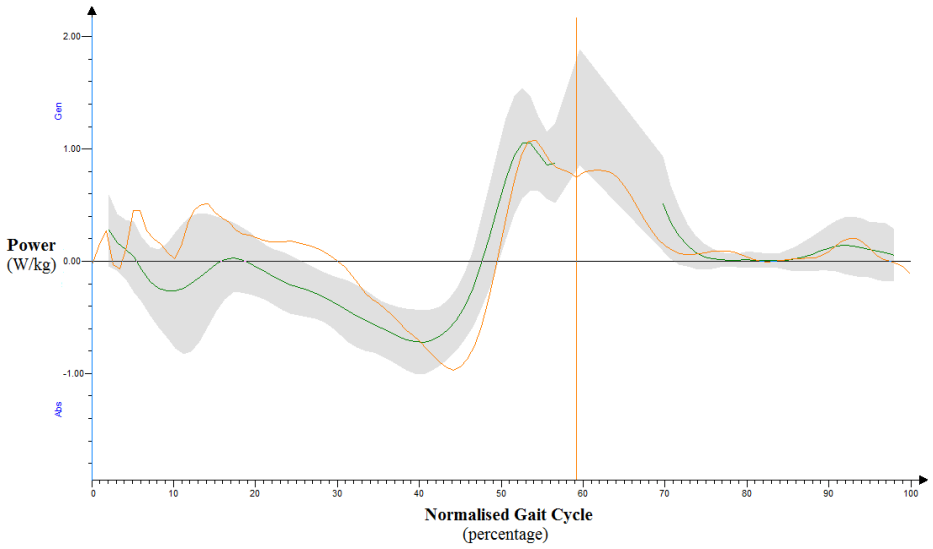

(j) Hip Power

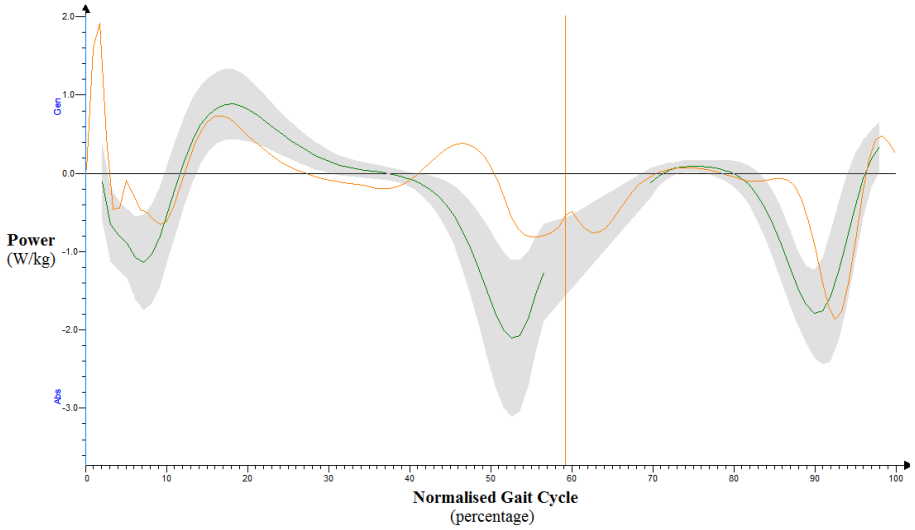

(k) Knee Power

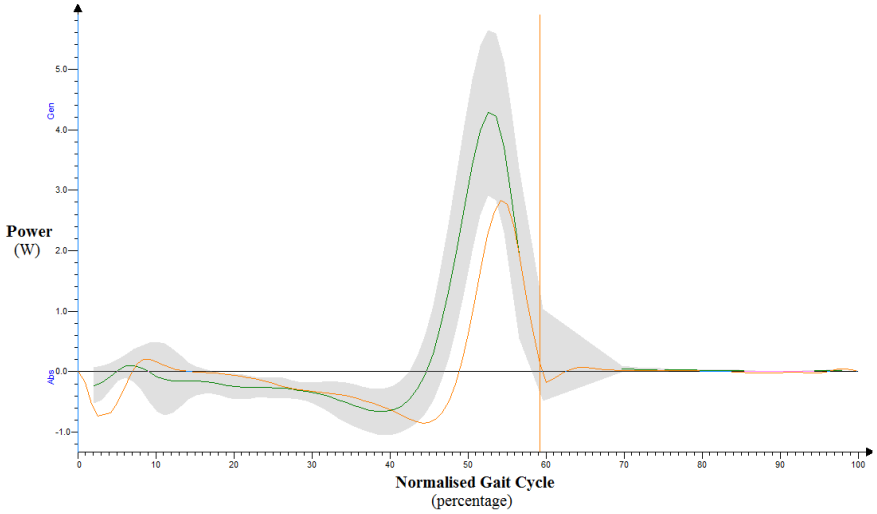

(l) Ankle Power

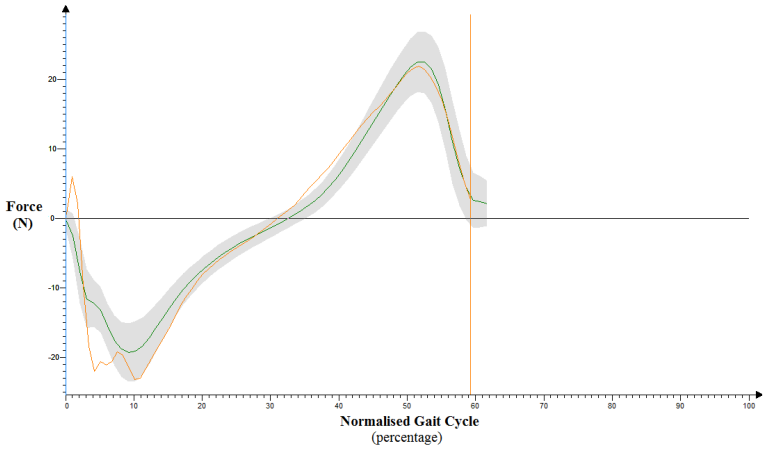

(m) Normalised GRF – X

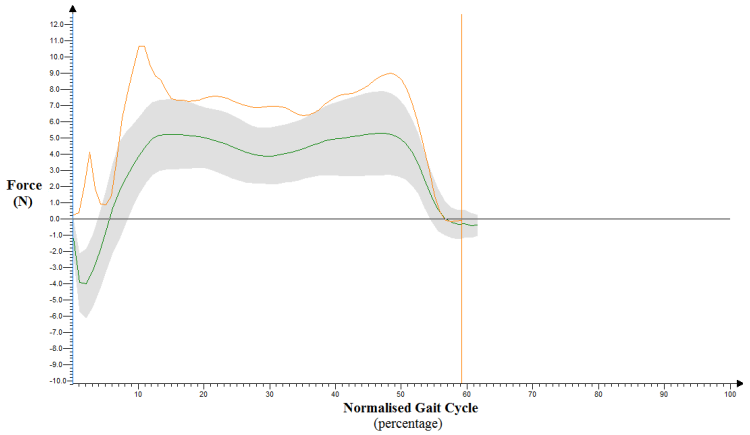

(n) Normalised GRF – Y

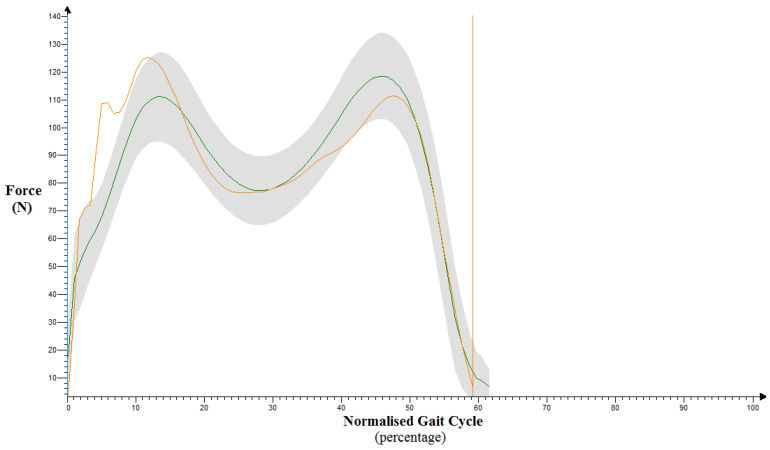

(o) Normalised GRF – Z

<u>Figures 4.26(a) to (o)</u> – Examples of the graphical kinetic outputs from Polygon® of one walking trial from the control group. The walking average range for the control group database is depicted by the grey shaded areas with the green line representing the mean. The orange line highlights the cycle of the left foot.

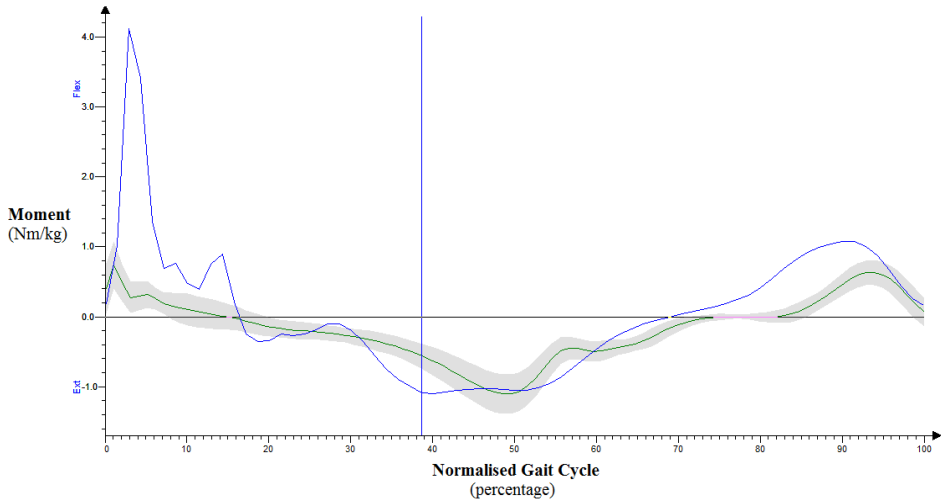

(a) Hip Flexion/Extension

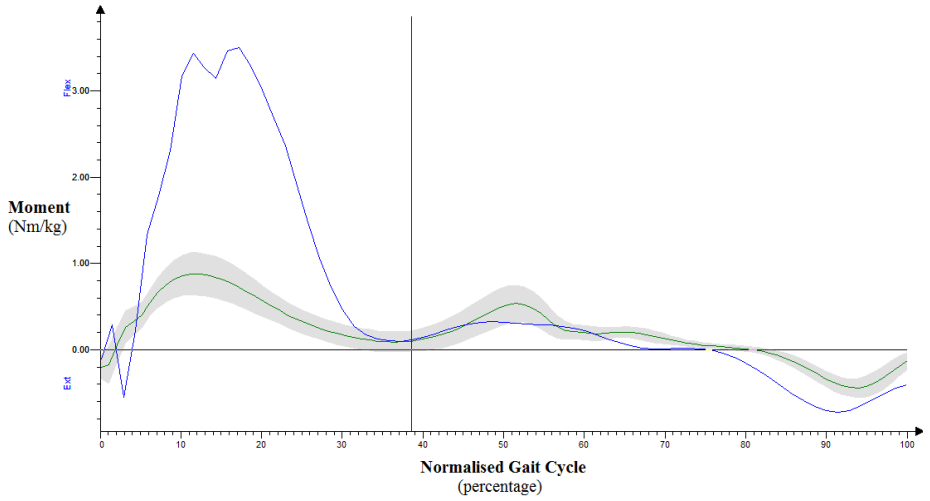

(b) Knee Flexion/Extension

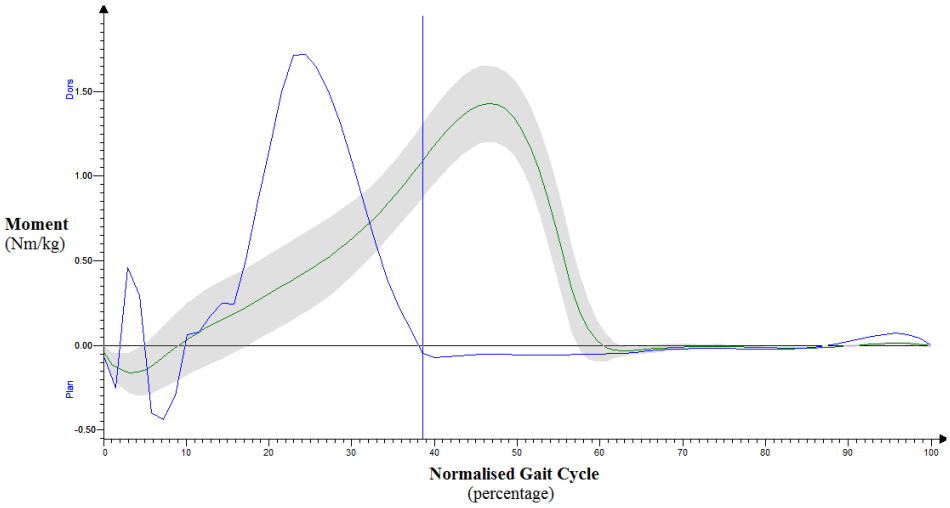

(c) Ankle Dorsiflexion/Plantarflexion

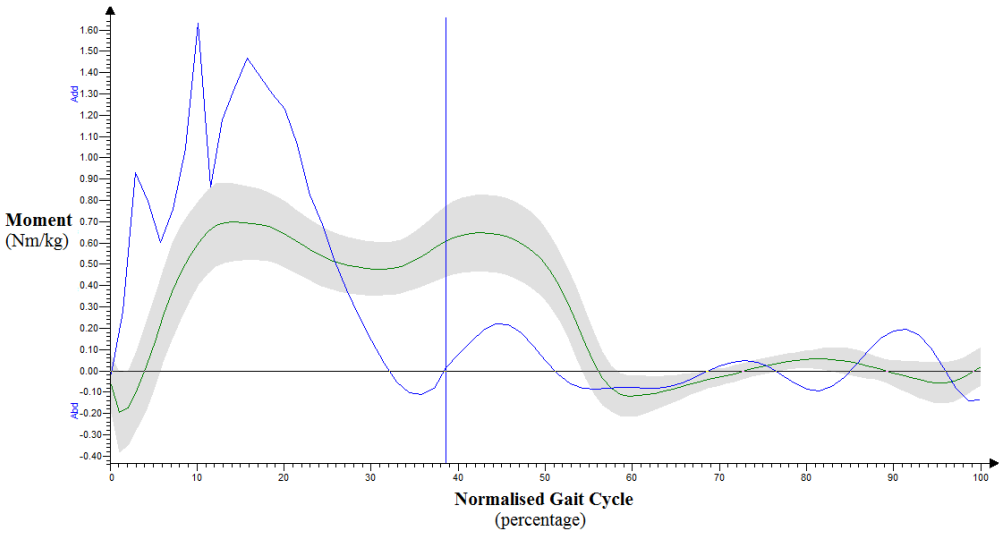

(d) Hip Abduction/Adduction

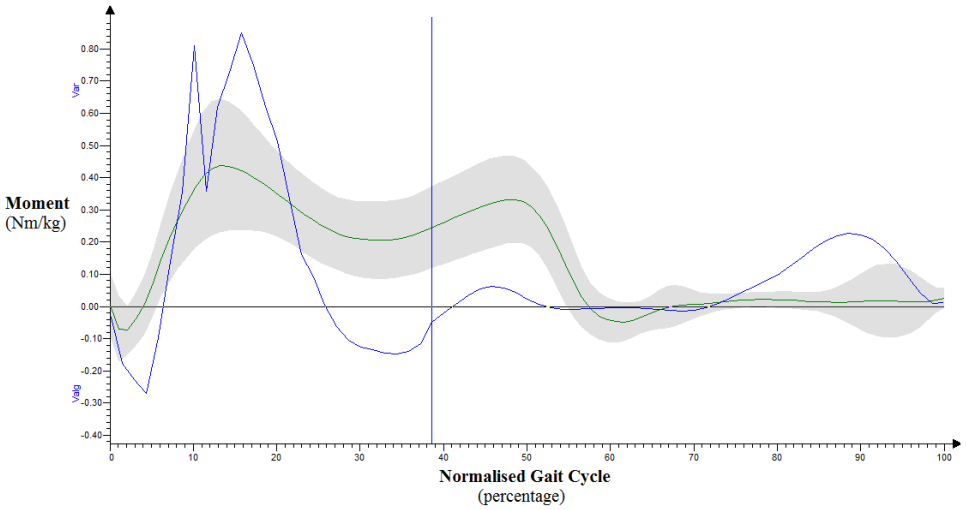

(e) Knee Valgus/Varus

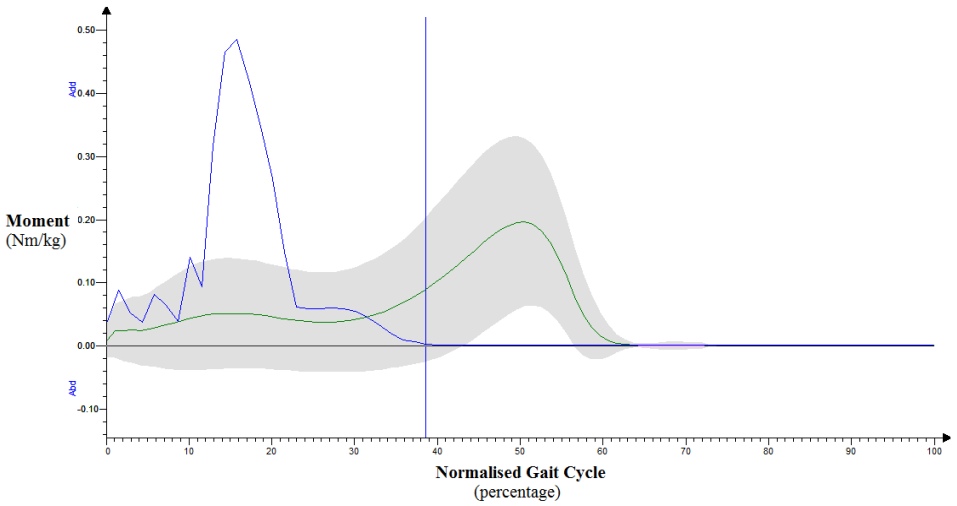

(f) Ankle Abduction/Adduction

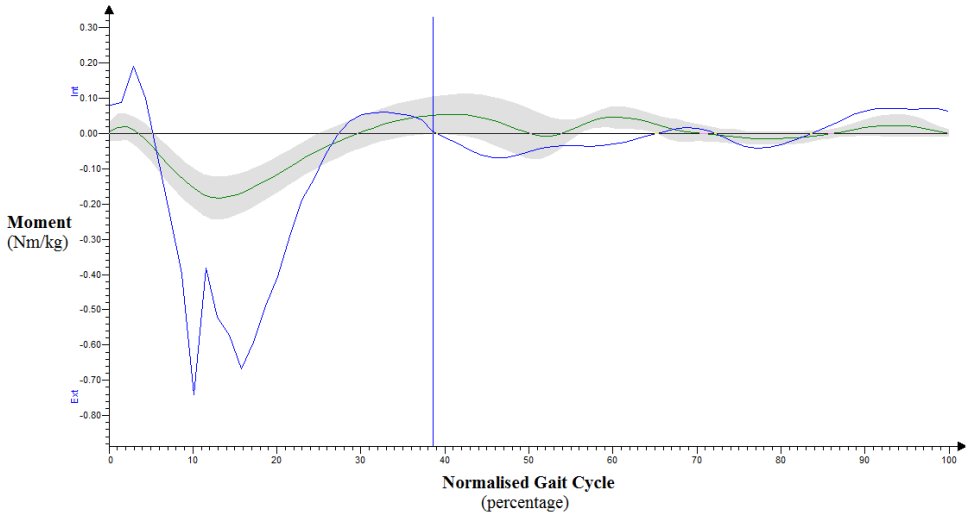

(g) Hip Rotation

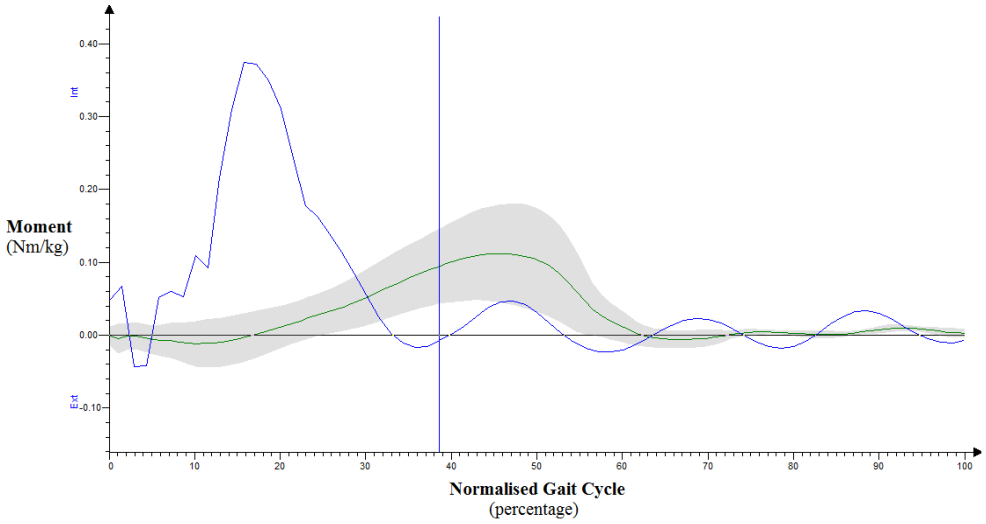

(h) Knee Rotation

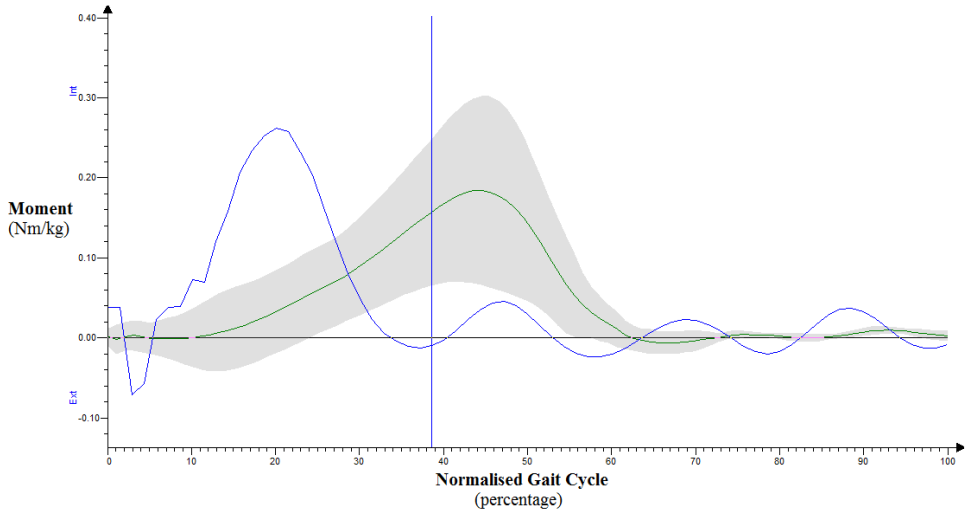

(i) Ankle Rotation

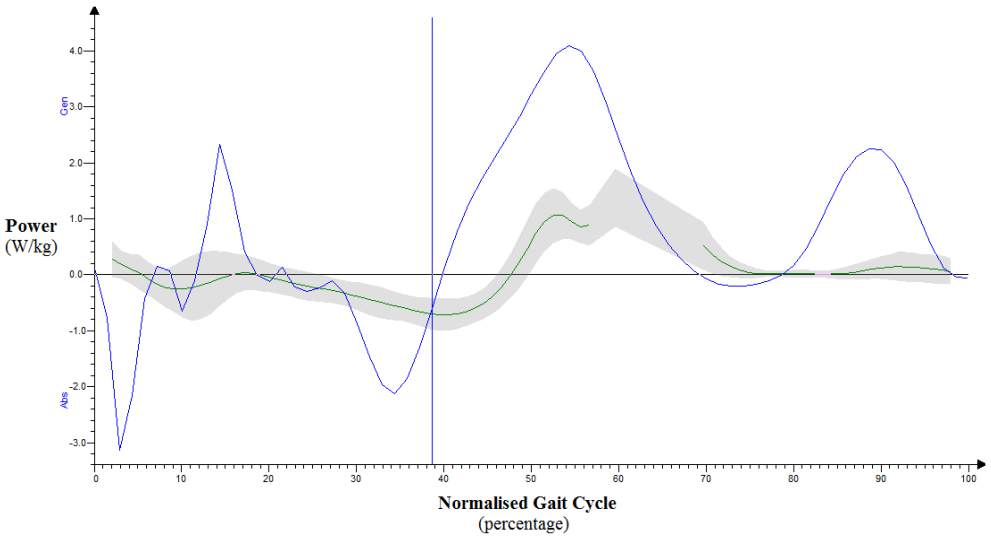

(j) Hip Power

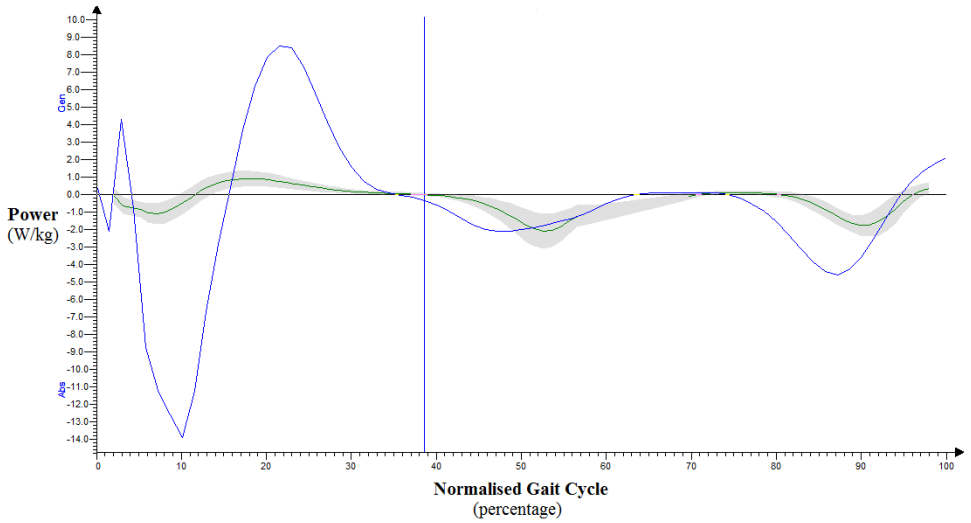

(k) Knee Power

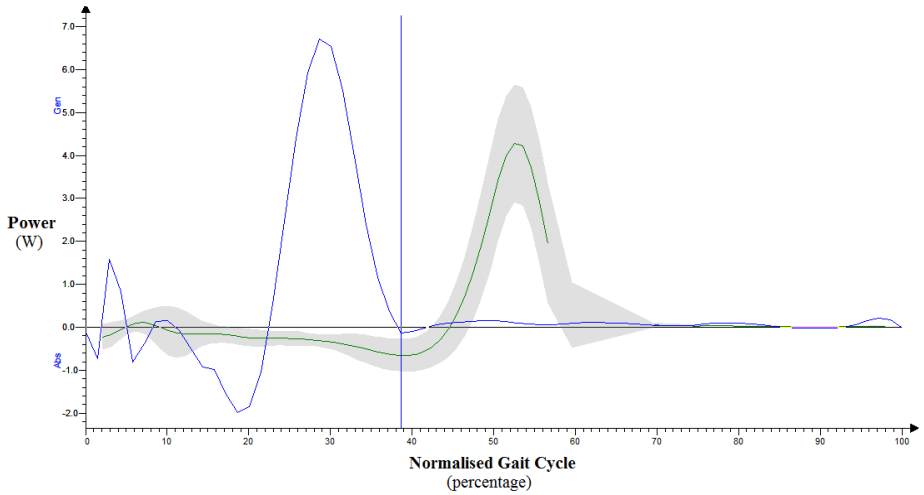

(l) Ankle Power

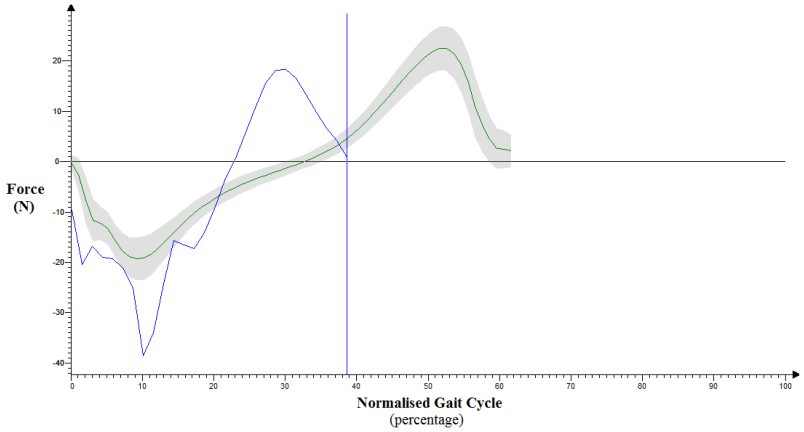

(m) Normalised GRF – X

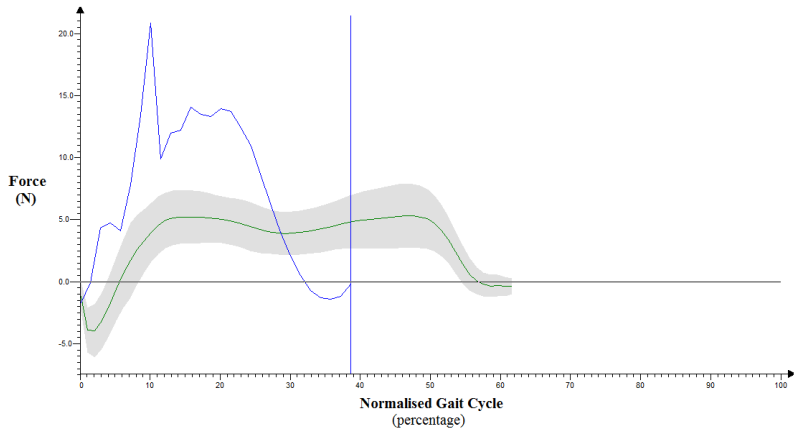

(n) Normalised GRF – Y

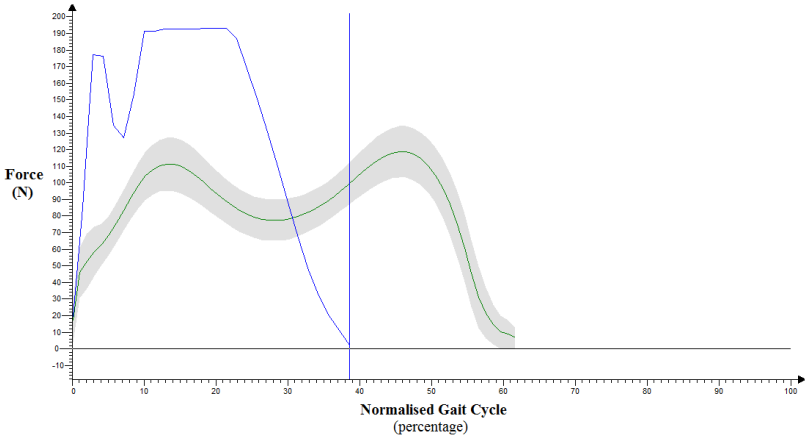

(o) Normalised GRF - Z

<u>Figure 4.27(a) to (o)</u> – Examples of the graphical kinetic outputs from Polygon® of one heel running trial from the control group. The grey shaded areas depict the average range of the control walking database (with the green line signifying the mean) to compare the difference bewteen running and walking. The blue line denotes the cycle of the right foot while running.

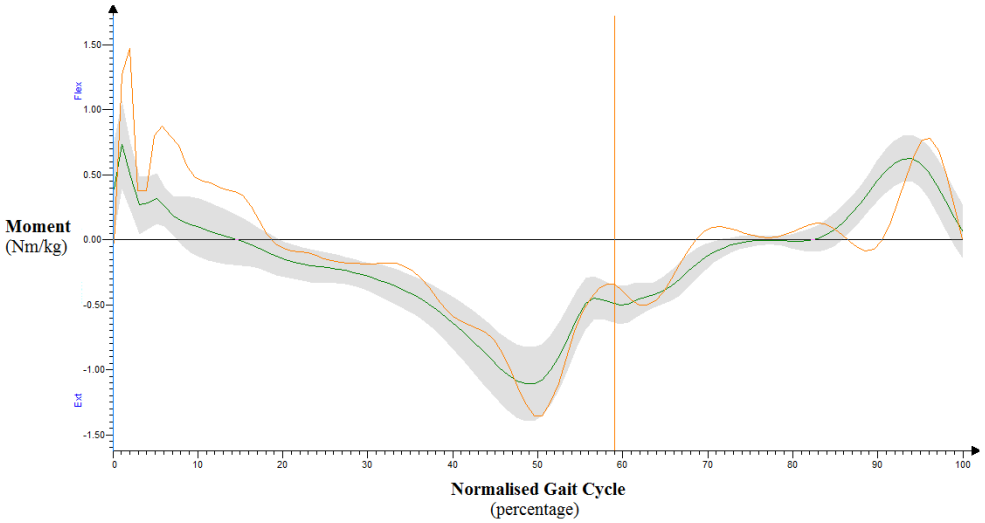

(a) Hip Flexion/Extension

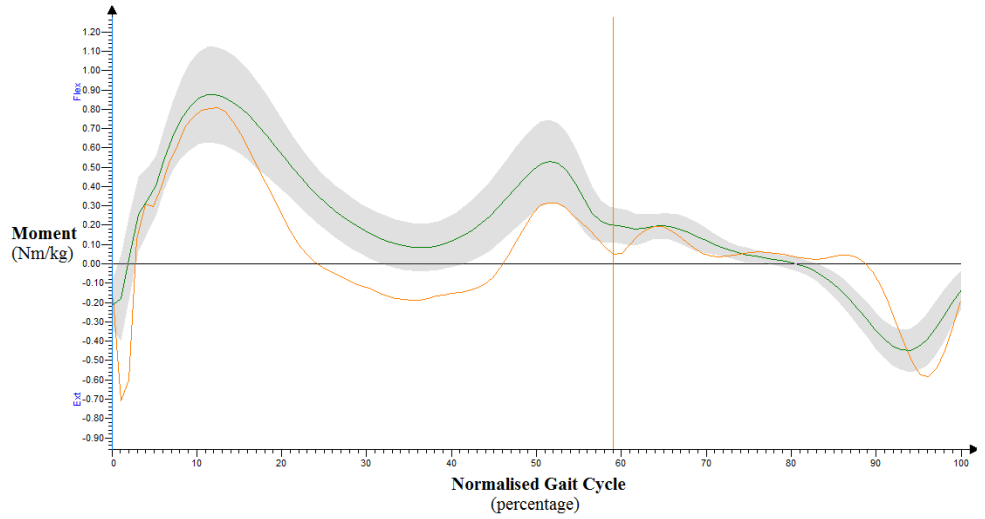

(b) Knee Flexion/Extension

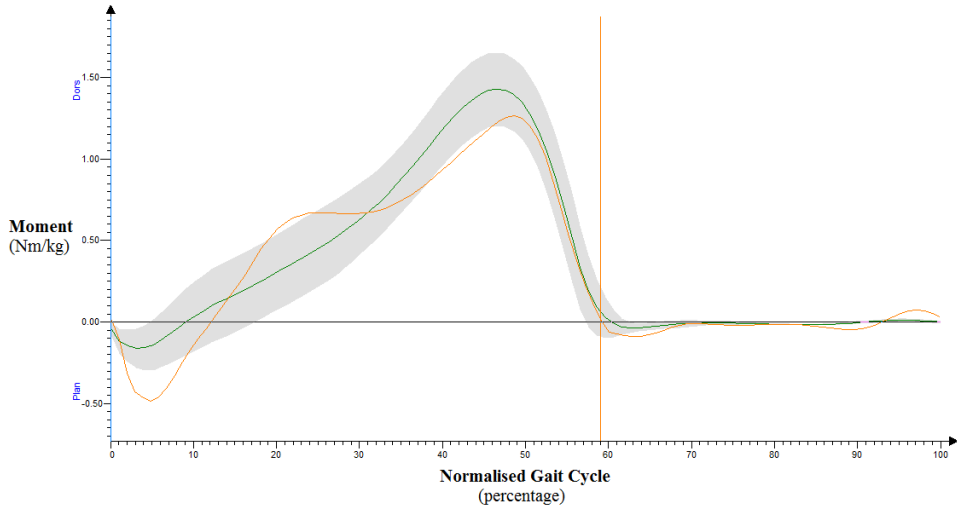

(c) Ankle Dorsiflexion/Plantarflexion

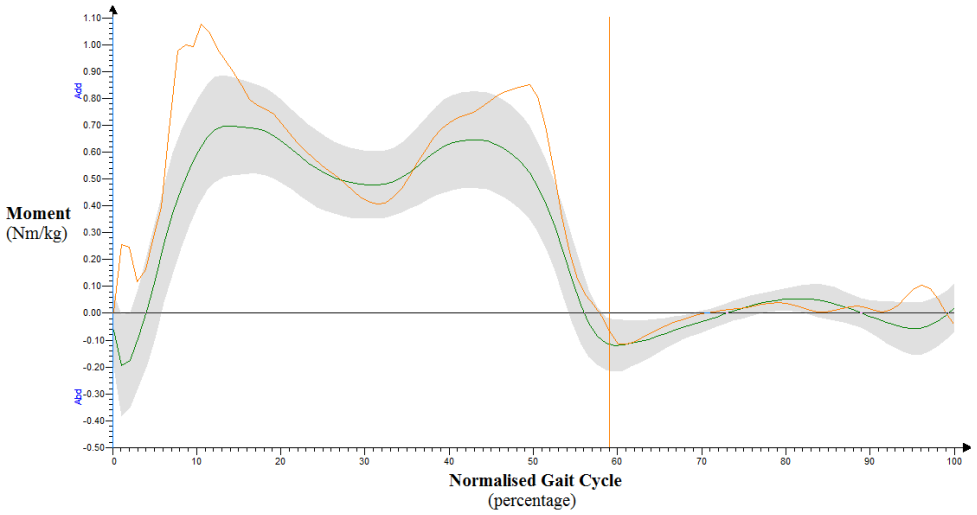

(d) Hip Abduction/Adduction

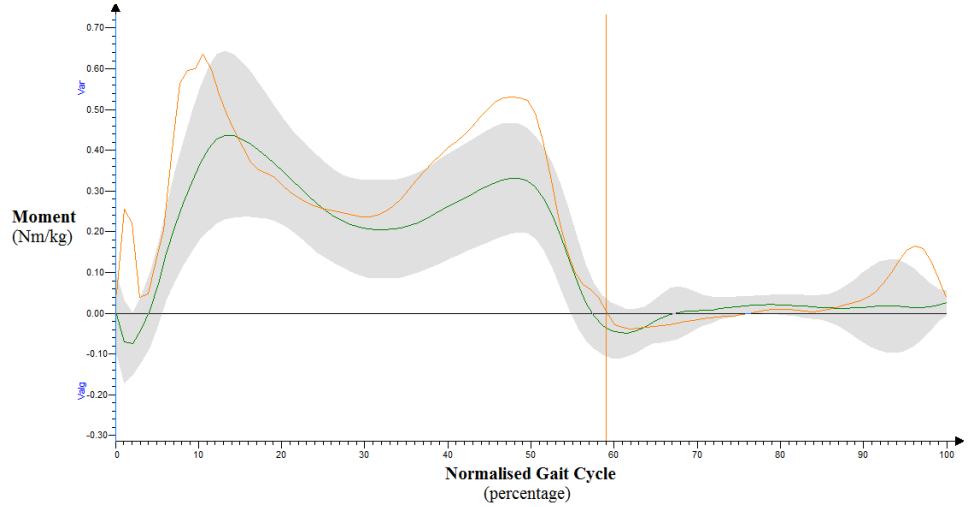

(e) Knee Valgus/Varus

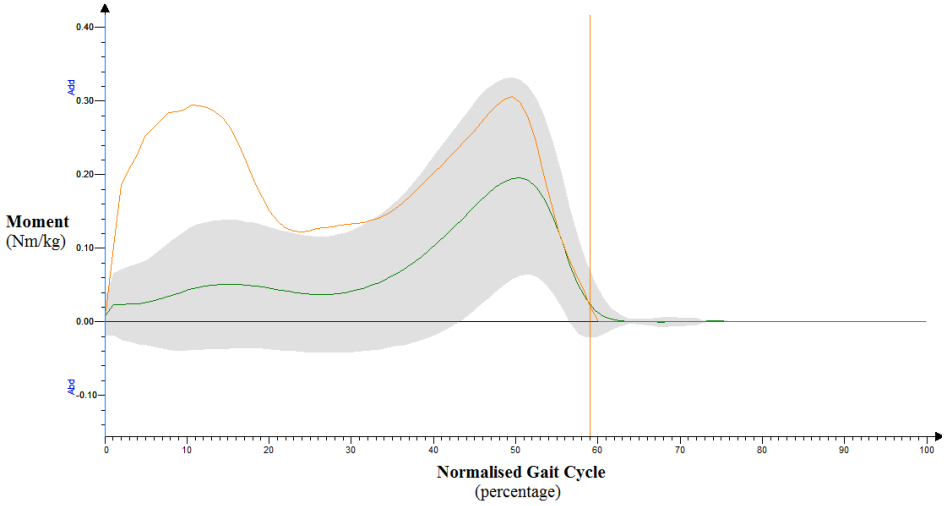

(f) Ankle Abduction/Adduction

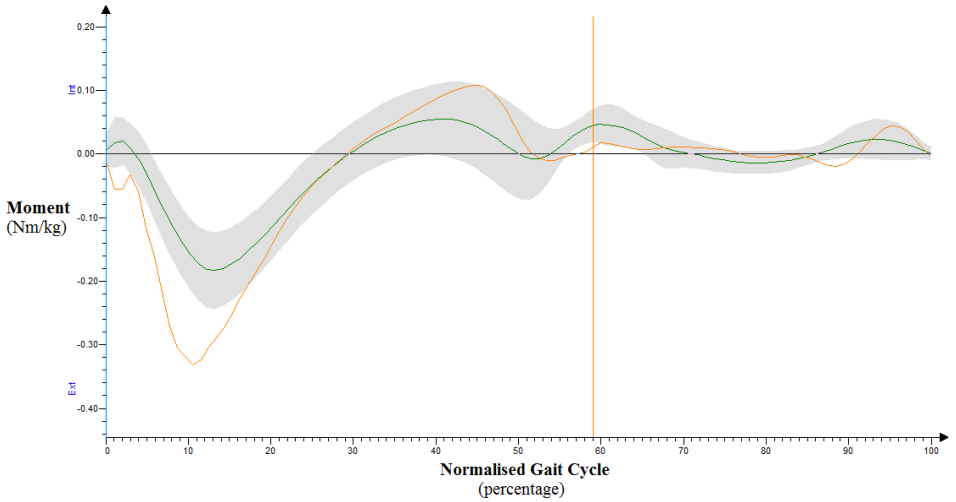

(g) Hip Rotation

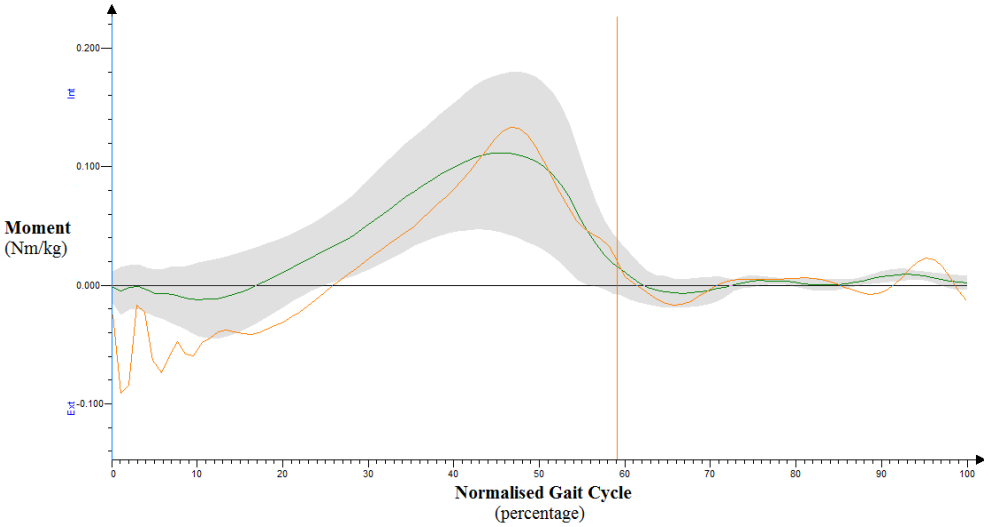

(h) Knee Rotation

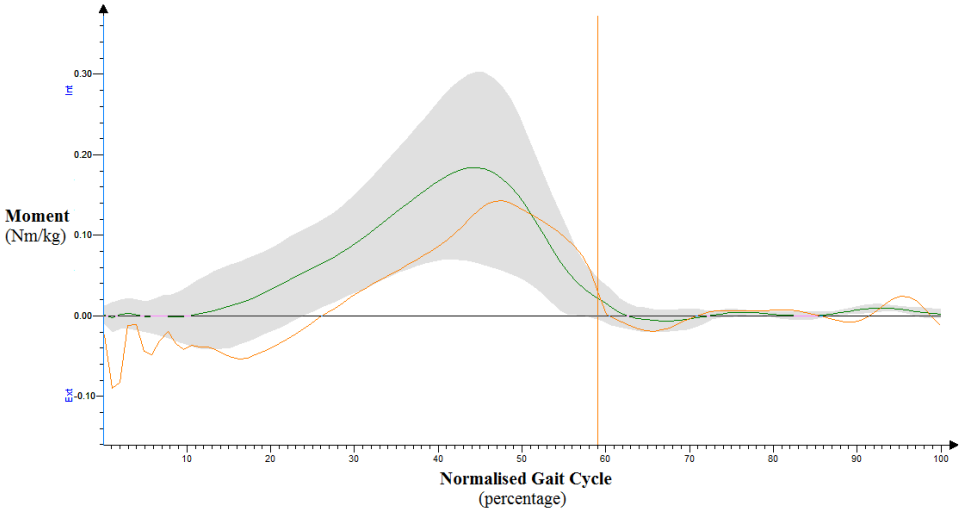

(i) Ankle Rotation

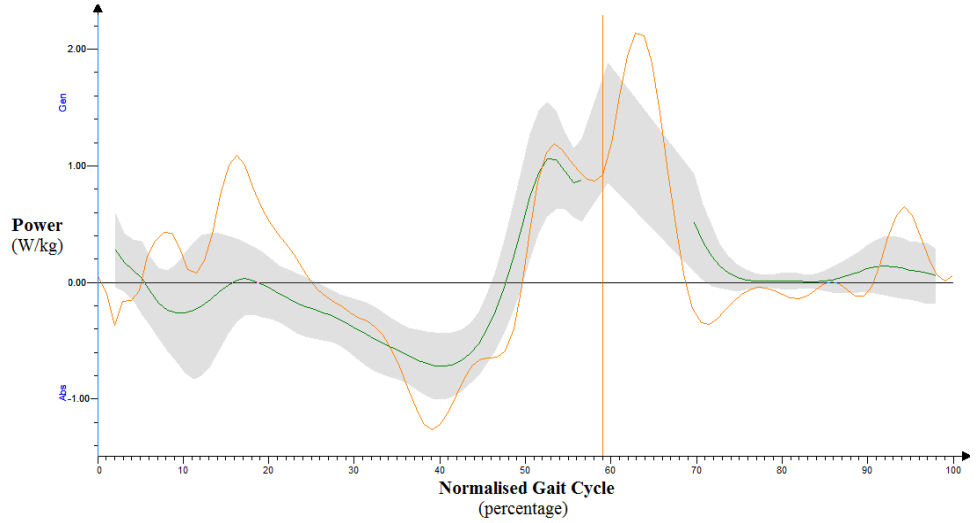

(j) Hip Power

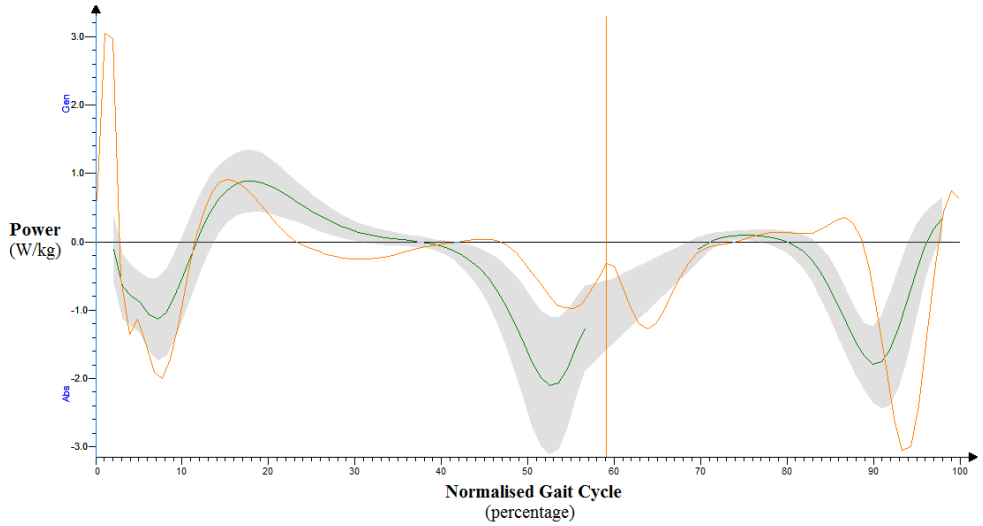

(k) Knee Power

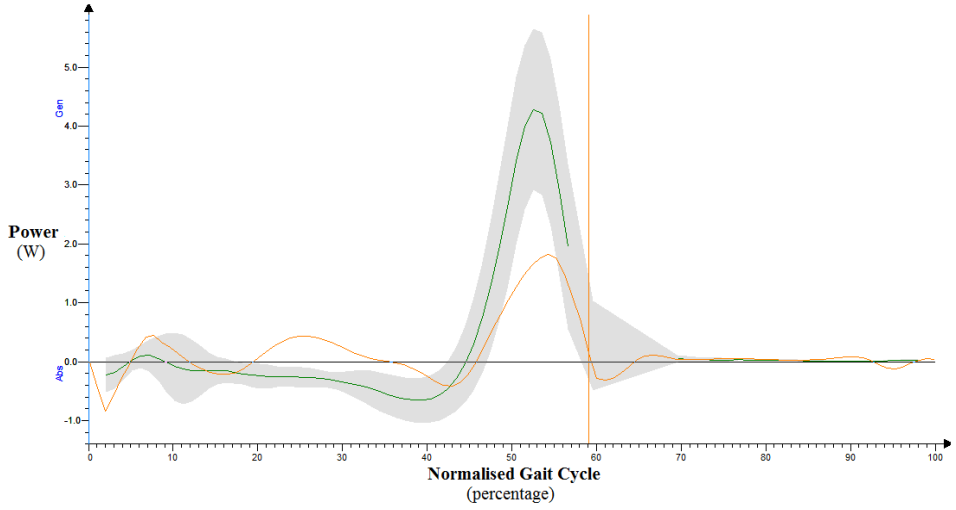

(l) Ankle Power

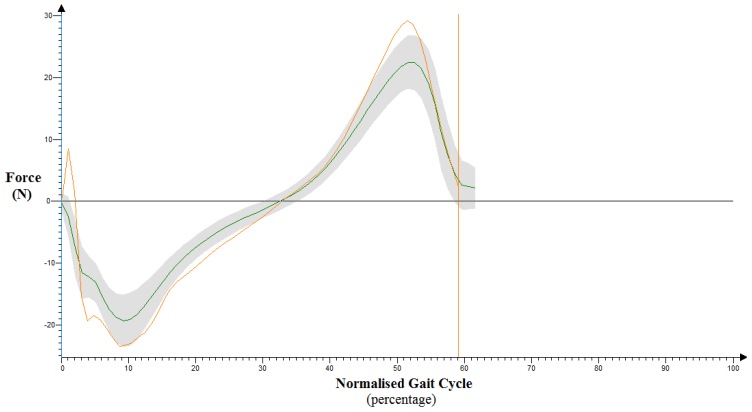

(m) Normalised GRF – X

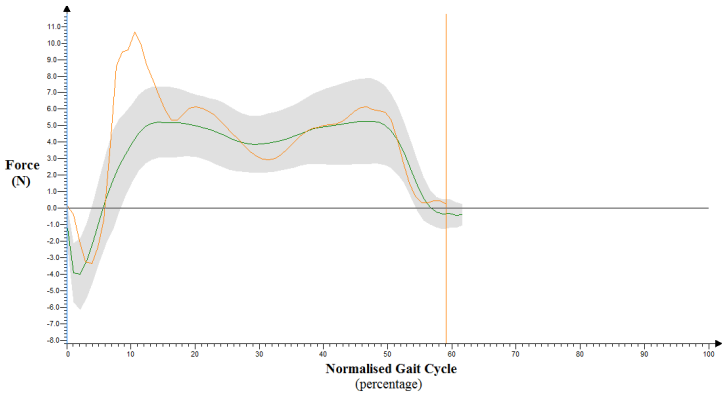

(n) Normalised GRF – Y

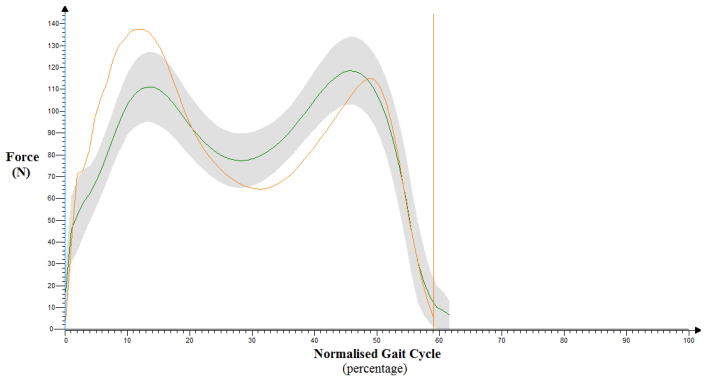

(o) Normalised GRF – Z

<u>Figure 4.28(a) to (o)</u> – Examples of the graphical kinetic outputs from Polygon® of one walking trial from the active group. The grey shaded areas depict the average range of the active walking database (with the green line signifying the mean) and the orange line highlights the left foot while walking.

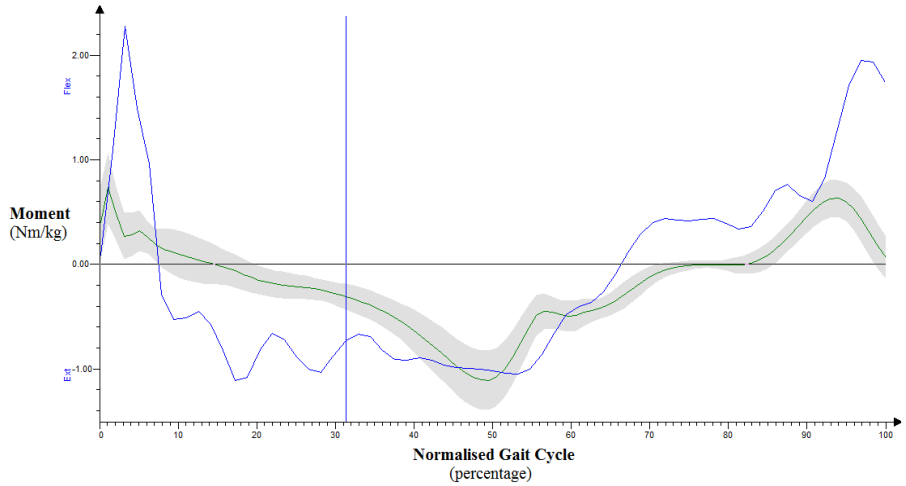

(a) Hip Flexion/Extension

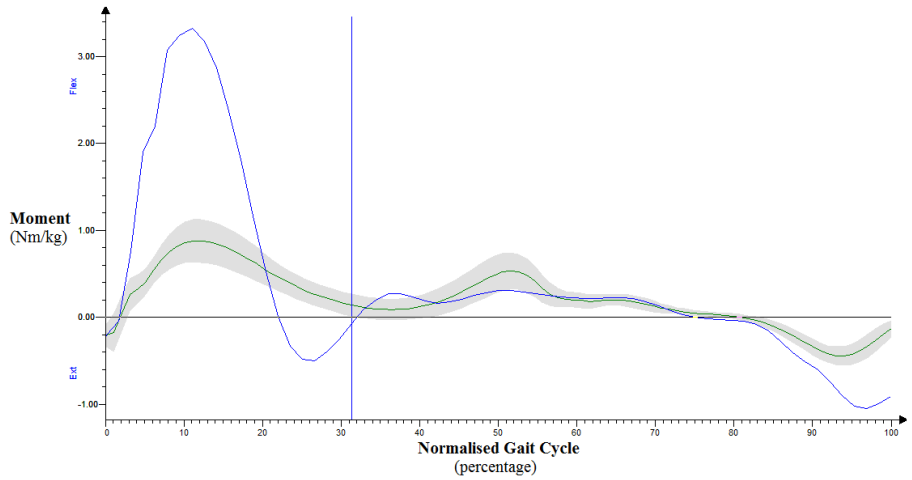

(b) Knee Flexion/Extension

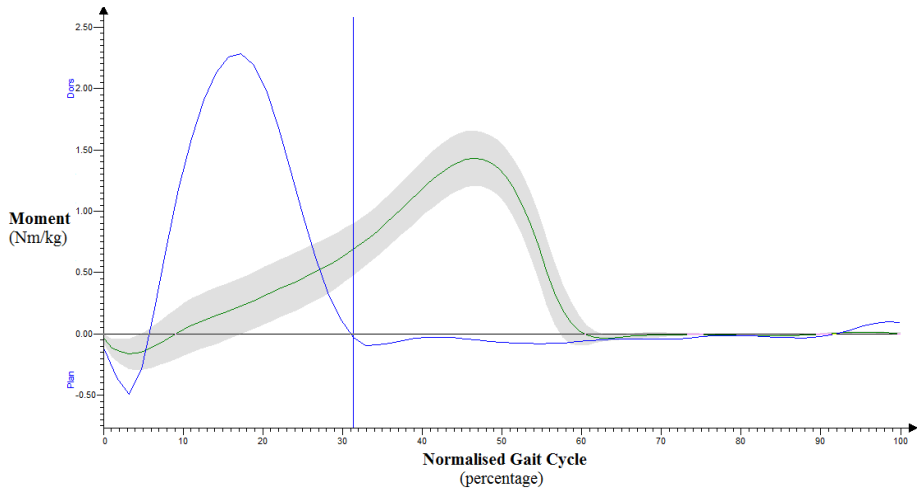

(c) Ankle Flexion/Extension

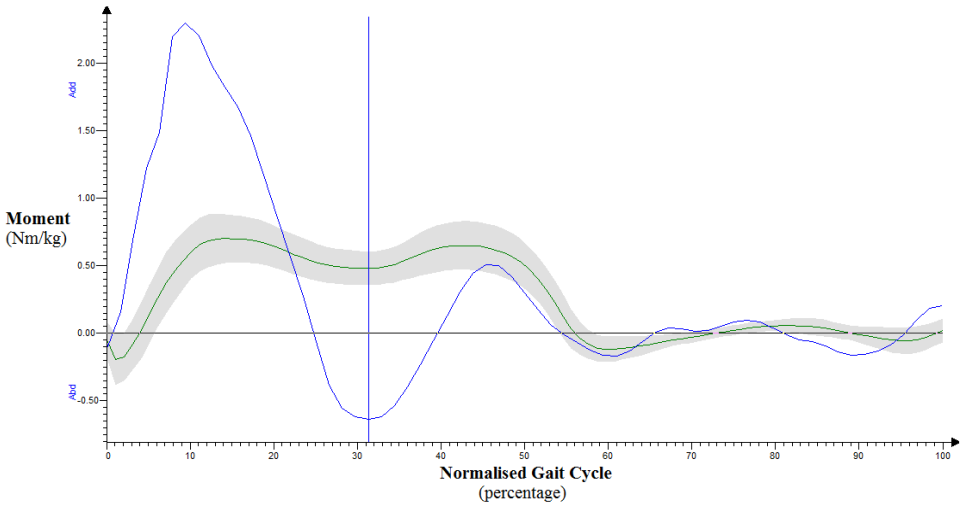

(d) Hip Abduction/Adduction

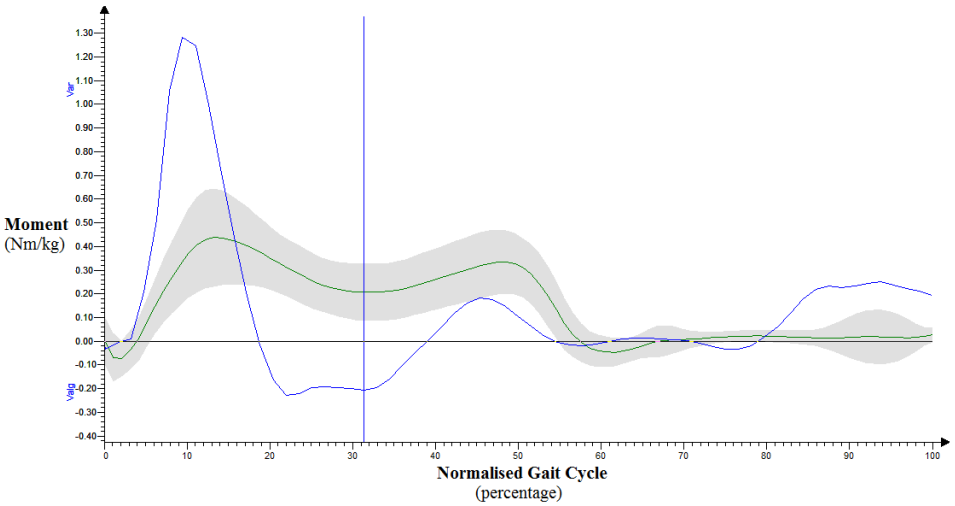

(e) Knee Valgus/Varus

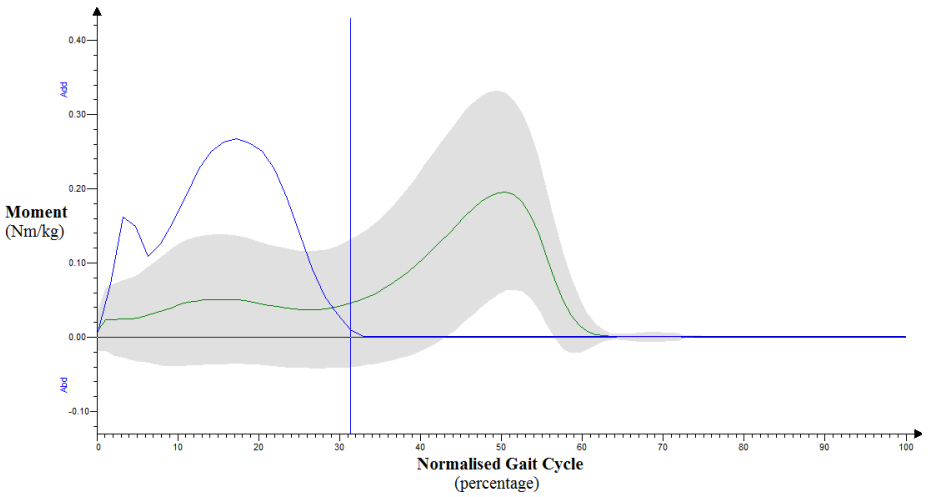

(f) Ankle Abduction/Adduction

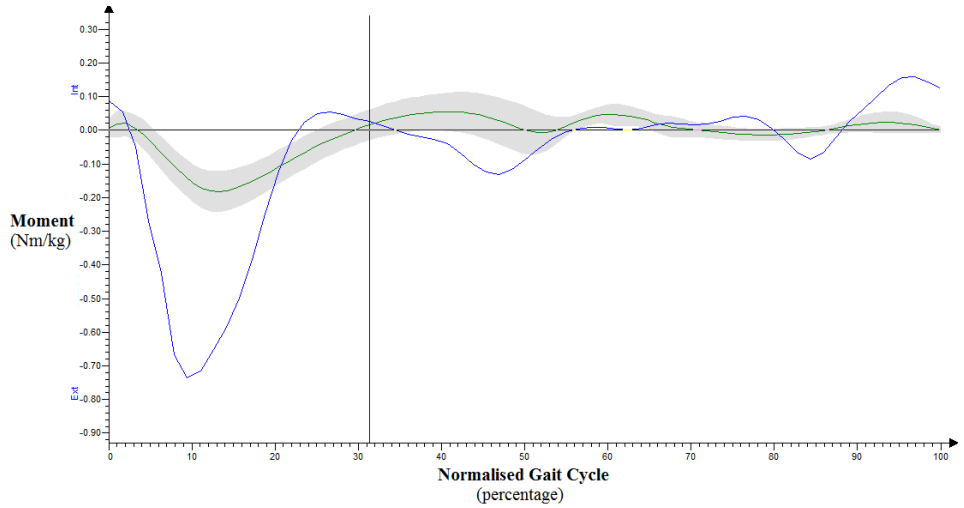

(g) Hip Rotation

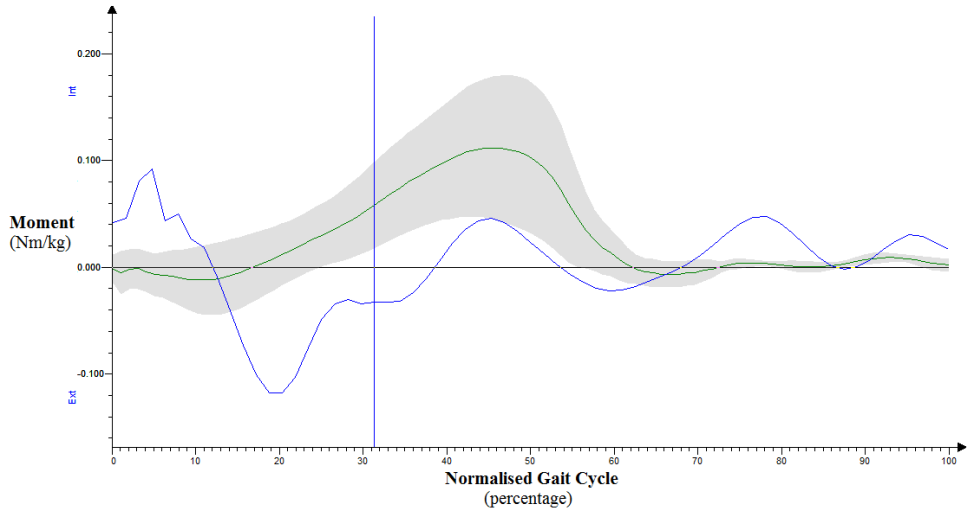

(h) Knee Rotation

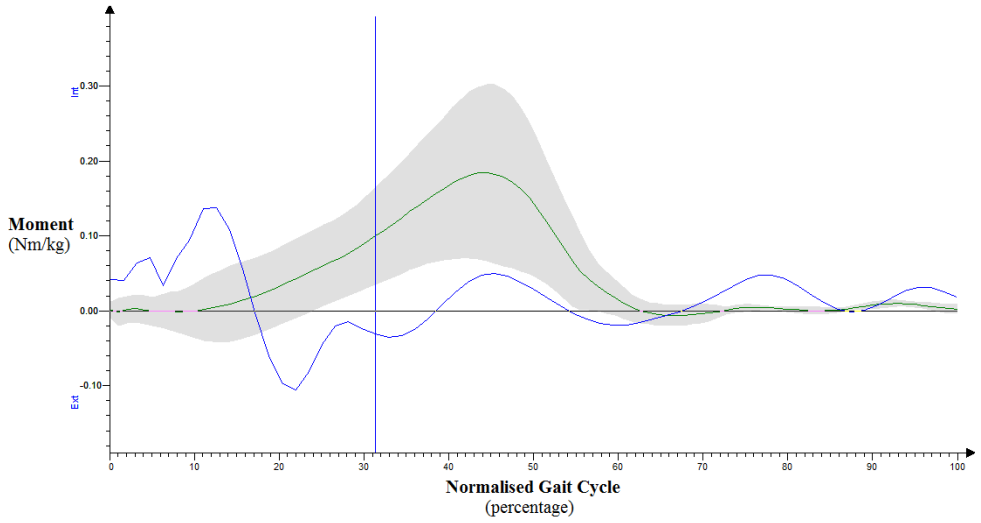

(i) Ankle Rotation

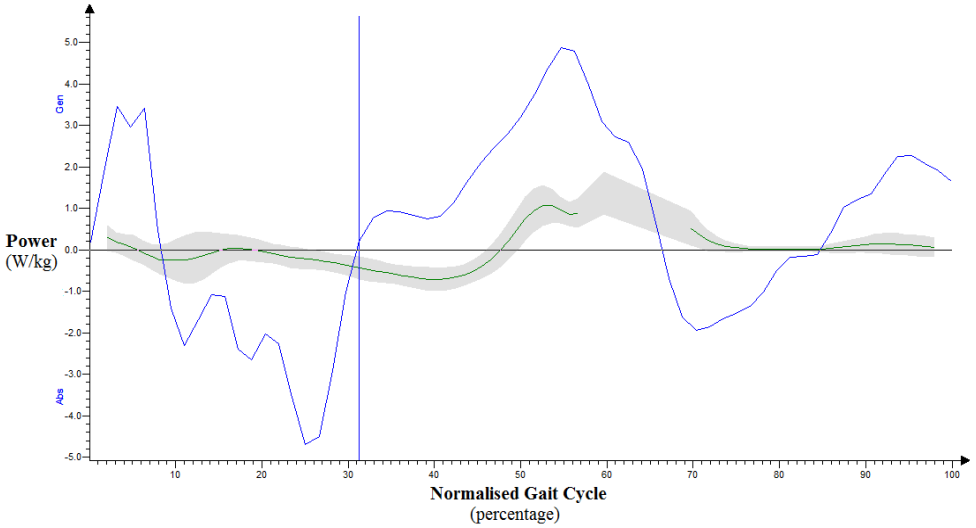

(j) Hip Power

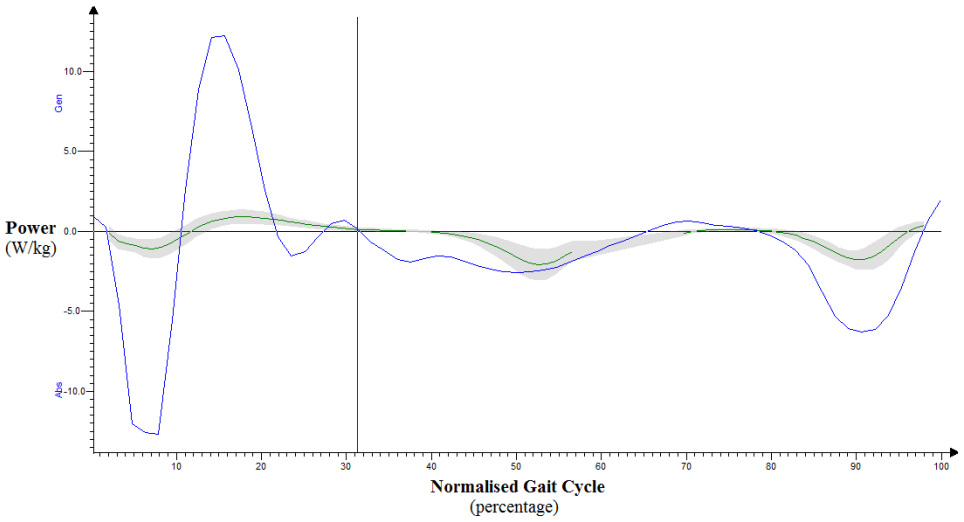

(k) Knee Power

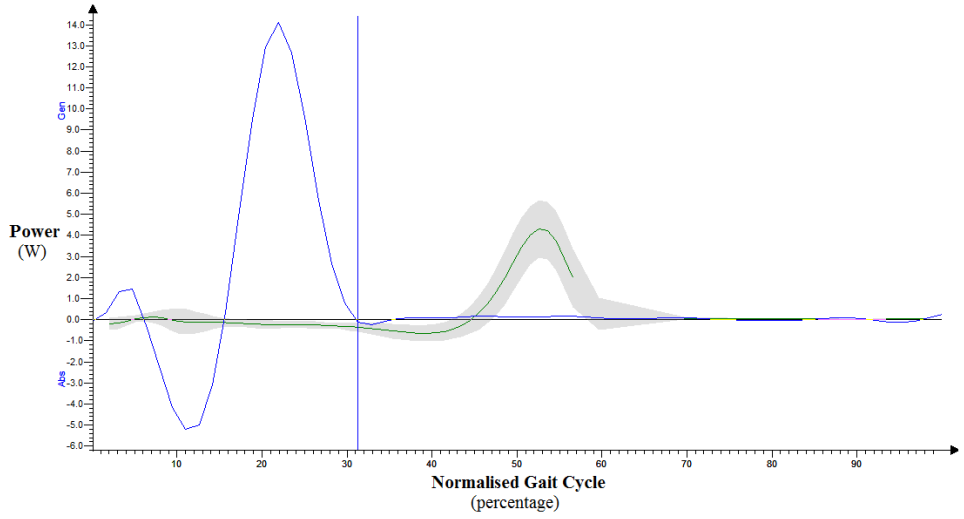

(l) Ankle Power

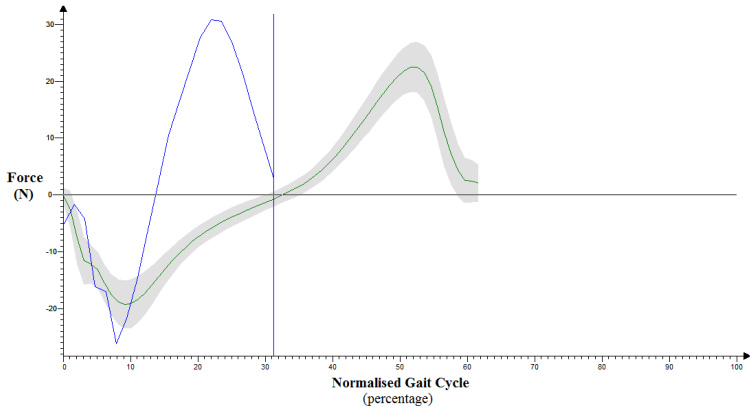

(m) Normalised GRF – X

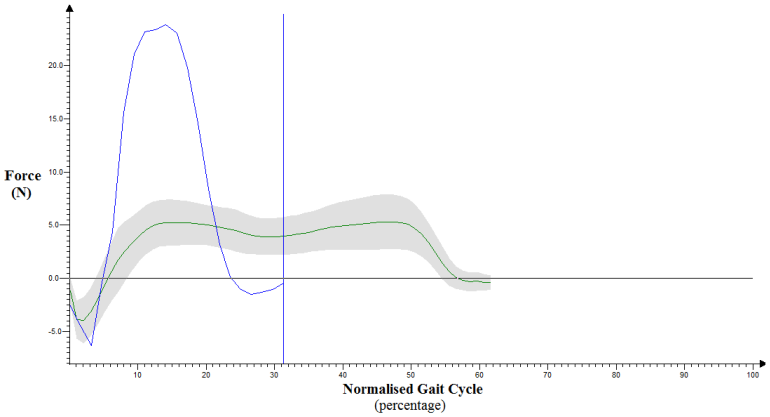

(n) Normalised GRF – Y

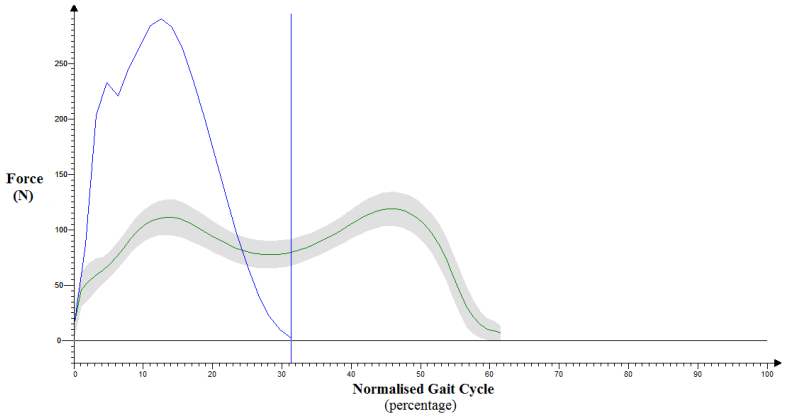

(o) Normalised GRF – Z

<u>Figure 4.29(a) to (o)</u> – Examples of the graphical kinetic outputs from Polygon® of one heel running trial from the same individual in the active group. The grey shaded areas depict the average range of the active walking database (with the green line signifying the mean) to compare the difference bewteen running and walking. The blue line denotes the cycle of the right foot while running.

Each foot (left and right) was analysed during the stance phase of walking and running and Tables 4.23 and 4.24 summarise the statistical significance of the difference between the minimum and maximum results. To allow easier comparison of the differences between the control and active kinetic data, Tables 4.25 and 4.26 detail the mean and standard deviation separately for each variable while walking and running respectively.

The assumption that individuals from the control group would walk in a similar manner to individuals from the active group would be a logical expectation for the kinetic results after observing no visual differences for the kinematic Polygon® graphs or divergence from the pattern of in-shoe pressure distribution while walking. Interestingly, this expectation was not supported by the results of the kinetic data, which instead found that significant differences were found between the control and active groups while walking as well as running. The results of the Mann-Whitney Tests demonstrate that the active group differs significantly from the control group; thus implying that the active group have not only modified their running technique, however the natural biomechanics of walking have additionally adapted as a consequence of intensive sports training.

Table 4.23 – Range of motion in the stance phase – Mann-Whitney Test comparing the maximum and minimum values for variables compared between the control and active groups when walking.

Mann-Whitney Test ***Active vs Control*** **Variables**	Active Range	Control Range	**p**
Right Centre of Mass (Z)			
Minimum	0	0	**0.022**
Maximum	1019	1060	**0.032**
Right Hip Angle (X)			
Minimum	-19	-15	0.140
Maximum	57	59	**0.034**
Right Knee Angle (X)			
Minimum	-6	2	**0.000**
Maximum	58	57	**0.000**
Right Ankle Angle (X)			
Minimum	-32	-27	**0.000**
Maximum	37	27	**0.000**
Right Hip Angle (Y)			
Minimum	-10	-13	0.365
Maximum	10	12	0.705
Right Knee Angle (Y)			
Minimum	-10	-10	0.268
Maximum	15	25	0.370
Right Ankle Angle (Y)			
Minimum	-22	-13	**0.003**
Maximum	16	11	**0.000**
Right Knee Power (Z)			
Minimum	-4	-8	0.399
Maximum	3	4	**0.000**
Right Ankle Power (Z)			
Minimum	-2	-4	0.705
Maximum	6	5	0.719
Right Knee Moment (X)			
Minimum	-839	-1009	**0.002**
Maximum	1390	1861	0.325
Right Ankle Moment (X)			
Minimum	-722	-329	0.680
Maximum	2163	1812	**0.004**
Right Knee Moment (Y)			
Minimum	-477	-472	0.424
Maximum	984	953	0.648

Mann-Whitney Test ***Active vs Control*** **Variables**	Active Range	Control Range	**p**
Left Centre of Mass (Z)			
Maximum	0	0	0.123
Maximum	1036	1067	0.167
Left Hip Angle (X)			
Minimum	-21	-21	0.918
Maximum	57	55	0.212
Left Knee Angle (X)			
Minimum	-9	-1	0.314
Maximum	58	61	**0.001**
Left Ankle Angle (X)			
Minimum	-40	-20	**0.000**
Maximum	13	24	**0.000**
Left Hip Angle (Y)			
Minimum	-14	-15	0.450
Maximum	11	12	0.638
Left Knee Angle (Y)			
Minimum	-13	-11	0.704
Maximum	13	29	**0.014**
Left Ankle Angle (Y)			
Minimum	-9	-12	0.080
Maximum	15	11	**0.000**
Left Knee Power (Z)			
Minimum	-4	-7	0.849
Maximum	3	3	**0.000**
Left Ankle Power (Z)			
Minimum	-1	-2	0.824
Maximum	6	6	0.918
Left Knee Moment (X)			
Minimum	-965	-794	**0.003**
Maximum	1603	2439	**0.029**
Left Ankle Moment (X)			
Minimum	-723	-1884	**0.026**
Maximum	2000	1831	0.847
Left Knee Moment (Y)			
Minimum	-265	-402	0.254
Maximum	1054	735	0.505

Right Ankle Moment (Y) *Minimum* *Maximum*	-366 540	-545 434	**0.002** **0.000**	Left Ankle Moment (Y) *Minimum* *Maximum*	-288 625	-510 269	0.236 **0.000**
Right Knee Force (X) *Minimum* *Maximum*	-3 5	-3 6	**0.000** **0.001**	Left Knee Force (X) *Minimum* *Maximum*	-4 5	-2 6	0.170 **0.002**
Right Ankle Force (X) *Minimum* *Maximum*	-1 14	0 14	**0.001** 0.233	Left Ankle Force (X) *Minimum* *Maximum*	-1 14	0 15	**0.023** 0.234
Right Knee Force (Y) *Minimum* *Maximum*	-3 2	-3 1	**0.001** 0.394	Left Knee Force (Y) *Minimum* *Maximum*	-1 3	0 2	0.327 **0.001**
Right Ankle Force (Y) *Minimum* *Maximum*	-2 1	-2 2	0.580 **0.018**	Left Ankle Force (Y) *Minimum* *Maximum*	-1 2	-1 2	0.090 0.737
Right Knee Force (Z) *Minimum* *Maximum*	-14 2	-13 1	0.082 **0.000**	Left Knee Force (Z) *Minimum* *Maximum*	-14 1	-14 1	**0.040** **0.002**
Right Ankle Force (Z) *Minimum* *Maximum*	-3 5	-2 4	**0.000** 0.206	Left Ankle Force (Z) *Minimum* *Maximum*	-2 5	-3 4	**0.000** 0.354

****Green* denotes p value is very highly significant (0.000-0.001), *yellow* denotes p value is highly significant (0.001-0.01) and *orange* denotes p value is significant (0.01-0.05).*

Table 4.24 – Range of motion in the stance phase – Mann-Whitney Test comparing the maximum and minimum values for variables compared between the control and active groups when running.

Mann-Whitney Test ***Active vs Control*** **Variables**	Active Range	Control Range	**p**
Right Centre of Mass (Z)			
Minimum	0	777	0.286
Maximum	990	1013	0.239
Right Hip Angle (X)			
Minimum	-13	-14	0.332
Maximum	66	67	**0.015**
Right Knee Angle (X)			
Minimum	6	6	**0.001**
Maximum	56	59	**0.001**
Right Ankle Angle (X)			
Minimum	-58	-29	**0.000**
Maximum	49	37	**0.000**
Right Hip Angle (Y)			
Minimum	-14	-10	**0.000**
Maximum	17	19	0.650
Right Knee Angle (Y)			
Minimum	-19	-19	0.150
Maximum	21	22	**0.032**
Right Ankle Angle (Y)			
Minimum	-21	-15	0.246
Maximum	20	10	**0.000**
Right Knee Power (Z)			
Minimum	-16	-21	**0.035**
Maximum	20	19	**0.000**
Right Ankle Power (Z)			
Minimum	-18	-9	**0.000**
Maximum	38	20	**0.000**
Right Knee Moment (X)			
Minimum	-1702	-1015	**0.002**
Maximum	4033	5376	0.673
Right Ankle Moment (X)			
Minimum	-1366	-250	**0.000**
Maximum	3937	620	**0.001**
Right Knee Moment (Y)			
Minimum	-1693	-1625	0.839
Maximum	2584	1561	0.169

Mann-Whitney Test ***Active vs Control*** **Variables**	Active Range	Control Range	**p**
Left Centre of Mass (Z)			
Maximum	0	774	**0.015**
Maximum	1003	1072	**0.003**
Left Hip Angle (X)			
Minimum	-14	-11	0.361
Maximum	65	72	0.462
Left Knee Angle (X)			
Minimum	6	7	0.064
Maximum	57	62	0.309
Left Ankle Angle (X)			
Minimum	-109	-35	**0.022**
Maximum	65	35	**0.000**
Left Hip Angle (Y)			
Minimum	-17	-18	**0.016**
Maximum	15	19	0.330
Left Knee Angle (Y)			
Minimum	-12	-18	0.608
Maximum	17	26	0.393
Left Ankle Angle (Y)			
Minimum	-71	-15	0.982
Maximum	78	13	0.143
Left Knee Power (Z)			
Minimum	-25	-17	0.083
Maximum	22	15	**0.001**
Left Ankle Power (Z)			
Minimum	-17	-10	**0.000**
Maximum	31	18	**0.000**
Left Knee Moment (X)			
Minimum	-1323	-1279	0.288
Maximum	3910	3544	0.401
Left Ankle Moment (X)			
Minimum	-1558	-1026	**0.006**
Maximum	5803	2843	**0.000**
Left Knee Moment (Y)			
Minimum	-1024	-784	0.547
Maximum	2435	1482	**0.006**

Right Ankle Moment (Y) *Minimum* *Maximum*	-333 605	-1214 852	**0.021** 0.542	Left Ankle Moment (Y) *Minimum* *Maximum*	-402 596	-858 873	**0.000** 0.783
Right Knee Force (X) *Minimum* *Maximum*	-4 16	-2 11	**0.000** **0.003**	Left Knee Force (X) *Minimum* *Maximum*	-4 17	-3 11	**0.001** 0.361
Right Ankle Force (X) *Minimum* *Maximum*	-13 29	-1 21	**0.000** 0.148	Left Ankle Force (X) *Minimum* *Maximum*	-2 31	-1 21	**0.000** 0.193
Right Knee Force (Y) *Minimum* *Maximum*	-9 7	-5 1	**0.001** **0.024**	Left Knee Force (Y) *Minimum* *Maximum*	-7 11	-1 6	**0.006** 0.176
Right Ankle Force (Y) *Minimum* *Maximum*	-9 19	-4 2	0.743 **0.001**	Left Ankle Force (Y) *Minimum* *Maximum*	-4 10	-1 4	**0.000** 0.302
Right Knee Force (Z) *Minimum* *Maximum*	-26 4	-19 2	**0.001** **0.000**	Left Knee Force (Z) *Minimum* *Maximum*	-26 5	-20 2	**0.028** **0.000**
Right Ankle Force (Z) *Minimum* *Maximum*	-7 10	-6 5	**0.000** **0.000**	Left Ankle Force (Z) *Minimum* *Maximum*	-7 10	-4 6	**0.000** **0.001**

****Green* denotes p value is very highly significant (0.000-0.001), *yellow* denotes p value is highly significant (0.001-0.01) and *orange* denotes p value is significant (0.01-0.05).*

Table 4.25 – Descriptive statistics detailing the mean and standard deviation of the range of motion in the stance phase while walking for the active and control groups respectively.

Descriptive Statistics for Variables	$\bar{x}$	σ
Right Centre of Mass (Z) *Active* *Control*	 670.72 903.18	 394.48 187.77
Right Hip Angle (X) *Active* *Control*	 15.69 18.84	 24.41 23.89
Right Knee Angle (X) *Active* *Control*	 24.19 29.54	 22.50 21.70
Right Ankle Angle (X) *Active* *Control*	 -4.79 3.21	 15.91 15.94
Right Hip Angle (Y) *Active* *Control*	 -0.28 0.12	 6.01 6.58
Right Knee Angle (Y) *Active* *Control*	 0.48 -0.20	 5.69 6.27
Right Ankle Angle (Y) *Active* *Control*	 1.36 -0.51	 7.65 6.81
Right Knee Power (Z) *Active* *Control*	 -0.06 -0.47	 1.70 2.16
Right Ankle Power (Z) *Active* *Control*	 1.46 1.37	 2.43 2.45
Right Knee Moment (X) *Active* *Control*	 80.10 219.48	 656.06 772.74
Right Ankle Moment (X) *Active* *Control*	 543.25 599.62	 943.54 845.23
Right Knee Moment (Y) *Active* *Control*	 135.95 111.79	 327.76 313.86
Right Ankle Moment (Y) *Active* *Control*	 24.40 -45.70	 146.71 162.81

Descriptive Statistics for Variables	$\bar{x}$	σ
Left Centre of Mass (Z) *Active* *Control*	 662.94 908.42	 408.17 152.03
Left Hip Angle (X) *Active* *Control*	 16.16 17.89	 25.01 24.33
Left Knee Angle (X) *Active* *Control*	 23.88 26.95	 22.29 20.74
Left Ankle Angle (X) *Active* *Control*	 -5.19 2.81	 13.44 14.26
Left Hip Angle (Y) *Active* *Control*	 -0.53 -0.19	 6.87 7.04
Left Knee Angle (Y) *Active* *Control*	 0.90 0.05	 5.39 4.46
Left Ankle Angle (Y) *Active* *Control*	 1.74 -0.20	 5.31 6.01
Left Knee Power (Z) *Active* *Control*	 -0.02 -0.57	 1.82 2.35
Left Ankle Power (Z) *Active* *Control*	 1.19 1.27	 2.16 2.21
Left Knee Moment (X) *Active* *Control*	 58.08 235.04	 683.83 765.06
Left Ankle Moment (X) *Active* *Control*	 532.88 485.86	 898.44 836.49
Left Knee Moment (Y) *Active* *Control*	 196.88 158.98	 336.43 294.30
Left Ankle Moment (Y) *Active* *Control*	 30.52 -40.24	 146.89 141.53

Right Knee Force (X)		
Active	1.14	2.85
Control	1.60	2.87
Right Ankle Force (X)		
Active	5.98	6.35
Control	5.75	5.96
Right Knee Force (Y)		
Active	-0.30	0.94
Control	-0.47	0.88
Right Ankle Force (Y)		
Active	-0.20	0.84
Control	-0.09	0.77
Right Knee Force (Z)		
Active	-5.48	6.48
Control	-5.10	5.88
Right Ankle Force (Z)		
Active	0.98	2.57
Control	0.39	2.10

Left Knee Force (X)		
Active	0.99	2.85
Control	1.40	2.76
Left Ankle Force (X)		
Active	5.50	6.29
Control	5.71	5.94
Left Knee Force (Y)		
Active	0.40	0.96
Control	0.54	0.82
Left Ankle Force (Y)		
Active	0.31	0.84
Control	0.22	0.67
Left Knee Force (Z)		
Active	-5.00	6.40
Control	-5.05	5.87
Left Ankle Force (Z)		
Active	0.87	2.48
Control	0.42	2.11

Table 4.26 – Descriptive statistics detailing the mean and standard deviation of the range of motion in the stance phase while running for the active and control groups respectively.

Descriptive Statistics for Variables	$\bar{x}$	σ
Right Centre of Mass (Z)		
Active	844.53	195.01
Control	905.16	58.29
Right Hip Angle (X)		
Active	24.97	29.05
Control	22.72	25.08
Right Knee Angle (X)		
Active	29.36	15.55
Control	34.70	15.48
Right Ankle Angle (X)		
Active	-4.18	28.55
Control	7.50	23.12
Right Hip Angle (Y)		
Active	2.49	9.80
Control	4.67	7.74
Right Knee Angle (Y)		
Active	-0.26	9.02
Control	-2.54	8.05
Right Ankle Angle (Y)		
Active	2.28	11.49
Control	-1.75	8.13
Right Knee Power (Z)		
Active	1.93	10.34
Control	-1.66	9.28
Right Ankle Power (Z)		
Active	5.89	15.63
Control	4.04	8.21
Right Knee Moment (X)		
Active	865.44	1704.32
Control	990.52	1525.76
Right Ankle Moment (X)		
Active	1168.97	1561.38
Control	744.40	1204.43
Right Knee Moment (Y)		
Active	224.73	870.00
Control	120.32	615.51
Right Ankle Moment (Y)		
Active	43.26	221.64
Control	-64.62	424.89

Descriptive Statistics for Variables	$\bar{x}$	σ
Left Centre of Mass (Z)		
Active	793.06	271.72
Control	923.97	64.44
Left Hip Angle (X)		
Active	24.06	28.42
Control	23.91	26.76
Left Knee Angle (X)		
Active	31.60	16.64
Control	33.76	15.91
Left Ankle Angle (X)		
Active	-0.39	31.03
Control	4.96	24.61
Left Hip Angle (Y)		
Active	1.19	9.14
Control	2.87	9.25
Left Knee Angle (Y)		
Active	-0.38	5.74
Control	-0.48	8.68
Left Ankle Angle (Y)		
Active	-0.49	17.62
Control	-1.01	8.17
Left Knee Power (Z)		
Active	1.01	10.80
Control	-1.83	8.73
Left Ankle Power (Z)		
Active	5.81	15.68
Control	3.89	8.57
Left Knee Moment (X)		
Active	795.47	1613.94
Control	769.80	1402.85
Left Ankle Moment (X)		
Active	1281.77	1744.13
Control	716.24	1172.85
Left Knee Moment (Y)		
Active	427.38	905.80
Control	272.09	615.66
Left Ankle Moment (Y)		
Active	36.69	191.61
Control	-51.00	363.15

Right Knee Force (X)		
Active	4.53	6.90
Control	3.16	4.36
Right Ankle Force (X)		
Active	11.05	13.03
Control	7.40	7.95
Right Knee Force (Y)		
Active	-1.12	3.45
Control	-0.83	1.68
Right Ankle Force (Y)		
Active	-0.75	3.86
Control	-0.24	1.26
Right Knee Force (Z)		
Active	-8.97	11.81
Control	-6.23	7.52
Right Ankle Force (Z)		
Active	2.58	4.26
Control	0.29	2.74

Left Knee Force (X)		
Active	4.58	6.71
Control	3.00	4.25
Left Ankle Force (X)		
Active	10.80	11.95
Control	6.95	7.52
Left Knee Force (Y)		
Active	1.74	3.65
Control	1.15	1.78
Left Ankle Force (Y)		
Active	1.62	2.87
Control	0.66	1.39
Left Knee Force (Z)		
Active	-8.30	10.80
Control	-5.93	7.31
Left Ankle Force (Z)		
Active	2.15	3.84
Control	0.47	2.72

4.2.7 Relationship between Age, Skeletal Maturation and Group Statistics

Throughout the process of data collection, many opportunities arose which presented unique opportunities to investigate further some of the anthropometric measurements obtained as part of the research. This additional data is particularly helpful through the ability to compliment and provide a clear illustration of underlying trends and relationships regarding the data which otherwise would not enable reliable conclusions to be drawn from the results comparing the active and control groups.

An important area of scientific and clinical interest is the applicability of using radiographic atlases as a growth reference to gauge the development and progression of healthy skeletal maturation. Although this project is utilising MRI scans instead of radiographs, previous studies in the literature have concluded that three-dimensional data, including CT or MRI scans, can be substituted in place of the two-dimensional radiographs (Hackman, 2012; Dedouit *et al.*, 2012; Schmidt *et al.*, 2007; Schmeling *et al.*, 2006). Therefore, *The Radiographic Standard of Reference for the Growing Knee* (Pyle and Hoerr, 1969) and *The Radiographic Atlas of Skeletal Development of the Foot and Ankle* (Hoerr *et al.*, 1962) was used by the researcher to assign an estimated age to the knee and foot/ankle of each anonymous individual based on skeletal maturation. The appearance of key radiographic indicators were recognised and corresponded with the description and image of a plate in the atlas which best represented the stage of skeletal maturation, consequently estimating the expected chronological age of an individual. Table 4.27 depicts the results of a T-Test to determine whether any significant anthropometric differences between the active and control group were present.

Table 4.27 – T-Test for the equality of means of anthropometric independent samples between the active and control groups.

Independent Samples	$\bar{x}$	σ	Levene's Test		T-Test		
			F Value	p	t	Degrees of Freedom	p
Chronological Age (months) *Control* *Active*	 *161.80* *164.53*	 *10.25* *10.98*	0.513	0.480	-0.705[a]	28[a]	0.487[a]
Skeletal Age Knee (months) *Control* *Active*	 *163.80* *164.20*	 *10.50* *18.37*	1.524	0.227	-0.073[a]	28[a]	0.942[a]
Skeletal Age Foot (months) *Control* *Active*	 *163.20* *164.00*	 *11.83* *18.52*	4.043	0.054	-0.141[a]	28[a]	0.889[a]
Body Mass Index (BMI) *Control* *Active*	 *20.67* *18.81*	 *3.71* *1.96*	9.558	*0.004*	1.724[b]	21.249[b]	0.099[b]
Width of Dominant Knee (cm) *Control* *Active*	 *9.81* *9.14*	 *0.92* *0.49*	6.126	0.020	2.510[a]	28[a]	0.018[a]
Foot Size of Dominant Foot (UK) *Control* *Active*	 *7.23* *6.43*	 *1.80* *1.97*	0.583	0.451	1.160[a]	28[a]	0.256[a]
Height (cm) *Control* *Active*	 *162.77* *159.49*	 *8.49* *11.84*	2.417	0.131	0.870[a]	28[a]	0.392[a]

[a]*Equal variances assumed – F value defined at level of ≤ 0.01 significance.*
[b]*Equal variances not assumed – F value defined at level of ≤ 0.01 significance.*

As in the case of the growth plate volume T-Test results, no significant differences were found for the anthropometric measurements of the active and control groups. Due to a small sample size, the level of significance was set at $p \leq 0.01$. The only independent sample that was close to showing a significant difference between the two groups was the width of the dominant knee. This difference may be explained by the active group typically having toned and muscular limbs; thus resulting in the active individuals displaying a similar body mass index (BMI) to the control group yet not having

additional ‘fatty tissue’ around the knee joint. BMI correlates to the percentage of body fat composition, however, to correctly calculate the BMI of children and adolescents the method differs from the equation used for adults and instead uses centiles which factor age and sex differences against growth references and specialised charts (Cole, 2012). Ultimately BMI is not an ideal indicator for truly defining the health of growing individuals and is included in Table 4.27 to simply gauge that the combined height and weight of the individuals within each group were similar.

On the other hand, the Pearson correlation results for the anthropometric measurements signified a significantly different result and presence of an underlying trend that is evident in the active group. The relationship of skeletal age with the other independent variables best represents and mimics a close association with respect to the volume of the growth plates. The volume, area and size of each growth plate would be expected to depend and follow a similar trend as the associated stage of maturation. The relationships of chronological age, skeletal age of the knee and skeletal age of the foot can be visualised in Figures 4.30, 4.31 and 4.32. The graphs clearly signify that a stronger relationship exists within the active group when evaluating the expected skeletal age with the respective chronological age, as depicted by the black line, and when comparing this with the control group who typically present weaker correlations. The active group also have very highly significant correlations with BMI and both chronological and skeletal ages ($p \leq 0.001$); however these relationships were not significant for the control group. Although there was no significant difference with regards to the average heights of the active and control groups, the relationship of the height of active individuals with age, BMI, knee width and foot size was very highly significant ($p \leq 0.001$). This differs markedly from the control group where the height of individuals only has a significant relationship with foot size ($p < 0.001$). Figure 4.33

displays the differences in the trends set by the active and control groups in relation to the chronological age and respective height of each individual.

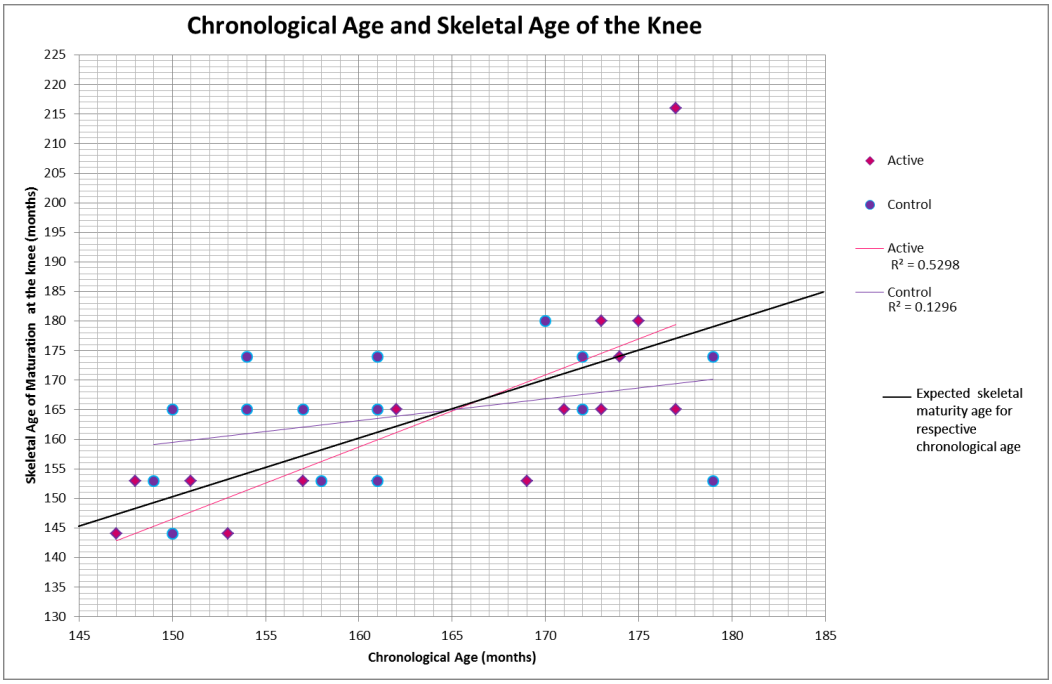

Figure 4.30 – Graph of chronological age plotted against skeletal age of the knee. Control correlation significance is 0.188 although active correlation significance is 0.002.

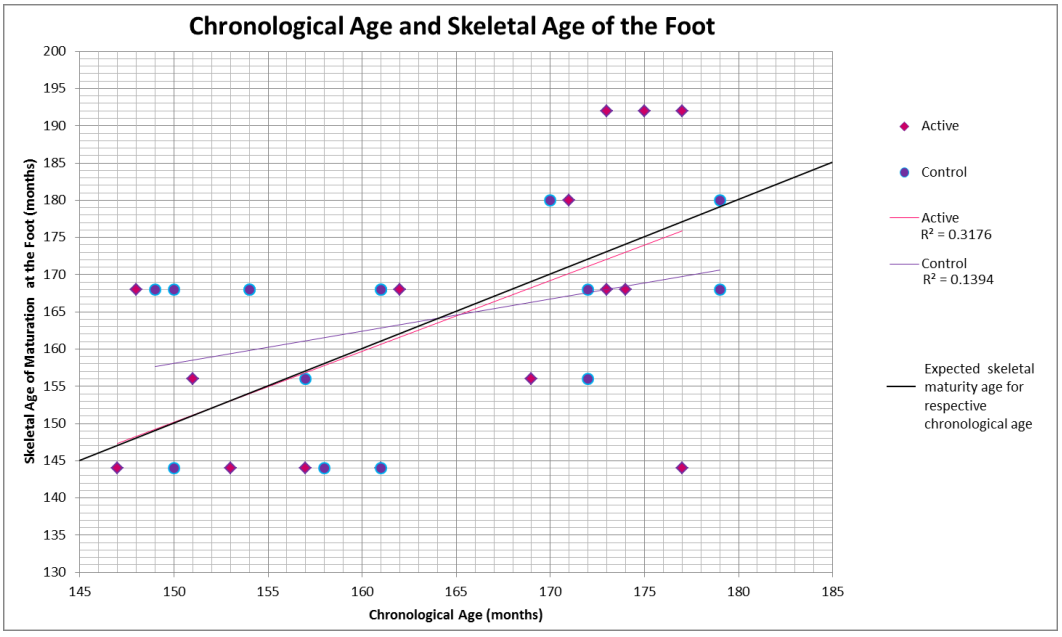

Figure 4.31 – Graph of chronological age plotted against skeletal age of the foot and ankle. Control correlation significance is 0.170 and active correlation significance is 0.029.

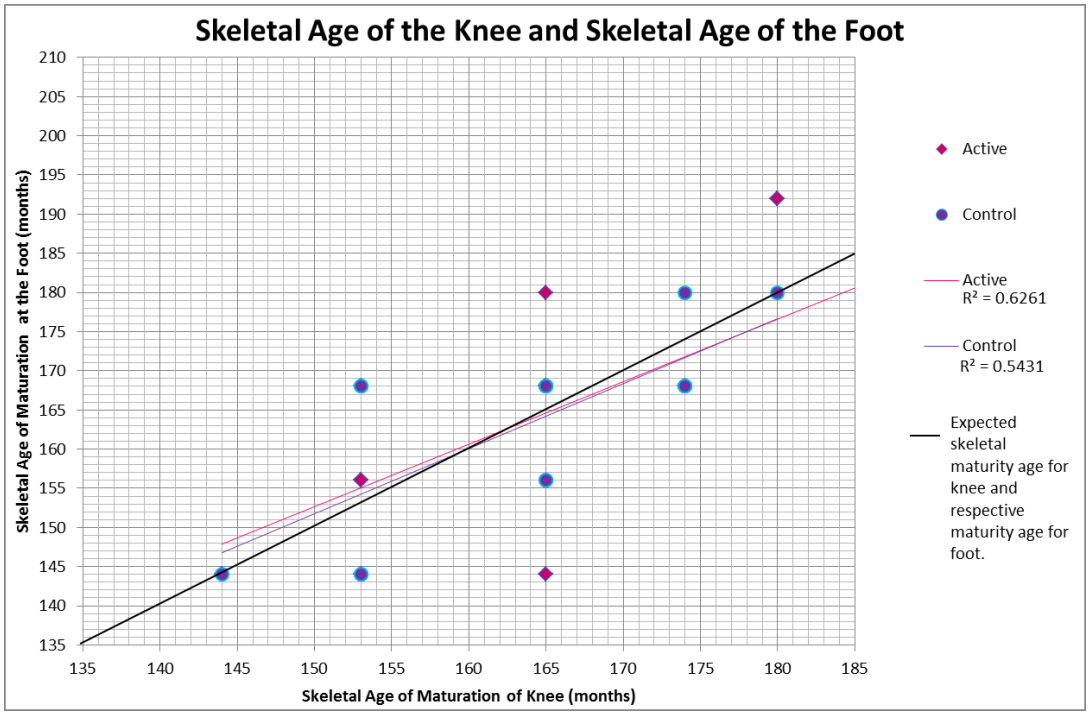

Figure 4.32 – Graph of skeletal age of the knee plotted against skeletal age of the foot. Control correlation significance is 0.002 and active correlation significance is 0.000.

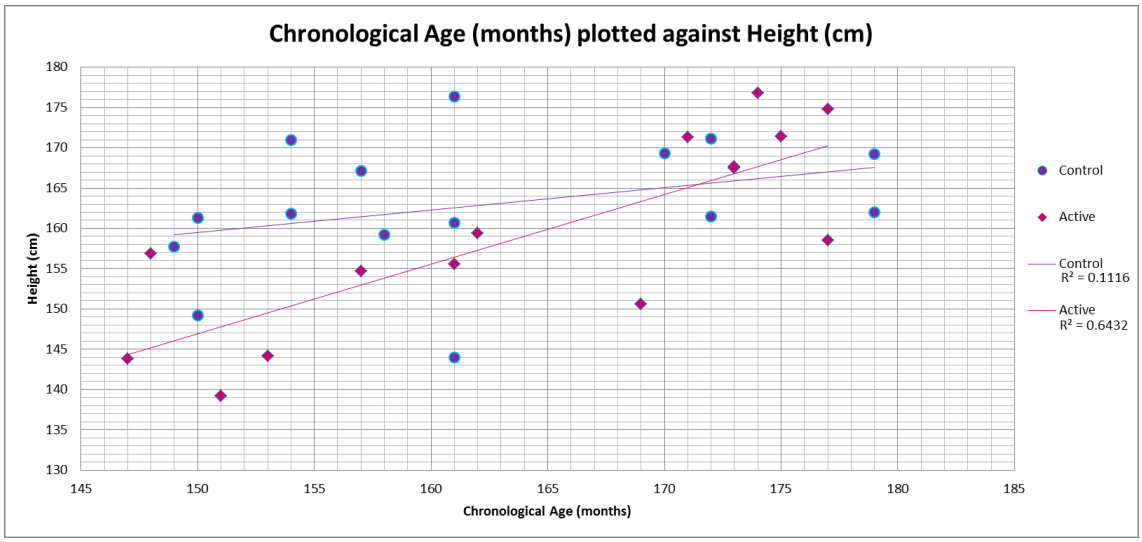

Figure 4.33 – Graph of chronological age plotted against height. Control correlation significance is 0.224 although active correlation significance is 0.000.

4.3 Chapter Summary

Ultimately, the results presented in Chapter 4 indicate that there is a complex relationship with regards to the level of activity and subsequent skeletal and biomechanical development of healthy individuals. The volumetric growth plate data did not reveal any significant differences between the active and control groups; however different trends are evident within the active and control group. Active individuals appear to follow a more closely connected pattern of skeletal development in relation to their chronological age, body mass index (BMI) and height, which has significantly stronger correlations in comparison to the control group. A particular concern regarding the active group is the increased prevalence of pathologies encountered through incidental MRI findings. The majority of individuals across both groups were asymptomatic; however 60% of the active group presented with disruption to skeletal development in the form of bone marrow oedema which greatly differs to the 13% of the control group who presented with bone marrow oedema.

The biomechanical data supports the trends outlined by the volumetric growth plate data by providing evidence that intensively trained active individuals adopt the most efficient running technique which mimics the natural style of barefoot running. This was verified through the in-shoe pressure data, which revealed the active group contact area and maximum force at the heel was significantly lower ($p < 0.001$) than the control group. The kinematic and kinetic data also highlighted significant differences in both running and walking gaits with respect to the range of motion, forces, angles, moments and power.

Chapter 5

Discussion

5.1 Interpretation of Results

Through the unique combination of techniques across the fields of biomechanics, anatomy and medical physics; this is the first study of its kind to investigate the effects of intensive sports training with respect to the growth plates and subsequent biomechanical development of the lower limbs. Ultimately there are numerous factors to consider with regards to drawing conclusions from the 'snap shot' nature of this pilot study, which aims to act as a robust platform to bridge the gap in scientific literature by highlighting the previously unknown impact that excessive sports training may have on the skeletal growth of the lower limb.

The final results of the 'incidental' observations discovered through this research support similar findings in the scientific literature with respect to interpreting that there is an increased likelihood of an active individual developing structural anatomical anomalies as a consequence of prolonged, intensive exercise (Nanni *et al.* 2005; Laor *et al.* 2006; Koh *et al*., 2007; Hreljac, 2004; Lohman *et al.*, 2002; Obembe *et al.*, 2007). As a consequence of clinical MRI scans typically not capturing similar levels of acquisition detail, unfortunately it is unknown whether the occurrence of bone bruising, or oedema-like signal of the bone marrow, is naturally encountered in the general population during the adolescent growth spurt. The increased occurrence of bone bruising at the ankle joint in the control group has likely equalled the active group as a consequence of the foot's design to disperse high impact demands which are encountered daily. The overall trend of bone bruising occurring at the knee, however, dramatically increases in prevalence in the active group which may cautiously suggest that this finding of bone marrow oedema in the distal femur and proximal tibia is unlikely to be found commonly in the general adolescent population.

The different dynamic and development attributes of the proximal tibia and calcaneus may explain why it was not possible to measure repeatedly or define accurately a 'TOTAL' outline for these volumes. The calcaneal growth plate is a traction epiphyses and by definition does not form at an articulation site. Interestingly, the findings at the proximal tibia may relate to the directionality of the histological cellular layers and their interaction with the internal stresses and strains travelling through the bones of the lower limb.

The results of this research highlight that important biomechanical differences were encountered when young athletes self selected a running speed and technique when compared to the self adopted running styles observed in less physically active schoolboys of the same age. This difference may be a consequence of the active group receiving one-to-one training to optimise and develop skilful techniques by reducing the excessive impacts encountered when running. Interestingly, the design concept of running shoes promotes the perception of reduced collision by impairing the sensory feedback mechanism encountered by the foot when striking the ground; therefore the overall stresses, which may appear to be cushioned, do not necessarily alter and could lead to over-pronation of the foot (Robbins and Hanna, 1987; Keenan *et al.*, 2011). The subsequent outcome is that athletes who exercise regularly at an intensive level will be more inclined to understand and recognise the most efficient and optimal biomechanical technique to limit the occurrence of overuse pain after repetitive training sessions. The results confirm that the active group typically mimic barefoot running by naturally striking the ground with the forefoot and toes; thus revealing that these individuals were either selected to play at the academy due to their natural athletic technique, or individually coached to modify and develop their personal skills to protect against injury.

The style and velocity of the running technique adopted by an individual can influence the shape of the kinetic graphical data (Cavanagh and LaFortune, 1980) yet it is also important to note that a variation in the type of shoe can alter the biomechanical interaction of weight, force and pressure distribution of the foot, ankle and lower limb (Keenan *et al.*, 2011; Bentley *et al.*, 2011). Although the control group are less physically active, on occasions when partaking in physical education classes at school, the individuals likely wear heavily cushioned sports shoes that interfere with the natural biomechanical feedback loop to alert an individual if excessive forces are negatively acting on the anatomical structures. The control group do not exercise at intensive levels, therefore any cushioned impacts encountered while running that would normally induce repetitive strain and micro-damage, would unlikely amount to a noticeably painful level for these individuals to alter the style of running. Overall there was only one control participant to adopt the toe-running technique. On closer examination of all of the information relating to this individual, he may be an outlier for both the control group and active group as he was the only individual to present with low longitudinal foot arches. Subsequently, his feet had a flatter appearance and this may explain the natural biomechanical adoption of running on his toes to reduce excessive impaction forces of his feet with the ground.

Power is defined as the product of joint angular velocity and the joint moment; therefore the positive relationship between the significant differences between the ankle moments and ankle angles in the sagittal (X) plane complement the significance of the interaction with ankle power in the transverse (Z) plane, particularly evident during running. A common cause of increased ground reaction forces travelling along the medial aspect of the foot is usually a consequence of excessive over-pronation of the foot and ankle (Dugan and Bhat, 2005). The active group walking trials and control group walking

trials are similar as expected; however one significant difference is the contact areas for the left and right feet are significantly smaller in the active group as a whole. This suggests that the active group typically walk with a similar pressure distribution path as they run; therefore are naturally lighter on their feet and have efficient biomechanical function. The difference in running style adopted by the active group also illustrates a clear difference in pressure distribution when compared to the control group. Ultimately this research indicates that intensive sports training regimes have a substantial role in influencing the biomechanical development of long bones.

5.1.1 Aims and Objectives

The main aim and objectives of the study were fulfilled successfully as the results enabled the hypothesis (H_1) to be tested and investigated. The division of the hypothesis into segments illustrates the importance of analysing the data separately in order to formulate an objective conclusion based on the combined, multifactorial aspects which affect skeletal growth and biomechanical development. Consequently, the following four statements can be accepted:

$H_{01\text{-}1}$ – The growth plate volumes in the active group **do not differ** significantly from those of the control group.

$H_{1\text{-}2}$ – There is a **significant difference** in plantar pressures exhibited by the active group compared to the control group.

$H_{1\text{-}3}$ – The lower limb kinetics of the active group **differ significantly** compared to those of the control group.

$H_{1\text{-}4}$ – The lower limb kinematics of the active group **differ significantly** compared to those of the control group.

Careful deliberation of the individual components of the results was required prior to concluding the final acceptance of the hypothesis (H_1) based on $H_{1\text{-}2}$, $H_{1\text{-}3}$ and $H_{1\text{-}4}$ all showing significant differences between the active and control group biomechanics when walking and running. Although $H_{1\text{-}1}$ was not found to be statistically significant overall; the relationship of active growth plate volumes and control group volumes follow different trends and a greater number of incidental findings were observed in the active group. This difference in relationship trend is also supported by evident differences in relation to the maturation stages of the epiphyseal regions and significantly different correlation results.

In relation to concisely categorising whether the effect of intensive sports training has a positive, negative or neutral influence on the growth and development of the epiphyseal plate, this is unfortunately difficult to determine. Further longitudinal research with larger sample sizes could reveal significant results in relation to the complex interaction that intensive sports training has on the volumetric size, and likely histological morphology, at vulnerable developmental stages.

Although the biomechanical function and form of the lower limb appears to adapt in a beneficial nature to efficiently distribute the stresses and forces incurred while running for the active individuals; the incidental findings from the MRI results contradict this theory. These incidental pathologies indicate negative disruption of the growth plates with regard to bone bruising. The observation of bone bruising suggests that micro-damage and overuse injuries are occurring at the epiphyseal plates, however this does not necessarily mean that subsequent growth is inhibited in a negative manner. This disruption, if not over exerted, could increase the flow of nutrients by improving the blood supply at times of increased biomechanical loading, thus potentially improving

the final bone mineral density and stimulating long term healthy growth. However, as this is out with the scope of the research at this stage, the fact remains that pathological findings are observed in asymptomatic individuals across both groups. There is an evident trend of bone bruising and marrow oedema that is far greater in active individuals which should not be ignored.

5.1.2 Nutrition and Lifestyle

One important point to consider is that there was an interesting outlier included in the active group who did not display even a rudimentary trace of an epiphyseal scar at the age of 14 years. This could be entirely unrelated to the effects of intensive sports training and may well be within the range of normal variation; however for a male individual this age is predominantly precocious for complete closure and obliteration of the growth plates, particularly when radiopaque epiphyseal scars have been found to persist long into adulthood (Davies *et al.*, 2013). This active individual encountered a serious injury (which was muscle/tendon damage and not a fracture to the bone) earlier during the previous year which resulted in physiotherapy sessions at Murray Park while he was out of action. The incidence of injury dramatically increases when training is increased (Clinghan *et al.*, 2008); therefore it is important to consider this increased risk that could confound and negate the positive influence moderate exercise has on growth, by resulting in irreversibly damaging the growth plate and ceasing longitudinal growth altogether.

Previous studies in the scientific literature have also observed that reduced skeletal maturation can occur in individuals who regularly partake in excessive physical activities (De Smet *et al.*, 1994). One particularly evident difference in the size and

maturation status of growth plates was found by De Smet *et al*. (1994) who researched a group of competitive gymnasts, with a chronological age range spanning from 13.1 to 20.6 years, who presented with an unusually high number of female gymnasts to still have open growth plates. On comparison of radiographs, the gymnasts had younger bone ages and reduced skeletal maturation than expected for their chronological age.

The research undertaken by Hackman (2012) is particularly appropriate to consider due to the population also being local to Dundee, as in the case of the control group. Interestingly, Hackman (2012) found that the cohorts of 11 year old and 13 year old males showed the largest mean difference in skeletal maturity (±7.54 and ±8.81 months respectively), with the exception of the final age bracket of 19 year olds. This assists in supporting the understanding of why the strength and significance of the control group correlations may have a generally weaker relationship when compared to the overall relationship trends found within the active group. An example is that the active group follow the expected trend that chronological age is strongly correlated with the skeletal maturity age at the knee ($p = 0.002$); therefore it is surprising that the control group fail to show a statistically significant trend ($p = 0.188$). This may be explained by the active group consistently having independent samples of the growth plate volumes with a larger standard deviation when compared with the standard deviations found in the control group. Intriguingly, the mean value tends to present as larger values for the average growth plate volumes of the control group with the exception of the T2 data for the distal femoral and distal tibial growth plates. These observations once again illustrate that there are evidently complex interactions with respect to the effect that intensive sports training has on the functional development of each growth plate and reiterates the fact that a larger sample size may find significant differences that are otherwise hidden behind correlation trends.

5.2 Limitations

The control group were selected for by sedentary characteristics prevalent in their lifestyle; however, the true definition of sedentary is difficult to define (Pate *et al*., 2008). Although physical activity was not measured by empirical raw data, the level of weekly activity was gauged by interviewing the individuals with their parents present and the extent of exercise was categorised by how many hours each activity was exerted during a typical week. Ultimately this could introduce errors as each individual is subjective with classifying their own level of activity and what they perceive to be moderate exercise. This small limitation was reduced by being able to listen, discuss and question each individual at the time of completing the questionnaire and ample space was provided for the boys to go into as much detail as possible to create a complete representation of daily life.

Of all of the software used for the MRI analysis, all three software were useful for different reasons in their own right. T2 for quickness and this was the one method to show a similar level of relationship across different regions. The Endpoint software had the livewire tool which made it ideal for precision which was proven to have a highly significant inter- and intra-observer error rate ($p < 0.001$). The one limitation with Endpoint software is that the version is now obsolete and therefore not readily available for other research groups to test the reproducibility of alternative segmentations of MRI data. OsiriX™ was ideal in the fact that the software is free and operates on the basis of open-source versions, ultimately resulting in the continual development and improvement of features at the forefront of technological advances. The 3D graphics are outstanding and provide anatomical reconstructions and views in exceptional detail which would otherwise be unattainable. The only drawback with the software in

comparison to the other two systems is the requirement to develop a sufficient tool which would assist in the semi-automatic detection of regions of interest. The number of manual outlines required to complete the entire growth plate region is almost double (OsiriX has a minimum number of 160 slices compared to 80 slices for Endpoint and 23/25 slices for T2 map program) and without the semi-automatic recognition of the live wire tool to help guide the researcher consequently resulted in this technique being the least efficient with respect to the dependence on time which is not optimal for large, longitudinal studies.

An additional consideration is that the control group were found to skeletally mature in advance of the active group, which may result in the endpoint outlines and boundaries of the control growth plates becoming more difficult to discern; therefore introducing a potential explanation as to why the growth plate volume relationships did not have significantly strong a correlation. The analysis of each growth plate segmentation was randomised at all stages; therefore the possibility of introducing observer variables is negated. Additionally through the testing of inter-observer error, the ability to recognise that both observers independently calculated similar results leads to the conclusion that this difference is not random. Although the Independent Samples T-Test did not indicate any significant differences between the two sample groups, if the research is expanded to include a larger sample size this may affect the significance as the small sample size may limit the statistical power to discern more subtle trends.

Chapter 6

Future Work and Conclusions

6.1 Future Work

Ideally, this research would be suited to being extended longitudinally in order to follow the progression and development of the same individuals. The active individuals can be recruited to intensive sports training academies from the age of nine years; therefore the opportunity to sequentially record the anatomical form of the growth plate (via MRI) and the respective biomechanical developments (via Motion Analysis) every year until the beginning of a professional career at the age of seventeen would ultimately provide a robust platform to further explore how much relevance should be weighted on the observation of incidental pathologies. In order to improve the ability of accurately determining the developmental stage an individual has reached in relation to the peak growth spurt, testosterone levels could be measured if a blood sample was incorporated into the research protocol. This technique could provide valuable developmental information in relation to potential differences that may be observed in the growth plates of similarly aged individuals who could be at opposite sides of the adolescent growth spurt; thus presenting entirely different levels of skeletal maturation, and consequently growth plate volumes, which could otherwise present as more challenging to compare. Due to the young age of this sample group, the invasive nature of needles would likely be disconcerting for the volunteers and would therefore always be a supplementary factor which would require independent consent.

If an additional group of amateur football players were included in the study, this could perhaps impart a better understanding with regards to the importance of combining intensive exercise with the nutritional balance that youth academies like Murray Park emphasise as being fundamental to their success. The elite active group would perhaps confirm that, when compared with an amateur group, fewer injuries are likely to be

incurred in relation to the number of hours spent training as a consequence of the different extent of professional protection.

During the biomechanical phase of data collection in the sports laboratory, EMG data was recorded as an area of interest outside the scope of this study. Future development prospects of this research could implement a program, which is currently being developed in IMAR, to combine and synchronise EMG muscle activity with the kinematic and kinetic data collected. Figure 6.1 depicts a screen shot of the prototype program developed in-house which combines all of the trial data in one program. Once the Vicon® and EMG ASCII files are aligned to the same radio pulse, the different frequencies can then be synchronised to scale, to compare the timings of events at the same percentage of the gait cycle. This advancement could further highlight potential hidden biomechanical weaknesses within the muscles due to repetitive strain injury.

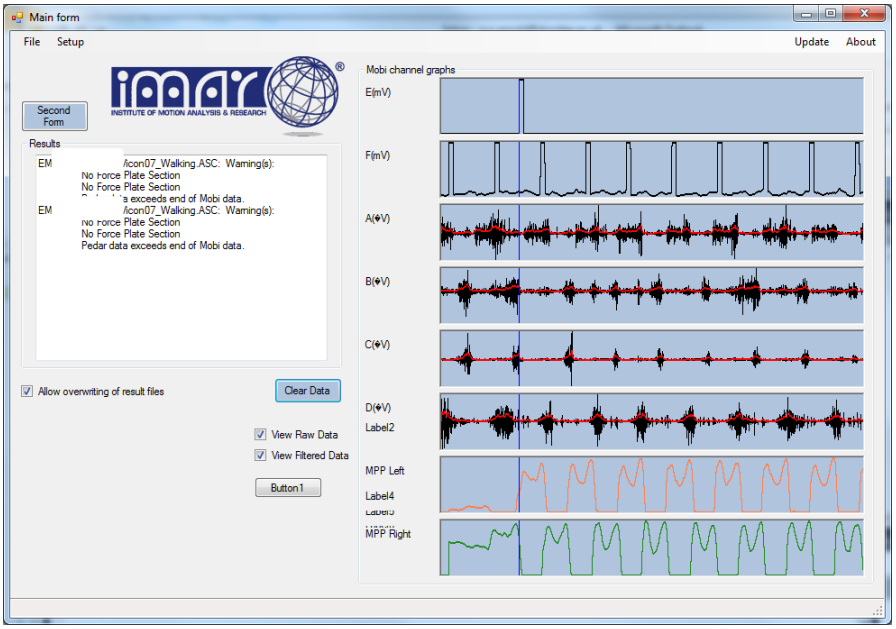

Figure 6.1 – IMAR program developed in-house and created in MATLAB® which synchronises Vicon®, Pedar®, and EMG trial files together to enable analysis of the holistic gait parameters.

6.2 Conclusions of the research

The powerful combination of analysing both biomechanical and anatomical aspects of the developing lower limb in professionally trained individuals is unique to this research project. Combining the kinetic and kinematic data with the complementary volumetric data of the growth plate ultimately permits realistic and reliable conclusions to be drawn from the findings. Further expansion of this project, both in terms of increased sample size and scope for repeated collection of an individual's data on a yearly/longitudinal basis, would ultimately create a significantly robust platform to support the results and conclusions of this research.

Intensive training activities should remain an important focus for young athletes in order to enhance future performance and long-term health benefits, with the negative association of developing an irreversible injury being negated through the careful implementation of health and safety guidelines. The long-term health of individuals is of the foremost importance and this research could ultimately improve professional training guidelines, in addition to the health support mechanisms available to society as a whole. This could not come at a more influential time for young school children and young athletes following the increased supportive, enthusiastic passion for sports created in the aftermath of the 2012 Olympic Games and anticipation for the 2014 Commonwealth Games.

References

Abboud, R.J. (2002) Mini-Symposium: The Elective Foot (i) Relevant Foot Biomechanics. *Current Orthopaedics* **16**: 165-179.

Abboud, R.J., Rowley, D.I. and Newton, R.W. (2000) Lower Limb Muscle Dysfunction May Contribute to Foot Ulceration in Diabetic Patients. *Clinical Biomechanics.* **15** (1): 37-45.

Adirim, T.A. and Barouh, A. (2006) Common Orthopaedic Injuries in Young Athletes. *Current Paediatrics.* **16** : 205-210.

Advanced Mechanical Technology, Inc. (2013) *Force and Motion.* (Last accessed - 2013): http://www.amti.biz/.

AeRang, K., Dombi, E., Solomon, J., Fox, E., Balis, F.M., and Widemann, B.C. (2011) Automated Volumeric Growth Plate Measurement Using Magnetic Resonance Imaging for Monitoring Skeletal Toxicity in Children Treated on Investigational Drug Trials. *Clinical Cancer Research.* **17** (18): 5982-5990.

Afshar, A.N. and Ren, L. (2012) Dynamic Stability of Passive Bipedal Walking on Rough Terrain: A Preliminary Simulation Study. *Journal of Bionic Engineering*. **9** : 423-433.

Agur, A.M.R. and Dalley, A.F. (2005) *Grant's Atlas of Anatomy – Eleventh Edition.* Lippincott Williams and Wilkins, Baltimore, USA.

Almosnio, S., Kajaks, T., and Costigan, P.A. (2009) The Free Moment in Walking and its Change With Foot Rotation Angle. *Sports Medicine, Arthroscopy, Rehabilitation, Therapy and Technology.* **1** (19) : 1-9.

Amini, S., Veilleux, D., and Villemure, I. (2010) Tissue and Cellular Morphological Changes in Growth Plate Explants Under Compression. *Journal of Biomechanics.* **43** : 2582-2588.

Andersson, E.A., Nilsson, J. and Thorstensson, A. (1997) Intramuscular EMG From the Hip Flexor Muscles During Human Locomotion. *Acta Physiologica Scandinavica*. **161** (3): 361-370.

Arkin, A.M. and Katz, J.F. (1956) The Effects of Pressure on Epiphyseal Growth: The Mechanism of Plasticity of Growing Bone. *The Journal of Bone and Joint Surgery.* **38-A**: 1056-1076.

Armitage, P., Berry, G. and Matthews, J.N.S. (2002) *Statistical Methods in Medical Research*. Blackwell Science Ltd., Cornwall. Pgs 138-140.

Ayyappa, E. (1997) Normal Human Locomotion - Part 2: Motion, Ground Reaction Force and Muscle Activity. *Journal of Prosthetics and Orthotics.* **9** (2): 42-57.

Babraj, J.A., Vollaard, N.B.J., Keast, C., Guppy, F.M., Cottrell, G., and Timmons, J.A. (2009) Extremely Short Duration High Intensity Interval Training Substantially Improves Insulin Action in Young Healthy Males. *BioMed Central Endocrine Disorders.* **9** (3): 1-8.

Bartlett, R. (1999) *Sports Biomechanics: Reducing Injury and Improving Performance.* E & FN Spon, London.

Basmajian, J.V. and De Luca, C.J. (1985) *Muscles Alive – Fifth Edition*. Williams and Wilkins, Baltimore, USA.

Beltran, L., Ghazikhanian, V., Padron, M. and Beltran, J. (2012) The Proximal Hamstring Muscle-Tendon-Bone Unit: A Review of the Normal Anatomy, Biomechanics and Pathophysiology. *European Journal of Radiology*. **81** (12): 3772-3779.

Bentley, J.A., Ramanathan, A.K., Arnold, G.P., Wang, W. and Abboud, R.J. (2011) Harmful Cleats of Football Boots: A Biomechanical Evaluation. *Foot and Ankle Surgery*. **17** (3): 1-4.

Bertsch, C., Unger, H., Winkelmann, W., and Rosenbaum, D. (2004) Evaluation of Early Walking Patterns from Plantar Pressure Distribution Measurements - First Year Results of 42 Children. *Gait and Posture*. **19** : 235-242.

Boisseau, N., Vermorel, M., Rance, M., Duché, P., and Patureau-Mirand, P. (2007) Protein Requirements in Male Adolescent Soccer Players. *European Journal of Applied Physiology*. **100** : 27-33.

Bosch, K. and Rosenbaum, D. (2010) Gait Symmetry Improves in Childhood – A 4-Year Follow-up of Foot Loading Data. *Gait and Posture.* **32** : 464-468.

Bovi, G., Rabuffetti, M., Mazzoleni, P., and Ferrarin, M. (2011) A Multiple-task Gait Analysis Approach: Kinematic, Kinetic and EMG Reference Data for Healthy Young and Adult Subjects. *Gait and Posture*. **33** : 6-13

Brenner, J.S., and the Council on Sports Medicine and Fitness. (2007) Overuse Injuries, Overtraining, and Burnout in Child and Adolescent Athletes. *Pediatrics.* **119** : 1242-1245.

Brewis, A. (2012) Obesity and Human Biology: Toward A Global Perspective. *American Journal of Human Biology* **24**: 258-260.

Bright, R.W., Burstein, A.H., and Elmore, S.M. (1974) Epiphseal-Plate Cartilage: A Biomechanical and Histological Analysis of Failure Modes. *The Journal of Bone and Joint Surgery.* **56** : 688-703.

Brookes, M. (1971) *The Blood Supply of Bone*. Butterworths, London.

Brown, W.J., McLaughlin, D., Leung, J., McCaul., K.A., Flicker, L., Almeida, O.P., Hankey, G.J., Lopez, D., and Dobson, A.J. (2012) Physical Activity and All-Cause Mortality in Older Women and Men. *British Journal of Sports Medicine.* **46** : 664-668.

Bush, P.G., Hall, A.C., and Macnicol, M.F. (2008) New Insights into Function of the Growth Plate: Clinical Observations, Chondrocyte Enlargement and a Possible Role for Membrane Transporters. *Journal of Bone and Joint Surgery.* **90-B** (12): 1541-1547.

Byers, S., Moore, A.J., Byard, R.W., and Fazzalari, N.L. (2000) Quantitative Histomorphometric Analysis of the Human Growth Plate From Birth to Adolescence. *Bone* **27** (4): 495-501.

Caine, D., DiFiori, J., and Maffulli, N. (2006) Physeal Injuries in Children's and Youth Sports: Reasons for Concern? *British Journal of Sports Medicine* **40** : 749-760.

Cappellini, G., Ivanenko, Y.P., Poppele, R.E. and Lacquaniti, F. (2006) Motor Patterns in Human Walking and Running. *Journal of Neurophysiology.* **95** (6): 3426-3437.

Carson Jr, W.G. and Gasser, S.I. (1998) Little Leaguer's Shoulder: A report of 23 Cases. *American Journal of Sports Medicine.* **26** (4): 575-580.

Carter, S. (2009) *The Genetic Basis of Human Height: The Role of Estrogen*. PhD Thesis. Queensland University of Technology, Brisbane, Australia.

Cavanagh, P.R. and Lafortune, M.A. (1980) Ground Reaction Forces in Distance Running. *Journal of Biomechanics*. **13** : 397-406.

Choudhri, A.F. and Radvany, M.G. (2011) Initial Experience with a Handheld Device Digital Imaging and Communications in Medicine Viewer: OsiriX Mobile on the iPhone. *Journal of Digital Imaging.* **24** (2): 184-189.

Christou, M., Smilios, I., Sotiropoulos, K., Volaklis, K., Pilianidis, T., and Tokmakidis, S.P. (2006) Effects of Resistance Training on the Physical Capacities of Adolescent Soccer Players. *The Journal of Strength and Conditioning Research.* **20** (4): 783-791.

Cifrek, M., Medved, V., Tonković, S., and Ostojić, S. (2009) Surface EMG Based Muscle Fatigue Evaluation in Biomechanics. *Clinical Biomechanics.* **24** : 327-340.

Clinghan, R., Arnold, G.P., Drew, T.S., Cochrane, L.A., and Abboud, R.J. (2008) Do You Get Value for Money When You Buy an Expensive Pair of Running Shoes. *British Journal of Sports Medicine.* **42** : 189-193.

Cole, T.J. (2012) The Development of Growth References and Growth Charts. *Annals of Human Biology*. **39** (5): 382-394.

Colvin, A.C. and Lynn, A. (2010) Sports-Related Injuries in the Young Female Athlete. *Mount Sinai Journal of Medicine.* **77** : 307-314.

Craig, J.G., Cody, D.D. and van Holsbeek, M. (2004) The Distal Femoral and Proximal Tibial Growth Plates: MR Imaging, Three-Dimensional Modelling and Estimation of Area and Volume. *Skeletal Radiology*. **33** : 337-344.

Cram, J.R. (2003) The History of Surface Electromyography. *Applied Psychophysiology and Biofeedback*. **28** (2): 81-91.

Damavandi, M., Dixon, P.C., and Pearsall, D.J. (2012) Ground Reaction Force Adaptations During Cross-Slope Walking and Running. *Human Movement Science.* **31**: 182-189.

Davies, C., Hackman, L. and Black, S. (2013) The Persistence of Epiphyseal Scars in the Adult Tibia. *International Journal of Legal Medicine*. DOI: 10.1007/s00414-013-0838-3.

De Andrea, C.E. and Hogendoom, P.C.W. (2012) Epiphyseal Growth Plate and Secondary Peripheral Chondrosarcoma: The Neighbours Matter. *Journal of Pathology* **226** : 219-228.

Dedouit, F., Auriol, J., Rousseau, H., Rougé, D., Crubézy, E., and Telmon, N. (2012) Age Assessment by Magnetic Resonance Imaging of the Knee: A Preliminary Study. *Forensic Science International*. **217** : 232.e1-232.e7.

Desloovere, K., Molenaers, G., Feys, H., Huenaerts, C., Callewaert, B., and Van de Walle, P. (2006) Do Dynamic and Static Clinical Measurements Correlate with Gait Analysis Parameters in Children with Cerebral Palsy? *Gait and Posture.* **24** : 302-313.

De Smet, L., Claessens, A., Lefevre, J., and Beunen, G. (1994) Gymnast Wrist: An Epidemiologic Survey of Ulnar Varience and Stress Changes of the Radial Physis. *American Journal of Sports Medicine*. **22** : 846-850.

Diebal, A.R., Gregory, R., Alitz, C., and Gerber, J.P. (2011) Effects of Forefoot Running on Chronic Exertional Compartment Syndrome: A Case Series. *The International Journal of Sports Physical Therapy*. **6** : 312-321.

Drake, R.L., Vogl, W., and Mitchell, A.W.M. (2005) *Gray's Anatomy for Students.* Churchill Livingstone, Elsevier, London.

Ducher, G., Daly, R.M., and Bass, S.L. (2009) Effects of Repetitive Loading on Bone Mass and Geometry in Young Male Tennis Players: A Quantitative Study Using MRI. *Journal of Bone and Mineral Research.* **24** (10): 1686-1692.

Dugan, S.A. and Bhat, K.P. (2005) Biomechanics and Analysis of Running Gait. *Physical Medicine & Rehabilitation Clinics of North America.* **16** (3): 603-621.

Dunning, E. (2000) Towards a Sociological Understanding of Football Hooliganism as a World Phenomenon. *European Journal on Criminal Policy and Research.* **8** (2): 141-162.

Dvorak, J., Fuller, C.W., and Junge, A. (2012) Planning and Implementing a Nationwide Football-Based Health-Education Programme. *British Journal of Sports Medicine.* **46** : 6-10.

Edwards, M.R., Jack, C. and Singh, S.K. (2008) Tibialis Posterior Dysfunction. *Foot and Ankle.* **22** (3): 185-192.

ElBaradie, K., Wang, Y., Boyan, B.D., and Schwartz, Z. (2011) Rapid Membrane Responses to Dihydrotestosterone are sex dependent in Growth Plate Chrondrocytes. *Journal of Steroid Biochemistry and Molecular Biology.* **132** : 15-23.

Emery, K.H. (2009) MR Imaging in Congenital and Acquired Disorders of the Pediatric Upper Extremity. *Magnetic Resonance Imaging Clinics of North America.* **17** : 549-570.

Emons, J.A.M., Boersma, B., Baron, J., and Wit, J.M. (2005) Catch-up Growth: Testing The Hypothesis of Delayed Growth Plate Senescence in Humans. *Journal of Pediatrics*. **47** : 843-846.

Ericsson, K.A., Krampe, R.T., and Tesch-Römer, C. (1993) The Role of Deliberate Practice in the Acquisition of Expert Performance. *Psychological Review*. **100** (3): 363-406.

Fiedler, K.E., Stuijfzand, W.J.A., Harlaar, J., Dekker, J., and Beckerman, H. (2011) The Effect of Shoe Lacing on Plantar Pressure Distribution and In-shoe Displacement of the Foot in Healthy Participants. *Gait and Posture*. **33** : 396-400.

Figueirdo, A.J., Coelho e Silva, M.J., and Malina, R.M. (2010) Predictors of Functional Capacity and Skill in Youth Soccer Players. *Scandinavian Journal of Medical Science Sports*. **21**: 446- 454.

Forwood, M.R., Baxter-Jones, A.D., Beck, T.J., Mirwald, R.L., Howard, A., and Bailey, D.A. (2006) Physical Activity and Strength of the Femoral Neck During the Adolescent Growth Spurt: A Longitudinal Analysis. *Bone.* **38** : 576-583.

Franklin, D., Flavel, A., Kuliukas, A., Cardini, A., Marks, M.K., Oxnard, C. and O'Higgins, P. (2012) Estimation of Sex from the Sternal Measurements in a West Australian Population. *Forensic Science International.* **217** : 1-5.

Frost, H.M. (1994) Wolff's Law and Bone's Structural Adaptations to Mechanical Usage: An Overview for Clinicians. *The Angle Orthodontist.* **64** (3): 175-188.

Fujii, T., Takai, S., Arai, Y., Kim, W., Amiel, D., and Hirasawa, Y. (2000) Microstructural Properties of the Distal Growth Plate of the Rabbit Radius and Ulna: Biomechanical, Biochemical, and Morphological Studies. *Journal of Orthopaedic Research.* **18** (1): 87-93.

Gelander, L., Karlberg, J., and Albertsson-Wikland, K. (1994) Seasonality in Lower Leg Length Velocity in Prepubertal Children. *Acta Paediatrica.* **83** : 1249-1254.

Gerrard, D.F. (1993) Overuse Injury and Growing Bones: The Young Athlete at Risk. *British Journal of Sports Medicine*. **27** : 14-18.

Girard, O., Eicher, F., Fourchet, F., Micallef, J.P., and Millet, G.P. (2007) Effects of the Playing Surface on Plantar Pressures and Potential Injuries in Tennis. *British Journal of Sports Medicine*. **41** : 733-738.

Goldblatt, J.P. and Richmond, J.C. (2003) Anatomy and Biomechanics of the Knee. *Operative Techniques in Sports Medicine*. **11** : 172-186.

Goryachev, Y., Debbi, E.M., Haim, A., and Wolf, A. (2011) The Effect of Manipulation of the Centre of Pressure of the Foot During Gait on the Activation Patterns of the Lower Limb Musculature. *Journal of Electromyography and Kinesiology.* **21** : 333-339.

Granata, K.P., Abel, M.F. and Damiano, D.L. (2000) Joint Angular Velocity in Spastic Gait and the Influence of Muscle-Tendon Lengthening. *Journal of Bone and Joint Surgery*. **82** (2): 174-186.

Greulich, W.W. and Pyle, S.I. (1959) *Radiographic Atlas of Skeletal Development of the Hand and Wrist – Second Edition.* Stanford University Press, California.

Hackman, L. (2012) *Age Estimation in the Living: A Test of Six Radiographic Methods.* PhD Thesis. Dundee University, Dundee, UK.

Hackman, L. and Black, S. (2013) The Reliability of the Greulich and Pyle Atlas When Applied to a Modern Scottish Population. *Journal of Forensic Sciences.* **58** (1) : 114-119.

Hall, M.C. (1961) The Trabecular Patterns of the Neck of the Femur with Particular Reference to Changes in Osteoporosis. *Canadian Medical Association Journal*. **85** (18): 1141-1144.

Hartwig, T.B., Naughton, G., and Searl, J. (2009) Load, Stress, and Recovery in Adolescent Rugby Union Players During a Competitive Season. *Journal of Sports Sciences.* **27** (10): 1087-1094.

Haskell, W.L., Lee, I.M., Pate, R.R., Powell, K.E., Blair, S.N., Franklin, B.A., Macera, C.A., Heath, G.W., Thompson, P.D., and Bauman, A. (2007) Physical Activity and Public Health: Updated Recommendation for Adults From the American College of Sports Medicine and the American Heart Association. *Circulation*. **116** : 1081-1093.

Hidler, J., Wisman, W., and Neckel, N. (2008) Kinematic Trajectories While Walking Within the Lokomat Robotic Gait-Orthosis. *Clinical Biomechanics.* **23** : 1251-1259.

Hochberg, Z. (2002) Clinical Physiology and Pathology of the Growth Plate. *Best Practice and Research Clinical Endocrinology and Metabolism* **16** (3): 399-419.

Hodson, A. (1999) Too Much Too Soon? The Risk of 'Overuse' Injuries in Young Football Players. *Journal of Bodywork & Movement Therapies*. **3** (2): 85-91.

Hoerr, N.L., Pyle, S.I., and Francis, C.C. (1962) *Radiographic Atlas of Skeletal Development of the Foot and Ankle.* Charles C. Thomas, Illinois, USA.

Hogrel, J.Y. (2005) Clinical Applications of the Surface Electromyography in Neuromuscular Disorders. *Clinical Neurophysiology.* **35** : 59-71.

Hreljac, A. (2004) Impact and Overuse Injuries in Runners. *Medicine and Science in Sports and Exercise* **36** (5): 845-849.

Institute of Motion Analysis and Research Manual (Last accessed – 2013). Tayside Orthopaedic and Rehabilitation Technology (TORT) Centre, Department of Orthopaedic and Trauma Surgery, University of Dundee. https://secure.dundee.ac.uk/orthopaedics/dundeeonly/plugin4.pdf

Johannsen, N., Binkley, T., Englert, V., Neiderauer, G., and Specker, B. (2003) Bone Response to Jumping is Site-specific in Children: A Randomized Trial. *Bone* **33** : 533-539.

Johnson, A., Doherty, P.J., and Freemont, A. (2009) Investigation of Growth, Development, and Factors Associated with Injury in Elite Schoolboy Footballers: Prospective Study. *British Medical Journal*. **338** : 1-4.

Kakihana, W., Torii, S., Akai, M., and Ohtake, Y. (2007) Secondary Gait Changes in Subjects with Recurrent Ankle Sprain – Subtalar and Knee Joint Moments During Stance -Presentation 0048. *Journal of Biomechanics.* **40** (S2): 43.

Kapoor, S., Gibbs, S., Abboud, R. and Wang, W. (2009) Comparison of Lower Limb Joint Powers in Cerebral Palsy Before and After Botulinum Toxin Injection. *Gait and Posture*. **30** (2) : 91.

Karol, L.A. and Jeans, K.A. (2011) Assessment of Clubfoot Treatments Using Movement Analysis. *Journal of Experimental and Clinical Medicine*. **3** (5): 228-232.

Keenan, G.S., Franz, J.R., Dicharry, J., Croce, U.D., and Kerrigan, C. (2011) Lower Limb Joint Kinetics in Walking: The Role of Industry Recommended Footwear. *Gait and Posture*. **33** : 350-355.

Kerssemakers, S.P., Fotiadou, A.N., deJonge, M.C., Karantanas, A.H., and Maas, M. (2009) Sport Injuries in the Paediatric and Adolescent Patient: A Growing Problem. *Pediatric Radology*. **39** : 471-484.

Kirane, Y.M., Michelson, J.D. and Sharkey, N.A. (2008) Evidence of Isometric Function of the Flexor Hallucis Longus Muscle in Normal Gait. *Journal of Biomechanics.* **41** : 1919-1928.

Knudson, D. (2003) *Fundamentals of Biomechanics*. Plenum Publishers, New York, USA.

Koh, E.S., Lee, J.C., and Healy, J.C. (2007) MRI of Overuse Injury in Elite Athletes. *Clinical Radiology.* **62** : 1036-1043.

Koh, T.J. and Grabiner, M.D. (1992) Cross Talk in Surface Electromyograms of Human Hamstring Muscles. *Journal of Orthopaedic Research.* **10** : 701-709.

Kontulainen, S., Sievänen, H., Kannus, P., Pasanen, M., and Vuori, I. (2003) Effect of Long-Term Impact-Loading on Mass, Size, and Estimated Strength of Humerus and Radius of Female Racquet-Sports Players: A Peripheral Quantitative Computed Tomography Study Between Young and Old Starters and Controls. *Journal of Bone and Mineral Research.* **18** (2): 352-359.

Kuczmarski, R.J., Ogden, C.L., Guo, S.S., Grummer-Strawn, L.M., Flegal, K.M., Mei, Z., Wei, R., Curtin, L.R., Roche, A.F., Johnson, C.L. (2002) 2000 CDC Growth Charts for the United States: Methods and Development. *Vital Health Statistics*. **11** (246): 1-190.

Kumar, A. and Sharma, T. (2011) Rare Variation of Flexor Digitorum Longus Muscle of Leg – A Case Report. *International Journal of Anatomical Variations.* **4** : 69-71.

Kushner, A. (1940) Evaluation of Wolff's Law of Bone Formation. *American Journal of Bone and Joint Surgery.* **22** (3): 589-596.

Lanyon, L.E., Hampson, W.G.J., Goodship, A.E., and Shah, J.S. (1975) Bone Deformation Recorded in Vivo From Strain Gauges Attached to the Human Tibial Shaft. *Acta Orthopaedica Scandinavica*. **46** : 256-268.

Laor, T., Wall, E.J., and Vu, L.P. (2006) Physeal Widening in the Knee Due to Stress Injury in Child Athletes. *American Journal of Roentgenology.* **186** : 1260-1264.

Larson, R.L. and McMahan, R.O. (1966) The Epiphyses and the Childhood Athlete. *Journal of the American Medical Association* **196** (7): 607-612.

LeVeau, B.F. and Bernhardtm D.B. (1984) Developmental Biomechanics: Effects of Forces on the Growth, Development, and Maintenance of the Human Body. *Physical Therapy*. **64** (12): 1874-1882.

Lieberman, D.E., Raichlen, D.A., Pontzer, H., Bramble, D.M. and Cutright-Smith, E. (2006) The Human Gluteus Maximus and its Role in Running. *The Journal of Experimental Biology.* **209** : 2143-2155.

Lieberman, D.E., Venkadesan, M., Werbel, W.A., Daoud, A.I., D'Andrea, S., Davis, I.S., Mang'Eni, R.O., and Pitsiladis, Y. (2010) Foot Strike Patterns and Collison Forces in Habitually Barefoot Versus Shod Runners. *Nature*. **436** : 531-536.

Liebling, M.S., Berdon, W.E., Ruzal-Shapiro, C., Levin, T.L., Roye Jr, D., and Wilkinson, R. (1995) Gymnast's Wrist (Pseudorickets Growth Plate Abnormality) in Adolescent Athletes: Findings on Plain Films and MR Imaging. *American Journal of Roentgenology.* **164** : 157-159.

Liikavainio, T., Isolehto, J., Helminen, H.J., Perttunen, J., Lepola, V., Kiviranta, I., Arokoski, J.P.A. and Komi, P.V. (2007) Loading and Gait Symmetry During Level and Stair Walking in Asymptomatic Subjects with Knee Osteoarthritis: Importance of Quadriceps Femoris in Reducing Impact Force During Heel Strike? *The Knee.* **14** (3): 231-238.

Lilley, K., Dixon, S., and Stiles, V. (2011) A Biomechanical Comparison of the Running Gait of Mature and Young Females. *Gait and Posture* **33** : 496-500.

Loh, R. (13th March 2012) Barca Academy Coach's Advice To S'Pore: 'Invest In Your Youth' - Press Release. The New Paper. (Last accessed - 2013): fcbarcelonasg.com/press-release/press-release-on-13-march-2012/

Lohman, M., Kivisaari, A., Vehmas, T., Kallio, P., Puntila, J. and Kivisaari, L. (2002) MRI in the Assessment of Growth Arrest. *Pediatric Radiology* **32** : 41-45.

Long, J.T., Klein, J.P., Sirota, N.M., Wertsch, J.J., Janisse, D., and Harris, G.F. (2007) Biomechanics of the Double Rocker Sole Shoe: Gait Kinematics and Kinetics. *Journal of Biomechanics.* **40** : 2882-2890.

Lovejoy, C.O. (1988) Evolution of Human Walking. *Scientific American*. **259** : 118-125.

Lujan, B.F. and White, R.J. (Last accessed: 2013) Human Physiology in Space http://www.nsbri.org/humanphysspace/focus6/f6-245.jpg

Lynch, N.A., Ryan, A.S., Evans, J., Katzel, L.I., and Goldberg, A.P. (2007) Older Elite Football Players Have Reduced Cardiac and Osteoporosis Risk Factors. *Medicine and Science in Sports and Exercise.* **39** (7): 1124-1130.

Mackie, E.J., Tatarczuch, L., and Mirams, M. (2011) The Skeleton: A Multi-functional Complex Organ. The Growth Plate Chondrocyte and Endochondral Ossification. *Journal of Endocrinology.* **211** : 109-121.

Malina, R.M., Eisenmann, J.C., Cumming, S.P., Ribeiro, B., and Aroso, J. (2004) Maturity-associated Variation in the Growth and Functional Capacities of Youth Football (Soccer) Players 13-15 Years. *European Journal of Applied Physiology.* **91** : 555-562.

Malina, R.M., Peña Reyes, M.E., Eisenmann, J.C., Horta, L., Rodrigues, J., and Miller, R. (2000) Height, Mass and Skeletal Maturity of Elite Portuguese Soccer Players Aged 11-16 Years. *Journal of Sports Sciences*. **18** : 685-693.

Minina, E., Wenzel, H.M., Kreschel, C., Karp, S., Gaffield, W., McMahon, A.P., and Vortkamp, A. (2001) BMP and Ihh/PTHrP Signalling Interact to Coordinate Chondrocyte Proliferation and Differentiation. *Development.* **126** : 4523-4534.

Monaghan, C.C., Hermens, H.J., Nene, A.V., Tenniglo, M.J.B. and Veltink, P.H. (2010) The Effect of FES of the Tibial Nerve on Physiological Activation of the Leg Muscles During Gait. *Medical Engineering and Physics.* **32** : 332-338.

Moreland, M.S. (1980) Morphological Effects of Torsion Applied to Growing Bone: An *In Vivo* Study in Rabbits. *Journal of Bone and Joint Surgery*. **62-B** (2): 230-237.

Moritani, T., Stegeman, D., and Merletti, R. (2004) Basic Physiology and Biophysics of EMG Signal Generation. In: Merletti, R. and Parker, P. *Electromyography: Physiology, Engineering, and Noninvasive Applications.* Wiley and Sons, New Jersey. **Chapter 1** : 1-25.

Muniz, A.M.S. and Nadal, J. (2009) Application of Principal Component Analysis in Vertical Ground Reaction Force to Discriminate Normal and Abnormal Gait. *Gait and Posture*. **29** : 31-35.

Murley, G.S., Buldt, A.K., Trump, P.J. and Wickham, J.B. (2009) Tibialis Posterior EMG Activity During Barefoot Walking in People with Neutral Foot Posture. *Journal of Electromyography and Kinesiology.* **19** (2): 69-77.

Nanni, M., Butt, S., Mansour, R., Muthukumar, T., Cassar-Pullicino, V.N., and Roberts, A. (2005) Stress-induced Salter-Harris I Growth Plate Injury of the Proximal Tibia: First Report. *Skeletal Radiology.* **34** : 405-410.

Neely, F.G. (1998) Biomechanical Risk Factors for Exercise-Related Lower Limb Injuries. *Sports Medicine*. **26** (6): 395-413.

Ng, D. and Vesely, M. (2012) The Free Sartorius Flap: Clinical Cases and Anatomical Study. *Journal of Plastic, Reconstructive and Aesthetic Surgery*. **65** : 1671-1677.

Nilsson, O. and Baron, J. (2004) Fundamental Limits on Longitudinal Bone Growth: Growth Plate Senescence and Epiphyseal Fusion. *Endocrinology and Metabolism.* **15** (8): 370-374.

Nilsson, O., Marino, R., De Luca, F., Philip, M. and Baron, J. (2005) Endocrine Regulation of the Growth Plate. *Hormone Research.* **64** : 157-165.

Obembe, O.O., Gaskin, C.M., Taffoni, M.J. and Anderson, M.W. (2007) Little Leaguer's Shoulder (Proximal Humeral Epiphysiolysis): MRI Findings in Four Boys. *Pediatric Radiology.* **37** : 885-889.

Ogden, J.A. (2000) *Skeletal Injury in the Child – Third Edition*, Springer-Verlag, New York.

Orlin, M.N. and McPoil, T.G. (2000) Plantar Pressure Assessment. *Physical Therapy*. **80** (4): 399-409.

Õunpuu, S. (1994) The Biomechanics of Walking and Running - in Kwong, P.K. (1994) *Clinics in Sports Medicine: Foot and Ankle Injuries*. W.B Saunders, Philadelphia. Pages 843-863.

Palastanga, N., Soames, R., and Palastanga, D. (2008) *Anatomy and Human Movement Pocketbook.* Churchill Livingstone, Elsevier, Philadelphia.

Panghaal, V., Janow, G., Trinh, A., Ilowite, N., and Levin, T.L. (2012) Normal Epiphyseal Cartilage Measurements in the Knee in Children: An Alternative Sonographic Approach. *Journal of Ultrasound Medicine.* **31** (1): 49-53.
Pate, R.R., O'Neill, J.R., and Lobelo, F. (2008) The Evolving Definition of "Sedentary." *Exercise and Sport Sciences Reviews.* **36** (4): 173-178.

Pearson, O.M. and Lieberman, D.E. (2004) The Aging of Wolff's "Law": Ontogeny and Responses to Mechanical Loading in Cortical Bone. *Yearbook of Physical Anthropology*. **47** : 63-99.

Perry, J. (1992) *Gait Analysis: Normal and Pathological Function.* SLACK Incorporated, New York.

Poon, M., Hamarneh, G., and Abugharbieh, R. (2008) Efficient Interactive 3D Livewire Segmentation of Complex Objects with Arbitrary Topology. *Computerized Medical Imaging and Graphics.* **32** (8): 639-650.

Prendergast, P.J. and Huiskes, R. (1995) The Biomechanics of Wolff's Law: Recent Advances. *Irish Journal of Medical Sciences.* **164** (2): 152-154.

Putti, A.B., Arnold, G.P., Cochrane, L. and Abboud, R.J. (2007) The Pedar In-shoe System: Repeatability and Normal Pressure Values. *Gait and Posture.* **25** (3): 401-405.

Pyle, S.I. and Hoerr, N.L. (1969) *The Radiographic Standard of Reference for the Growing Knee.* Charles C. Thomas, Illinois, USA.

Queen, R.M., Gross, M.T. and Liu, H.Y. (2006) Repeatability of Lower Extremity Kinetics and Kinematics for Standardized and Self-Selected Running Speeds. *Gait and Posture*. **23** : 282-287.

Ramanathan, A.K. and Abboud, R. (2010) Clubfoot Assessment: The Complete IMAR Footprint. *Orthopaedics and Trauma*. **24** (4) : 303-308.

Ramanathan, A.K., Kiran, P., Arnold, G.P., Wang, W. and Abboud, R.J. (2010) Repeatability of the Pedar-X® In-Shoe Pressure Measuring System. *Foot and Ankle Surgery.* **16** (2): 70-73.

Rand, M.K., and Ohtsuki, T. (2000) EMG Analysis of Lower Limb Muscles in Humans During Quick Change in Running Directions. *Gait and Posture*. **12** : 169-183.

Rang, M. (1969) *The Growth Plate and its Disorders.* E & S Livingstone Ltd., Edinburgh.

Ratib, O. and Rosset, A. (2006) Open-Source Software in Medical Imaging: The Development of OsiriX. *International Journal of Computer Assisted Radiology and Surgery*. **1** : 187-196.

Rennie, W.J. and Saifuddin, A. (2005) Pes Anserine Bursitis: Incidence in Symptomatic Knees and Clinical Presentation. *Skeletal Radiology*. **34** : 395-398.

Reynard, F., Dériaz, O. and Bergeau, J. (2009) Foot Varus in Stroke Patients: Muscular Activity of Extensor Digitorum Longus During the Swing Phase of Gait. *The Foot.* **19** (2): 69-74.

Riggs, B.L., Melton III, L.J., Robb, R.A., Camp, J.J., Atkinson, E.J., Peterson, J.M., Rouleau, P.A., McCollough, C.H., Bouxsein, M.L., and Khosla, S. (2004) Population-Based Study of Age and Sex Differences in Bone Volumeric Density, Size, Geometry, and Structure at Different Skeletal Sites. *Journal of Bone and Mineral Research.* **19** (12): 1945-1954.

Robbins, S.E. and Hanna, A.M. (1987) Running-related Injury Prevention Through Barefoot Adaptations. *Medicine and Science in Sports and Exercise.* **19** (2): 148-156.

Rodgers, M.M. (1988) Dynamic Biomechanics of the Normal Foot and Ankle During Walking and Running. *Physical Therapy* **68** (12): 1822-1830.

Rogol, A.D., Roemmich, J.N. and Clarke, P.A. (2002) Growth at Puberty. *Journal of Adolescent Health.* **31** : 192-200.

Rolian, C., Lieberman, D.E., Hamill, J., Scott, J.W., and Werbel, W. (2009) Walking, Running and the Evolution of Short Toes in Humans. *The Journal of Experimental Biology*. **212** : 713-721.

Rose, J. and Gamble, J.G. (1994) *Human Walking – Second Edition*. Williams and Wilkins, Maryland.

Rosset, A., Spadola, L., and Ratib, O. (2004) OsiriX: An Open-Source Software for Navigating in Multidimensional DICOM Images. *Journal of Digital Imaging*. **17** (3): 205-216.

Rowland, T.W. (1996) *Children's Exercise Physiology – Second Edition*. Human Kinetics, Champaign, IL.

Ryan, T.M. and Krovitz, G.E. (2006) Trabecular Bone Ontogeny in the Human Proximal Femur. *Journal of Human Evolution.* **51** : 591-602.

Sailhan, F., Chotel, F., Guibal, A., Gollogly, S., Adam, P., Bérard, J., and Guibaud, L. (2004) Three-Dimensional MR Imaging in the Assessment of Physeal Growth Arrest. *European Radiology*. **14** : 1600-1608.

Salter, R.B. and Harris, W.R. (1963) Injuries Involving the Epiphyseal Plate. *Journal of Bone and Joint Surgery.* **45-A** : 587-622.

Saul, L. (2013) Human Anatomy Lab - Photo Gallery of Anatomy Models. Collarado University. (Last accessed – 2013):http://www.colorado.edu/intphys/iphy3415/models/.

Scheuer, L. and Black, S. (2000) *Developmental Juvenile Osteology*. Elsevier Academic Press, London.

Schmeling, A., Schulz, R., Danner, B., and Rösing, F.W. (2006) The Impact of Economic Progress and Modernization in Medicine on the Ossification of Hand and Wrist. *International Journal of Legal Medicine.* **120** : 121-126.

Schmidt, S., Mühler, M., Schmeling, A., Reisinger, W., and Schulz, R. (2007) Magnetic Resonance Imaging of the Clavicular Ossification. *International Journal of Legal Medicine.* **121** : 321-324.

Shih, C., Chang, C., Penn, I., Tiu, C., Chang, T., and Wu, J. (1995) Chronically Stressed Wrists in Adolescent Gymnasts: MR Imaging Appearance. *Radiology.* **195** : 855-859.

Sicurezza, E., Palazzo, G. and Leonardi, R. (2011) Three-dimensional Computerised Tomographic Orbital Volume and Aperture Width Evaluation: A Study in Patients Treated with Rapid Maxillary Expansion. *Oral Surgery, Oral Medicine, Oral Pathology, Oral Radiology and Endodontics.* **111** : 503-507.

Siegling, J.A. (1941) Growth of the Epiphyses. *Journal of Bone and Joint Surgery* **23** : 23-36.

Soames, R.W. (1985) Foot Pressure Patterns During Gait. *Journal of Biomedical Engineering.* **7** (2): 120-126.

Soler, T. and Calderón, C. (2000) The Prevalence of Spondylolysis in the Spanish Elite Athlete. *The American Journal of Sports Medicine*. **28** (1): 57-62.

Spina, A.A. (2007) The Plantaris Muscle: Anatomy, Injury, Imaging and Treatment. *The Journal of the Canadian Chiropractic Association*. **51** (3): 158-165.

Stokes, I.A.F. (2002) Mechanical Effects on Skeletal Growth. *Journal of Musculoskeletal Neuron Interaction*. **2** (3): 277-280.

Tanner, J.M., Whitehouse, R.H., and Takashi, M. (1966) Standards From Birth to Maturity for Height, Weight, Height Velocity and Weight Velocity: British Children. *Archives of Disease in Childhood* **41** : 613-617.

Tervo, T., Nordström, P., Neovius, M., and Nordström, A. (2009) Reduced Physical Activity Corresponds with Greater Bone Loss at the Trabecular than the Cortical Bone Sites in Men. *Bone.* **45** : 1073-1078.

Thomas, S.S. and Supan, T.J. (1990) A Comparison of Current Biomechanical Terms. *American Academy of Orthotists and Prosthetics.* **2** (2): 107-114.

Tobias, J.H., Steer, C.D., Mattocks, C.G., Riddoch, C., and Ness, A.R. (2007) Habitual Levels of Physical Activity Influence Bone Mass in 11-Year-Old Children From the United Kingdom: Findings From a Large Population-Based Cohort. *Journal of Bone and Mineral Research* **22** (1): 101-109.

Ulijaszek, S.J., Johnston, F.E. and Preece, M.A. (1998) *The Cambridge Encyclopedia of Human Growth and Development*, Cambridge University Press, Cambridge.

Vaughan, C.L. (2003) Theories of Bipedal Walking: An Odyssey. *Journal of Biomechanics.* **36** : 513-523.

Vaughan, C.L., Davis, B.L. and O'Connor, J.C. (1999) *Dynamics of Human Gait – Second Edition.* Kiboho Publishers, Cape Town.

Vicente-Rodriguez, G., Jimenez-Ramirez, J., Ara, I., Serrano-Sanchez, J.A., Dorado, C., and Calbet, J.A.L. (2003) Enhanced Bone Mass and Physical Fitness in Prepubescent Footballers. *Bone*. **33** : 853-859.

Villemure, I. and Stokes, I.A.F. (2009) Growth Plate Mechanics and Mechanobiology. A Survey of Present Understanding. *Journal of Biomechanics*. **42** : 1793-1803.

Wardak, E., Gill, S., Wardak, M., Sen, R., Singh, P., Kumar, V., Saini, R., and Jha, N. (2009) Role of MRI in Detecting Early Physeal Changes Due to Acute Osteoarticular Infection Around the Knee Joint: A Pilot Study. *International Orthopaedics (SICOT).* **33** : 1707-1711.

Wearing, S.C., Urry, S.R. and Smeathers, J.E. (2000) The Effect of Visual Targeting on Ground Reaction Force and Temporospatial Parameters of Gait. *Clinical Biomechanics*. **15** : 583-591.

Whittle, M.W. (2007) *Gait Analysis: An Introduction – Fourth Edition*. Elsevier Ltd, Philadelphia.

Willy, C., Schneider, P., Engelhardt, M., Hargens, A.R., and Mubarak, S.J. (2008) Richard von Volkmann: Surgeon and Renaissance Man. *Clinical Orthopaedics and Related Research*. **466** (2): 500-506.

Witvrouw, E., Borre, K.V., Willems, T.M., Huysmans, J., Broos, E. and De Clercq, D. (2006) The Significance of Peroneus Tertius Muscle in Ankle Injuries – A Prospective Study. *The American Journal of Sports Medicine.* **34** (7): 1159-1163.

Woo, S.L., Kuei, S.C., Amiel, D., Gomez, M.A., Hayes, W.C., White, F.C., and Akeson, W.H. (1981) The Effect of Prolonged Physical Training on the Properties of Long Bone: A Study of Wolff's Law. *The Journal of Bone and Joint Surgery.* **63** : 780-787.

Woods, C., Hawkins, R.D., Maltby, S., Hulse, M., Thomas, A. and Hodson, A. (2004) The Football Association Medical Research Programme: An Audit of Injuries in Professional Football – Analysis of Hamstring Injuries. *British Journal of Sports Medicine.* **38** : 36-41.

Wright, C.M, Booth, I.W., Buckler, J.M.H., Cameron, N., Cole, T.J., Healy, M.J.R., Hulse, J.A., Preece, M.A., Reilly, J.J. and Williams, A.F. (2002) Growth Reference Charts for Use in the United Kingdom. *Archives of Disease in Childhood.* **86** : 11-14.

Yarrow, K., Brown, P., and Krakauer, J.W. (2009) Inside the Brain of an Elite Athlete: The Neural Processes that Support High Achievement in Sports. *Nature Reviews Neuroscience*. **10** : 585-597.

Zackowski, K.M., Dromerick, A.W., Sahrmann, S.A., Thach, W.T. and Bastian, A.J. (2004) How Do Strength, Sensation, Spasticity and Joint Individuation Relate to the Reaching Deficits of People with Chronic Hemiparesis? *Brain.* **127** : 1035-1046.